

REPORT DOCUMENTATION PAGE

Form Approved OMB No. 0704-0188

Public reporting burden for this collection of information is estimated to average 1 hour per response, including the time for reviewing instructions, searching existing data sources, gathering and maintaining the data needed, and completing and reviewing the collection of information. Send comments regarding this burden estimate or any other aspect of this collection of information, including suggestions for reducing the burden, to Department of Defense, Washington Headquarters Services, Directorate for Information Operations and Reports (0704-0188), 1215 Jefferson Davis Highway, Suite 1204, Arlington, VA 22202-4302. Respondents should be aware that notwithstanding any other provision of law, no person shall be subject to any penalty for failing to comply with a collection of information if it does not display a currently valid OMB control number.

PLEASE DO NOT RETURN YOUR FORM TO THE ABOVE ADDRESS.

1. REPORT DATE (DD-MM-YYYY) 18-06-2004	2. REPORT TYPE Final Report	3. DATES COVERED (From - To) 01-Feb-02 - 01-Feb-04
--	---------------------------------------	--

4. TITLE AND SUBTITLE Development of Methods for Diagnostics of Discharges in Supersonic Flows	5a. CONTRACT NUMBER ISTC Registration No: 2247p
	5b. GRANT NUMBER
	5c. PROGRAM ELEMENT NUMBER

6. AUTHOR(S) Dr. Alexei Ershov	5d. PROJECT NUMBER
	5d. TASK NUMBER
	5e. WORK UNIT NUMBER

7. PERFORMING ORGANIZATION NAME(S) AND ADDRESS(ES) M.V. Lomonosov Moscow State University (MSU) Faculty of Physics Moscow 119899 Russia	8. PERFORMING ORGANIZATION REPORT NUMBER N/A
--	--

9. SPONSORING/MONITORING AGENCY NAME(S) AND ADDRESS(ES) EOARD PSC 802 BOX 14 FPO 09499-0014	10. SPONSOR/MONITOR'S ACRONYM(S)
	11. SPONSOR/MONITOR'S REPORT NUMBER(S) ISTC 01-7038

12. DISTRIBUTION/AVAILABILITY STATEMENT
Approved for public release; distribution is unlimited.

13. SUPPLEMENTARY NOTES

14. ABSTRACT

This report results from a contract tasking M.V. Lomonosov Moscow State University (MSU) as follows: The contractor will develop methods of measurements of plasma parameters of the electric discharges in supersonic air flows of propane-air mixtures. The experimental investigation of spatial and temporary evolution of parameters of plasma discharges of various types of the discharges (longitudinal direct current, transversal pulsed-periodic, plasma dynamic discharges) and combustion plasma in supersonic flows will be carried out at Mach number M=2 in a pressure range 10-400 Torr. The following plasma parameters will be measured: charged particle densities, gas and vibrational temperatures, floating and plasma potential, transversal and longitudinal electric field in plasma. He will also develop the laboratory prototype of a compact automated diagnostic probe complex for measurement of local parameters plasma in supersonic flows in a real time mode. This Project consists of two tasks. Task 1 is devoted to development of the complex of diagnostic methods (probe and spectroscopic) that will enable to indicate ignition and combustion of air-fuel mixture in supersonic flow and to measure parameters of discharge and combustion plasma. Task 2 will be devoted to creation of the laboratory prototype of a compact automated diagnostic complex for measurement of local parameters of plasma supersonic flows in a real time mode.

15. SUBJECT TERMS
EOARD, Physics, Plasma Physics & Magnetohydrodynamics

16. SECURITY CLASSIFICATION OF:			17. LIMITATION OF ABSTRACT UL	18. NUMBER OF PAGES 148	19a. NAME OF RESPONSIBLE PERSON WAYNE A. DONALDSON
a. REPORT UNCLAS	b. ABSTRACT UNCLAS	c. THIS PAGE UNCLAS			19b. TELEPHONE NUMBER (Include area code) +44 (0)20 7514 4299

ISTC 2247p

**FINAL
PROJECT TECHNICAL REPORT
of ISTC 2247p**

**Development of Methods for Diagnostics
of Discharges in Supersonic Flows
(From 1 February 2002 to 31 January 2004)**

Department of Physics of Moscow State University

Dean of Department of Physics

Professor

V.I. Trukhin

Project Manager

Associated Professor

A. P. Ershov

Moscow

March 2004

**This work was supported financially by EOARD and performed under the contract to the
International Science and Technology Center (ISTC), Moscow**

**Development of Methods for Diagnostics
of Discharges in Supersonic Flows
(From 1 February 2002 to 1 February 2003)**

Alexey Petrovich Ershov (Project Manager)
Department of Physics of Moscow State University

The objectives of this project are the development of a complex of techniques, which will allow to measure parameters of discharge plasma and flame plasma in a supersonic flows and the development of laboratory prototype of an automated diagnostic probe circuit.

Keywords: electric discharge, supersonic flow, diagnostic methods, electric probe, measurement circuit, propane-air mixture, ignition.

Participating Institution: Department of Physics of Moscow State University
Adress: Department of Physics, Moscow State University, 119899, Moscow, Russia
Tel: (095) 939-31-60
Fax: (095) 932-88-20
E-mail: dean@phys.msu.su / ershov@ph-elec.phys.msu.su

Partner: The European Office of Aerospace Research and Development (EOARD)
Adress: 223/231 Old Marylebone Road NW1 5TH London, UK
Tel: +44(20) 7514 4953
Fax: +44(20) 7514 4960
E-mail : wayne.donaldson @london.af.mil

CONTENTS

ABSTRACT	5
NOMENCLATURE	9
INTRODUCTION	10
CHAPTER I. TECHNICAL SUPPORT OF INVESTIGATIONS	12
§ 1. Draft scheme of the experimental setup	12
§ 2. The modernization of plasma jet generator and input system of plasma jet in a supersonic flow	15
CHAPTER II. DEVELOPMENT OF A LABORATORY PROTOTYPE OF AN AUTOMATED DIAGNOSTIC PROBE CIRCUIT	17
§ 1. The operation principle and block diagram of probe circuit	17
§ 2. The user interface	20
CHAPTER III. ANALYSIS OF PROBE VOLTAGE CURRENT CHARACTERISTICS FOR CONDITIONS OF IGNITING DISCHARGES	22
Introduction	22
§1 Background of Probe-Plasma Interaction Detailed Description	23
§2 Electric Field Distribution around a Double Probe. Effect of a Second Wire	25
§ 3 Plasma Parameter Distributions and Ion Probe Current in Drift, Diffusion and Intermediate Modes	27
§ 4 Account to the Electron Current Leakage	29
§ 5 Probe Voltage Current Characteristics	31
§ 6 Difference in Diagnostics of Pure Air and Air-Hydrocarbon Mixture	35
§ 7 Mathematical Modeling of a Double Probe in the Air-Fuel Plasma	38
§ 8 Analysis of Interaction of Probes with Flame Plasma High-Speed Flows	43
CHAPTER IV. COMPUTER SIMULATIONS OF PLASMA-PROBE INTERACTION IN A SUPERSONIC FLOW	68
§ 1. 1D numerical model	68
§ 2. Results of computation	70
§ 3. Comparison with experimental data	77
§ 4. Electron part of probe characteristic	80

CHAPTER Y. METHODS OF THE DETECTION OF THE IGNITION PROCESS AND MEASUREMENTS OF PLASMA PARAMETERS OF A DISCHARGES IN A SUPERSONIC FLOW	85
§ 1. Spectroscopic method of the detection of the ignition process	85
1.1 Temporary measurement of relative intensities of active radicals in plasma of pulsed transversal discharge in a supersonic propane-air flow	85
1.2 Temporary measurement of relative intensities of active radicals in plasma of plasmadynamic discharge in a supersonic propane-air flow	88
§ 2. Probe method of the detection of the ignition process	91
§ 3. The measurements of gas and vibrational temperatures	92
§ 4. Probe measurements of plasma density	94
4.1. Double probe characteristics in plasma of igniting discharges	94
4.2 Single probe characteristics in plasma	101
CHAPTER YI. PLASMA PARAMETERS OF IGNITING DISCHARGES IN A SUPERSONIC FLOW	106
§1. Parameters of electrode discharges in a supersonic airflow	106
§ 2. Parameters of electrode ignition discharge in supersonic propane – air mixture flows	116
§ 3. Macroscopic parameters of a plasmadynamic discharge in a supersonic air and propane – air mixture flows	120
§ 4. Plasma density of a plasmadynamic discharge in a supersonic air and propane – air mixture flows	124
CHAPTER YII. SIMULATION OF AN IGNITING DISCHARGE IN A SUPERSONIC PROPANE-AIR MIXTURE FLOW	131
§ 1. Unsteady heat source model of the discharge in a supersonic propane-air mixture flow	131
§ 2. Results of simulation of an ignition discharge in a supersonic propane-air flow	135
CONCLUSION	142
LIST OF PUBLISHED PAPERS AND REPORTS	145

ABSTRACT

The complex of probe and spectroscopic methods which allow to determine parameters of discharge plasma of a fuel-air mixture, fact of ignition of propane - air mixture in a supersonic flows and parameters of flame plasma has been developed in the current project.

Experiments have been produced with an application of a wind tunnel of short action. Measurements have been performed in supersonic air and air-propane flows at Mach number $M = 2$ under total pressures $P_0 = 1 - 5$ atm, stagnation temperature $T_0 = 300$ K, vacuum chamber pressures $p = 50 - 300$ Torr. Pulse modulator with output voltage up to 24 kV, current up to 40 A and pulse duration $\tau = 2 - 1000$ μ s have been used to generate pulsed transversal and longitudinal discharges. Magnetoplasma compressor type electrode unit generated a pulsed plasma jet injected into the supersonic flow. The quasi-period of the discharge current was about 60 μ s, the maximal value of current was $I_{\max} \approx 10$ kA, and discharge voltage was $U_{\max} = 5$ kV.

The complex of diagnostic instruments was used for a measurement of microscopic parameters of the discharges: schlieren set-up, high-speed photography, scheme of a PC-controlled probe, a PC-controlled analyser of optical spectra based on a spectrograph with CCD image sensor and digital storage oscilloscopes Tektronix TDS-210.

The new type of the probe measurement device fundamentally improving the temporary resolution was developed. Laboratory prototype of an automated diagnostic probe circuit has been manufactured and tested. The operation principle of this device is based on the use of ADSP-type signal processor, installed near an investigation object, the transformation of measured analogue signal to digital sequence, temporal storing data in the ADSP memory and the transmission of data to the main computer.

An analytical model for drift, diffusion and intermediate modes of probe operation in high-speed flows of dense weakly ionized plasma is suggested. New analytical model for the modes, in which the probe current is limited by processes in the Debye double layer and in the ion drift region, has been developed for the characteristic high-speed flows of flame plasmas.

A computer simulation of one-dimensional probe diagnostic problem has been carried out for the cases when processes in the Debye layer are important. Both cases of the steady plasma and the

plasma flow with the Blasius gas dynamical profile have been considered. These results are in a reasonable agreement with the new experimental data.

I-V probe characteristics of double probe were measured in plasma of electrode and plasmadynamic igniting discharges in the supersonic air and air-propane mixture. Comparison with results of numerical modeling has shown, that the model of ion saturation current can be applied for a determination of ion density.

Voltage - current characteristics of single probe in the propane-air flame plasma in the supersonic propane-air flow was measured. Comparison with results of numerical modeling has shown, that electron probe current is determined by electron drift in the region of the undisturbed flow and the known formula of a drift current can be used for voltage - current characteristics interpretation.

The method of electric field measurement in plasma of the transversal discharge in the supersonic air and air-propane mixture flow was suggested and tested. It's based on the fact that the discharge channel represents a current loop, drifting with speed of a flow v , and the value E is determined by the first derivative on time of electrode voltage: $\partial U / \partial t \approx 2Ev$.

The method of gas temperature measurement was adapted to experimental conditions. The intensities of lines of the rotational structure of the second positive system of N_2 , which has been used for measurements of gas (rotational) temperature of air plasma, falls at growth of full pressure $P_0 > 1$ atm very sharp. Especially it is true in case of air-propane plasmas. As result, plasma temperature has to be evaluated over the relative intensities of the molecular bands of CN (0,0) и (1,1) with quantum wavelengths $\lambda=388,3$ и $387,2$ nm.

Mechanism of transversal electric discharge sustention in supersonic air and propane-air flows was investigated. It was experimentally shown that secondary breakdown between anode and cathode discharge streams, formed along a flow, causes transversal discharge's instability in supersonic flows. Due to this phenomenon a discharge is temporary and spatially quasi-stationary, even if a current's generator acts as a source for discharge feeding. Spatial discharge structure consists of two parts: a stationary of extension L_0 -, and a quasi-stationary of extension $L_t = vt$, where v – is a velocity of a flow, t – current time between two consequent breakdowns $0 < t < T$. Period of the voltage vibration T in the discharge is a function of the macroscopic discharge parameters – discharge current, interelectrode distance and full pressure.

An electric field - current relation were measured in wide ranges of discharge current and full pressure of a flow, when a current's generator acts as a source for discharge feeding. The found dependencies $E(I)$ are the falling ones, a connection between a current and a field is close to the power dependence $I \sim E^{-m}$, where $2 < m < 3$, and the electric field in a region of respectively small currents $I < 1$ A reaches values close to 1 kV/cm, whereas the values of the electric field at $I > 1$ A are ones lower 10^2 V/cm.

The temperature of plasma of the transversal discharge in a supersonic airflow was measured in wide ranges of discharge current and pressure of a flow. The temperature - current dependence has a direct power law $T \sim I^{1/3}$ in studied range of parameters. The temperature has a tendency to decrease when a density of gas flowing out of a nozzle increases. The temperature - current dependence is qualitatively opposite to changing of the electric field with current. The value of temperature reaches its maximum value near electrodes and slowly decreases down a flow.

Measured gas temperature absolute values at high currents reach several thousands degrees. These values are smaller than the values of the electron temperature $T_e \approx 10^4$ K calculated for these conditions. Thus, plasmas in conditions under the investigation are nonequilibrium one, it is insufficient to know the gas temperature value for determining of its conductivity, and direct measurements of the plasma density are necessary.

Results of charged particle measurements in the transversal discharge obtained by electric probes and by Stark-effect method show that ion density values at $P_0 \approx 1$ and currents up to 40 A do not exceed 10^{14} cm^{-3} . Electron density of flame plasma flow was equal to about 10^{10} cm^{-3} .

Checking technique of ignition and combustion of propane- air mixture in supersonic flows was suggested. Experimentally was shown that the fact of ignition and combustion of propane-air mixture supersonic flow may be tested by complex (joint application) of two methods: a) investigation of CH radicals band, $\lambda = 431.5$ nm, luminescence evolution and b) investigation of the single electric probe currents evolution.

The investigations of ignition of supersonic propane-air mixture flow by different type of discharge were performed. The range of parameters of the pulsed transversal electric discharge, in which the ignition of the propane-air mixture flow is observed, is determined. It's shown experimentally, that there are the thresholds of ignition, due the length of discharge across the

supersonic air-propane mixture flow, the discharge current in the case of discharge feeding from the generator of current or of electric power density. The growth of the electric power density results in reduction of the pulse duration. The temperature of plasma of electrode discharges in case of ignition of supersonic air-propane mixture flow was equal to about 3000 K, whereas the gas temperature in the discharge in the supersonic airflow was up to 2000 K.

Numerical model of electric discharge in a supersonic airflow and air-propane mixture flow as energy-releasing zone was developed. The laminar flow is described by Navier-Stokes equations with additional source term in energy equation. For description of the fuel gas ignition and consequent burning were used two chemical models: 11 species thermally equilibrium quasiglobal chemical models with one global reaction and some detailed reaction model with detailed reactions mechanism, including 30 species and 70 chemical reactions.

The effects of the heat source power, geometry and time expansion type on the ignition process were studied. The results are computed for experimental conditions: $P_0 = 4$ atm, $T_0 = 300$ K, $M = 2$ and stoichiometric composition of fuel mixture. The threshold specific power value, at which the ignition takes place and the threshold value of a discharge length were obtained. These values were consistent with experimental data for transversal and longitudinal electric discharges.

NOMENCLATURE

- e – Magnitude of electron charge
 M – Mach number flow
 u -flow velocity
 P_0 – receiver pressure
 p – chamber pressure
 I – discharge current,
 j - density of current
 U – discharge voltage,
 L –discharge length
 U_p – probe bias,
 I_i – ion probe current
 r_p – probe radius,
 L_p – probe length,
 r_D – Debye length
 $\varepsilon = (r_D / r_p)^2$
 n - neutral particle density,
 n_i, n_e - density of ions and electrons
 T - gas temperature
 T_e – electron temperature
 $\tau = T_e / T$
 D_i - Diffusion coefficient of ions,
 Re_e –electric (diffusion) Reynolds number
 μ_e, μ_i - electrons and ions mobilities accordingly
 μ - viscosity
 Pr – Prandtl number
 z – axial coordinate
 $L_W(\alpha)$ - Lambert W function with an argument α

INTRODUCTION

The problem of organization of ignition and stabilization of combustion of an air-fuel mixture is one of basic problems of aircraft at transition to hypersonic velocity of flight. The gas discharges of a various type can be the perspective tool of the decision of this problem.

The definition of the most effective type of the discharge and its optimization from the point of view of ignition are impossible without development of diagnostics methods of discharge plasma in supersonic flows and measurement of their parameters. The complex of diagnostic methods (spectroscopic, probe, microwave) of discharge plasma in supersonic airflows was developed in frameworks of EOARD partner Project of the ISTC #1867p.

The application of such discharges as the systems of ignition of fuel-air mixtures requires in the first place revision of techniques, caused the necessity of the account of influence of gaseous fuel on properties of plasma.

Next, direct application of developed methods in case of combustion plasma is impossible. The reason of impossibility of these methods is the basic difference of the characteristics of plasma supported by an electrical field, and plasma created due to chemical energy of air-fuel mixture combustion. The existing methods of combustion plasma measurements are intended for case of stationary burning of a flame and subsonic velocities of flows.

At last, after the combustion of fuel-air mixture with the help of discharge system there is a problem of separation of discharge plasma from flame plasma.

The objectives of the project are:

1. The development of a complex of techniques, which will allow to determine:
 - parameters of discharge plasma of a fuel-air mixture
 - the fact of ignition of fuel - air of a mixture in a supersonic flows,
 - parameters plasma of a flame.
2. The development of laboratory prototype of an automated diagnostic probe circuit for measurement of local parameters of plasma in supersonic flows

Expected results

- The methods of measurements of parameters of gas discharge plasma and combustion plasma in supersonic propane-air mixtures flows will be developed.
- The experimental investigation of spatial and temporary evolution of parameters of plasma of various types of the discharges in supersonic flows of propane-air combustible

mixtures and combustion plasma created by these discharges will be carried out with Mach number $M=2$ in a pressure range 10-400 Torr.

- Checking technique of ignition and combustion of an air-fuel mixture in a supersonic flow will be developed.
- The mathematical model of interaction of plasma with a probe
- Laboratory prototype of an automated diagnostic probe circuit for measurement of local parameters of plasma in supersonic flows in a real time mode will be developed and performed.
- The mathematical model of the discharge in a supersonic gas flow.

Technical Approach and Methodology

During the first year the following investigations have been planned:

upgrade the experimental set up;

development of spectroscopic methods of a measurement spatially - temporary evolutions of parameters of plasma;

modelling of probe voltage-current characteristics in high-speed flows of the discharge plasma of the propane-air mixture;

investigation of parameters of plasma and physical processes in a supersonic flow of non-equilibrium plasma of the gas discharges of a various type;

development of mathematical model of the discharge in a supersonic gas flow;

development of the technical project on model sample of the automated probe diagnostic complex.

During the second year the following investigation have been planned:

simulation of interaction weakly ionized plasma of propane-air flame with a probe.

development of technique of probe measurements of parameters of flame plasma in a supersonic gas flow

measurements of combustion plasma parameters

technique of indication of ignition and combustion of propan - air- mixture in a supersonic flow.

production of an automated probe diagnostic circuit.

CHAPTER I. TECHNICAL SUPPORT OF INVESTIGATIONS

§ 1. Draft scheme of the experimental setup

Draft scheme of the experimental setup for development and testing of diagnostic methods is shown in Fig.1.1. The experimental setup is built around a stainless steel cylindrical gas/vacuum chamber. The chamber is three meters long and one meter in diameter. It consists of two sections that can form a vacuum-tight junction with help of a lever-operated gate. At the installation and adjustment of diagnostic and experimental equipment inside the chamber its section can be easily separated. Twenty-six windows with different diameters (10-50 cm) are located on its lateral surface, that allows to visualize discharge processes and to provide the vacuum-tight transport of electric current and electric signals.

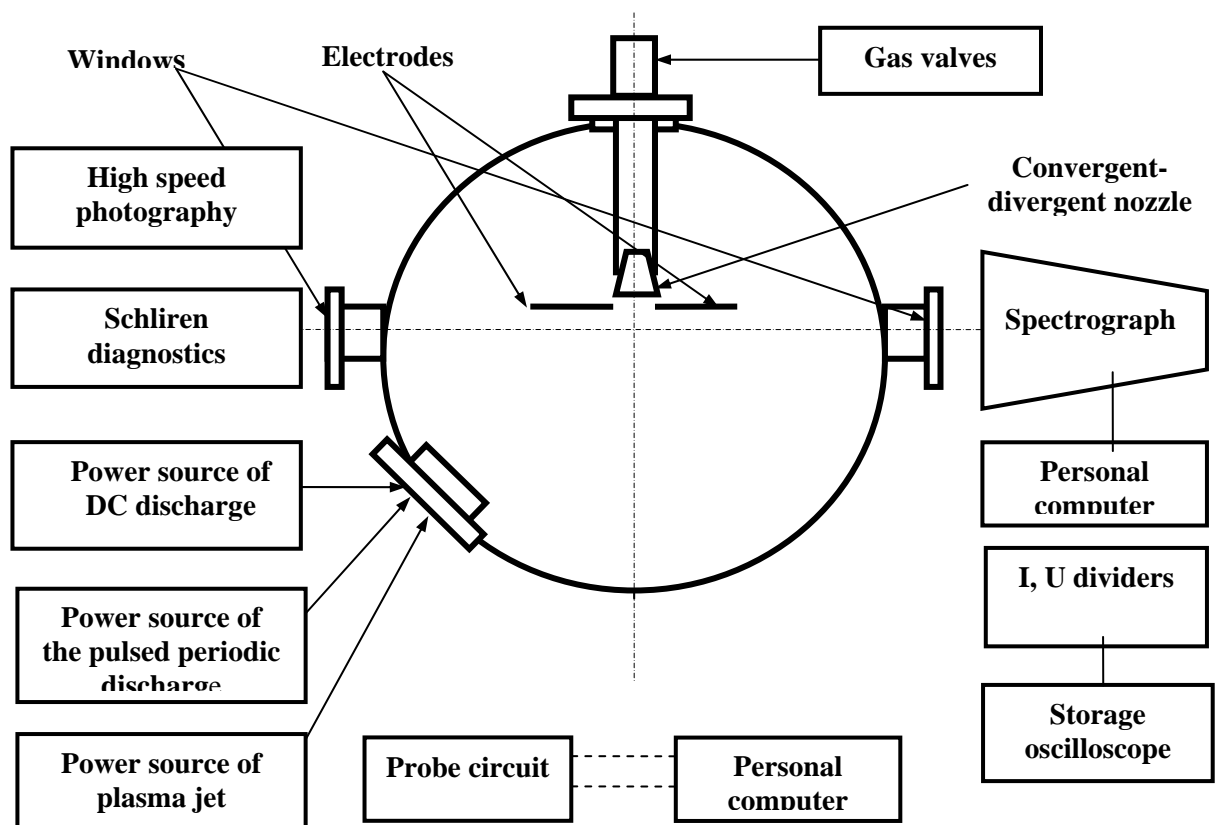


Fig. 1.1. Draft scheme of the experimental setup.

The supersonic channel (Fig.1.2) was mounted along chamber's vertical diameter. The air supply and propane-butane supply (further in the text for brevity - propane) were connected with the channel through the electric valves. Vacuum pumps allow achieving a pressure into chamber up

to 1 Torr. Supersonic flow was formed in the channel (or in the chamber) by opening an electric valves and filling with the air or air-propane mixture through a converging-diverging nozzle with Mach number $M = 2$. A cylindrical dielectric nozzle had diameter of its critical cross section 15.4 mm and an outlet diameter 26 mm.

The pressure in the gas/vacuum chamber was varied in a range $p = 50 - 400$ Torr. The pressure in the receiver of the compressor was varied in a range $P_0 = 1 - 5$ atm, the pressure in the receiver of propane tank is about 5 atm. The flow duration was about 2 seconds.

The experiments were carried out for the transversal pulsed discharge, longitudinal pulsed discharge and pulse plasmadynamic discharge.

The pulsed discharges were fed by a power supply unit with voltage up to 24 kV, current up to 40 A and pulse duration 2 - 1000 μ s.

The plasmadynamic discharge was created with use of a magnetoplasma compressor type electrode unit. New design of plasma jet generator and the input system of a plasma jet in a supersonic flow has been developed in contrast to project [1]. The pulse energy was stored in a 50 μ F capacitor, which was charged by the power supply unit up to the voltage of 5 kV. The pulsed discharge switch joined the capacitor and magnetoplasma compressor type electrode unit.

The valves, power supplies and recording equipment were controlled by the system of synchronization. Detailed description of synchronization system has been performed in [1].

The complex of diagnostic methods was used for a measurement of microscopic parameters of the discharges:

- schlieren method
- high-speed photography
- spectroscopic methods
- probe method

Detailed description of schlieren setup has been performed in [1].

High-speed photography was used for the investigation of dynamics of pulse transversal

A PC-controlled analyzer of optical spectra based on a spectrograph was used for registration of plasma radiation spectra in the spectral band 300 – 900 nm. Detailed description of PC-controlled analyzer has been performed in [1].

The electrical probes were used for a measurement of a plasma density, floating potential and electric field in plasma. The special scheme of a PC-controlled double probe has been developed and used (Chapter II).

Two digital storage oscilloscopes Tektronix TDS-210 registered another signals.

Some experiments were performed in free airflow. The investigations of discharges into propane- air mixture supersonic flow were performed in the supersonic channel. Schematic of the channel was shown on Fig.1.2, and its photo – on Fig.1.3.

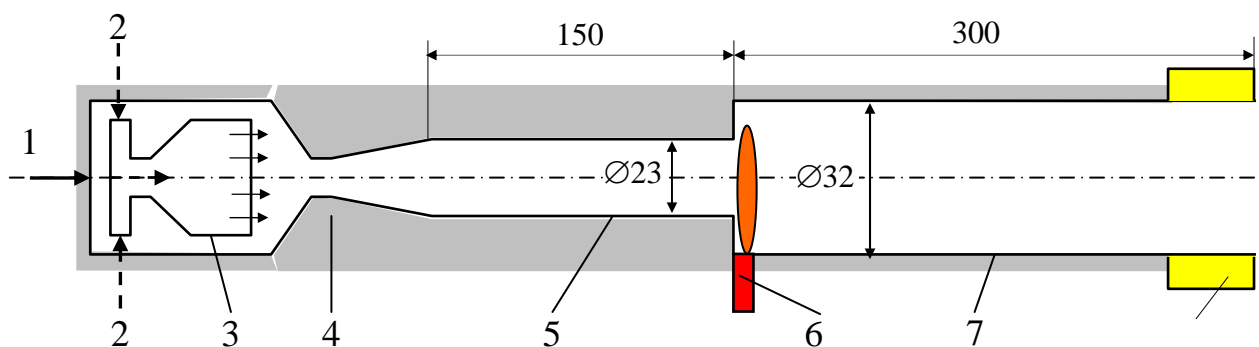


Fig.1.2 Schematic of the supersonic channel

1 – propane supply, 2 – air supply, 3 – mixer, 4 – supersonic nozzle, 5 – insulator section, 6 – plasma generator (electric discharge or plasma jet), 7 – combustor section.

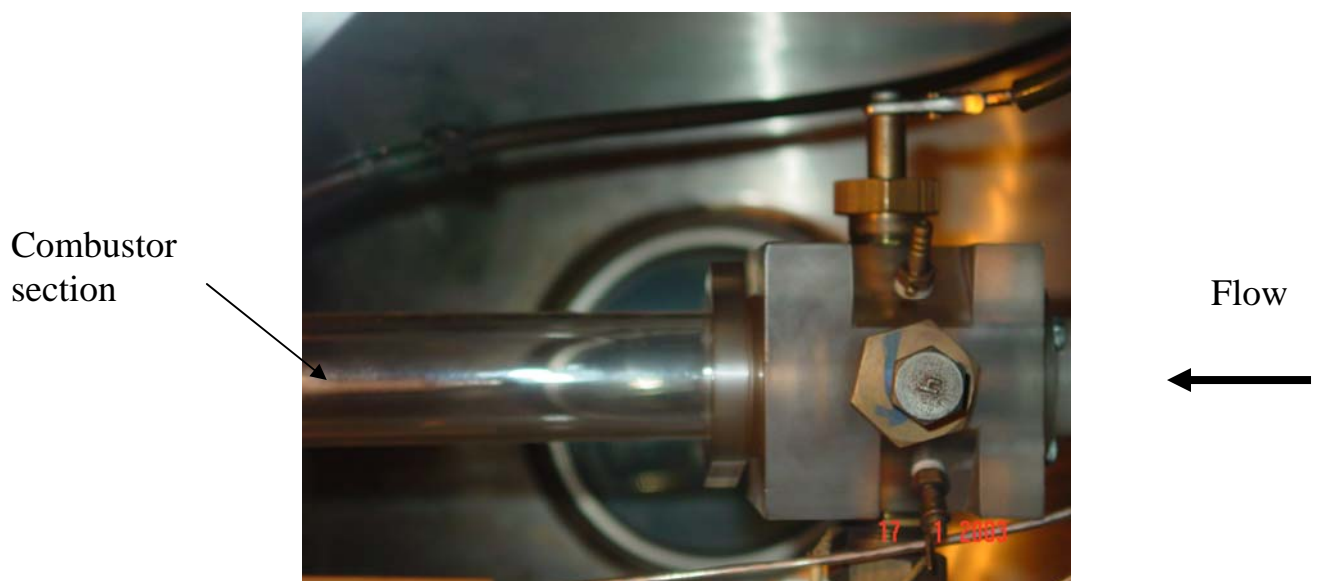


Fig.1.3 Photo of the supersonic channel.

§ 2. The construction of plasma jet generator and input system of a plasma jet in a supersonic flow

Our earlier experiments on studying possibility of ignition of air-fuel mixtures by pulsed plasma generator (plasmatron) had been carried out under conditions of normal position of axes of the plasma jets and the mixture flow. Besides that, rather powerful plasmatron with the stored pulse energy $800 \div 1250$ J had been applied primarily. In the present experiments these features have been changed. For bias (45°) positioning of the plasma jet relatively the supersonic airflow, a new, improved discharge chamber has been created. Besides that, new design of plasmatron has been developed, which permits minimization of the threshold discharge voltage and thus minimization of the energy store.

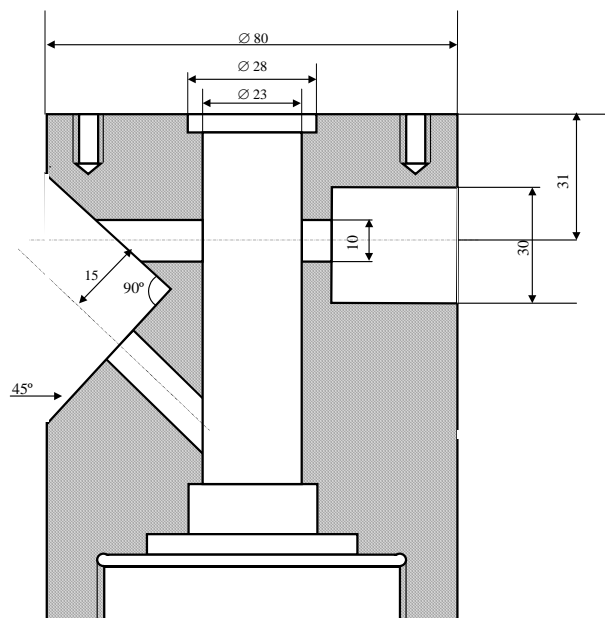


Fig.1.4. Schematic draft of the discharge chamber.

A schematic draft of the discharge chamber is shown in Fig.1.4. The chamber is made of an acrylic plastic, it has a form of a $\varnothing 80 \times 120$ mm cylinder. The work channel is made in the upper part of the chamber, the channel's diameter (23 mm) is equal to the supersonic nozzle output diameter. In the lower part of the chamber the channel becomes wider ($\varnothing 28$ mm) to fit the diameter of the quartz tube, which is applied as a work channel of the supersonic airflow. Several holes are made in the chamber walls. Two of them can be used for transversal discharges with normal initial position of electrodes or plasma generators relatively the gas flow. One more hole makes it possible to position a plasmatron in an angle of 45° relatively the flow axis.

Fig.1.5 shows the new plasmatron design and its power supply scheme. The plasmatron contains a brass carrier hollow disc (1), which is also the negative electrode. The dielectric (acrylic plastic) separator (2) is screwed into the hollow disc. A brass coupler (3) is screwed to the separator. A brass rod positive electrode (4) is screwed into the coupler. The plasmatron was supplied by a DC source (5) with maximal voltage of 5 kV. This power supply unit charged a 50 μF capacitor C. The plasmatron was fed through an additional discharge triggering unit (6), which was switched on by a synchronization circuit. As the working voltage reached the plasmatron electrodes, a breakdown appeared between the internal diameter of the carrier (1) and the external surface of the rod (4).

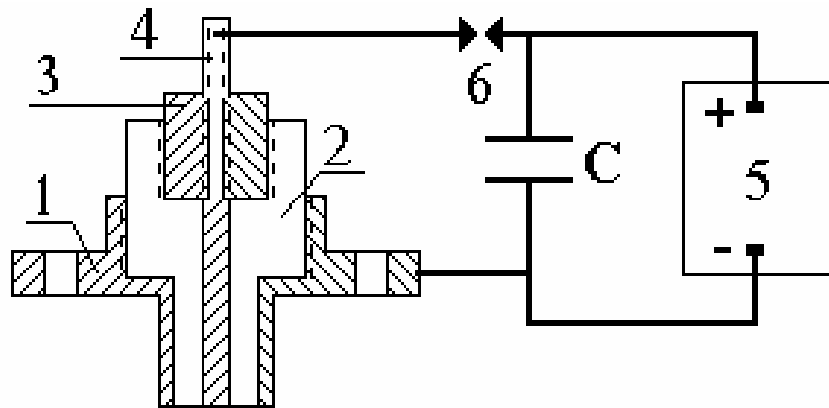


Fig.1.5. Plasmatron design and power supply scheme.

1 - negative electrode, 2 – isolator, 3 - brass coupler, 4 - positive electrode, 5 – high-voltage DC source, 6 – discharge triggering unit (spark gap).

Characteristic sizes of the units 2, 3 and 4 were varied in order to vary the discharge gap length and thus to change the breakdown voltage. Under conditions of the current experiments, the ratio of the internal diameter of the carrier (1) and the external diameter of the rod electrode (4) was equal to 3 / 7, 4 / 7 и 5 / 7, which corresponded to variation of the discharge gap length between 1 and 2 mm. Note that in the earlier experiments we had applied a constant ratio 4/10, with a 3 mm discharge gap.

Decreasing of the discharge gap length made it possible to apply lower working voltage (down to 2.5 kV) and the energy stored in the capacitor. For further decreasing of the pulse energy, the capacity C was taken twice as less. This made it possible to vary the discharge energy in a range from ≈ 150 J to ≈ 600 J.

REFERENCES TO CHAPTER I

1. Ershov A.P. Final Project Technical Report of ISTC 1867p. Moscow State University, Department of Physics, September 2001.

CHAPTER II.

DEVELOPMENT OF THE LABORATORY PROTOTYPE OF AN AUTOMATED DIAGNOSTIC PROBE CIRCUIT

§ 1. The operation principle and block diagram of probe circuit

To choose the operation principle of probe circuit several different alternate designs cases have been considered.

A PC-controlled probe measurement device type with an opto-galvanic isolation based on optocoupler and a fiber optical waveguide have been developed and tested to measure the double probe characteristics in electrical discharge in supersonic airflows [1]. The system with the galvanic separation of the analog and digital parts on base of the optron pairs does not provide the required temporary resolution because of comparatively slow operation of the optocouples. This scheme is also sensitive to noises.

The design with the optic waveguide fiber data transfer channel is more progressive. Updating variant of this device [2] is based on the transformation of measured analogue signal to digital sequence, the transmission of the said sequence via optic fiber line for the required distance and the inverse transformation of the digit code to the analogue signal.

However, since the measurement part of the diagnostic device is positioned outside the wind tunnel, the capacity of connecting wires limits the speed of the probe voltage -current characteristic measurements. For an improvement of the temporary resolution another type of the probe measurement device has been developed.

In the autonomous regime, the device is to provide the synchronization of the measurements switching on, registration and storing of no less than 10^2 voltage-current characteristics, and their further transfer to the main computer with use of standard interface means. To provide better temporary resolution, the device will be installed near the object under investigation; a low-power accumulator battery should provide its power supply. The device must be mobile, small size, and cheap.

An analysis has shown that the demands listed above are most likely to be met in a device based on an ADSP-type signal processor. This device may apply the principle of conversion of the measured analog signal into a digital form, its temporal storing in the ADSP memory, and its sequent transfer to the main computer via either the standard interface RS232, or the infrared port.

The simplified block diagram of the device is presented in Fig. 2.1.

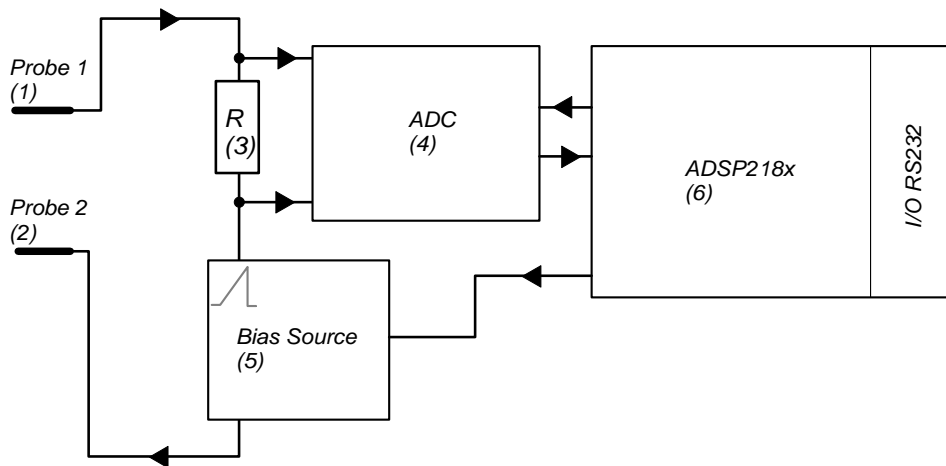


Fig.2.1 The simplified block diagram of the laboratory prototype of an automated diagnostic probe circuit

1-2 – a double probe, 3 – a resistor, 4 – analog-digital converter, 5 – a voltage integrator on a base of a powerful operational amplifier, 6 – ADSP-type signal processor.

Timing and controlling of the device are governed by ADSP - type signal processor (6). At the moment of time t_0 (start point of measurement of the probe voltage-current characteristic) ADSP (6) forms a start pulse of ADC (4). ADC (4) transforms the value of voltage on the resistor R (3) to a digital sequence, which is transmitted to ADSP (6) for temporal storing in the ADSP memory. ADC word size is 12 bit, and the conversion time is 50 ns, which provides the necessary dynamic range and speed of processing.

At the same time, the start pulse is transmitted to the unit of formation of the linearly growing bias voltage (5). The electric circuit of measuring of the double probe voltage-current characteristic consists of the unit (5), the plasma under investigation, the probes (1) and (2), and the 10-Ohm resistor (3). . The unit (5) is designed as a voltage integrator on base of a powerful operational amplifier.

The voltage bias $U(t)$ in the probe circuit changes linearly from a minimal voltage of -30 V to a maximal voltage of $+30$ V during $10 \mu\text{s}$. The resulting probe current $i(t)$ in this circuit is continuously transformed by ADC (4) .

For measurement of one voltage-current characteristic the ADSP (6) starts N of conversions, which are carried out by the ADC (4) with fixed time lags ($0.1 \mu\text{s}$). As the bias voltage temporal dependence is known, the array of N pairs of values $\{U(t_i), i(t_i)\}$ is formed in the ADSP memory

(6), this array represents the voltage-current characteristic. The device can record about 500 voltage-current characteristics during one experiment.

After filling of the ADSP memory the measuring section has to connect to the basic PC through a standard interface RS232, and the data are transported for further processing and analysis. The program (or reprogram) of measuring section is produced by the interface converter, which is disconnected from the measuring section. The photo of these devices is

The parameters of the device are shown in the Table 1.

Table 1.

Duration of a single probe measurement	10 μ s
Voltage of probe VAC measurement	\pm 30 V
Probe current limits	\pm 50 mA
Bandwidth (-3 dB level)	1 MHz
ADC	12 bit
Separation from the main computer	not limited
High voltage isolation	not limited

The experienced variant of the block of probe diagnostics was manufactured. The view of the block of probe diagnostics is shown in Fig.2.2.

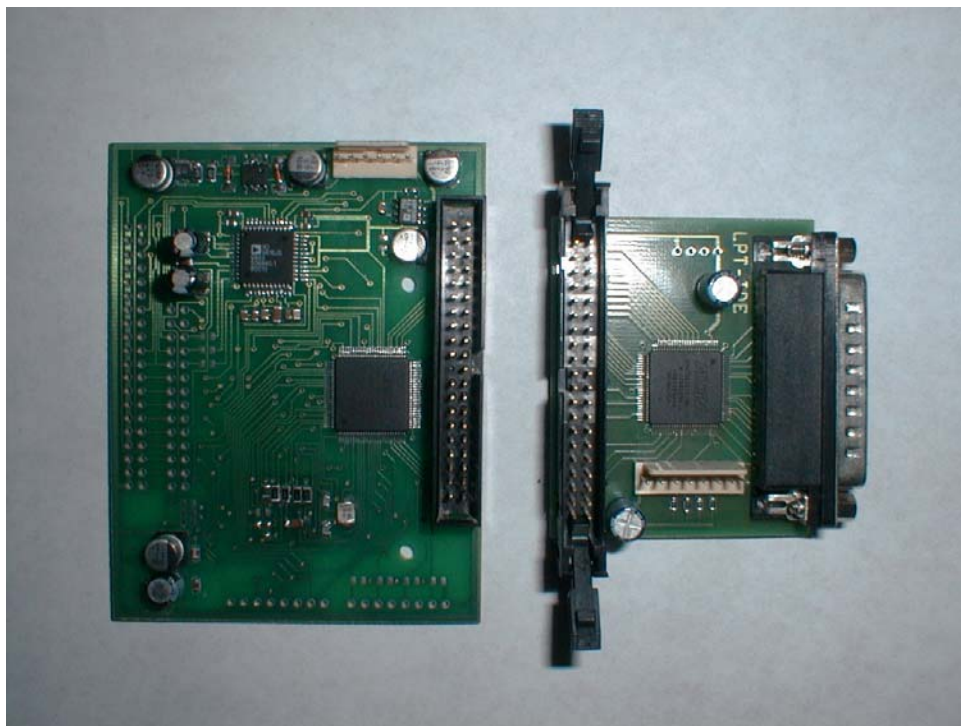


Fig.2.2. Photos of the block of probe diagnostics

An analog-digital measuring section and interface converter of LPT port. Top view.

§ 2. User interface

The program for user interface was design.

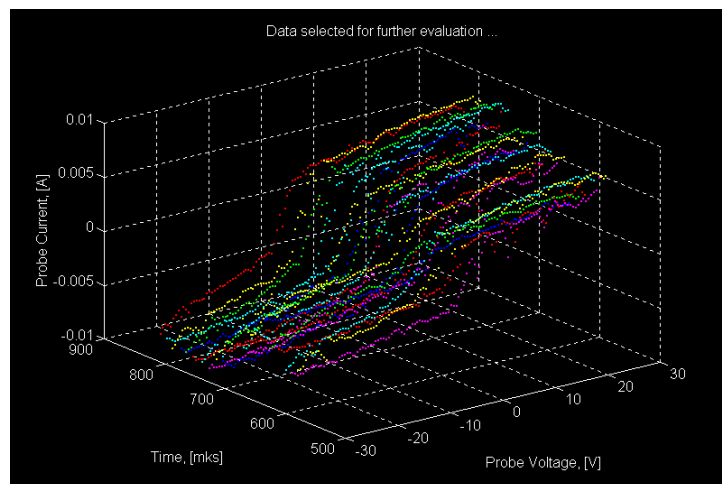
The program was oriented on the ultimate user and was designed for visualization, process experimental data and it's analysis. The program allow:

- to examine the original sequence of probe characteristics
- to choose from this sequence the series of probe characteristics to process
- to investigate the dynamics of probe current at fixed probe potential
- to determinate the average probe I-V characteristic on base of select series
- to analyze the form of probe I-V characteristic and to set the algorithm of determination of plasma parameters (automatically or according to the choose of users)
- to retain the results in during to phase of procedure and to transmit these results to another MS Windows' applications.

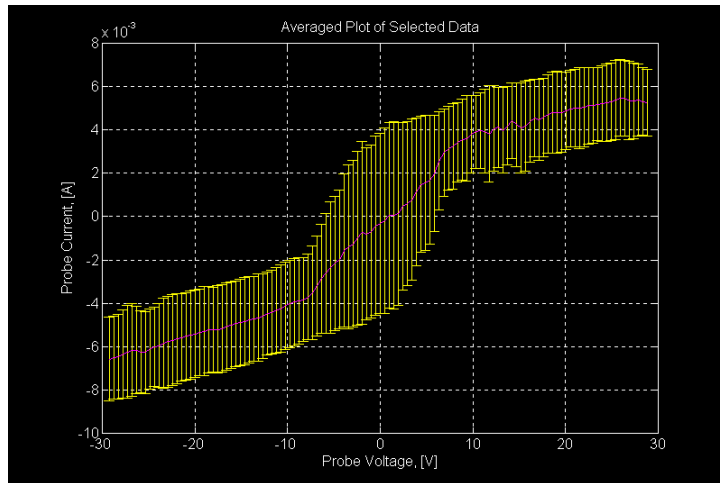
The program is realized in MATLAB. It's allowed to routine update all algorithms by means of the change Script files.

As an illustration of the test of the diagnostic circuit consider the sequence of the process of examination of probe characteristics. The user chooses from the original sequence of probe characteristics the series of probe characteristics to process (Fig.2.3a.), and can to determinate the average probe I-V characteristic on base of select series (Fig.2.3b) or investigate the dynamics of probe current at fixed probe potential (Fig.2.3c).

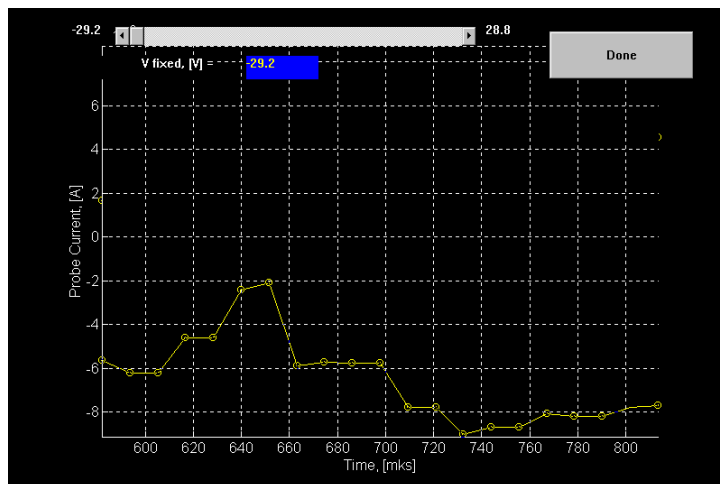
Fig.2.3 The illustration the process of examination of probe characteristics. Double probe.



a) The series of probe characteristics selected by the user to process.



b) The average probe I-V characteristic on base of select series



c) An investigation of the dynamics of probe current at fixed probe potential ($V_{\text{fixed}} = -29,2 \text{ V}$).

REFERENCES TO CHAPTER II

1. Ershov A., Ardelyan N., Chuvashov S., Shibkov V., Timofeev I. // AIAA Journal, Vol.39, No 11. P.2180, 2001.
2. Ershov A.P. Final Project Technical Report of ISTC 1867p, Moscow State University, Department of Physics, September 2001.

CHAPTER III.

ANALYSIS OF PROBE VOLTAGE CURRENT CHARACTERISTICS FOR THE CONDITIONS OF IGNITING DISCHARGES

Introduction

It seems very easy for illiterate people to insert a wire into a plasma volume and to get a probe signal. However, the problem is then far from solution yet: in the one hand, the signal must be informative in regard to plasma parameters, i.e. the noise problem must be solved; in the other hand, it is not easy to extract this information.

Modes of probe-plasma interaction are numerous, and for a great part of them there exists no sufficient theory, which would make it possible to bind probe signals with plasma properties. No skilled in art specialist can report probe diagnostic results without detailed consideration of the actual mode and substantiation of the applied method.

Our previous studies of probe interaction with weakly ionized plasma flows with high speed \mathbf{v}_g [1,2] have shown that under conditions in the discharge plasmas of interest the probe ion current is defined either by the ambipolar diffusion, or by the ion drift in the local electric field \mathbf{E}_0 ; analytical formulae for the drift mode in the case of normally positioned \mathbf{E}_0 and \mathbf{v}_g had been deduced. The field has components bound with the probe bias voltage, the charging of the active probe wire, the external discharge field, and charging of the second, passive wire of the double probe; the last component has not been accounted for in the previously deduced analytical formulae. These formulae had also neglected the electron component of the probe current. The model corresponded to the model discharges in supersonic airflows [1,2].

However, our further studies of the double probe interaction with plasma flows under conditions close to the optimum for air-fuel flows ignition (transversal discharges with comparatively higher electric current and lower electric field) have shown that the vectors \mathbf{E}_0 and \mathbf{v}_g are often not normal to each other; drift and diffusion can play comparable roles in formation of the voltage current characteristic; charging of the second, passive wire of the double probe can be important in formation of the electric field distribution near the active probe surface; the electron current can

sometimes affect the voltage current characteristic. Neither the probe models known from the literature ([3-7] a.o.), nor our previous studies describe this situation.

All these aspects have been accounted for in our new analytical effort. The complexity of the set of processes accounted for made it impossible to deduce analytical formulae, but the resulting procedure of calculation is simple and fast enough to be applicable for diagnostic purposes.

The further development of the project is bound with diagnostics of flames. Flame plasmas are characterized by comparatively low values of ion density. Then the probe ion current is defined either by processes in the Debye layer, or by the ambipolar diffusion. The Debye layer is nearly one-dimensional. For description of such modes of plasma-probe interaction, the quasi-neutral approximation is invalid in the Debye layer, and it is necessary to solve the Poisson equation. Such computations have been carried out in a one- dimensional approximation. The studies of probe modes in flame plasma flows are to be continued in the next stage of the project.

§ 1. Background of a Detailed Description of Probe-Plasma Interaction

An interpretation of probe voltage-current characteristics in terms of plasma parameters is based on consideration of transport of charged particles in the vicinity of the sounding probe surface, see, e.g., References [3-7]. The consideration in the case of discharge plasma flows characteristic for plasma aerodynamic applications should be based on the following equations [1,2,8,9].

The Navier-Stokes equations for neutral components dynamics:

$$\partial\rho_g/\partial t + \text{div}(\rho_g\mathbf{v}_g) = 0, \quad \rho_g d\mathbf{v}_g/dt = -\mathbf{grad}p_g + q + \mathbf{F}, \quad (1.1)$$

$$n_g dE_g/dt = -p_g \text{div} \mathbf{v}_g + Q + W,$$

(here n_g , ρ_g , p_g , \mathbf{v}_g , E_g are the gas concentration, density, pressure, velocity and internal energy of translations and rotations, q and Q are the viscous terms, the terms \mathbf{F} and W account for forces and energy flows from the plasma, $\rho_g = m_{\text{mol}}n_g$, m_{mol} is a molecule mass, k_B is the Boltzmann constant. In our case the force \mathbf{F} is negligible [1], as well as the effect of W for the characteristic size of the probe vicinity (0.1...1 mm). That's why the effect of plasma components on the neutral gas was neglected. In our case the Reynolds number is not very high ($\text{Re} = 1...300$), i.e. a laminar gas flow takes place.

In our previous works [1,2] it had been shown that the electron temperature T_e in the region of enhanced electric field near the probe surface can be considerably higher than in the ambient plasma. The current study deals with lower electric field values; that is why temperature of electrons here has been supposed to be a constant.

Balance of positive ions:

$$\partial n_i / \partial t + \text{div}(n_i \mathbf{v}_i) = K_I(T_e) - K_R(T_e). \quad (1.2)$$

Here \mathbf{v}_i is the positive ions velocity, K_I , K_R are the rates of ionization and (dissociative) recombination (see, e.g., [9]). The effect of reactions can take place in the region of enhanced T_e near the probe [1,2]. As the electron temperature was a constant, in the current study this effect was neglected ($K_I - K_R = 0$). The velocity of ions [10]

$$\mathbf{v}_i = \mathbf{v}_g - 1/n_i D_a \nabla n_i + \mu_i \mathbf{E} - D_i \nabla \ln T_g - D_i T_e / T_g \nabla \ln T_e, \quad D_a = D_i (1 + T_e / T_g) \quad (1.3)$$

$$\mu_i = e / (m_{mol} \nu_{im}), \quad D_i = k_B T_g / (\nu_{im} m_{mol}),$$

here μ_i is the ion mobility, ν_{im} is the cross section of elastic ion-molecule collisions, D_a is the ambipolar diffusion coefficient. This expression accounts for the ion-gas friction, the drift in the external electric field, the ambipolar diffusion and (approximately) the thermal diffusion.

As the characteristic temperature and positive ions concentration in discharge plasmas are relatively high, the effect of negative ions on the probe voltage-current characteristics is comparatively weak [1,2]; in the current studies it was neglected. For plasma regions, the quasi neutral approximation was applied instead of the Poisson equation:

$$|n_e - n_i| / n_i \ll 1, \text{ or } n_e = n_i \quad (1.4)$$

(n_e , n_i are concentrations of electrons and ions). The applicability of this approximation for discharge plasmas is considered below.

For the electromagnetic field in the plasma region, quasi steady ($\partial/\partial t \approx 0$) Maxwell equations (except the Poisson equation) at low values of the magnetic Reynolds number $\text{Re}_m \ll 1$ were applied:

$$\text{rot } \mathbf{E} = 0, \quad \mathbf{j} = \sigma \mathbf{E}, \quad \text{rot } \mathbf{B} = \mu_0 \mathbf{j}, \quad \text{div } \mathbf{B} = 0 \quad (1.5)$$

in a case ($\partial/\partial t \approx 0$), ($\sigma = e n_e \mu_e$ is the conductivity, $\mu_e = e / (m_e \nu_e)$ is the electron mobility in the electric field \mathbf{E} , \mathbf{B} is the magnetic field induction, \mathbf{j} is the density of current, $\mu_0 = 4\pi 10^{-7}$ H/m, e and m_e are the electron charge and mass, ν_e is the frequency of electron collisions). The last three

equations (1.5) with account to the expression of \mathbf{E} via the gradient of the electric potential φ and to the identity $\text{div rot } \mathbf{G} \equiv 0$ valid for any vector \mathbf{G} , yield

$$\text{div} (n_e \mu_e \mathbf{grad} \varphi) = 0. \quad (1.6)$$

This equation can be used for calculation of \mathbf{E} and φ in quasi-neutral plasma regions. However, it is invalid in the Debye double layer near the probe surface, where the medium is not quasi neutral.

As the active surface of a double probe is negatively charged relatively the plasma medium [1,2], in this layer $n_e \ll n_i$. The ions are accelerated to the probe surface in this layer, they pass through the double layer without a considerable resistance, and practically all the ions that enter the Debye layer will reach the surface. Electrons are repulsed from the negatively charged surface; only a high-energy fraction of electron distribution can overcome the potential barrier and take part in formation of the total probe current.

The total probe current is calculated by integration:

$$I_i = L'R \int [j_i(\psi) - j_e(\psi)] d\psi. \quad (1.7)$$

Here $j_i(\psi)$, $j_e(\psi)$ are the ion and electron components of the local probe current density, L' is the length of the probe that is in a contact with the plasma.

§ 2. Electric Field Distribution around the Double Probe. Effect of the Second Wire

Consider the electric field distribution in the plasma volume around the double probe (two cylinders with axes in a direction \mathbf{z} , $\mathbf{z} \perp \mathbf{E}_0$, $\mathbf{z} \perp \mathbf{v}_g$). The probe charge produces a electric field around its surface, this provides the probe current. The external (discharge) electric field \mathbf{E}_d must be also taken into account, as it can be much higher than the probe field, especially due to the well-known effect of field concentration by conductors.

One more aspect is bound with the fact that in the current experiments there are two parallel cylindrical probes with rather a small separation δ_{12} , and their plane is inclined relatively the discharge electric field \mathbf{E}_d for an angle $\beta_2 \approx \pi/4$. The charge of probe 1 can induce a considerable electric field \mathbf{E}_{12} in the position of another probe 2, and vice versa. Note that the resulting external electric field for the probe 2, $\mathbf{E}_d + \mathbf{E}_{12}$, is not equal to the electric field for the probe 1, $\mathbf{E}_d + \mathbf{E}_{21}$, primarily due to the difference of the angles between the field vectors (β_2 and $\pi - \beta_2$). This may result in different slopes of the voltage-current characteristics for positive and negative voltages U : the probe that is collecting primarily ions at $U > 0$ is in higher field \mathbf{E}_0 , and the ion drift current is relatively stronger at $U > 0$ than that at $U < 0$. Note that the angle $\Psi_{\mathbf{E}_0}$ between \mathbf{E}_0 and \mathbf{v}_g differs

from the angle between \mathbf{E}_d and \mathbf{v}_g , Ψ_{E_V} depends on U , as well as on β_2 , R , δ_{12} , E_d and other parameters.

These probes also have as a rule different potentials, for they are positioned in places with different values of the plasma potential. The difference in local plasma potential values is $E_d \delta_{12} \sin \beta_2$. This shifts the double probe zero current point from the $U = 0$ position.

The summary (probe and external) field (with no account to plasma effects) for a sufficiently long ($L/R \gg 1$) cylindrical probe with its axis normal to the ambient external electric field \mathbf{E}_0 in a medium with even conductance distribution can be approximated as [6]

$$\mathbf{E} = \mathbf{E}_0 \left(1 - \frac{R^2}{r^2}\right) + \mathbf{r}^0 2 \left(\frac{R^2}{r^2}\right) (\mathbf{E}_0 \mathbf{r}^0) + \mathbf{r}^0 V_p / (r \ln(L/R)), \quad (2.1)$$

here \mathbf{r}^0 is the unit radial vector, V_p is the probe voltage. The field component normal to the surface $E_n = (\mathbf{E}_0 \mathbf{r}^0)$ in the boundary $r = r_a$ between the diffusion and drift layers is

$$E_n = E_0 \cos \psi \left(1 + \frac{R^2}{(R+r_a)^2}\right) + V_p / ((R+r_a) \ln(L/R)), \quad (2.2)$$

here ψ is the probe surface azimuth angle coordinate (the same probe surface azimuth angle as in [1]), ψ is bound with the external electric field. If one neglects r_a in comparison with R , then

$$E_n \approx 2 E_0 \cos \psi + V_p / (R \ln(L/R)). \quad (2.3)$$

For the double probe the sum of the values of current to the probes equals to zero. One of the probes (say, probe 1) absorbs primarily ions, while the other one (probe 2) absorbs primarily electrons. The fact that $\mu_i / \mu_e \ll 1$ yields that both probes are necessarily charged so that the retarding potential would prevent electrons to flow to the surface, for the ion current on the probe 1 cannot be as high as the electron current on a zero potential surface of the probe 2. In the zero point of the voltage current characteristic, to keep zero total probe current, each probe must have a negative bias relatively the local plasma medium potential:

$$V_p^0 = 2 E_0 (R \ln(L/R)) + \Delta V, \quad (2.4)$$

here the first term is bound with the external field, the second term results from the fact that fast particles of the electron distribution function can overcome potential barriers. This term is bound with the Debye layer, where the corresponding electric field is concentrated, i.e. it is not taken into account at consideration of the plasma regions. If the distribution function is close to the

Maxwellian one, it is in a direct proportion to the electron temperature. The actual value of V_p^0 must be determined by integration of the currents over the entire probe surface.

A probe potential in other points of the voltage current characteristic can be expressed as $V_p = V_p^0 + \Delta V_p$. The normal field on the interface with the diffusion layer in accord with (2.3), (2.4) is

$$E_n \approx 2 E_0 \cos \psi + 2 E_0 + \Delta V_p / (R \ln(L/R)), \quad (2.5)$$

i.e. the field near the probe is defined by the external field, if $E_0 \gg E_0^* = \Delta V_p / (2R \ln(L/R))$, and by the difference of potentials between the two probes, if $E_0 \ll E_0^*$.

§ 3. Plasma Parameters Distributions and Ion Probe Current in Drift, Diffusion and Intermediate Modes

A double probe voltage-current characteristic is formed primarily by the ion current. The latter can be limited either by the processes of ion drift in the drift area (or the “non-viscous flow region”, where $|\mu_i \mathbf{E}_0| \gg |\mathbf{grad}(D_a n_i)|$), or by finite efficiency of the ambipolar diffusion in the diffusion layer (or the “viscous boundary layer”, where $|\mathbf{grad}(D_a n_i)| > |\mu_i \mathbf{E}_0|$), or by the ion-ion repulsion in the Debye sheath, where $n_i \gg n_e$. The least effective process defines the mode of probe operation.

Consider the case when the ions pass through the double layer without a considerable resistance. Such a situation is characteristic for the major part of the plasma parameters, especially for the cases of sufficiently high characteristic gas density, which are characteristic for realistic full-scale systems of plasma aerodynamics [1]. Then the double layer can be excluded from our speculations concerning the ion current.

Parts of the probe surface are under different conditions due to the distribution of the plasma parameters and the local normal electric field E_n . For some of the current tubes the ion current can be limited by the ion drift (drift mode), but for other current tubes the situation may be opposite (diffusion mode). The relative yield of the modes depends on external conditions and the probe bias voltage U .

Consider a current tube with drift, diffusion or intermediate mode. Its effective voltage for a cylindrical probe is bound with the local electric field as [6] $\Delta \phi_1 \approx E_n (R \ln(L/R))$, here R and L are the probe radius and length. The diffusion and drift layers can be represented as sequent resisting

parts of a current tube with voltages $\Delta\varphi_a$ and $\Delta\varphi_d$, respectively. The total voltage of a current tube for the ion current i_i can be calculated from the formula

$$\Delta\varphi_i = \Delta\varphi_a + \Delta\varphi_d = (\rho_a + \rho_d)i_i. \quad (3.1)$$

The values of partial resistances of the layers $\rho_a = \Delta\varphi_a/i_a$ and $\rho_d = \Delta\varphi_d/i_d$ can be determined from the values of ion currents i_a and i_d , which are calculated for the current tube from solution of the two partial problems with respect to only diffusion and only drift. Together with the condition of conservation of the ion current through a current tube $i_a = i_d = i_i$ it makes it possible to determine the values of the total ion current i_i , $\Delta\varphi_a$ and $\Delta\varphi_d$ for any current tube.

Consider the drift partial problem. The equations (1.2) and (1.3) with account to (1.5), (1.6), the equations $\mathbf{j} = \sigma\mathbf{E}$, $\sigma = en_e\mu_e$, $\mathbf{rot}\mathbf{B} = \mu_0\mathbf{j}$, $n_i\mu_i/(\mu_e n_e) \ll 1$, the mathematical identity $\mathbf{div}(\mathbf{rot}\mathbf{G}) \equiv 0$ valid for any vector \mathbf{G} , and in case that $(\mu_i/\mu_e) = \text{const}$, yield that the value $x = n_i/n_g$ is a constant, and on the interface of the drift and diffusion regions this value is equal to the unperturbed one in the ambient flow x_∞ . It makes it possible to determine the ion current density in the drift region: actually, neglecting variations of $T_g^{1/2}$, one can get the ion drift current density as [1]

$$\begin{aligned} j_{id}(\psi) &= en_i(\psi)\mu_i(\psi)E_n(\psi) = e^2 E_n(\psi) n_i(\psi) / [n_g m_{mol} \Sigma_{im} (2 k_B T_g / m_{mol})^{1/2}] = \\ &= e^2 x_i E_n(\psi) / [m_{mol} \Sigma_{im} (2 k_B T_g / m_{mol})^{1/2}] = en_{i\infty} \mu_{i\infty} E_n(\psi), \end{aligned} \quad (3.2)$$

here $n_{i\infty}$ and $\mu_{i\infty}$ are the unperturbed values of ion density and mobility in the ambient flow. The corresponding drift layer partial local resistance of a current tube with the cross section area A (near the boundary of the drift and diffusion layers)

$$\rho_a(\psi) = \Delta\varphi_i(\psi) / [j_{id}(\psi) \delta A]. \quad (3.3)$$

Consider now the partial problem with respect to the potential fall in the diffusion layer only. The diffusion characteristic length r_a for a temporary evolution of an initially stepwise profile of concentration is

$$r_a = (tD_a)^{1/2}, \quad (3.4)$$

here the time coordinate t can be expressed via the length l of a path of an element of plasma along the probe surface as

$$t = \int (1/v_g) dl \approx l/v_g, \quad l \approx R\psi_1, \quad (3.5)$$

here ψ_1 is the azimuth coordinate bound with the gas flow, $\psi_1 = \psi - \Psi_{E_v}$, Ψ_{E_v} is the angle between the vectors of the external (ambient) electric field and the unperturbed plasma flow velocity.

Assume a linear radial plasma density profile across the diffusion layer and a constant $x=x_\infty$ in the drift area; then the ion flux across the diffusion layer is

$$\Gamma(\psi) = -D_a(\psi) \nabla n_i(\psi) \approx D_{a\infty} n_{i\infty} / r_a(\psi). \quad (3.6)$$

Here $D_{a\infty}$ is the ambipolar diffusion coefficient in the ambient flow (we neglect variations of T_e). The corresponding ion current density and the diffusion layer partial local resistance are

$$j_{ia}(\psi) = e\Gamma(\psi), \quad \rho_a(\psi) = \Delta\phi_i(\psi) / [\delta A j_{ia}(\psi)]. \quad (3.7)$$

These formulae yield infinite j_{ia} at $\psi_1 = 0$. To eliminate it, a small but finite constant value of r_{a0} was added to the denominator in (3.6); it can be determined from a 2D solution of the diffusion problem for a flow over a cylinder, but calculations have shown that the resulting total ion current is practically independent on considerable variations of r_{a0} . Actually, if the partial resistance $\rho_a(\psi)$ is low, it can be neglected. That is why the additive to the denominator must be applied rather to provide non-stop calculations.

The value of j_{ia} is independent of $\Delta\phi_i$, and the higher is $\Delta\phi_i$, the higher is the effective resistance ρ_a corresponding to the constant j_{ia} . One can see that the diffusion mode can prevail at high $\Delta\phi_i$, i.e. when the drift processes are effective.

Together with the mentioned above, it makes it possible to calculate $j_i(\psi)$ for any current tube with account of the both drift and diffusion mechanisms.

§ 4. Account to the Electron Current Leakage

The electron distribution function contains a tail of high-energy electrons, which can overcome retarding potential barriers and enter the surface of the probe, which collects primarily ions. As the mobility of electrons is much higher than that of ions, the electron current leakage can affect the total probe current at low U .

Consider first the situation with the probe zero voltage $U = 0$. If the two probes are under the same conditions, then the total current $I = 0$, i.e. the electron and ion currents are equal to each other for both probes. The ion current flows through practically all the surface. The electron current leaks practically only into a portion of the probe surface, where the local retarding electric field is low. The electrons must overcome the local potential barrier $\Delta\phi_e(0)$ corresponding to the retarding

electric field. In case of the Boltzmann distribution function, it yields the exponential factor to the local values of the electron current:

$$j_e(T_e, U=0) = \exp[-\Delta\phi_e(U=0)/(k_B T_e)] j_e^+, \quad (4.1)$$

here j_e^+ is the local one-side electron current through a surface A near the probe, which potential relatively the probe surface is $\Delta\phi_e$. Consider A to be the boundary between the drift and diffusion regions, then one can estimate j_e^+ from the kinetic formula

$$j_e^+ = en_e v_e / 4, \quad (4.2)$$

here n_e is the local electron density, v_e is the mean thermal electron speed. The value $\Delta\phi_e$ can be calculated as a sum of the voltage of the diffusion layer $\Delta\phi_a$ and the voltage of the double layer near the surface $\Delta\phi_p$, which results from extra negative charging of the probe relatively the case of $T_e = 0$. The value of $\Delta\phi_e(U=0)$ can be calculated from the condition of zero total (ion and electron) current through the whole probe surface. Note that at $U=0$ the probes are under a considerable negative potential.

Now consider the case of the probe, which collects primarily ions at $U \neq 0$. The retarding potential barrier $\Delta\phi_e(U)$ grows for a value, which is less or equal to U . However, at low enough values of voltage U in the major part of the probe surface the relative changes of $\Delta\phi_d$ are not considerable due to the effect of preliminary charging of the probe in the external electric field. This makes it possible to assume that the ion current and the corresponding voltage drops do not depend on variations of U at low values of the external voltage $|U|$. Thus, to a first approximation, the total negative retarding potential

$$\Delta\phi_e(U) = \Delta\phi_a + \Delta\phi_p(U=0) + |U|. \quad (4.3)$$

At higher $|U|$ the errors bound with this approximation may grow, but then as a rule the electron current becomes negligible, and these errors do not affect the summary voltage-current characteristic considerably.

It makes it possible to calculate the voltage-current characteristic with respect to the electron current leakage at low values of $|U|$. This makes the growth of the total probe current not so quick at $|U| <$

$k_B T_e$ and $|U| \approx k_B T_e$. At higher $|U|$, the voltage-current characteristic approaches that calculated without the account for the electron current.

Thus, in accord with (4.1), (4.3), the electron current falls exponentially, as the probe voltage bias $|U|$ grows. This exponential fall of the probe electron current with $|U|$ can be seen in the results of our detailed 1D computations of the Debye and diffusion layers (see below).

Of course, it could be possible to neglect the region of a considerable effect of the electron current and to determine plasma parameters from the parts of a voltage-current characteristic with totally ion current (at high $|U|$), but the theoretical curve would be then somewhat dislike the corresponding experimental voltage-current characteristic, especially near the point of origin of the coordinates.

§ 5. Probe Voltage Current Characteristics

The resulting probe total (ion and electron) current I was calculated for a given probe bias voltage U with use of the above mentioned explicit analytical formulae by a direct calculation of the integral () over the probe surface (or over the azimuth angle ψ) with iterating of $\Delta\phi_p$ to meet the condition of the necessary suppression of the electron current. The computation time is negligible. Some results are shown in Fig.1–3.

The theoretical and experimental voltage current characteristics correlate at reasonable values of plasma parameters (Fig.1–3). They have regions of steeper (at lower $|U|$) and slower growth (at higher $|U|$), which, in accord with the model, correspond to the modes with ion plus electron and with only ion currents. They are all asymmetric: $\partial I/\partial U$ and maximal I are higher for $U > 0$ than for $U < 0$ (apparently, due to the difference in values of the external electric field E_0). The zero current point is as a rule shifted from the $U=0$ point (because of the difference in positions of the two probes). The electron component is considerable near the origin; the diffusion mode is important at higher voltages $|U|$; the drift mode plays an important role in the rest parts of the voltage-current characteristics.

The diagnostic problem solution on base of the newly developed model suggests best fitting of experimental and theoretical results by varying of unknown or poorly known plasma parameters, such as $T_e, T_g, n_{i\infty}$.

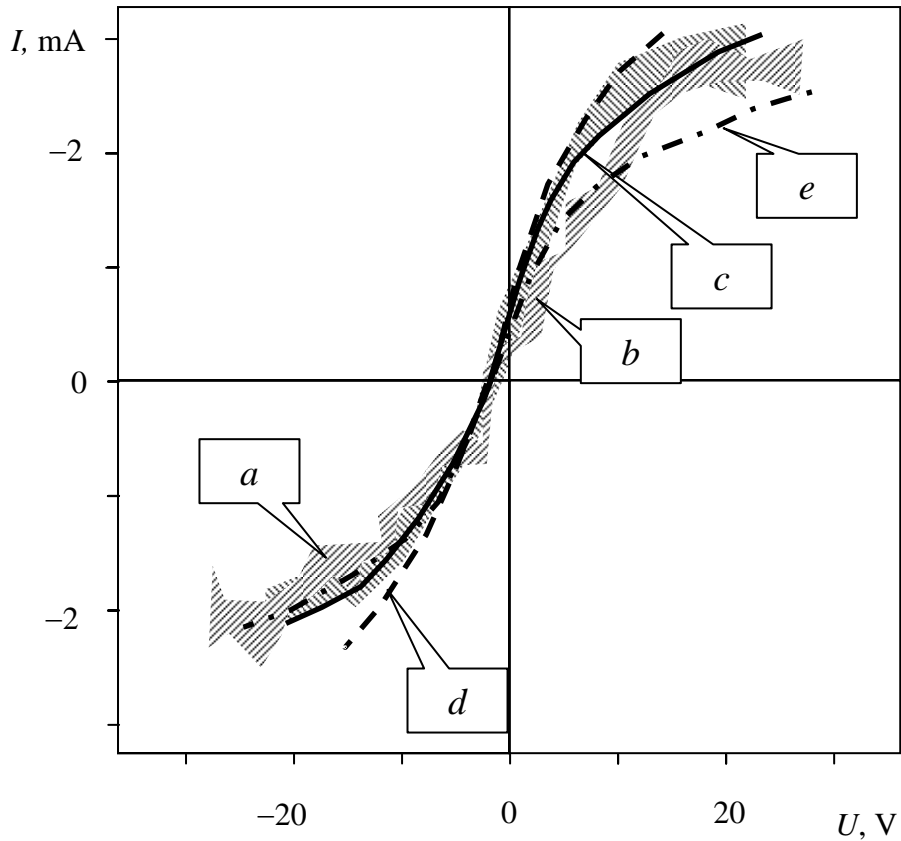


Fig. 1. Probe voltage-current characteristics for the transversal discharge at electric current 5 A, chamber gas pressure 100 Torr, gas speed 600 m/s, discharge electric field 43 V/cm, probe diameter 0.3 mm, probe-plasma contact length 2.3 mm, separation between the probes 2 mm, double probe plane – discharge electric field angle 45° , gas speed – discharge electric field angle 0° (the anode jet)

a, b – regions of scattering of experimental points at two sequent measurements, *c, d, e* – theoretical curves at ion density $1.2 \cdot 10^{14} \text{ cm}^{-3}$, with gas temperature 2000 K (*c,e*) and 3000 K (*d*), electron temperature 2 eV (*c,d*) and 1 eV (*e*)

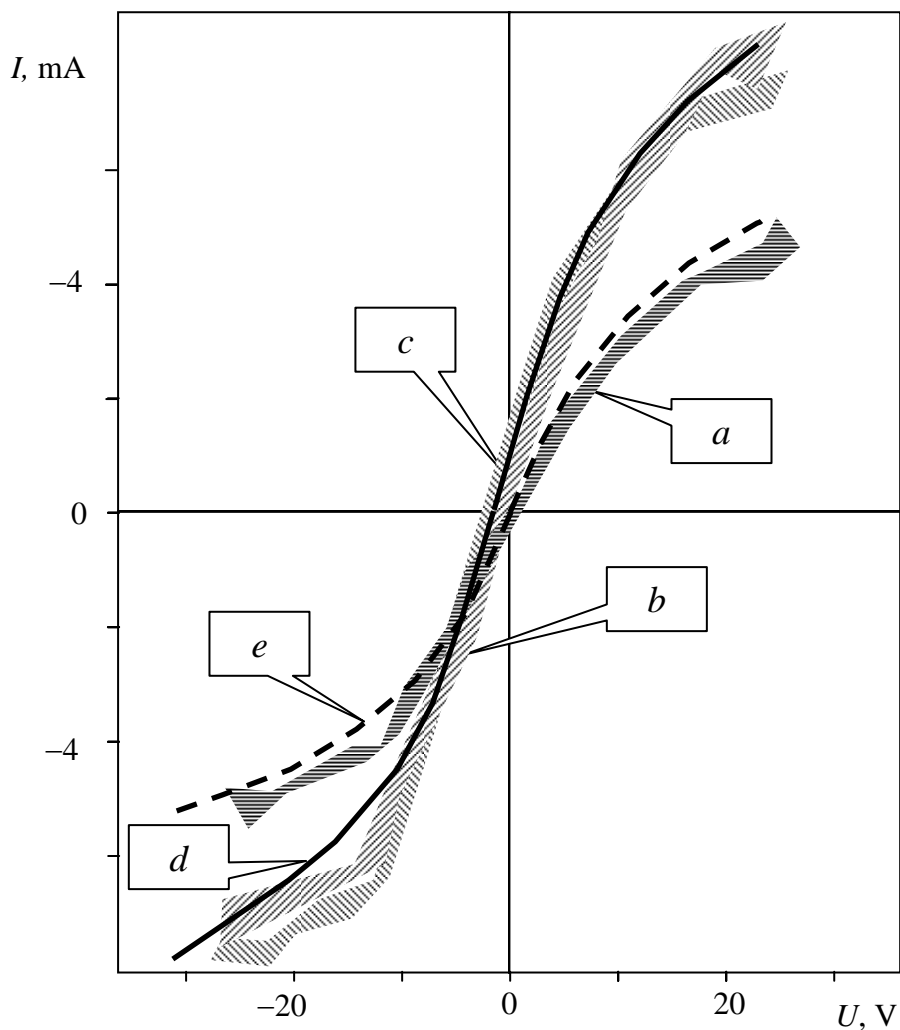


Fig. 2. Probe voltage-current characteristics for the transversal discharge at electric current 11 A, chamber gas pressure 100 Torr, gas speed 600 m/s, discharge electric field 23 V/cm, probe diameter 0.3 mm, probe-plasma contact length 2.8 mm, separation between the probes 2 mm, double probe plane – discharge electric field angle 45° , gas speed – discharge electric field angle 0° (the anode jet).

a, *b*, *c* – regions of scattering of experimental points at sequent measurements, *d*, *e* – theoretical curves at ion density $2.9 \cdot 10^{14} \text{ cm}^{-3}$, and $1.8 \cdot 10^{14} \text{ cm}^{-3}$, respectively.

Gas temperature 2000 K, electron temperature 2 eV

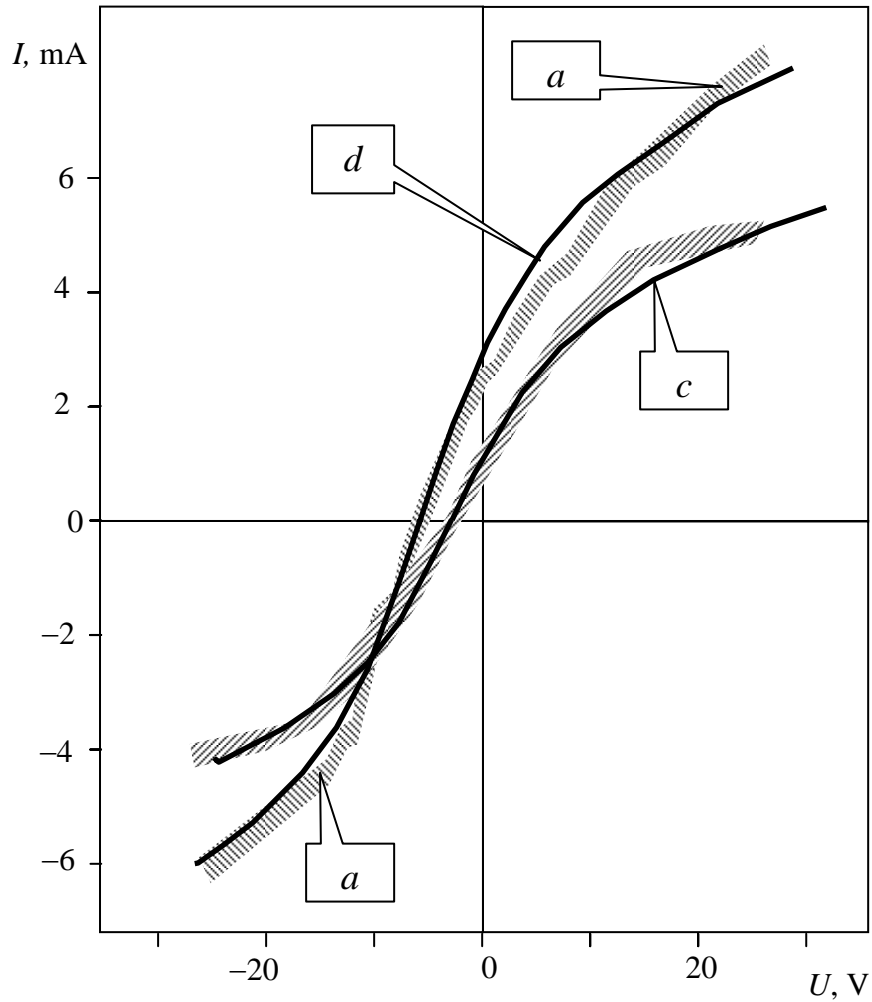


Fig. 3. Probe voltage-current characteristics for the transversal discharge at electric current 16 A, chamber gas pressure 100 Torr, gas speed 600 m/s, discharge electric field 17 V/cm, probe diameter 0.3 mm, probe-plasma contact length 3 mm, separation between the probes 2 mm, double probe plane – discharge electric field angle 45° , gas speed – discharge electric field angle 0° (the anode jet).

a, b – regions of scattering of experimental points at two sequent measurements, *c, d* – theoretical curves at ion density $1.4 \cdot 10^{14} \text{ cm}^{-3}$ and $2.3 \cdot 10^{14} \text{ cm}^{-3}$, respectively, with gas temperature 2000 K, electron temperature 2 eV

§ 6. Difference in Diagnostics of Pure Air and Air-Hydrocarbons Mixture

For the conditions characteristic for the plasma aerodynamic experiments, the theoretical methods for probe diagnostics have been previously developed. For a broad region of plasma flow parameters, in which the ion drift in the electric field is important, the analytical formulae have been deduced. Another regime (characterized by a great role of ion diffusion) has been studied numerically. These studies dealt with air plasma. Consider the plasma of air-fuel mixtures.

The stoichiometric amount of fuel in air-fuel mixtures is comparatively small (few percents). E.g., complete oxidation of 2 molecules of octane C_8H_{18} wants 25 molecules of oxygen, that in air corresponds to 125 molecules of nitrogen, i.e. the stoichiometric molecular composition of the octane-air mixture is 1.3% of octane and the rest 98.7% of air. It means that the effect of fuel presence on plasma properties with additive yields of components with comparable weight factors is negligible. E.g., the thermodynamic functions $p_g = p_g(\rho_g, T_g)$ and $\varepsilon_g = \varepsilon_g(\rho_g, T_g)$ and plasma viscosity $\eta_g = \eta_g(\rho_g, T_g)$ are practically unaffected, provided the values of ρ_g and T_g are specified (don't forget that a diagnostic problem is considered). The same can be deduced for electron mobility and plasma conductivity for a given electron density.

The presence of fuel, however, can make a considerable difference in cases where yields of minor components can be exponentially high. The balance of positive ions in weakly ionized plasma, e.g., depends on components with the lowest ionization potential. Some hydrocarbons have ionization potentials that are considerably lower than that of O_2 and N_2 . It means that the ionization rate and the positive ions characteristic composition in air-fuel mixtures will be different than in air plasmas under the same conditions.

One of important issues of probe diagnostics of hydrocarbon plasmas is reported to be deposition of polymeric films on probes surfaces [11]. The dielectric film insulates the surface and lowers the probe current. Polymerization and film deposition is well known for non-equilibrium plasmas of air-hydrocarbons mixtures. For preventing of such phenomena, probe heating to temperatures exceeding 800 K can be applied [11].

An ion has practically the same scattering targets in the air-fuel host gas as that in the air. However, hydrocarbons generally have lower ionization potentials than O_2 and N_2 . It causes dramatic changes in positive ions composition. It can be important for probe diagnostics.

The ion composition in a non-equilibrium plasma depends greatly on actual conditions and initial fuel sort, as well as on the process history. But it is likely that the general trend is to form positive ions with 2...4 carbon atoms. E.g., at discharges in both light methane CH_4 (16 a.u.m.) and several times as heavy n-octane C_8H_{18} (114 a.u.m.) major ions have medium weights (30...60 a.u.m.) [12],

[13]. Negative ions in hydrocarbon plasmas are light (primarily H⁻), they have much higher mobility than negative ions in air, but the probe current is practically unaffected by the negative ions movement however.

The previously developed (for air plasma) probe diagnostic method is based on measurement of an ion current, which is determined by mobility and diffusion of positive ions. The coefficients of mobility and diffusion are bound by the Einstein relation, so one can consider only one of them.

The mobility K_i of ions (mass M_i) in a host gas of different molecules (mass M_m) at moderate characteristic values of electric field (E/N_g less than 100 Td) is determined at a given temperature T by the reduced mass $\mu = M_i M_m / (M_i + M_m)$ [14],

$$K_i = 3\pi^{1/2} e / [8N_g \Sigma_{im}^*(\mu, T) (2k_B T \mu)^{1/2}],$$

$$\Sigma_{im}^*(\mu, T) = 0.5 \int_0^\infty \Sigma_{im}(x) \exp(-x^2) x^2 dx, \quad x = \mu g^2 / (2k_B T),$$

here g is the relative ion-molecule speed, k_B is the Boltzmann constant.

For O₂⁺ ions in the air, the resonance charge exchange at collisions with O₂ molecules is important, it lowers their mobility. Note that the hydrocarbon positive ions have practically no chances to meet the corresponding molecules, and the resonant charge exchange is not effective in the hydrocarbon plasmas. These ions collide with host gas molecules of other structure (N₂, O₂...). For gas molecules, which are not dipoles (that is the case for the air-fuel plasma), Σ_{ia} is determined primarily by polarization α_m of the neutral molecule in the ion electric field,

$$\Sigma_{ia} \approx 2\pi(\alpha_m / E_i)^{1/2},$$

E_i is the mean ion energy, which is close to the gas thermal energy. One can see that for this approximation (which has an accuracy of about 20%) the sort of ions i affects K_i only via square root of the reduced mass μ . The corresponding mobility of ions in a gas of different molecules is practically independent of gas temperature and ion distribution function, with an accuracy of $\approx 20\%$ an ion mobility at a gas with the density corresponding to the atmospheric pressure can be estimated as [14] $K_i \approx 36 (\alpha_m \mu)^{-1/2}$, here K_i is in cm²V⁻¹s⁻¹. The corresponding dependence on ion mass is rather weak for heavier ions: e.g., even for $M_i = 5M_m$, K_i is only 1.3 times as less as that for $M_i = M_m$. Light ions have much higher mobility (e.g., $M_i / M_m = 1/28$ for H⁺ in air corresponds to K_i being 3.8 times as high as K_i for $M_i = M_m$).

Thus, one of the major differences of probe voltage-current characteristics in air-fuel mixtures is bound with different scattering cross sections and with different masses of positive ions. The probe diagnostic signals depend on the sorts of abundant ions in plasma.

Heavier ions have poor mobility and give a little contribution in the total ion transport, lighter ions contribute much more. The positive ions that are possible to have the highest population in hydrocarbon non-equilibrium plasmas with different fuels and histories have ion masses, which are not very far from each other and from that of the air plasmas. It is important that a sufficiently low percentage of light hydrogen positive ions with high mobility is usually formed in hydrocarbon-air plasmas (H has a comparatively high ionization potential).

The reduced mobility $K_{i0} = K_i N_g / N_{g0}$ in nitrogen for $C_6H_7^+$ is $2.47 \text{ cm}^2/(\text{V}\cdot\text{s})$ (here $N_{g0} = 2.69 \cdot 10^{-19} \text{ cm}^{-3}$) [15]. The $\mu^{-1/2}$ dependence yields $K_{i0} \approx 3.45 \text{ cm}^2/(\text{V}\cdot\text{s})$ for, say, CH_5^+ . For the experimental conditions of [13] at $E/N_g \approx 100 \text{ Td}$ (heavier hydrocarbon ions in methane) the reduced mobility was $2.8 \text{ cm}^2/(\text{V}\cdot\text{s})$. Thus, the reduced mobility of the most abundant hydrocarbon ions is likely to be about $3 \text{ cm}^2/(\text{V}\cdot\text{s})$.

The value of ion mobility $\mu_{i\infty}$ affects both the processes of ion drift and ambipolar diffusion ($D_{a\infty}$ is proportional to $\mu_{i\infty}$). However, the ion drift current density is in a direct proportion to the mobility $\mu_{i\infty}$ (in accord with (3.2)), while the diffusion ion flow is proportional to $D_{a\infty}^{1/2}$ (see (3.4),(3.6)). It means that the total probe current dependence on $\mu_{i\infty}$ is nonlinear, and it is weaker than a direct proportion.

It altogether means that the ion transport characteristics are likely to be not very sensitive to an actual ion composition for characteristic air-fuel mixtures, and the corresponding errors are tolerable. However, the fact that ion mobility in an air-fuel mixture can be several (≈ 4) times higher than in pure air must be accounted for. The accuracy might be enhanced by experimental and/or theoretical studies of positive ions in actual plasmas.

Ionization rates may depend on presence of comparatively small fractions of molecules with low ionization potentials I_i . In the pure comparatively hot air those can be NO molecules ($I_i = 9.24 \text{ eV}$), in hydrocarbons – e.g., CH_3 ($I_i = 9.84 \text{ eV}$). The differences in ionization rates are not very dramatic (say, for air and methane the difference is within 5 times for $E/n_g > 100 \text{ Td}$, higher values for methane, as it follows from the approximation data cited, e.g., in [16]). Thus, the ionization thresholds of applicability of the probe diagnostics for air and air-fuel mixtures must be close to each other. For the first approximation of the current diagnostic problem, one can neglect the difference between ionization in the air and in an air-fuel mixture. For higher accuracy, one must specify the gas composition including small fractions, which depend on the process history and parameters.

Thus, the prospects of diagnostics are looking optimistic. Further studies are necessary however.

§ 7. Mathematical Modeling of the Double Probe in the Air-Fuel Plasma

A direct computer simulation of the double probe in the plasma of the air-fuel mixture has been carried out on base of the model similar to that developed in [1] for plasmas of air.

The neutral gas dynamics was simulated on base of (1.1) in the 2D planar approximation with the apparent boundary conditions, which are traditional for computations of flow over a body: zero velocity on the probe surface, ambient plasma flow parameters on the input boundary, and a free exit on the opposite side. The plasma concentration is defined by (1.2), (1.3) with $K_I - K_R = 0$, the electric potential was calculated from (1.6), the electron temperature was assumed to be a constant (1.5 eV). In accord with the above mentioned, the ion mobility was taken 4 times as high as that of the air plasma, and all the other plasma properties were the same as in the case of air plasma [1]. The plasma boundary conditions were analogous to [1]: on the boundary near the probe the mean normal component of the total ion velocity was computed as [1] $v_b = v_{in} + v_{iT}/2 \exp(-2 [v_{in} / v_{iT}]^2)$, here v_{iT} is the arithmetic mean thermal ion velocity, v_{in} is the drift velocity; the ‘probe’ boundary potential in computations φ_0 was taken C_b times less than the probe voltage V_p , $C_b = \ln(L/R) / \ln(R_b/R)$, R_b is the maximal radial coordinate of the mesh (in order to account for the finite size of the computational region). At $r = R_b$, the potential was a zero, and the ion velocity was equal to the gas flow velocity.

This model considers processes in the quasi-neutral part of the vicinity of a cylindrical probe. It pays no account for the Debye double layer. Of course, the model cannot be applied for such regimes of plasma-probe interaction, in which the double layer limits the ion current to the probe. Such regimes are considered below analytically and numerically. Here we consider the opposite case (i.e. for regimes with ion current limitation by ambipolar diffusion and/or ion drift). The Debye double layer potential drop $\Delta\varphi_q$ in such regimes can be considerable however ($\Delta\varphi_q$ can achieve 10 V and more). It means that the total probe-plasma potential drop $\Delta\varphi$ is divided between the Debye double layer $\Delta\varphi_q$ and the plasma region $\Delta\varphi_d$. One could suppose that neglecting of the Debye double layer drop may result in intolerable errors, but the situation is not so bad.

The values of $\Delta\varphi_q$ are high for the regimes, in which the ion current to the probe is limited by diffusion. For these regimes the ion current is independent on the plasma region potential drop, and the uncertainties in this value cannot affect the voltage-current characteristic. Thus, for the diffusion regimes it is possible to neglect the Debye double layer drop.

For the regimes, in which the ion current to the probe is limited by the ion drift, the latter depends on the potential drop in the plasma region, $\Delta\varphi_d = \Delta\varphi - \Delta\varphi_q$. For the double probe with cylindrical wires 1 and 2, the probe bias $U = \Delta\varphi_1 - \Delta\varphi_2 = (\Delta\varphi_{q1} - \Delta\varphi_{q2}) + (\Delta\varphi_{d1} - \Delta\varphi_{d2}) \approx \Delta\varphi_{d1} + (\Delta\varphi_{q1} - \Delta\varphi_{q2})$ (here

the voltage drop in the plasma near the passive probe $\Delta\phi_{d2}$ is neglected). One can see that the uncertainty bound with neglecting of processes in the Debye double layer depends on the difference of the two double layer drops ($\Delta\phi_{q1} - \Delta\phi_{q2}$), which is considerably less than $\Delta\phi_{q1}$. Moreover, the value of is much less for the ion drift regimes than that for the diffusion regimes. Thus, the uncertainty is tolerable, and the model is applicable for the drift regimes too.

The computer simulation of the gas dynamics of flow over the probe was carried out with use of the implicit free-LaGrange method and an irregular triangular mesh bound with the gas [1]. The mesh had a characteristic cell size that quickly decreased at approaching the probe surface; the mesh had about 200 cells along the probe surface, and about 20,000 cells total. The plasma part of the problem was solved with use of a fixed mesh, which had resulted from the solution of the gas dynamical part of the problem, and with the corresponding distributions of gas temperature, density and velocity.

Characteristic results of computations for air and air-fuel plasmas under similar conditions (probe diameter 1 mm, flow velocity 600 m/s, temperatures $T_e = 1.5$ eV, $T_g = 1000$ K, $M = 0.85$, gas and plasma densities $n_g = 10^{24} \text{ m}^{-3}$, $n_e = 10^{19} \text{ m}^{-3}$, probe potential $\phi_0 = 16$ V) are presented in Fig. 4...7. Major difference between the air and air-fuel plasmas is in the ion mobility (Fig.4), because different sorts of ions conduct the probe current in these species. This results in changes in other plasma parameters. Plasma density fall near the probe surface becomes relatively shallow in the air-fuel plasma (Fig.5), for the higher mobility makes it easier for ions to achieve a comparatively even spatial distribution. Electric field concentration near the probe surface becomes weaker (Fig.6): the field relaxes easier.

As it has been shown above, in the case of the ion drift mode, the growth of the ion mobility must result in 4 times higher probe current than that in the air plasma. In the case of the diffusion mode, the probe current is only twice as high. In our case the mode is intermediate between the drift and diffusion modes, i.e. for some current tubes the ion flow is limited primarily by drift, and for others – by diffusion. In accord with the analysis, the computed ion probe current is 2...4 times as high as in the air plasma (Fig. 7).

One can see that the differences in distributions of plasma density, ion mobility, electric field etc. are considerable. It means that the plasma composition should be accounted for at interpretation of probe voltage-current characteristics.

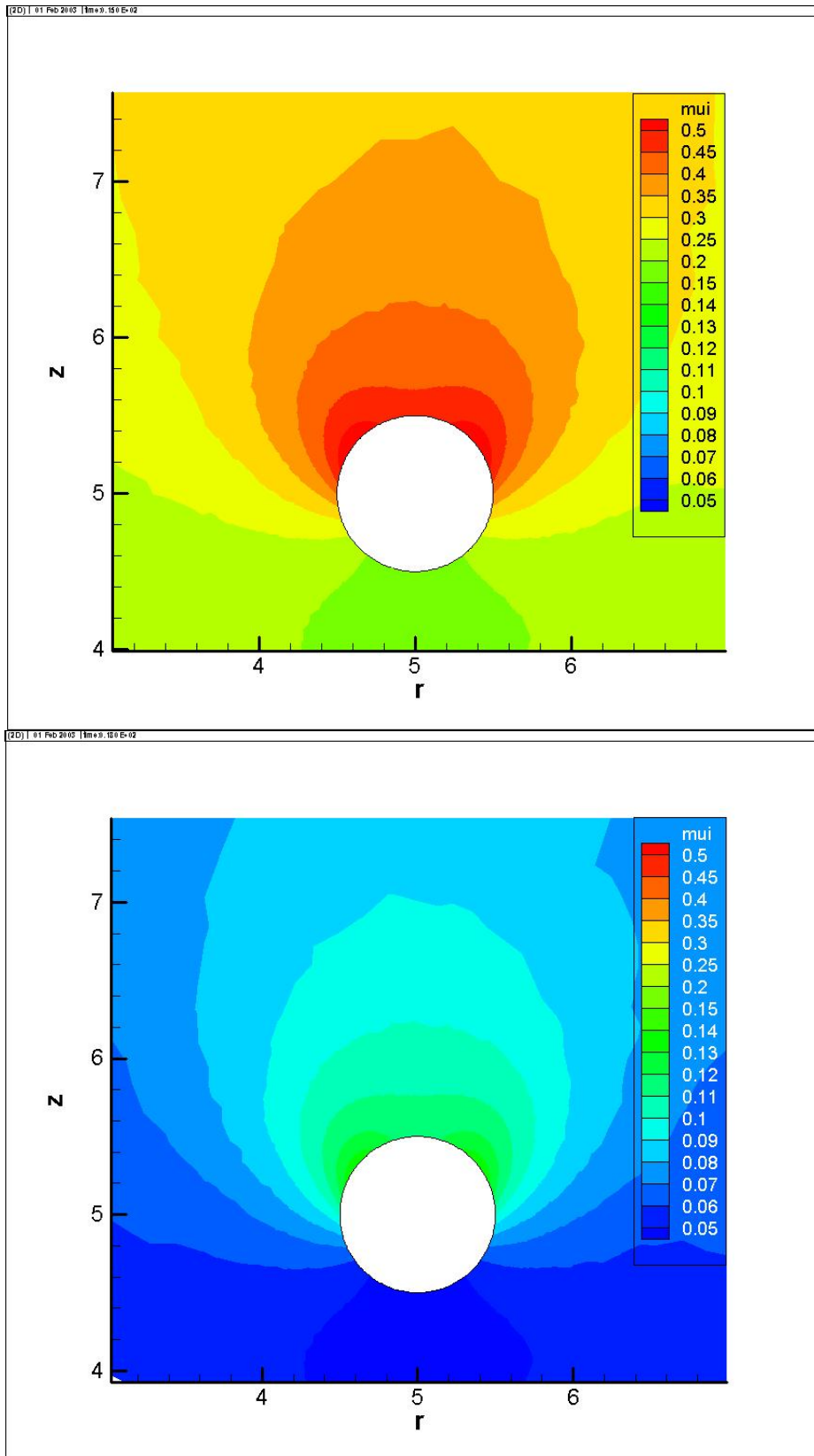


Fig. 4. Plasma ion mobility spatial distributions for air-fuel (a) and air (b) plasmas

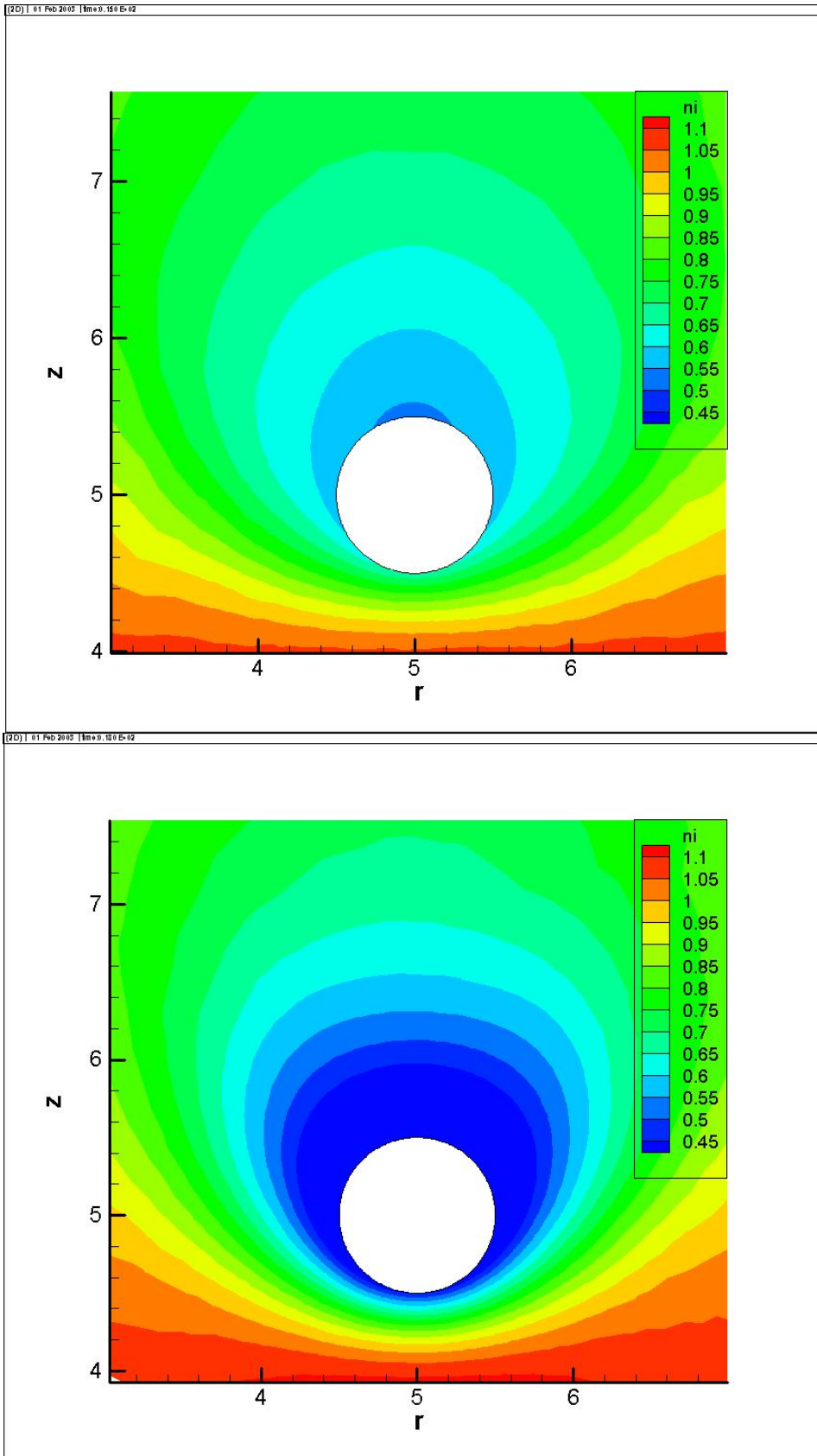


Fig. 5. Plasma density spatial distributions for air-fuel (a) and air (b) plasmas

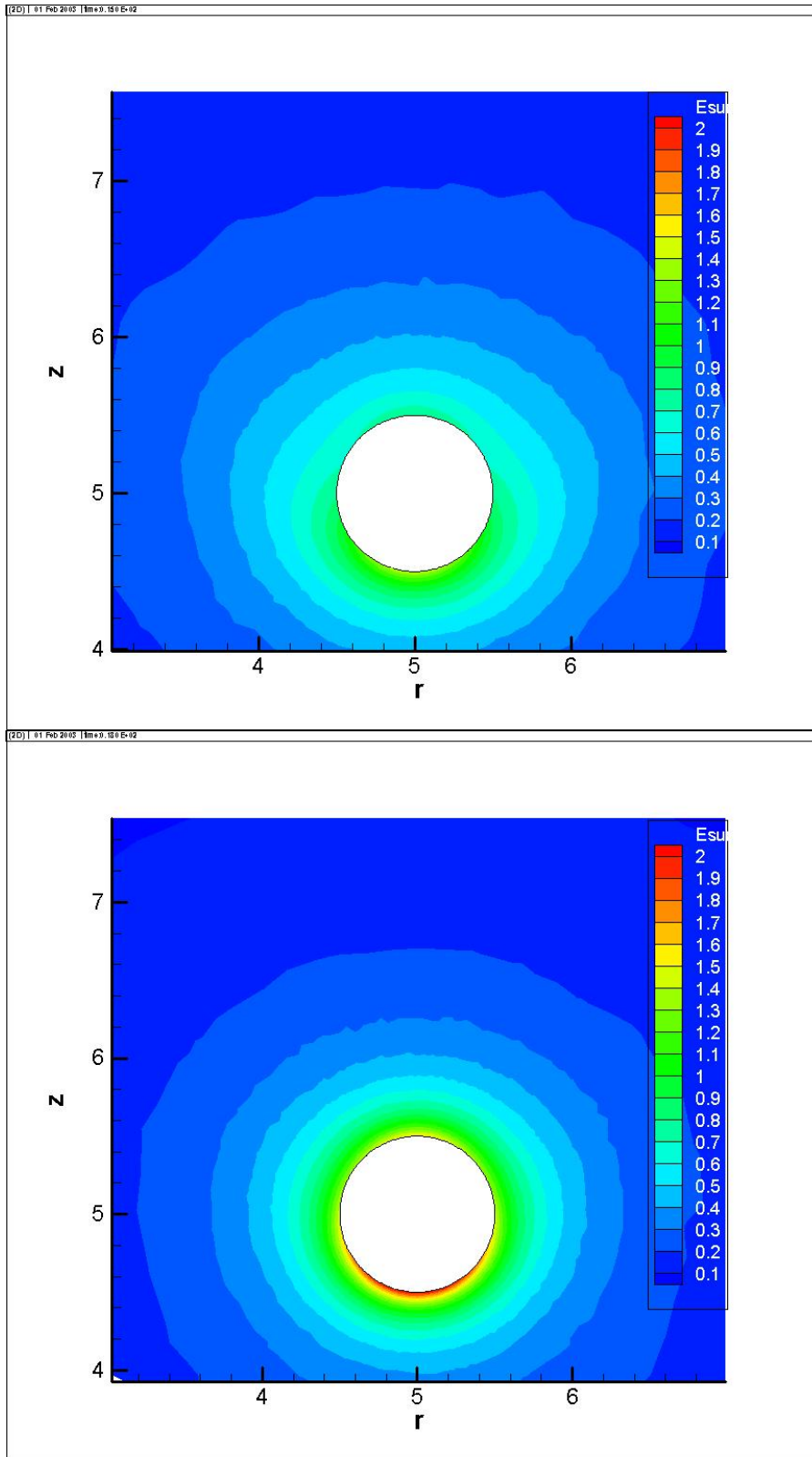


Fig. 6. Electric field modulus spatial distributions for air-fuel (a) and air (b) plasmas (the ambipolar field is excluded)

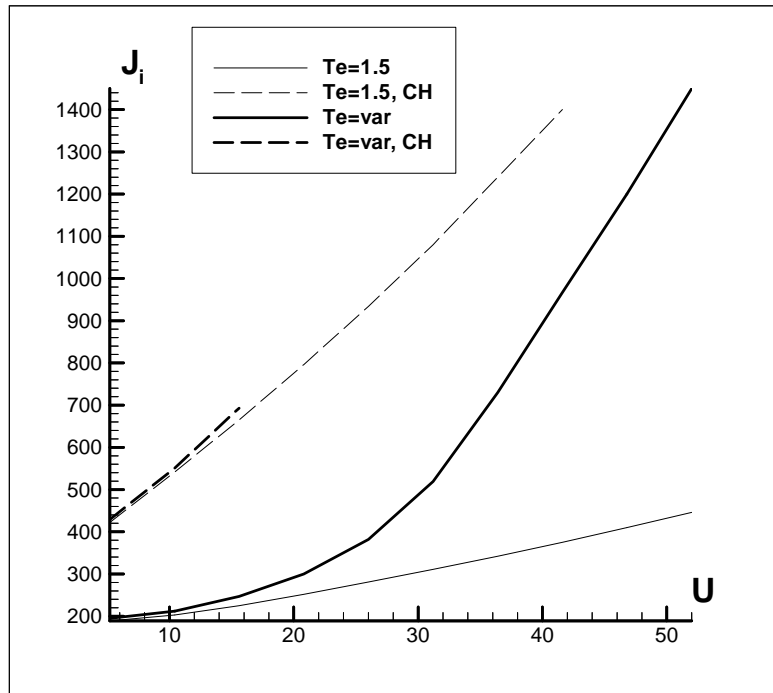


Fig. 7. The probe ion current density over the probe voltage bias for air-fuel (dashed lines) and air (solid lines) plasmas: computations with constant T_e (thin lines) and with direct computation of electron energy (thick lines)

§ 8. Analysis of Interaction of Probes with Flame Plasma High-Speed Flows

In most works concerning high pressure weakly ionized plasma flows [17] negatively biased probes are considered. They collect positive ions, which have comparatively low mobility. At low plasma density the ion probe current is too weak ($\sim \mu\text{A}$), and it is a considerable technical problem to measure this current at characteristic noisy environment. In [18], positively biased probes are considered, which collect much higher electron currents due to higher mobility of electrons. Such probes are more resistant to noises and therefore more suitable for application. We restrict our further study to the positively biased probes. These works deal with comparatively low-speed plasmas of hydrocarbon-air flames. As it is shown below, the regimes considered do not cover the region of parameters of high-speed flame plasma flows of interest.

1. Planar probes

Consider first the space charge sheath near a probe in a planar wall. Such planar geometry is the simplest for analysis, if one neglects field concentration and boundary effects near the frontal edge of the probe surface.

Consider the formation of the sheath. Ions are all swept out by drift in the electric field from the sheath, and the trajectories of ions, which are closest to the probe wall, define the shape of the sheath boundary. These trajectories are formed by convection along the axis x parallel to the probe surface (with the flow velocity v_f) and by ion drift in the normal direction y under the effect of the boundary sheath field E_0 . Thus, the sheath boundary coordinate x_s is defined by the equation

$$\partial x_s(y)/\partial y = E_0(y)\mu_i/v_f. \quad (1.1)$$

Here μ_i is the ion mobility. Traditionally, the zero sheath thickness $x_s = 0$ is assumed at $y = 0$, though actually the sheath must have a considerable thickness here due to field concentration.

The distribution of the electric field in the sheath is given by the Poisson equation with respect to the space charge of electrons,

$$\text{div } \epsilon_0 \mathbf{E}(x,y) = eN_e(x,y), \quad (1.2)$$

(here N_e is the electron density in the sheath, e is the electron charge, ϵ_0 is the permittivity of free space), or for the planar case with the only significant x -component of the field E

$$\partial \epsilon_0 E(x,y) / \partial x = eN_e(x,y). \quad (1.3)$$

Apparently, due to the definition of E_0 , $E(x = x_s, y) = E_0(y)$. The sheath voltage is

$$U = \int E(x,y)dx, \quad (1.4)$$

here the integration is carried out for $y = \text{const}$ from the probe surface $x = 0$ to x_s . If no ionization or recombination takes place in the sheath, then the conservation of electron current density j_e in the sheath yields

$$j_e(x,y) = N_e(x,y) \mu_e E(x,y) = N_{e0} \mu_e E_0(y), \quad (1.5)$$

here μ_e is the electron mobility, N_{e0} is the electron density of the plasma near the sheath boundary.

Substitution of $N_e(x,y)$ from (1.5) makes it possible to solve the Poisson equation (1.3):

$$E(x,y) = [2(x_s(y) - x) e E_0(y) N_{e0} / \epsilon_0 + E_0(y)^2]^{1/2}. \quad (1.6)$$

Integration of (1.4) gives the expression for $x_s(y)$ via $E_0(y)$ and U :

$$x_s(y) = E_0(y) \epsilon_0 \{1 - [1 - 3 U e N_{e0} / (\epsilon_0 E_0(y)^2)]^{2/3}\} / (2e N_{e0}) \quad (1.7)$$

This expression after substitution into (1) gives a differential equation for determination of $E_0(y)$, and then all the sheath distributions $x_s(y)$, $E(x,y)$, $N_e(x,y)$, $j_e(x,y)$ can be readily determined from (1.7), (1.6), (1.5). The solution of (1.1) however is not expressed with elementary functions.

To get more transparent relations, consider two opposite cases: $S \gg 1$ and $S \ll 1$, here

$$S = 3 U e N_{e0} / [\epsilon_0 E_0(y)^2]. \quad (1.8)$$

If $S \gg 1$, that corresponds to a great effect of the space charge, (1.7) becomes

$$x_s(y) = 3^{2/3} 2^{-1} \epsilon_0^{1/3} U^{2/3} e^{-1/3} N_{e0}^{-1/3} E_0(y)^{-1/3}. \quad (1.9)$$

In the opposite case $S \ll 1$, (1.7) is simplified to

$$x_s(y) = U/E_0(y). \quad (1.10)$$

Note that (1.10) gives values of $x_s(y)$, which are comparatively close (within a factor of 1.5...2) to those calculated from (1.7) for $S < 10$ (see Fig.1.1), i.e. the results based on (1.10) are valid not only for $S \ll 1$, but also for $S \approx 1$ and even for $S > 1$ up to $S \approx 10$. The formula (1.9) has a comparable accuracy (also within a factor of 1.5...2) at $1 < S < 10$ and is practically invalid at $S \ll 1$.

The solution of (1.1) with the approximation of (1.9) is

$$E_0(y) = (9U^2\varepsilon_0)/[8 x_s(y)^3 e N_{e0}], \quad (1.11)$$

(1.11) and (1.9) yield the formula [19] for the sheath size of the sheath-convection regime:

$$x_s(y) = [9 \mu_i U^2 \varepsilon_0 y / (2e N_{e0} v_f)]^{1/4}. \quad (1.12)$$

The sheath voltage-current characteristic results from (1.5), (1.11), (1.12):

$$j_e(y) = 4 \cdot 2^{1/4} 3^{1/2} \varepsilon_0^{1/4} e^{3/4} N_{e0}^{3/4} v_f^{3/4} \mu_e \mu_i^{-3/4} y^{-3/4} U^{1/2} \quad (1.13)$$

In accord with (1.8) and (1.11), the criterion of validity of (1.12) is expressed through external plasma parameters as

$$S_\infty = [(8 e N_{e0} y \mu_i) / (\varepsilon_0 v_f)]^{3/2} > 1 \quad (1.14)$$

i.e. for given plasma density this approximation is better for low flow velocity, big-size probes and high plasma mobility (lower gas pressure).

Note that this way of derivation of this well-known formula seems to be better substantiated than that based on model speculations of [19], it exposes implicit assumptions and the region of validity of this expression (1.12).

Consider now the application of the approximation (1.10). Solution of (1.1) then looks like

$$E_0(y) = [(U v_f) / (2 \mu_i y)]^{1/2}, \quad (1.15)$$

the sheath size

$$x_s(y) = [2 \mu_i U y / v_f]^{1/2}, \quad (1.16)$$

the criterion of validity of this approximation

$$S_0 = (6 e N_{e0} \mu_i y) / (\varepsilon_0 v_f) < 10. \quad (1.17)$$

Note that if $S_0 \approx 1$, then the other way of calculation of S also gives $S_\infty \approx 1$, so they do not contradict with each other.

The sheath voltage-current characteristic can be derived from (1.5) and (1.14) as

$$j_e(y) = e N_{e0} \mu_e [(U v_f) / (2 \mu_i y)]^{1/2}, \quad (1.18)$$

it is not linear (again $j_e(y)$ is directly proportional to $U^{1/2}$) although no space charge effect is taken into account in this approximation: the higher is the probe voltage, the thicker is the sheath.

Some results of calculations in both approximations are presented in fig.1.2 and fig.1.3 for plasma parameters characteristic for laboratory experiments and ramjet engine, respectively. The plasma density was taken from the experimental data [19] on atmospheric pressure propane-air flame ionization. The ion mobility was taken in accord with the data [20] for H_3O^+ ions with respect to gas density dependence.

For the laboratory flame plasma (fig.1.2) one can see that in the region of approximately equal validity (where $S = 1 \dots 10$) the two approaches yield results, which are very close to each other. The second approach (formulae (1.15)-(1.18)) is valid practically for the entire probe surface, while the first one fails in the frontal part of the probe, where the probe current density is the highest. Note that the level of plasma velocity in the plasma aerodynamic experiments is much higher than that in the studies of flames of burners ([19-20] etc.).

For the ramjet flame plasma parameters (fig.1.3) the first approximation [19] is invalid, for the parameter S is much less than unity on the entire probe surface. It is a result of still higher gas velocity and pressure characteristic for full-scale systems.

Thus, the second approach, which for planar probes is determined by formulae (1.15)-(1.18), can be recommended for broad regions of parameters corresponding to plasma aerodynamic applications.

2. Cylindrical probes

Cylindrical probes are more practical than planar probes; the resulting expressions here are comparatively complicated, though major features of probe-plasma interaction are the same. Similarly, the trajectories of ions, which are closest to the probe wall, define the shape of the sheath boundary. These trajectories are formed by convection along fluid flow tubes (with the flow velocity v_f) and by ion drift in the normal direction r under the effect of the radial boundary sheath field E_0 . Before the probe, near the critical point of the cylinder $\psi = 0$ (here ψ is the azimuth angle of the cylindrical probe surface) the flow tubes have directions with a considerable radial component. Near the rest, major part of the probe surface the flow tubes are positioned primarily along the surface, and one can neglect the radial component of flow velocity. Then the boundary ions trajectories $r_s = r_s(\psi)$ (in cylindrical coordinates r, ψ) are defined by the equation

$$(1/r_s(\psi)) \partial r_s(\psi) / \partial \psi = E_0(\psi) \mu_i / v_f. \quad (2.1)$$

The dependence between $E_0(\psi)$ and $r_s(\psi)$ is determined below, and (2.1) can be expressed as a differential equation for the function $E_0(\psi)$. In the flow tubes near the critical point of the cylinder $\psi = 0$ the drift velocity $E\mu_i$ is opposite to v_f ; the sheath field increases quickly at $r \rightarrow r_p$ (here r_p is the probe radius), and in the point with $E(\psi)\mu_i = v_f$ the ions are stopped, and the sheath boundary is formed. It provides the boundary condition for (2.1):

$$E_0(\psi=0)\mu_i = v_f. \quad (2.2)$$

The Poisson equation and electron current conservation in the cylindrically symmetric sheath look like

$$\partial E(r,\psi)/\partial r + E(r,\psi)/r = e N_e(r,\psi)/\epsilon_0, \quad (2.3)$$

$$2\pi r e N_e(r,\psi) E(r,\psi) \mu_e = 2\pi r_s e N_{e0} E_0(\psi) \mu_e. \quad (2.4)$$

The differential equation resulting from (2.3) and (2.4) with the boundary condition $E(r=r_s,\psi) = E_0(\psi)$ has the solution

$$E(r,\psi) = E_0(\psi) \{ r_s(\psi)^2 - K [r_s(\psi)^2 - r^2] \}^{1/2}/r, \quad (2.5)$$

here the dimensionless criterion is defined as $K = e r_s(\psi) N_{e0}/[E_0(\psi)\epsilon_0]$; $0 < K < 1$. The sheath voltage U is determined by integration of (2.5) over r at $\psi = \text{const}$ from r_p to $r_s(\psi)$:

$$U/[E_0(\psi) r_p] = \rho - [\rho^2 - K(\rho^2 - 1)]^{1/2} + \rho (1 - K)^{1/2} \ln \{ \{ \rho(1 - K) + (1 - K)^{1/2} [\rho^2 - K(\rho^2 - 1)]^{1/2} \} / \{ (1 - K) + (1 - K)^{1/2} \} \}, \quad (2.6)$$

here $\rho = r_s(\psi)/r_p$; $\rho > 1$. The formula (2.6) determines, in an implicit form, the required dependence between $E_0(\psi)$ and $r_s(\psi)$. This dependence however can be calculated only numerically. The resulting expression for the equation (2.1) also must be solved numerically.

Analogously to the planar probe geometry, the problem can be analyzed with additional assumptions. As it is shown above, the most attractive analytical approach corresponds to a weak space charge effect. If $K \ll 1$ (that also means a weak space charge effect), then (2.5), (2.6) reduce to

$$E(r,\psi) = E_0(\psi) r_s(\psi)/r, \quad (2.5)$$

$$U = E_0(\psi) r_s(\psi) \ln[r_s(\psi)/r_p], \quad (2.6)$$

the equation (2.1) can be expressed as

$$\partial r_s / \partial \psi = U \mu_i / \{ v_f \ln[r_s(\psi)/r_p] \}, \quad (2.7)$$

the boundary condition (2.2) looks like

$$\mu_i U / \{ r_s(\psi=0) \ln[r_s(\psi=0)/r_p] \} = v_f, \quad (2.8)$$

or explicitly

$$r_s(\psi=0) = r_{s0} = \mu_i U / \{ v_f L_W[\mu_i U / (r_p v_f)] \}, \quad (2.9)$$

here $L_W(\alpha)$ is the principal branch of the Lambert W function with an argument α , see fig. 2.1 [22].

The solution of (2.7) is

$$r_s(\psi) = r_p \exp\{ L_W[\mu_i U v_f^{-1} r_p^{-1} \exp(-1) (\psi + r_{s0} v_f \mu_i^{-1} U^{-1} [\ln(r_{s0}/r_p) - 1])] + 1 \}. \quad (2.10)$$

After substitution of (2.10) into (2.6), the boundary field expression via the external plasma parameters and ψ looks like

$$E_0(\psi) = U r_p^{-1} \exp\{ -L_W[\mu_i U v_f^{-1} r_p^{-1} \exp(-1) (\psi + r_{s0} v_f \mu_i^{-1} U^{-1} [\ln(r_{s0}/r_p) - 1])] - 1 \} \\ \times \{ L_W[\mu_i U v_f^{-1} r_p^{-1} \exp(-1) (\psi + r_{s0} v_f \mu_i^{-1} U^{-1} [\ln(r_{s0}/r_p) - 1])] + 1 \}^{-1}. \quad (2.11)$$

The probe current density can be derived from (2.4), (2.11) as

$$j_e(\psi) = e N_{e0} \mu_e U r_p^{-1} \{ L_W[\mu_i U v_f^{-1} r_p^{-1} \exp(-1) (\psi + r_{s0} v_f \mu_i^{-1} U^{-1} [\ln(r_{s0}/r_p) - 1])] + 1 \}^{-1}. \quad (2.12)$$

This approach is valid if

$$K = e N_{e0} U^{-1} \varepsilon_0^{-1} r_p^2 \{ L_W[\mu_i U v_f^{-1} r_p^{-1} \exp(-1) (\psi + r_{s0} v_f \mu_i^{-1} U^{-1} [\ln(r_{s0}/r_p) - 1])] + 1 \} \quad (2.13)$$

$$\times \exp\{2L_w[\mu_i U v_f^{-1} r_p^{-1} \exp(-1) (\psi + r_{s0} v_f \mu_i^{-1} U^{-1} [\ln(r_{s0}/r_p) - 1])] + 2\} \ll 1.$$

Some results of calculations are presented in fig.2.2 and fig.2.3 for plasma parameters characteristic for laboratory experiments and a ramjet engine, respectively. The plasma density was taken from the experimental data [18] on atmospheric pressure propane-air flame ionization. The ion mobility was taken in accord with the data [20] for H_3O^+ ions with respect to gas density dependence.

One can see that for the both cases the condition of validity of the approximation $K \ll 1$ is met, the reserve is especially large for the conditions of ramjet engine. It means that the Debye layer is compressed by the flow so that no space charge effects prevent the electron current to cross the layer. Actually, the sheath thickness is only a fraction of millimeter.

On the fore side of the probe ($\psi = 0$) the electric field and electron current density are considerably (5...10 times) higher, and the sheath thickness is narrower (2...3 times), than that at the back side ($\psi = \pi$). Note that most of the earlier approaches neglected this dependence on the angle ψ by accepting the approximation of cylindrical symmetry. Such neglecting is inapplicable at plasma flows with so high velocities.

The angular dependence of the electric current density is approximately in a direct proportion to $\psi^{1/2}$, and the voltage-current characteristic of the sheath is approximately a root parabola $I = U^\beta$, the exponent β varies from 0.25 for plasma parameters characteristic for the laboratory experiments to 0.4 for a ramjet engine (Fig. 2.4,2.5).

3. Total voltage-current characteristics

The next question is the influence of the other mechanisms of formation of the probe voltage-current characteristic, – the drift and diffusion mechanisms.

A voltage-current characteristic of a positive probe is formed by the electron current. The latter, in the principle, can be limited either by the processes of electron drift in the plasma area with the practically unperturbed relative plasma density n_e/n_g (i.e. the usual conductive charge transfer), or by a finite efficiency of the ambipolar diffusion in the diffusion layer, where plasma is quasi-neutral, but its relative density is lower than the unperturbed value, or by the abovementioned processes in the Debye space charge sheath, where $n_i \ll n_e$. The least effective process defines the mode of probe operation.

Parts of the probe surface are under different conditions due to the distribution of the plasma parameters. For some of the current tubes the total current can be limited by one of the mechanisms, but for other current tubes the situation may be different. The relative yield of the modes depends on external conditions and the probe bias voltage U .

Consider a current tube with drift, diffusion, space charge sheath or intermediate mode. Its effective voltage for a cylindrical probe is bound with the local electric field as [6] $\Delta\varphi \approx E_n(R \ln(L/R))$, here R and L are the probe radius and length. The diffusion, drift and Debye space charge layers can be represented as sequent resisting parts of a current tube with voltages $\Delta\varphi_a$, $\Delta\varphi_d$ and $\Delta\varphi_c$, respectively. The total voltage of a current tube for the current i can be calculated from the formula

$$\Delta\varphi = \Delta\varphi_a + \Delta\varphi_d + \Delta\varphi_c = (\rho_a + \rho_d + \rho_c)i . \quad (3.1)$$

The values of partial resistances of the layers $\rho_a = \Delta\varphi_a/i_a$, $\rho_d = \Delta\varphi_d/i_d$ and $\rho_c = \Delta\varphi_c/i_c$ can be determined from the values of ion currents i_a , i_d and i_c , which are calculated for the current tube from solution of the partial problems with respect to only diffusion, only drift and only space charge sheath processes. Together with the condition of conservation of the ion current through a current tube $i_a = i_d = i_c = i$ it makes it possible to determine the values of the total ion current i , and the total voltage $\Delta\varphi$ for any current tube.

Consider the drift partial problem. As it has been mentioned in the previous reports, the value $x=n_i/n_g = n_e/n_g$ is approximately a constant in the drift region, and on the boundary of the drift region this value is approximately equal to the unperturbed one in the ambient flow x_∞ . It makes it possible to determine the electron current density in the drift region as

$$\begin{aligned} j_d(\psi) &= en_e(\psi)\mu_e(\psi)E_n(\psi) = e^2 E_n(\psi) n_e(\psi)/[n_g m_{mol}\Sigma_{im} (2 k_B T_g / m_{mol})^{1/2}] = \\ &= e^2 x E_n(\psi) / [m_{mol}\Sigma_{im} (2 k_B T_g / m_{mol})^{1/2}] = en_{e\infty}\mu_{e\infty}E_n(\psi), \end{aligned} \quad (3.2)$$

here $n_{e\infty}$ and $\mu_{e\infty}$ are the unperturbed values of ion density and mobility in the ambient flow, E_n is the normal to the surface electric field component,

$$E_n = 2 E_0 \cos \psi + 2 E_0 + \Delta V_p / (R \ln(L/R)), \quad (2.5)$$

here $\Delta V_p = U - V_p^0$, V_p^0 is the negative bias relatively the local plasma medium potential:

$$V_p^0 = 2 E_0 (R \ln(L/R)) + \Delta V, \quad (2.4)$$

here the first term is bound with the external field, the second term results from the fact that fast particles of the electron distribution function can overcome potential barriers.

The corresponding drift layer partial local resistance of a current tube with the cross section area δA (near the boundary of the drift layer) is

$$\rho_d(\psi) = \Delta\varphi_d(\psi)/[j_d(\psi) \delta A]. \quad (3.3)$$

Consider now the partial problem with respect to the potential fall in the diffusion layer only. Note that the diffusion mechanism is to be taken into account in case that the diffusion layer thickness is higher than the Debye sheath. In the opposite case no ambipolar diffusion is present. Formally, if the diffusion characteristic length $r_a(\psi)$ is less than $r_s(\psi) - r_p$, then $\rho_a(\psi) = 0$. The value of r_a for a temporary evolution of an initially stepwise profile of concentration is

$$r_a = (tD_a)^{1/2}, \quad (3.4)$$

here the time coordinate t can be expressed via the length l of a path of an element of plasma along the probe surface as

$$t = \int (1/v_g) dl \approx l/v_g, \quad l \approx R\psi. \quad (3.5)$$

Assume a linear radial plasma density profile across the diffusion layer and a constant $x=x_\infty$ in the drift area; then the electron flux across the diffusion layer is

$$\Gamma(\psi) = -D_a(\psi) \nabla n_e(\psi) \approx D_{a\infty} n_{e\infty} / r_a(\psi). \quad (3.6)$$

Here $D_{a\infty}$ is the ambipolar diffusion coefficient in the ambient flow (we neglect variations of T_e). The corresponding current density and the diffusion layer partial local resistance are

$$j_a(\psi) = e\Gamma(\psi), \quad \rho_a(\psi) = \Delta\varphi_a(\psi)/[\delta A j_a(\psi)]. \quad (3.7)$$

These formulae yield infinite j_a at $\psi=0$. To eliminate it, a small but finite constant value of r_{a0} was added to the denominator in (3.6); it can be determined from a 2D solution of the diffusion problem for a flow over a cylinder, but calculations have shown that the resulting total current is practically independent on considerable variations of r_{a0} . Actually, if the partial resistance $\rho_a(\psi)$ is low, it can be neglected. That is why the additive to the denominator must be applied rather to provide non-stop calculations.

The value of j_a is independent of $\Delta\phi_a$, and the higher is $\Delta\phi_a$, the higher is the effective resistance ρ_a corresponding to the constant j_a . One can see that the diffusion mode can prevail at high $\Delta\phi_a$, i.e. when the field-dependent processes are effective.

Together with the mentioned above, it makes it possible to calculate $j(\psi)$ for any current tube with account of the mechanisms prevailing in the drift and diffusion regions and in the space charge sheath.

Some results of calculations of the probe electric current distributions and the total voltage-current characteristics are presented in Fig.3.1, 3.2 for plasma parameters characteristic for laboratory experiments and a ramjet engine, respectively. The probe diameter was $2r_p = 0.2$ mm and the length was $L_p = 1$ cm. No external electric field E_0 has been accounted for; it means that the drift component of the electric current is practically in a direct proportion to U and is independent on ψ .

Under the conditions characteristic for laboratory experiments the situation is intermediate. The voltage-current characteristic is formed by processes in the drift plasma region and in the Debye space charge sheath. The diffusion layer is too thin, and the diffusion component can be neglected. The effect of the Debye space charge sheath results in a considerable blockage of the electron current in the hind part of the probe ($|\psi| = \pi/2 \dots \pi$, see Fig. 3.1,a). The total voltage-current characteristic at high ψ is close to that of the Debye space charge sheath (root parabola). On the fore part of the probe surface ($|\psi| < \pi/2$) the sheath is thin, and the drift processes define the voltage-current characteristic: it is practically linear. The total voltage-current characteristic is not exactly linear, but no current saturation is observed.

Under the conditions characteristic for ramjet engines the Debye space charge sheath is thinner than in the previous case, and its blocking is less efficient. As a result, the total voltage-current characteristic is practically linear; it is characteristic for the drift regime. However the lack of the azimuth symmetry of the probe electric current distributions says that the processes in the Debye space charge sheath are still affecting the charge transfer.

$$x_s(y) = 2eN_{e0} / [E_0(y)\epsilon_0]$$

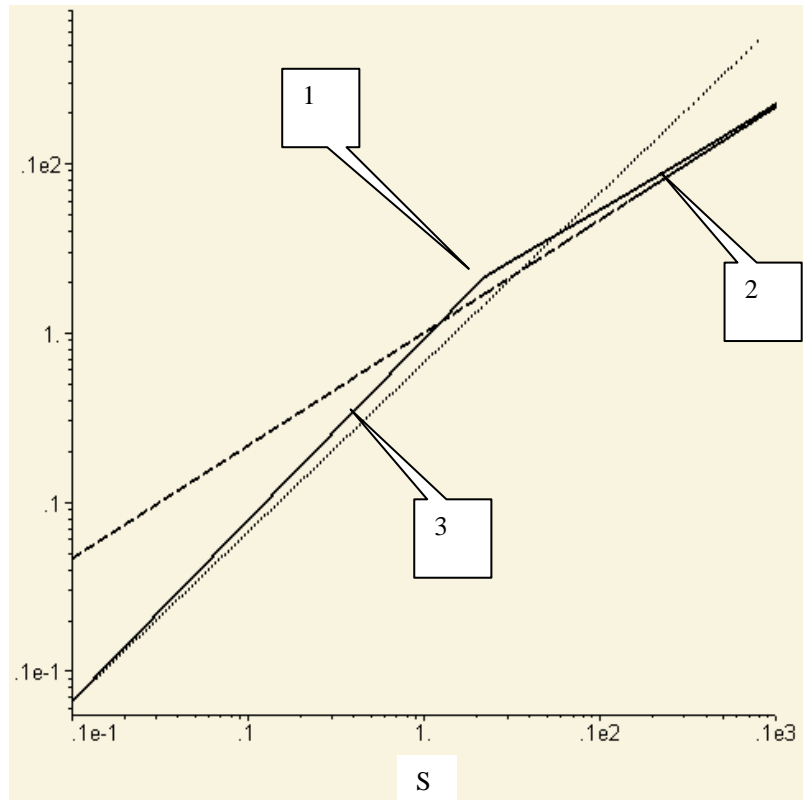
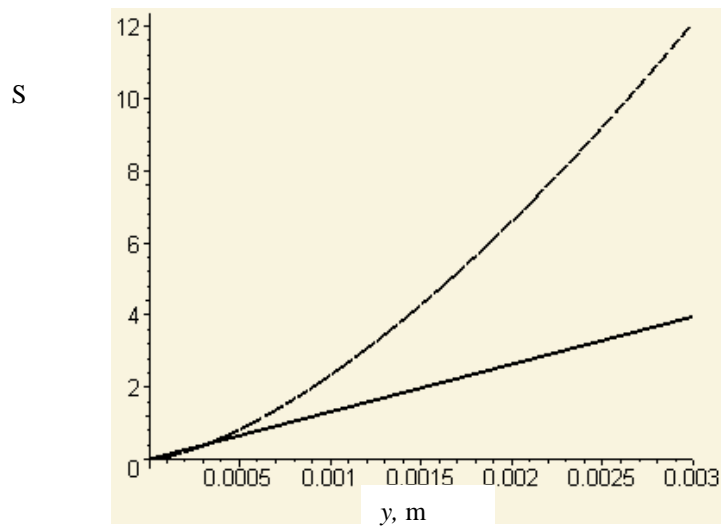
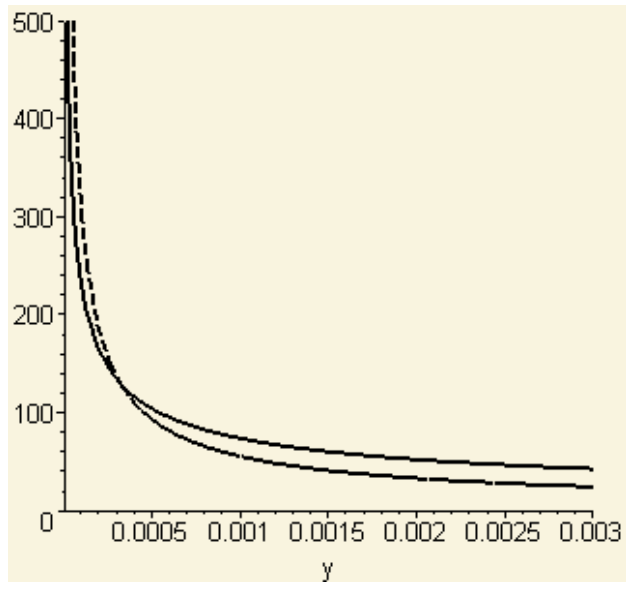


Fig. 1.1. Planar positively biased probe space charge sheath: comparison of the expression (7) (curve 1) with its approximations for $S \gg 1$ (9) (curve 2) and $S \ll 1$ (10) (curve 3).

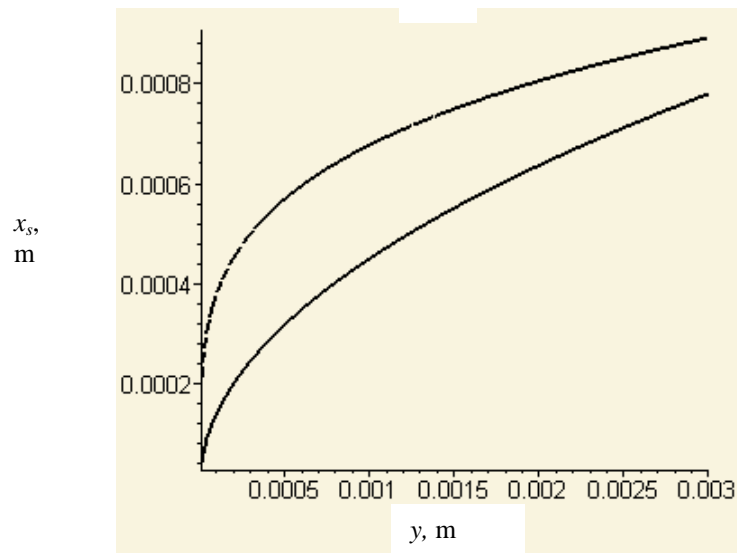
a)



b)



c)



d)

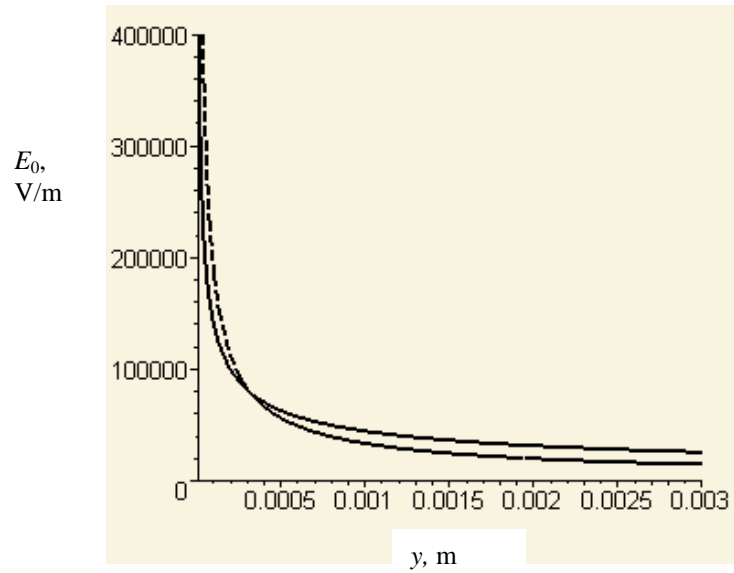
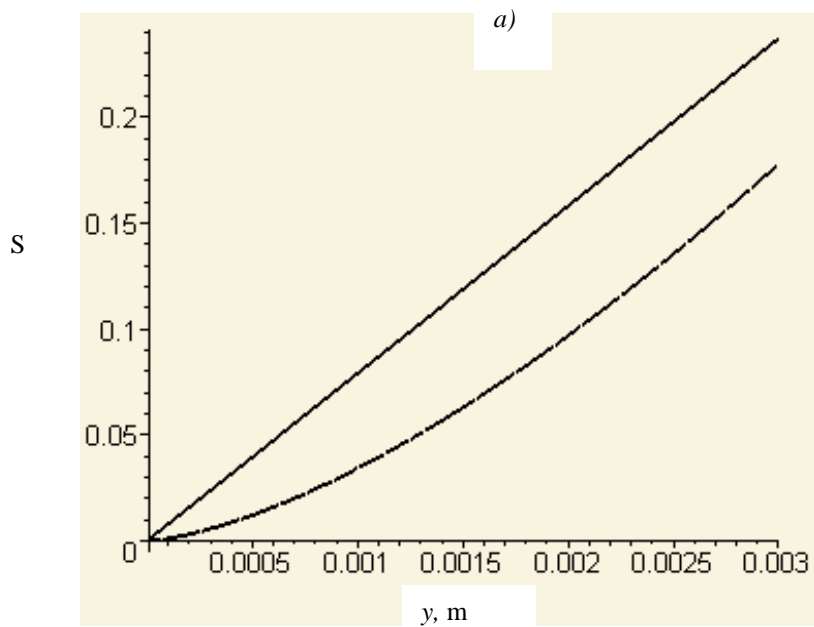
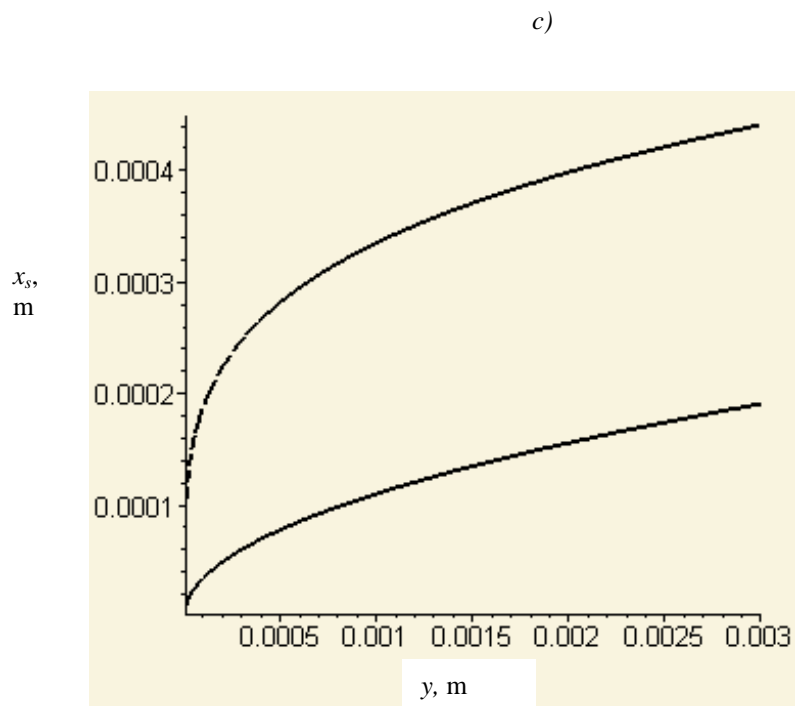
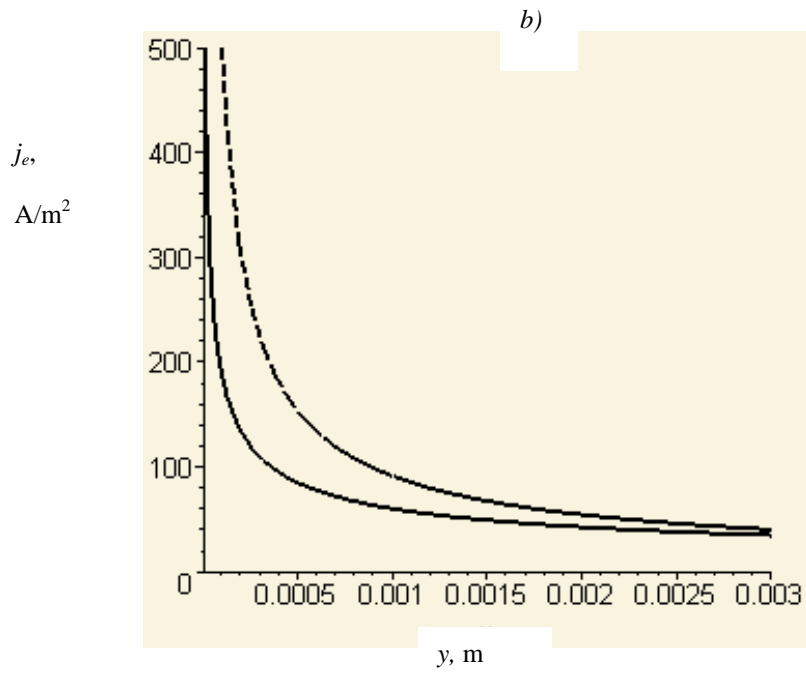


Fig. 1.2. Planar positively biased ($U = 20$ V) probe space charge sheath: spatial distributions of the validity criterion (a), probe current density (b), sheath size (c) and electric field (d) calculated with the $S \gg 1$ and $S \ll 1$ approximations (dashed and solid lines, respectively) for flame plasma flow parameters: $N_{e0} = 2.4 \cdot 10^{15} \text{ m}^{-3}$, $v_f = 600 \text{ m/s}$, $p = 200 \text{ Torr}$, $T_g = 1500 \text{ K}$.





d)

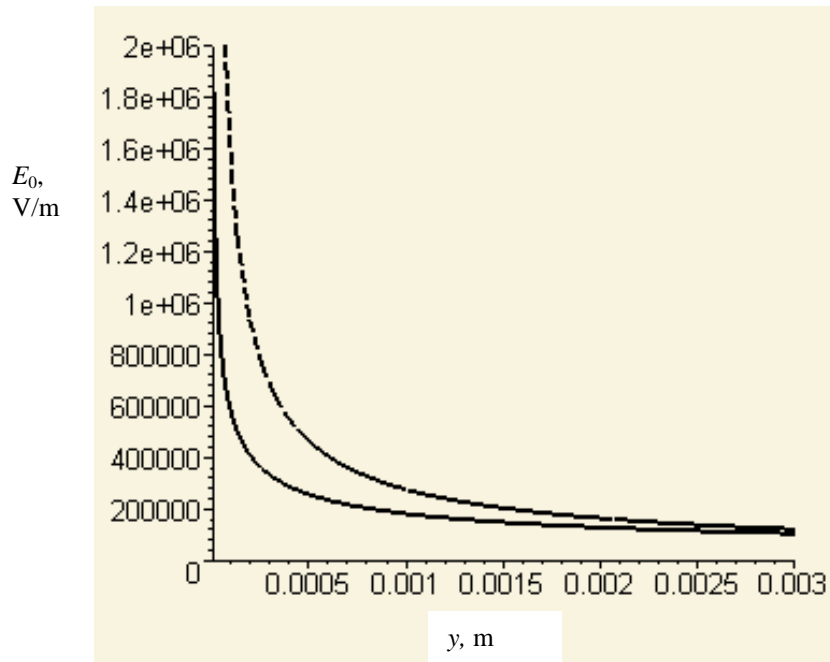


Fig. 1.3. Planar positively biased ($U = 20$ V) probe space charge sheath: spatial distributions of the validity criterion (a), probe current density (b), sheath size (c) and electric field (d) calculated with the $S \gg 1$ and $S \ll 1$ approximations (dashed and solid lines, respectively) for flame plasma flow parameters: $N_{e0} = 2.4 \cdot 10^{15} \text{ m}^{-3}$, $v_f = 2000 \text{ m/s}$, $p = 1000 \text{ Torr}$, $T_g = 1500 \text{ K}$

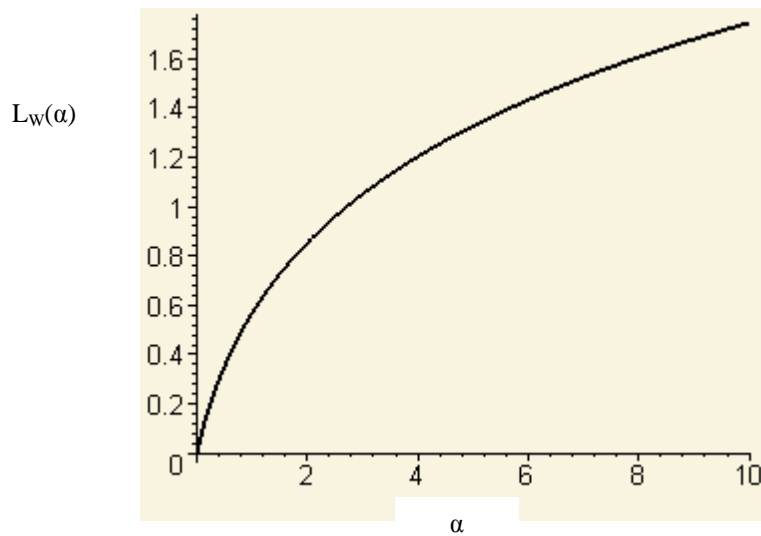
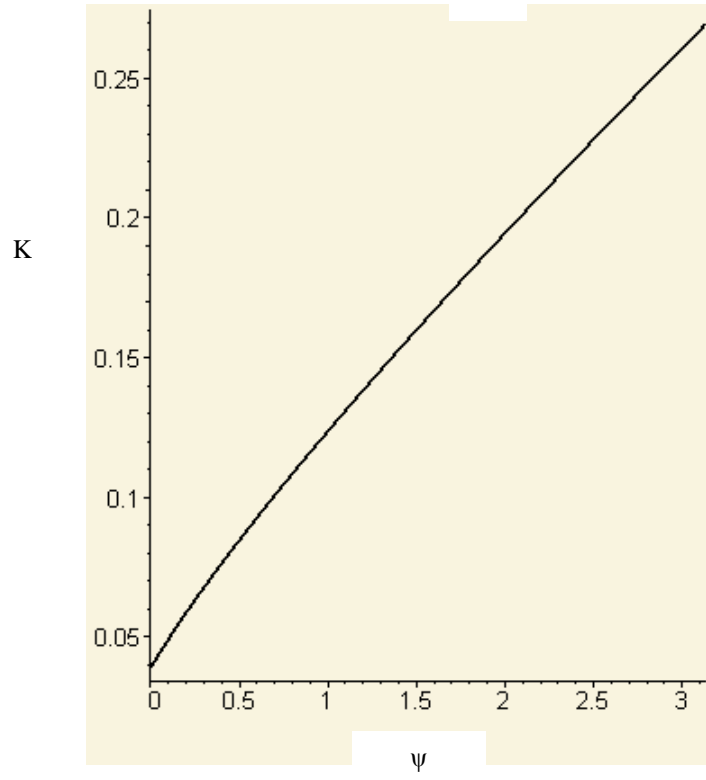
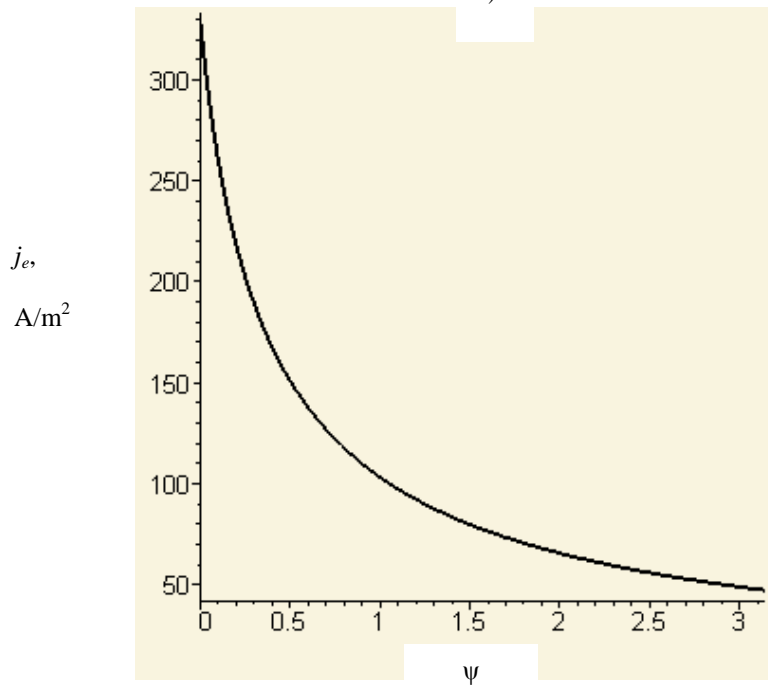


Fig. 2.1. The principal branch of the Lambert W function

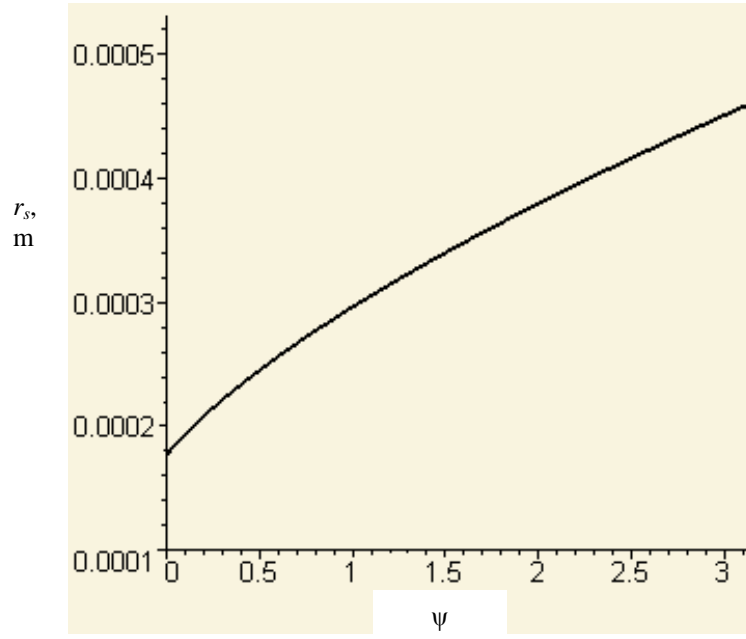
a)



b)



c)



d)

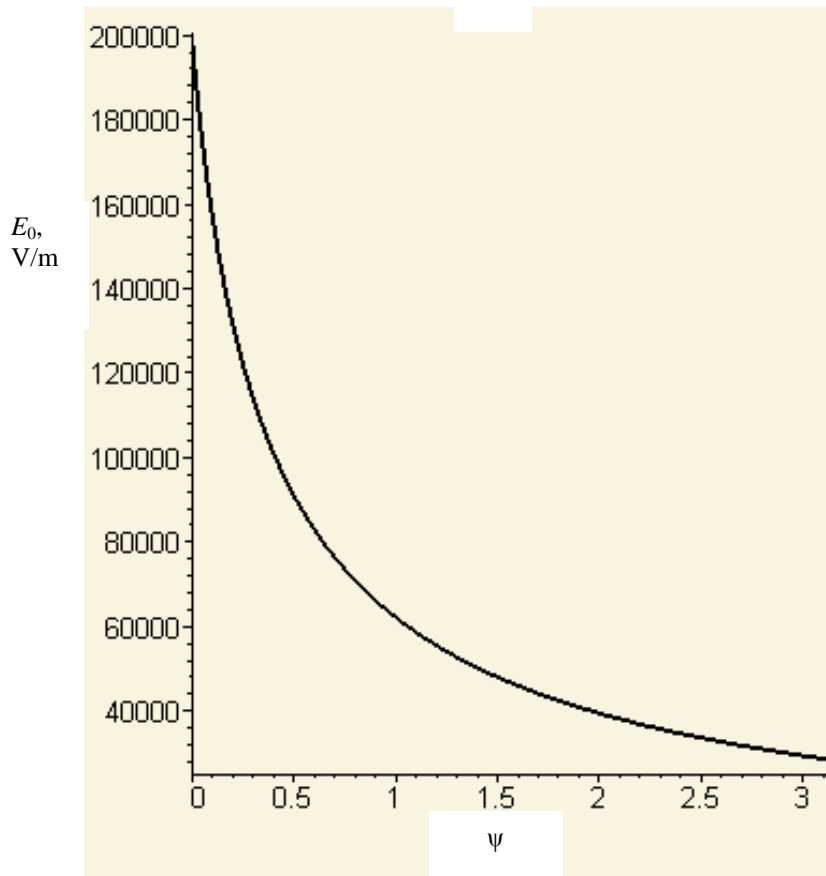
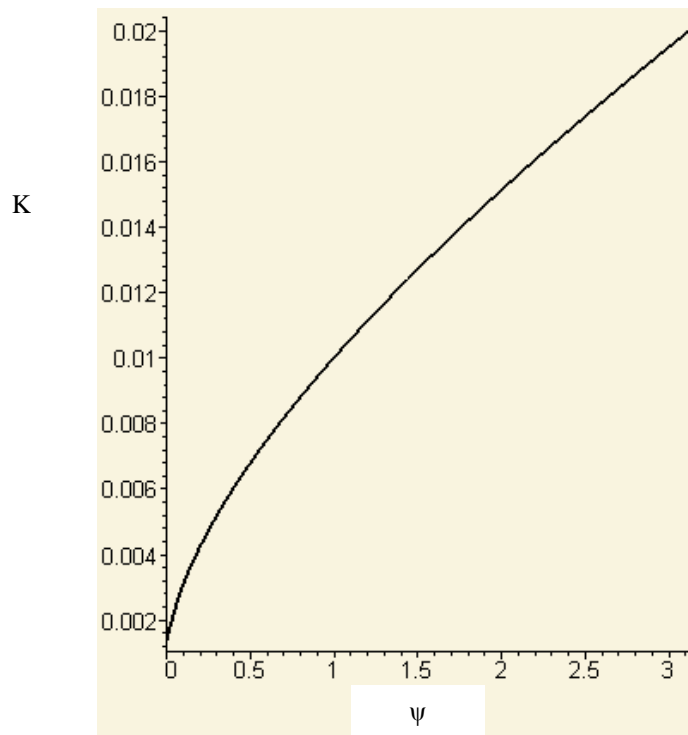
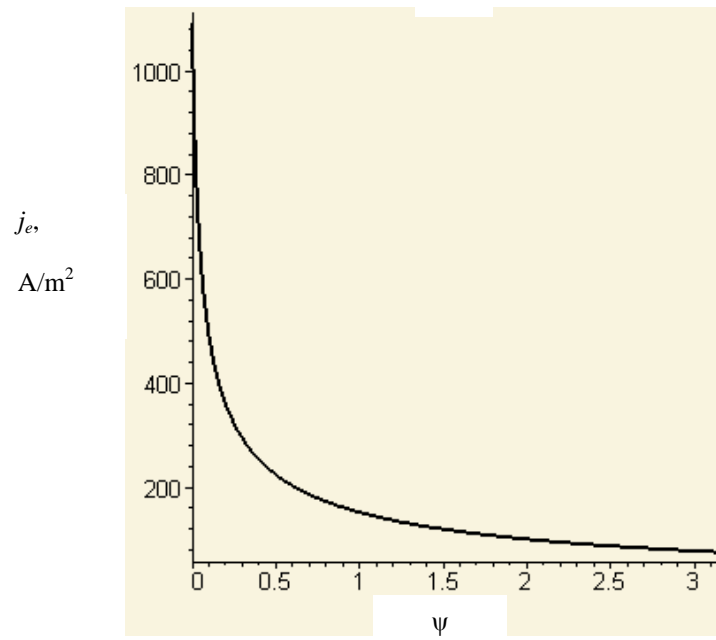


Fig. 2.2. Cylindrical ($2r_p = 0.2$ mm) positively biased ($U = 20$ V) probe space charge sheath: spatial distributions of the validity criterion (a), probe current density (b), sheath size (c) and electric field (d) calculated with the $K \ll 1$ approximation for flame plasma flow parameters: $N_{e0} = 2.4 \cdot 10^{15} \text{ m}^{-3}$, $v_f = 600$ m/s, $p = 200$ Torr, $T_g = 1500$ K

a)



b)



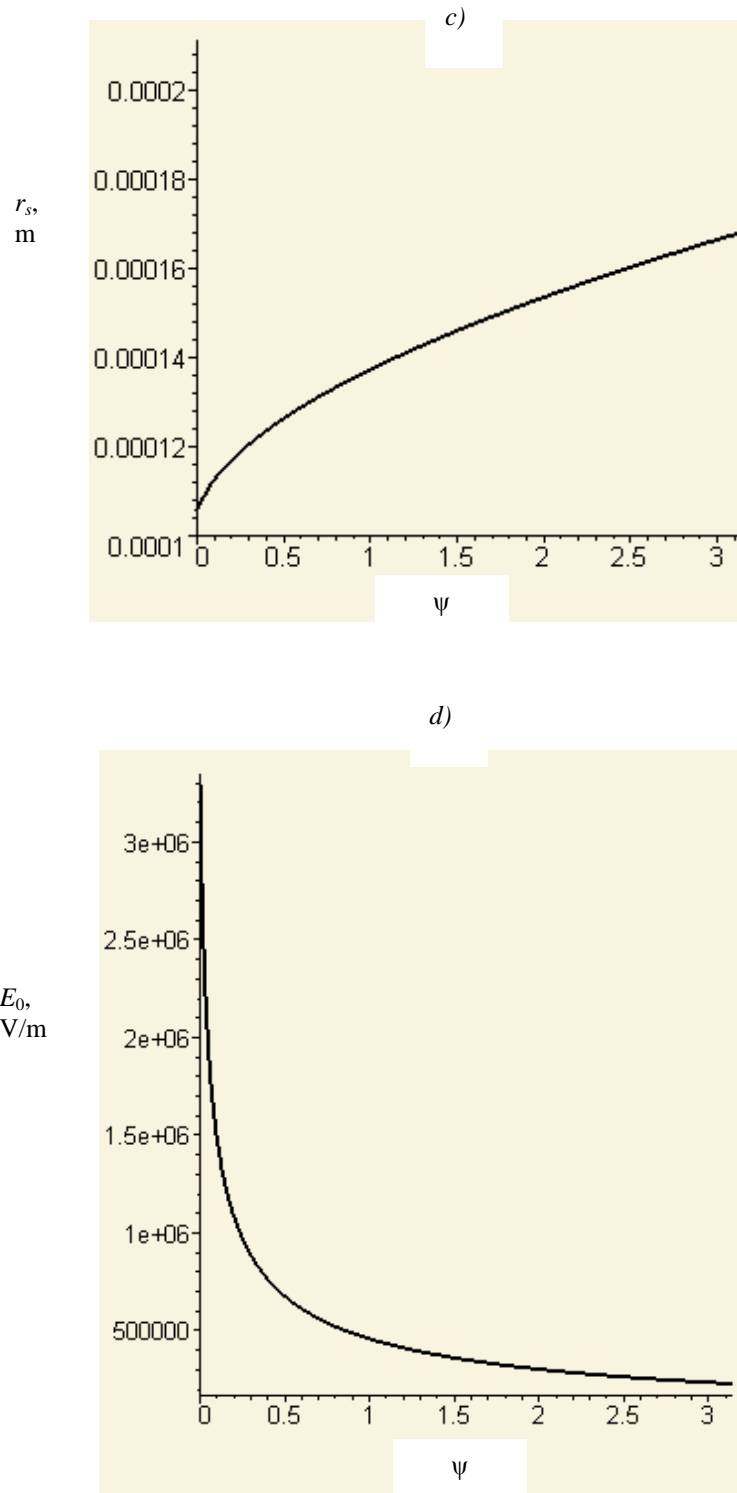


Fig. 2.3. Cylindrical ($2r_p = 0.2$ mm) positively biased ($U = 20$ V) probe space charge sheath: spatial distributions of the validity criterion (a), probe current density (b), sheath size (c) and electric field (d) calculated with the $K \ll 1$ approximation for flame plasma flow parameters: $N_{e0} = 2.4 \cdot 10^{15} \text{ m}^{-3}$, $v_f = 2000$ m/s, $p = 1000$ Torr, $T_g = 1500$ K

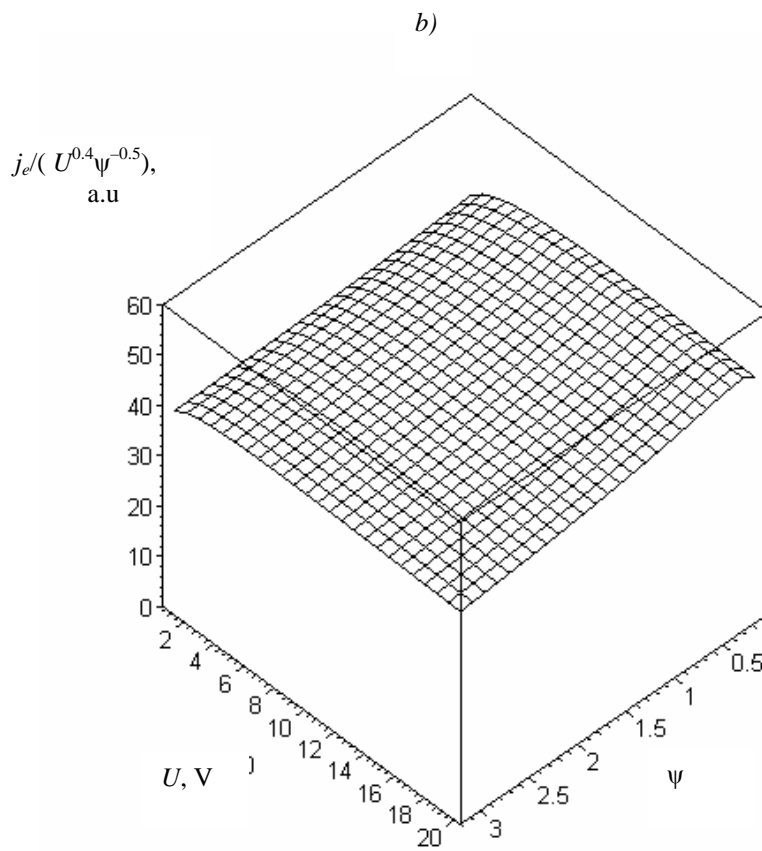
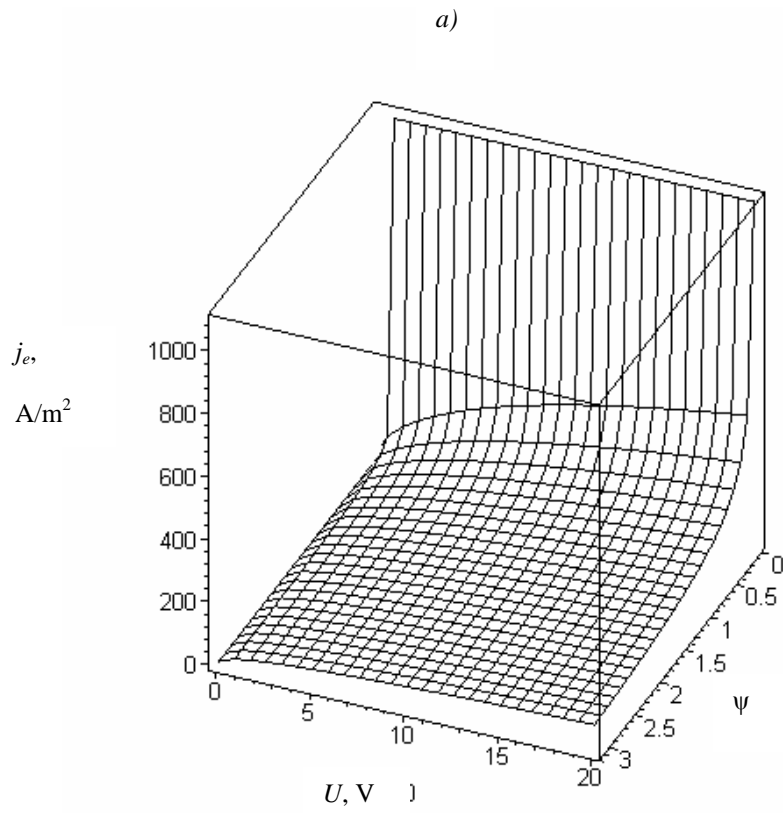


Fig.2.5. Electric current density (a) and that divided by $U^{0.4}\psi^{-1/2}$ (b) for flame plasma flow parameters: $N_{e0} = 2.4 \cdot 10^{15} \text{ m}^{-3}$, $v_f = 2000 \text{ m/s}$, $p = 1000 \text{ Torr}$, $T_g = 1500 \text{ K}$

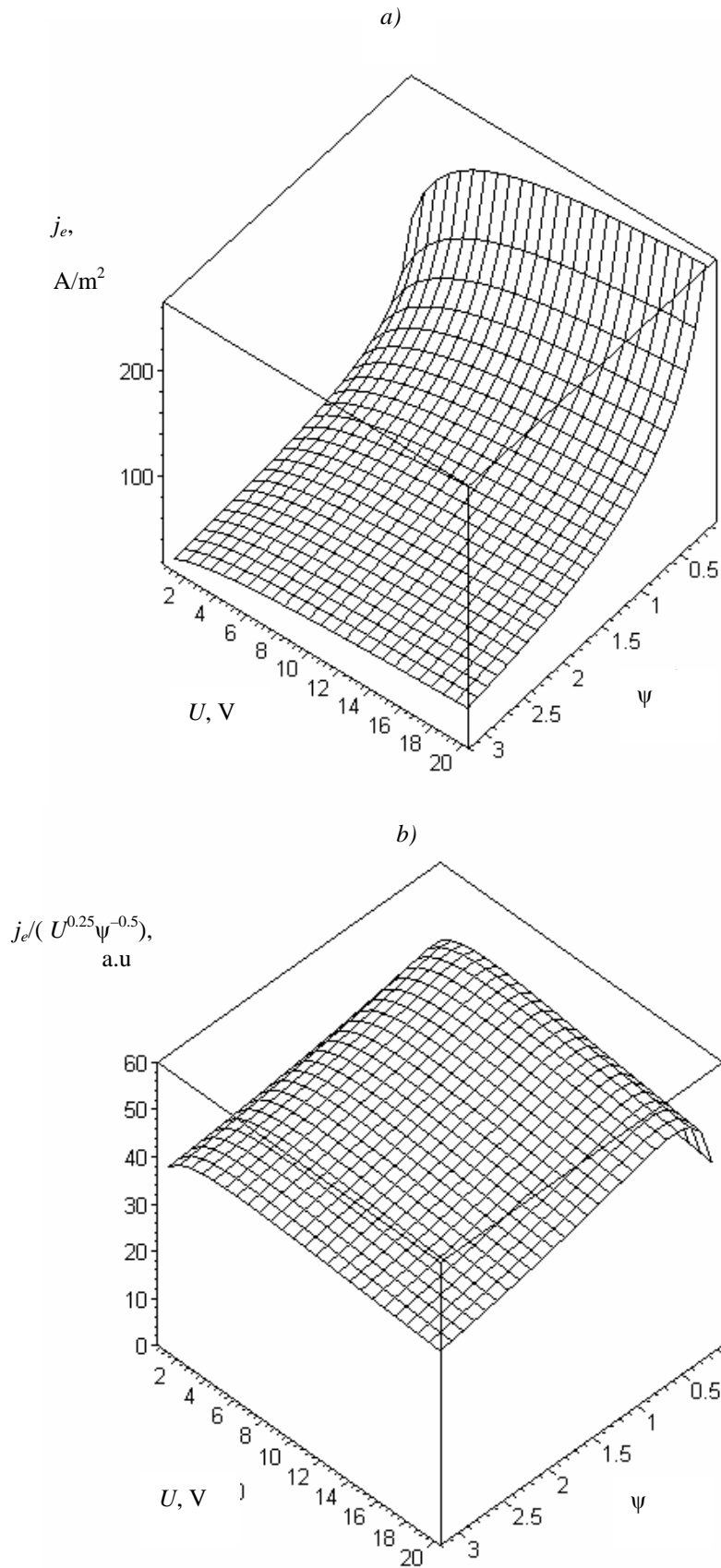


Fig.2.4. Electric current density (a) and that divided by $U^{1/4}\psi^{-1/2}$ (b) for flame plasma flow parameters: $N_{e0} = 2.4 \cdot 10^{15} \text{ m}^{-3}$, $v_f = 600 \text{ m/s}$, $p = 200 \text{ Torr}$, $T_g = 1500 \text{ K}$

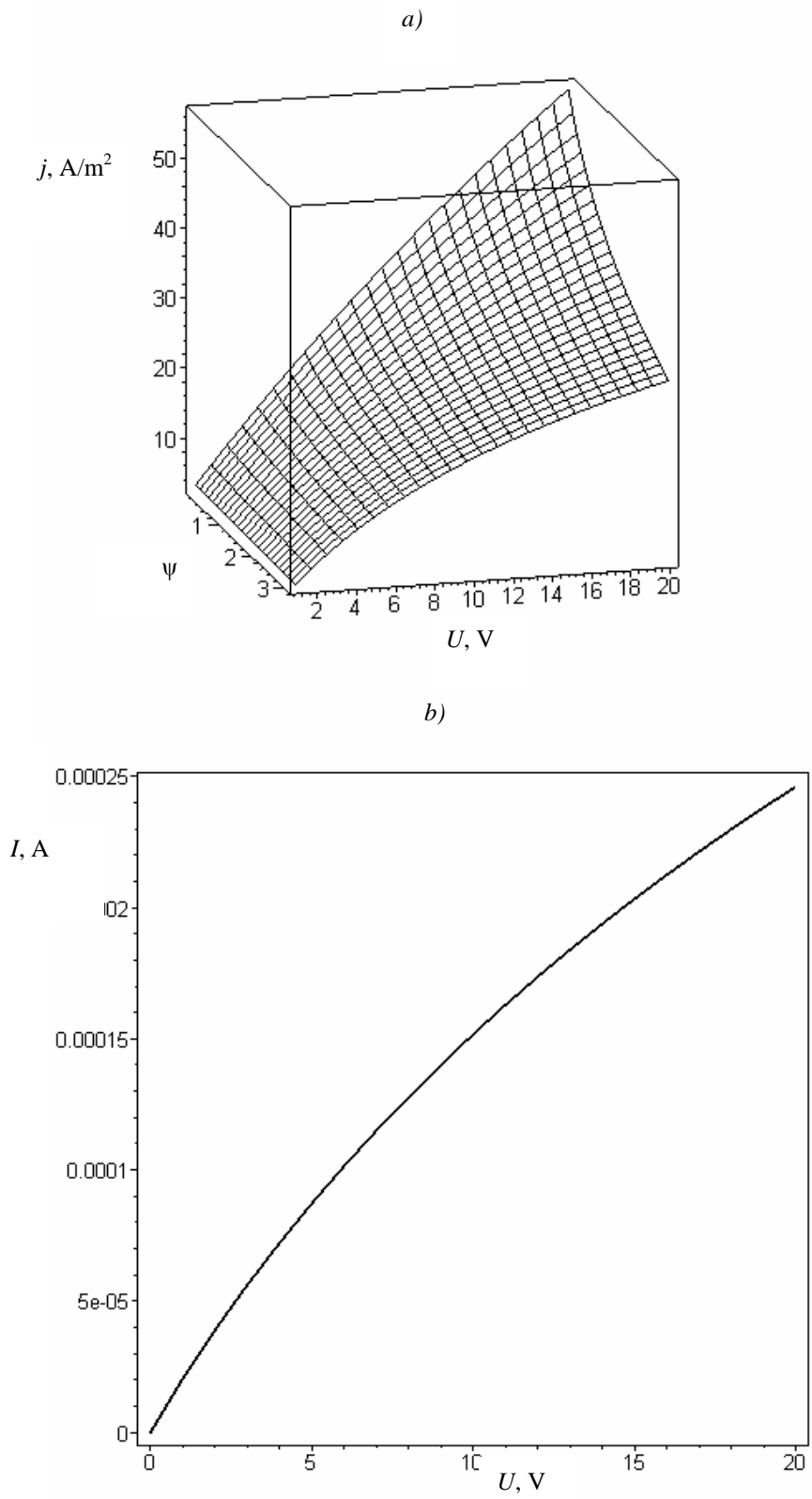


Fig.3.1. Electric current density distribution over the azimuth angle at different voltage (a) and the probe voltage-current characteristic (b) for flame plasma flow parameters: $N_{e0} = 2.4 \cdot 10^{15} \text{ m}^{-3}$, $v_f = 600 \text{ m/s}$, $p = 200 \text{ Torr}$, $T_g = 1500 \text{ K}$

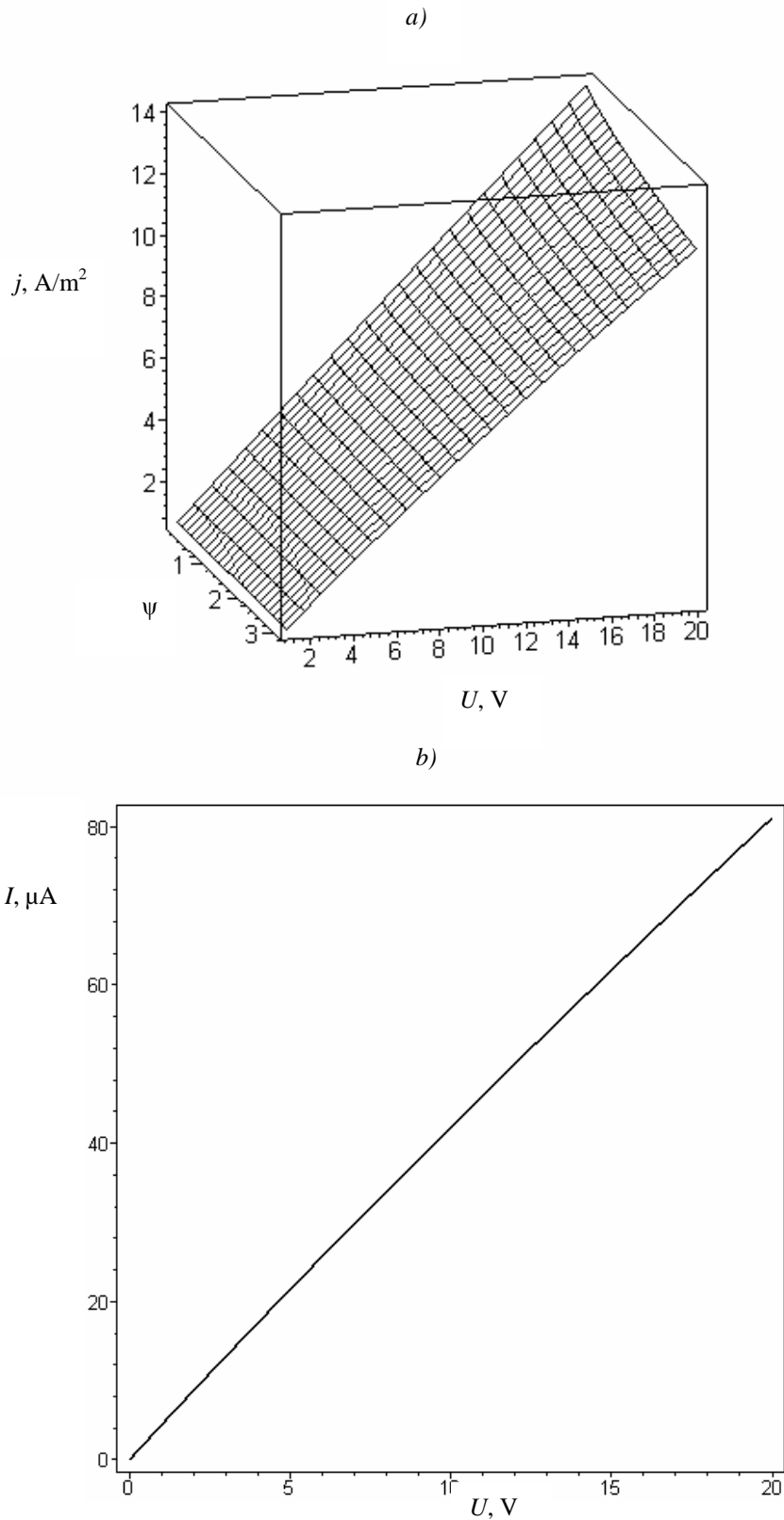


Fig.3.2. Electric current density distribution over the azimuth angle at different voltage (a) and the probe voltage-current characteristic (b) for flame plasma flow parameters: $N_{e0} = 2.4 \cdot 10^{15} \text{ m}^{-3}$, $v_f = 2000 \text{ m/s}$, $p = 1000 \text{ Torr}$, $T_g = 1500 \text{ K}$

REFERENCES TO CHAPTER III

1. Ershov A.P. Final Project Technical Report of ISTC 1867p, Moscow State University, Department of Physics, September 2001.
2. Ershov A., Ardelyan N., Chuvashv S., Shibkov V., Timofeev I. // AIAA Journal, Vol.39, No 11. P.2180, 2001.
3. Benilov M.S. Theory of Electric Probes in Weakly Ionized High Density Plasma Flows: Review //High Temperature. Vol.26. No. 5. Pp.993-1003, 1985.
4. Benilov M.S., Bochkarev G.G., Buznikov A.E., German V.O., Kovbasyuk V.I. Electrical Probe Characteristics in a Subsonic Plasma Flow// Academy of Science News. Liquid and Gas Mechanics. No.1. Pp.150-160, 1983.
5. Chen Xi. Ion Saturation Current Density and Specific Heat Flux on a Cylindrical Probe Immersed in a Dense Plasma Flow.// J.Phys.D: Applied Physics. Vol. 15. Pp. 1695-1708, 1982.
6. Akishev Yu.S., Napartovich A.N. On the Probe Diagnostics of a High Pressure Glow Discharge. Sov. Physics: Doklady. Vol.242. Pp. 812-815, 1978.
7. Mal'kov M.A., Devyatov A.M., Kuzovnikov A.A., Ershov A.P. Probe Diagnostics of the Plasma of Gas Discharge Light Sources. Moscow: MSU, 1991.
8. Protasov Yu.S., Chuvashv S.N. Physical Electronics of Gas Discharge Devices: Plasma Electronics. Moscow:Vysshaya Shkola. 1993; Protasov Yu.S., Chuvashv S.N. On Elementary Processes in Plasma// Encyclopedia of Low Temperature Plasma. Moscow: Nauka, 2000. V.1. P.43.(In Russian)
9. Biberman L.M., Vorobiov V.S., Iakubov I.T. Kinetics of Non-equilibrium Low Temperature Plasma. Moscow: Nauka, 1982.(In Russian).
10. Zhdanov V.M., Son E.E. Phenomenological and Kinetic Description of Transport Phenomena in Low Temperature Plasmas. // Encyclopedia of Low Temperature Plasma. Moscow: Nauka, 2000. V.1. P.508. (In Russian).
11. Ivanov Ju.A. Probe Diagnostics of Chemically Active Non-Equilibrium Plasma// In: Encyclopedia of Low Temperature Plasma. Moscow: Nauka, 2000. V.2. Pp.466-470. (In Russian)
12. C.Q.Jiao, C.A.DeJoseph, Jr, A.Garscadden. Weakly Ionized Gases Conference, Anaheim, CA, 2001. AIAA 2001-2950
13. J. de Urquijo, C.A. Arriaga, C. Cisneros, I. Alvarez. A Time-Resolved Study of Ionization, Electron Attachment and Positive-Ion Drift in Methane. // J.Phys. D: Appl.Phys. V. 32 (1999), pp. 41-45
14. Eletsky A.V., Smirnov B.M. Elementary Processes with Ions. // In: Encyclopaedia of Low

- Temperature Plasma. Moscow: Nauka, 2000. V.1. Pp.231-238. (In Russian)
15. Shen Nan Lin, Griffin G.W., Horning E.C., Wentworth W.E. J.Chem.Phys., 60, 4994 (1074)
 16. . Raizer Yu.P. Physics of Gas Discharges. Moscow: Nauka. 1992 (In Russian).
 17. Smy P.R. The use of Langmuir probes in the study of high pressure plasmas. Advances in Physics, V.25, No.5, Pp.517-553.
 18. Clements R.M., Smy P.R. The positively biased Langmuir probe in a high-pressure plasma. J. Phys. D: Appl.Phys. V. 26 (1993). P. 1916-1920.
 19. James Dawe, Syed A.H.Rizvi and Peter R. Smy. Electron current to a cylindrical probe in a moving high pressure plasma. IEEE Transactions of Plasma Science. 1993. V.21.No.1.P.202.
 20. Bradley D., Ibrahim S.M.A. The effects of electrical fields upon electron energy exchanges in flame gases. Combustion and Flame, v.22, pp.43-52. 1974.
 21. R.M. Corless, G.H. Gonnet, D.E.G. Hare, D.J. Jeffrey, and D.E. Knuth. "On The Lambert W Function". *Advances in Computational Mathematics* 5 (1996): 329-359

CHAPTER IV.

COMPUTER SIMULATIONS

§ 1. 1D numerical model

Most works on probe diagnostics for the cases when processes in the Debye layer are important are based on an asymptotic analysis for extreme cases, the number of works based on a detailed computer simulation seems insufficiently low [1], which makes it difficult interpret intermediate regimes.

A computer simulation of one-dimensional probe diagnostic problems has been carried out for the cases when processes in the Debye layer are important. Both cases of the steady plasma and the plasma flow with the Blasius gas dynamical profile have been considered.

Consider one-dimensional problem of plasma-probe interaction for cases of steady plasma and high-speed flows. The latter is based on the well-known Blasius gas dynamic boundary layer problem solution. A similar approximation has been applied in a semi-analytical approach of [2].

Characteristic parameters of the experiments are: probe radius $R \sim 0.2$ mm, length $L \sim 10$ mm, flow speed $v \sim 600$ m/s, gas temperature $T_g \sim 1000 - 3000$ K, probe potential $\varphi_p \sim 1 - 30$ V, electron temperature $T_e \sim 0.5-3$ eV, electron density $n_e \sim 10^{18} - 10^{21} \text{ m}^{-3}$, gas density $n_g \sim (1 - 3) 10^{24} \text{ m}^{-3}$.

The main dimensionless parameters of the problem are [1]:

- the Reynolds number $Re = vR/D_i$ ($D_i \approx 10^{-18}(2n_g)^{-1}\{k_B T_g/(2m_a)\}^{0.5}$ is the ion diffusion coefficient, k_B – is the Boltzmann constant, m_a is the mass of a neutral particle);
- $\varepsilon = k_B T_g \varepsilon_0 / (n_e e^2 R^2)$ (ε_0 is the dielectric constant, e is the electron charge), R is the probe radius;
- the dimensionless probe potential $\varphi_m = e \varphi_p / (k_B T_e)$.

Under experimental conditions of interest, $Re \approx (0.6-1) \cdot 10^3$, $\varepsilon \approx (1-3) \cdot 10^{-4}$ at $n_e = 10^{18} \text{ m}^{-3}$, $\varepsilon \approx (1-3) \cdot 10^{-7}$ at $n_e = 10^{21} \text{ m}^{-3}$.

No chemical reactions and electron temperature variations have been accounted for. The applied steady system of equations of electrons (indices “e”) and positive ions (indices “i”) and the Poisson equation in the dimensionless form looked like

$$\begin{aligned}\nabla \cdot (n_e \vec{v}_e) &= 0, \quad \vec{v}_e = \vec{v}_g - \varepsilon_e \mu_e \left(\frac{1}{n_e} \nabla (T_e n_e) + \chi \vec{E} \right), \\ \vec{E} &= -\nabla \varphi, \\ \nabla \cdot (n_i \vec{v}_i) &= 0, \quad \vec{v}_i = \vec{v}_g - \varepsilon_i \mu_i \left(\frac{1}{n_i} \nabla (T_i n_i) - \tau \chi \vec{E} \right), \\ \varepsilon_\varphi \nabla \cdot \nabla \varphi &= (n_e - n_i), \quad T_e = T_i = 1, \quad \mu_e = \mu_i = 1.\end{aligned}$$

Here

$$\begin{aligned}\varphi^M &= \varphi^M, \quad E^M = \frac{\varphi^M}{L}, \\ n_e^M &= n_i^M = n_\infty, \quad v^M = U = v_\infty, \\ \varepsilon_e &\equiv \frac{k_B T_e^M \mu_e^M}{e LU}, \quad \chi \equiv \frac{e \varphi^M}{k_B T_e^M}, \\ \varepsilon_i &\equiv \frac{k_B T_i^M \mu_i^M}{e LU} = \frac{T_i^M \mu_i^M}{T_e^M \mu_e^M} \varepsilon_e, \\ \tau &\equiv \frac{T_e^M}{T_i^M}, \quad \left\{ \left(\frac{\mu_i^M}{\mu_e^M} \right)^2 \cong 2 \frac{T_e^M m_e}{T_i^M m_i} \right\}, \\ \varepsilon_\varphi &\equiv \frac{\varepsilon_0 \varphi^M}{L^2 e n_\infty} = \chi \left(\frac{\lambda_D}{L} \right)^2, \quad \lambda_D^2 \equiv \frac{\varepsilon_0 k_B T_e^M}{e^2 n_\infty}.\end{aligned}$$

There are three small parameters in the system: two diffusion parameters ε_e , ε_i and the Debye parameter ε_φ . The ion diffusion parameter can be much less than the electron one:

$$\left(\frac{\varepsilon_i}{\varepsilon_e} \right)^2 \cong 2 \frac{T_i^M m_e}{T_e^M m_i}, \quad \frac{m_e}{m_i} \approx 10^{-4}, \quad \frac{T_i^M}{T_e^M} \approx 10^{-1}$$

Assume [2] that the densities depend on a variable $\eta = y \sqrt{\frac{U}{v x}}$ only, here x , y are the longitudinal and transversal special coordinates, $r = y + r_0$, r_0 is the probe radius. Then in a one-dimensional case the system of model equations looks like

$$\begin{aligned}
\nabla \cdot (n_e \vec{v}) - \varepsilon_e \nabla \cdot [\mu_e (\nabla (T_e n_e) + \chi n_e \vec{E})] &= 0, \\
\vec{E} &= -\nabla \varphi, \\
\nabla \cdot (n_i \vec{v}) - \varepsilon_i \nabla \cdot [\mu_i (\nabla (T_i n_i) - \chi \tau n_i \vec{E})] &= 0, \\
\vec{v} &\equiv \vec{v}_g, \\
\varepsilon_\varphi \nabla \cdot \nabla \varphi &= (n_e - n_i), \\
T_e = T_i = 1, \mu_e = \mu_i &= 1. \\
r^{-\alpha} \frac{\partial}{\partial r} \left(r^\alpha n_e \left[v_y - \frac{y}{2x} v_x \right] \right) + \left(1 + \frac{\alpha y}{r} \right) \frac{n_e v_x}{2x} \\
- \varepsilon_e r^{-\alpha} \frac{d}{dr} \left[\mu_e r^\alpha \left(\frac{d}{dr} (T_e n_e) + \chi n_e \vec{E} \right) \right] &= 0, \\
r^{-\alpha} \frac{\partial}{\partial r} \left(r^\alpha n_i \left[v_y - \frac{y}{2x} v_x \right] \right) + \left(1 + \frac{\alpha y}{r} \right) \frac{n_i v_x}{2x} & \quad (1) \\
- \varepsilon_i r^{-\alpha} \frac{d}{dr} \left[\mu_i r^\alpha \left(\frac{d}{dr} (T_i n_i) - \chi \tau n_i \vec{E} \right) \right] &= 0, \\
\varepsilon_\varphi r^{-\alpha} \frac{d}{dr} \left(r^\alpha \frac{d}{dr} \varphi \right) &= (n_e - n_i), \\
T_e = T_i = 1, \mu_e = \mu_i = 1, \vec{E} &= -\frac{d}{dr} \varphi.
\end{aligned}$$

($\alpha = 0, 1$ for planar and cylindrical symmetry, correspondingly). The values of v_x, v_y are tabulated from the Blasius problem solution. In case of $a = 1$ the value of v_y is divided by r to conserve the gas mass. The boundary conditions are:

$$n_{i,e}(1) = 0, n_{i,e}(\infty) = 1, \varphi(1) = \varphi_z, \varphi(\infty) = 0 \quad (2)$$

Assume $r_0 = x = 1$.

The problem (1), (2) has been solved at various conditions.

§ 2. Results of computation

2.1 Steady plasma. Spherical probe.

The only small parameter is ε_φ , it was varied in a wide range ($10^{-14} \leq \varepsilon_\varphi \leq 10^{-2}$) for testing the method of computation. Dimensionless profiles of electron and ion densities, the electric potential are shown in Fig.1 for $\varepsilon_\varphi = 10^{-12}$, spatial electron and ion current density distribution and

view of the voltage-current characteristic for this value of ε_ϕ are shown in Fig.2. Here and below J_{iDR} , J_{iDF} , J_{ic} (J_{eDR} , J_{eDF} , J_{ec}) are the densities of currents of ions (electrons) due to diffusion (indices “DF”), drift (indices “DR”), and convection (indices “C”); Φ_i is the electric field potential, POT_z is the potential of the probe relatively the plasma, TA is the ratio of T_e/T_i , N_i (N_e) are the densities of ions (electrons). All the values are dimensionless, the values of J_e are divided by $\sqrt{500\tau}$. The results are in a good agreement with the ambipolar diffusion formulae [4].

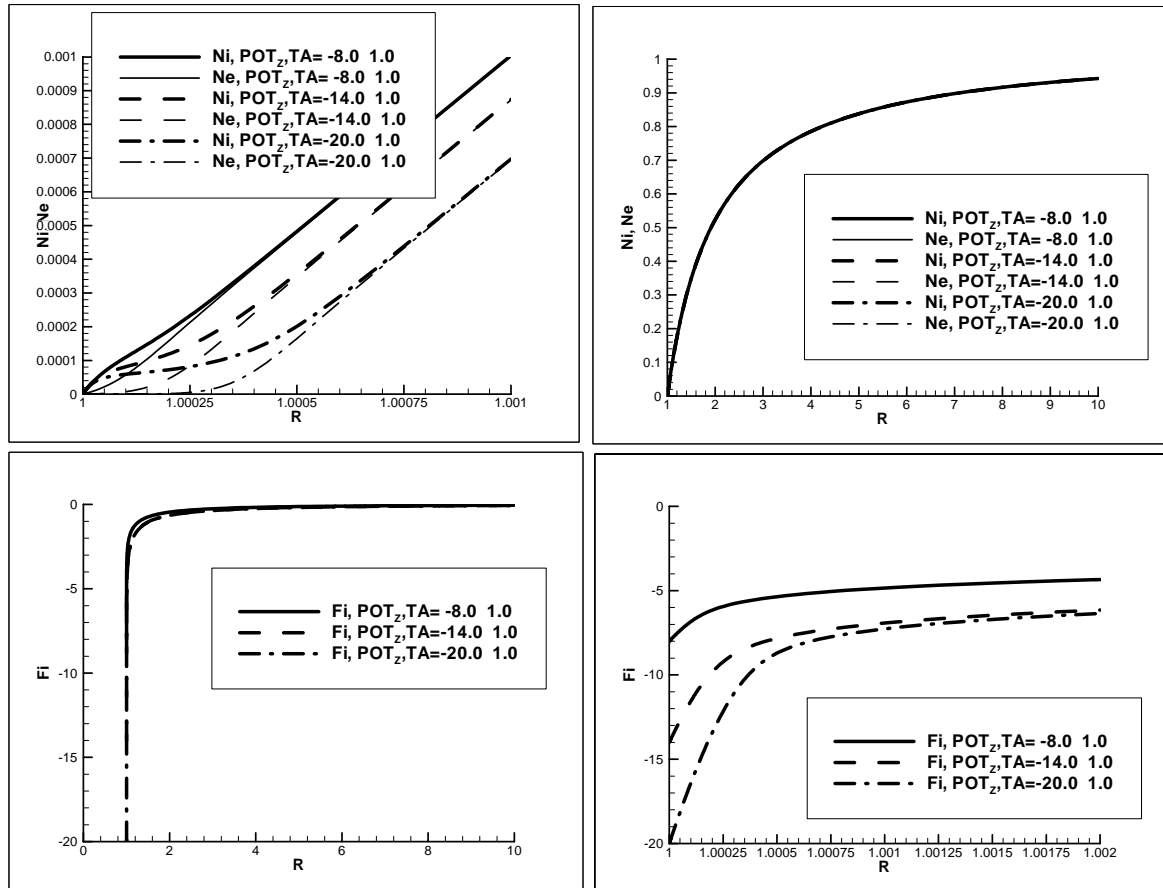


Fig.1. Spatial electron and ion density distribution (upper figures), potential distribution (lower figures) around probe in case of different value of probe potential.

$$\varepsilon_\phi = 10^{-12} \quad \varepsilon_i = 1, \quad \varepsilon_e = \sqrt{500\tau}$$

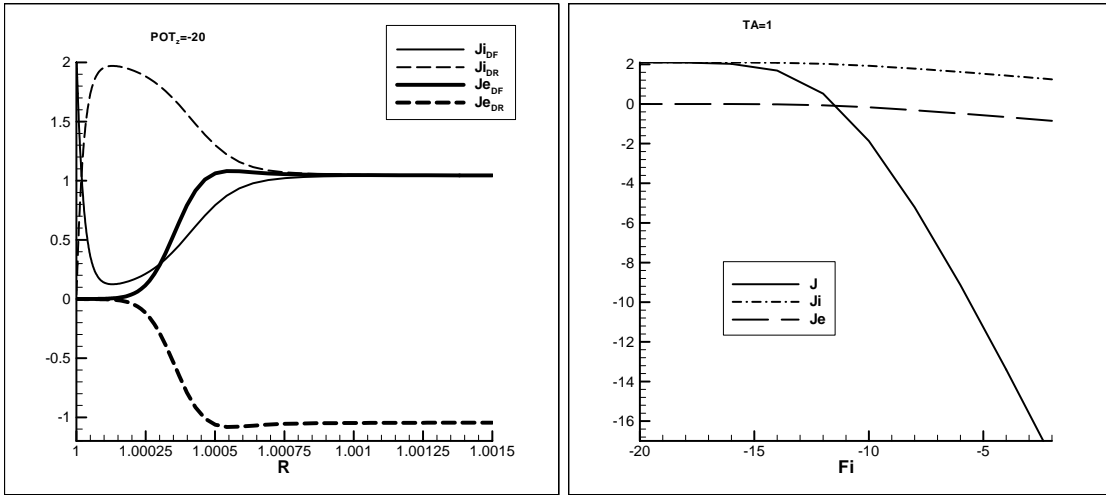


Fig.2. Spatial electron and ion current density distribution in case of $\varphi = -20$, the probe voltage-current characteristic and its components (from left to right). $\varepsilon_\varphi = 10^{-12}$, $\varepsilon_i = 1$, $\varepsilon_e = \sqrt{500\tau}$.

2.2. Plasma flow. Cylindrical symmetry

The computations were carried out for $\alpha = 1$ (cylindrical symmetry), at $Re = \varepsilon_i^{-1}$, $\varepsilon_e = \sqrt{500\tau}\varepsilon_i$. The plasma perturbation zone around an electric probe can be divided into three main regions [4]. The space-charge region (Debye sheath) adjoins to a probe directly. In this region it is impossible to neglect separation of charges, i.e. the solution of the Poisson equation is necessary. The sheath width depends on the value of Debye radius r_d and also the value of applied voltage.

The quasineutral layer is located further (diffusion region), in which charge separation is small, the Poisson equation is superfluous, and charge transfer by ambipolar diffusion is essential. The thickness of this region depends on the magnitude of electrical Reynold's number

Behind diffusion region there is the layer of quasineutral nonviscous flow (drift region) with the thickness about a probe radius, in which drift of charge particles in electrical field is main process of current collection.

Saturation mode.

The spatial profiles of parameters and the voltage-current characteristic for the classical [4] case of small Debye layer (as compared to the diffusion layer), which corresponds to current saturation, is shown in Fig.3-4. One can see that the voltage drop in the quasi-neutral zone amounts here to 30...50%. Note that earlier estimates [1] yielded a complete domination of the Debye layer drop under these conditions ($\varepsilon Re^2 = 10^{-6} \ll 1$).

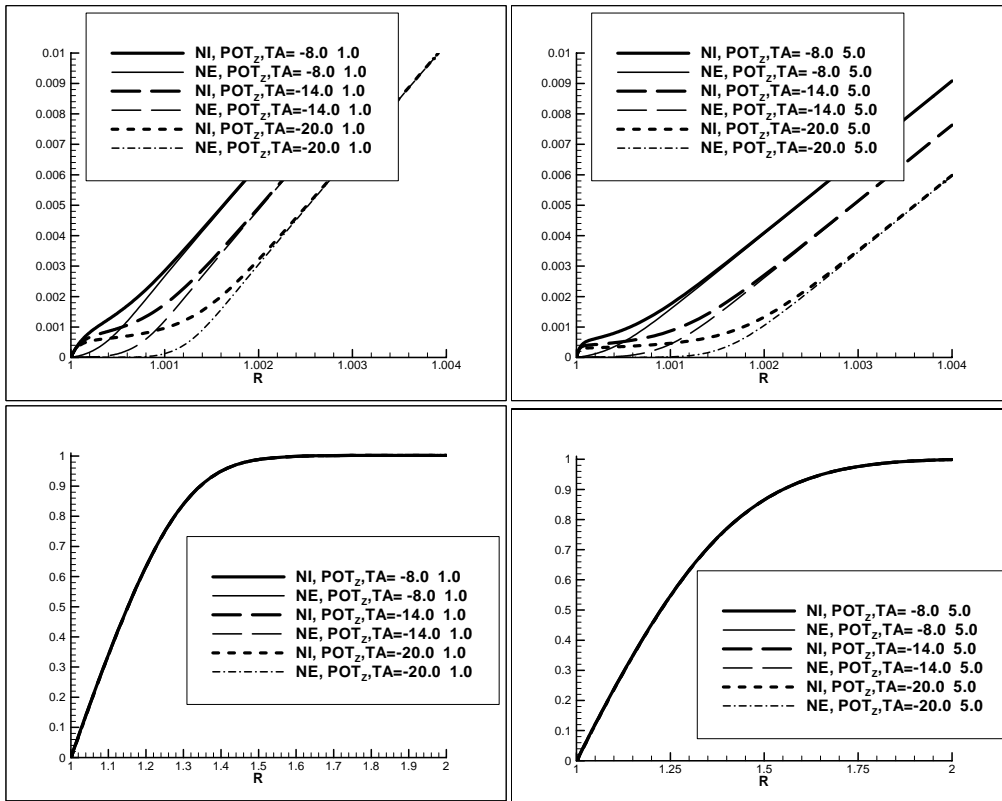


Fig.3. Spatial electron and ion density distribution around probe in case of different value of probe potential. $\epsilon = 10^{-10}$, $Re = 10^2$.

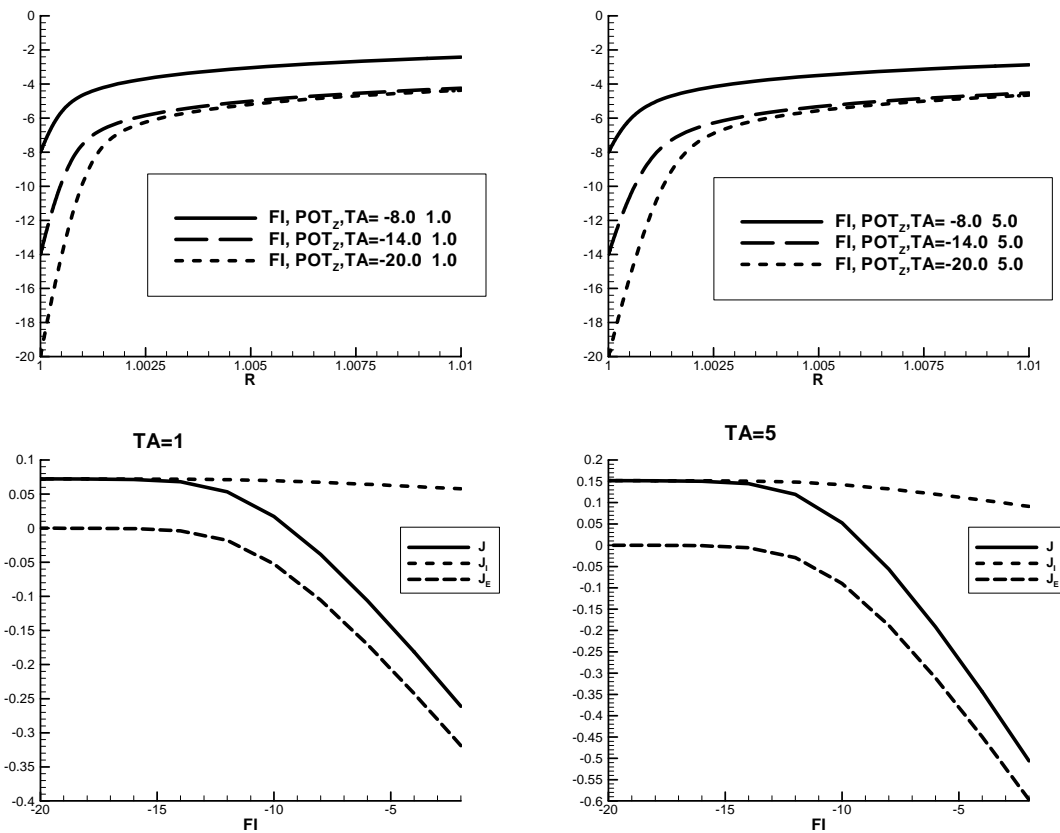


Fig.4. Spatial potential distribution and probe characteristic. $\epsilon = 10^{-10}$, $Re = 10^2$.

Intermediate mode.

In accord with [1,2], the plasma-probe interaction parameters must depend only on εRe^2 . However, computations presented below have shown that this parameter is not the only one: modes with different values of the ratio of the Debye and the diffusion probes $a = \sqrt[3]{\varepsilon} \sqrt{Re}$ appear to be considerably different. Results of computations for two cases with different values of a (0.68 and 1.47) with the same $\varepsilon Re^2 = 100$ ($\varepsilon = 10^{-8}$, $Re = 10^5$ and $\varepsilon = 10^{-4}$, $Re = 10^3$) are presented in fig. 5 and fig.6.

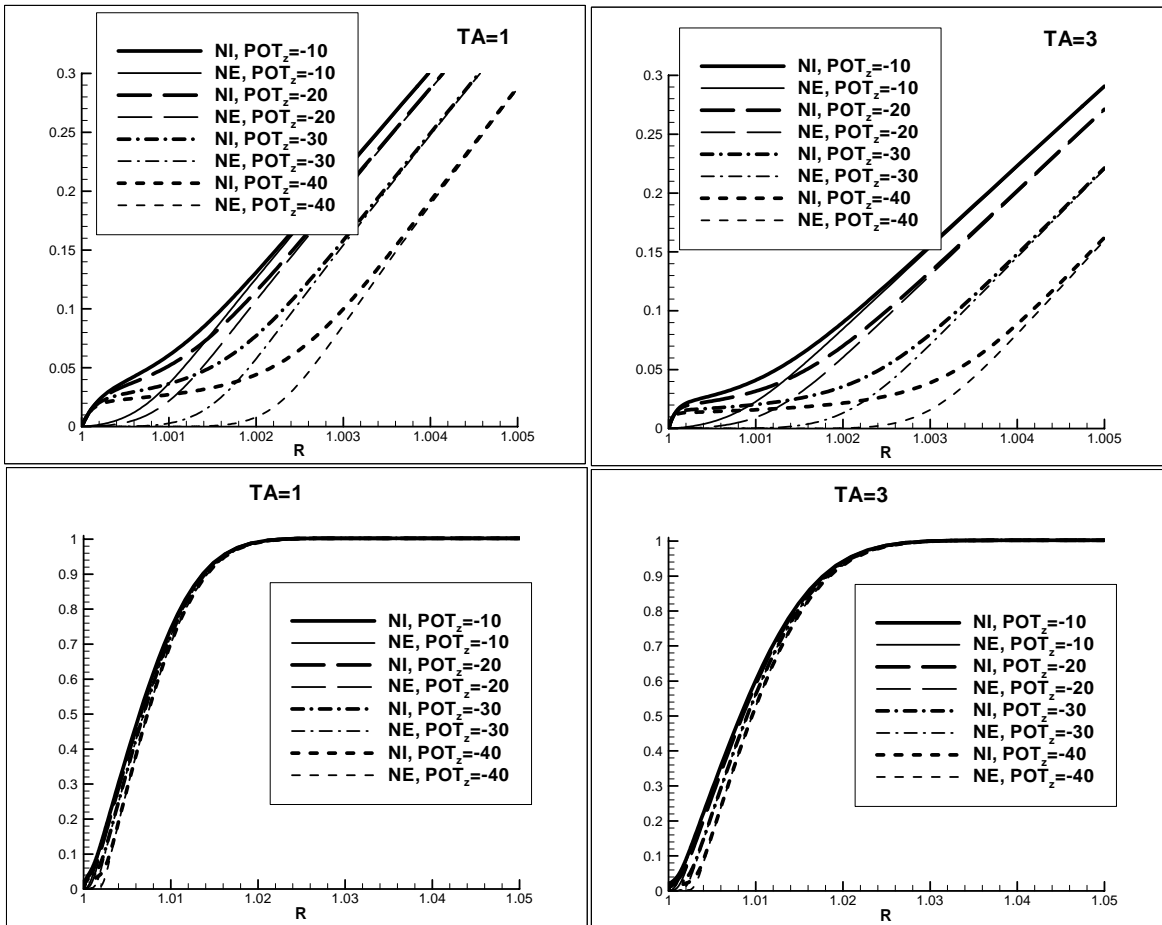


Fig.5. Spatial electron and ion density distribution around probe in case of different value of probe potential. $\varepsilon = 10^{-8}$, $Re = 10^5$

The first case the Debye layer size amounts to 10% of the diffusion layer, i.e. the situation is close to the current saturation mode, but the diffusion layer becomes shorter with voltage growth (due to the growth of the Debye layer size), which gives a slowly rising voltage current characteristic at saturation (Fig.6). Note that the probe current depend on τ : at $\tau = 1$ it is about twice as less than that at $\tau = 3$.

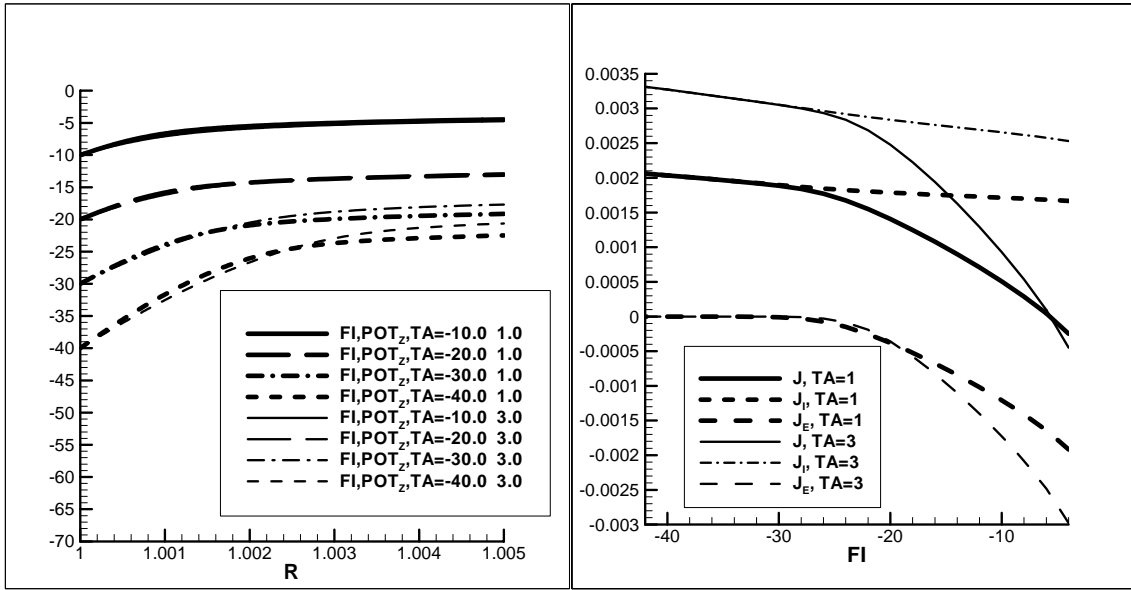


Fig.6. The probe voltage-current characteristic and it's components in case of isothermal (TA=1) and nonisothermal (TA=3) plasma. $\epsilon = 10^{-8}$, $Re = 10^5$

In the second case the sizes of the Debye and diffusion layers (Fig.7) are close to each other; no quasi-neutral diffusion layer is formed. The main voltage drop corresponds to the Debye layer.

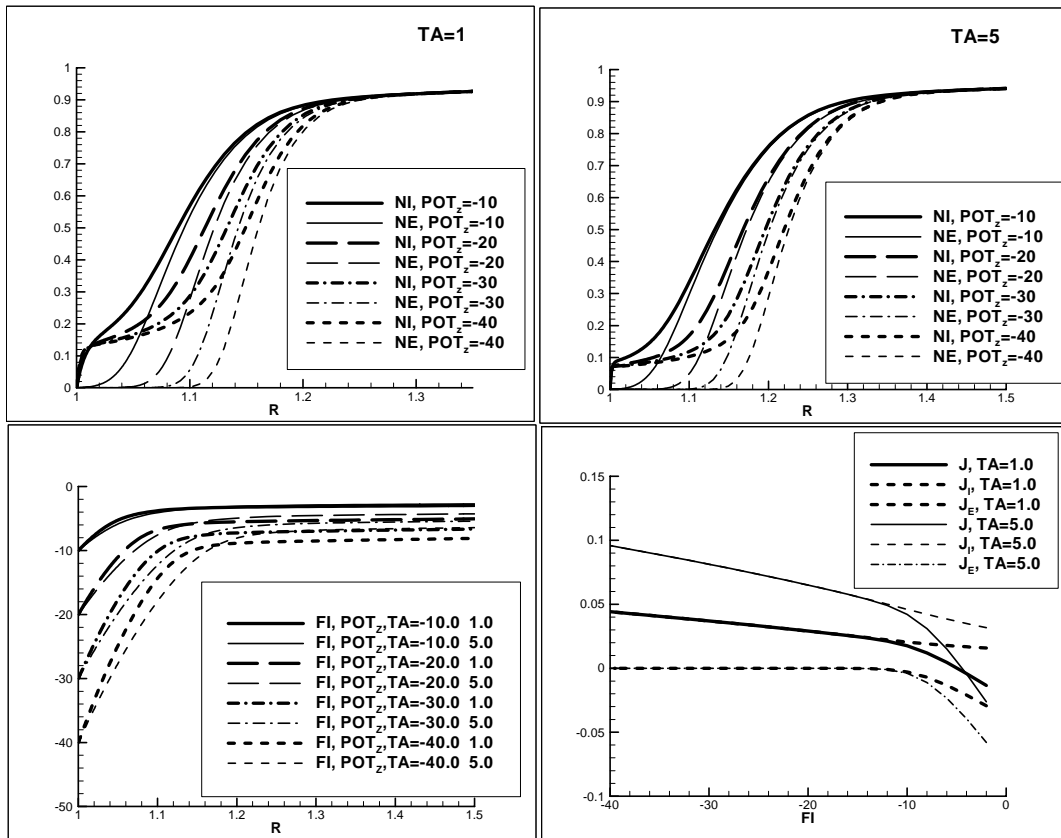


Fig.7. Spatial electron and ion density, potential distribution around probe in case of different value of probe potential. $\epsilon = 10^{-4}$, $Re = 10^3$

The ion probe current grows with growth of the probe voltage due to growth of the Debye layer. Instead of saturation one can observe a fall of the voltage current characteristic slope for 3...5 times.

Note that from the viewpoint of the earlier analytical works [2,3] these two cases are the same.

Fig.8 shows the case of $\varepsilon = 10^{-4}$, $Re = \frac{10^4}{3}$, in which the diffusion layer is absent at all.

About a half of the total voltage falls in the unperturbed flow region, the current slope change is much less than in the previous cases. The diagnostic problem is difficult to be solved here.

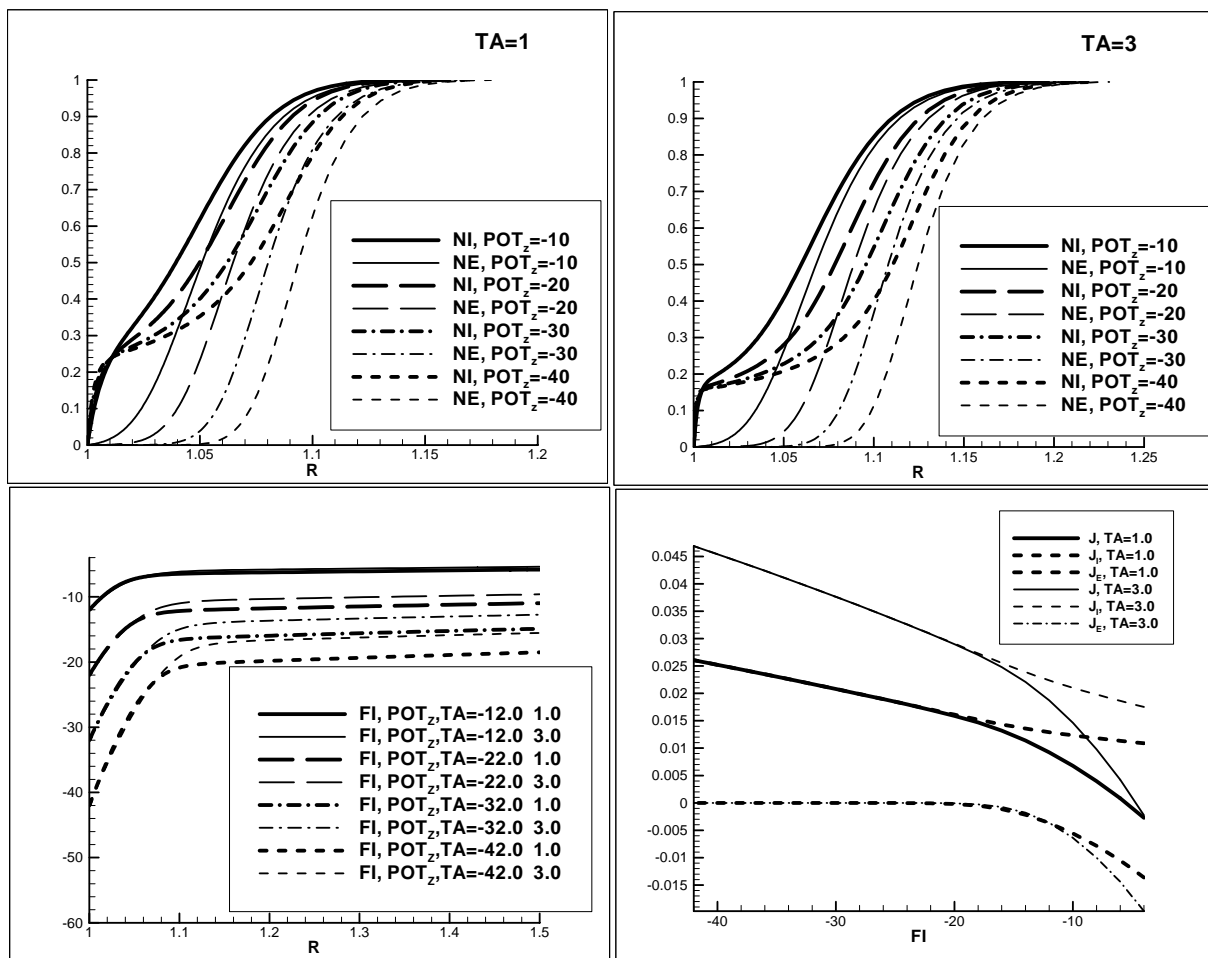


Fig.8. Spatial electron and ion density, potential distribution and probe characteristic.
 $\varepsilon = 10^{-4}$, $Re = 10^4/3$

Thus, significant differences with the analytical estimates [1, 4] have been observed. E.g, the spatial profiles of parameters and the voltage-current characteristic for the classical [1] case of small Debye layer (as compared to the diffusion layer), which corresponds to current saturation, have shown that the voltage drop in the quasi-neutral zone in case of flow plasma amounts here to 30...50%. Note

that earlier estimates [2] yielded a complete domination of the Debye layer drop under these conditions. For intermediate values of ratios of Debye to diffusion sizes, a considerable impact of the relative probe size is observed. Note that from the viewpoint of the earlier analytical works [2] these two cases are the same.

§ 3. Comparison with experimental data

The previous computations corresponded to the longitudinal positioning of the probe, which corresponds to the probe axis parallel to the flow velocity. Consider now the results of computations on base of the model (1), (2) for longitudinal and transversal cylindrical probes under conditions corresponding to the experiments with the pulsed plasmatrons (Fig. 9 - 15.).

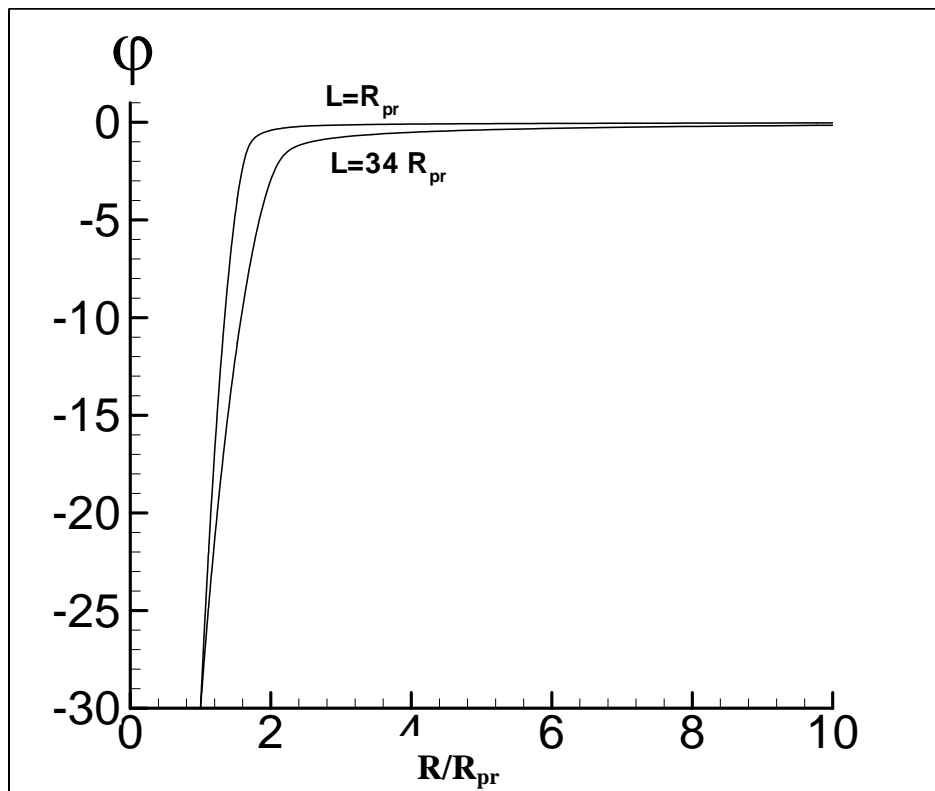


Fig.9 Radial potential distribution around the longitudinal probe, V , for two values of the axial coordinate L .

$R = 0.15 \text{ mm}$, $T = 5000 \text{ K}$, $N = 4 \cdot 10^{17} \text{ cm}^{-3}$, $v = 660 \text{ m/s}$, $D_i = 70 \text{ cm}^2/\text{s}$, $N_i = 4 \cdot 10^{12} \text{ cm}^{-3}$, $U = 30 \text{ V}$

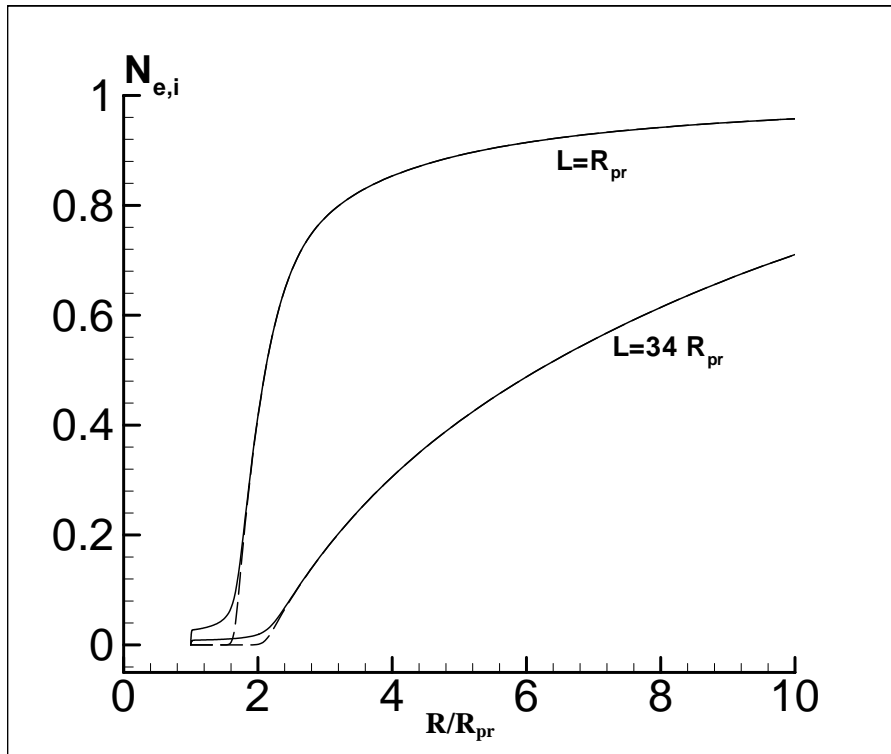


Fig.10. Radial distributions of relative densities of ions (solid lines) and electrons (dashed lines) around the longitudinal probe for two values of the axial coordinate L .

$R = 0.15 \text{ mm}$, $T = 5000 \text{ K}$, $N = 4 \cdot 10^{17} \text{ cm}^{-3}$, $v = 660 \text{ m/s}$, $D_i = 70 \text{ cm}^2/\text{s}$, $N_i = 4 \cdot 10^{12} \text{ cm}^{-3}$, $U = 30 \text{ V}$

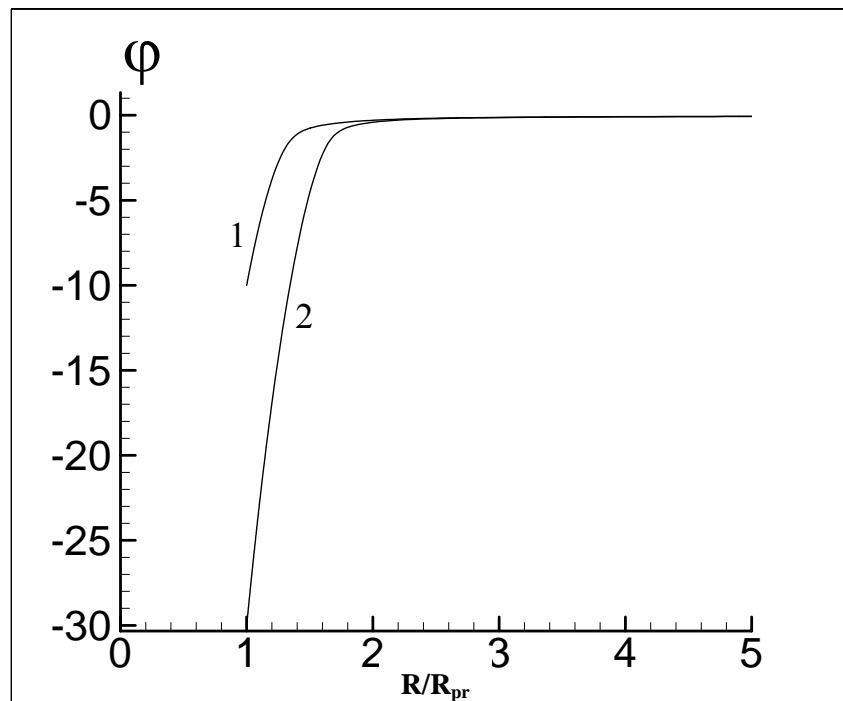


Fig.11. Radial potential distribution around the transversal probe, V , for two values of the probe potential: 1 – $U = 10 \text{ V}$, 2 – $U = 30 \text{ V}$.

$R = 0.15 \text{ mm}$, $T = 5000 \text{ K}$, $N = 4 \cdot 10^{17} \text{ cm}^{-3}$, $v = 660 \text{ m/s}$, $D_i = 70 \text{ cm}^2/\text{s}$, $N_i = 4 \cdot 10^{12} \text{ cm}^{-3}$

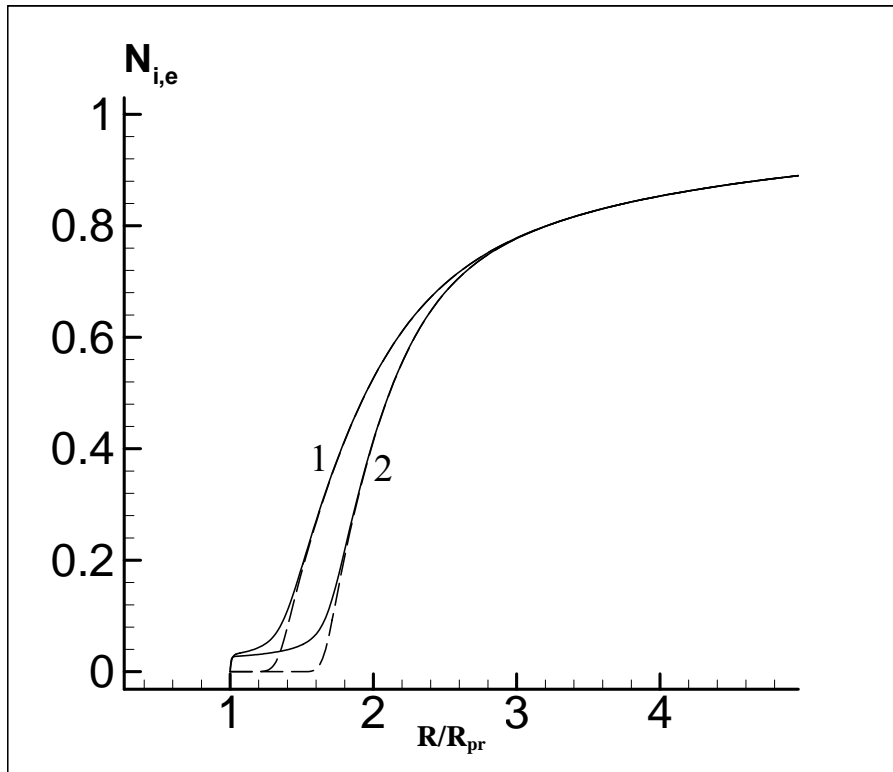


Fig.12. Radial distributions of relative densities of ions (solid lines) and electrons (dashed lines) around the transversal probe for two values of the probe potential: 1 – $U=10$ V, 2 - $U=30$ V. $R = 0.15$ mm, $T = 5000$ K, $N = 4 \cdot 10^{17}$ cm^{-3} , $v=660$ m/s, $D_i = 70$ cm^2/s , $N_i = 4 \cdot 10^{12}$ cm^{-3}

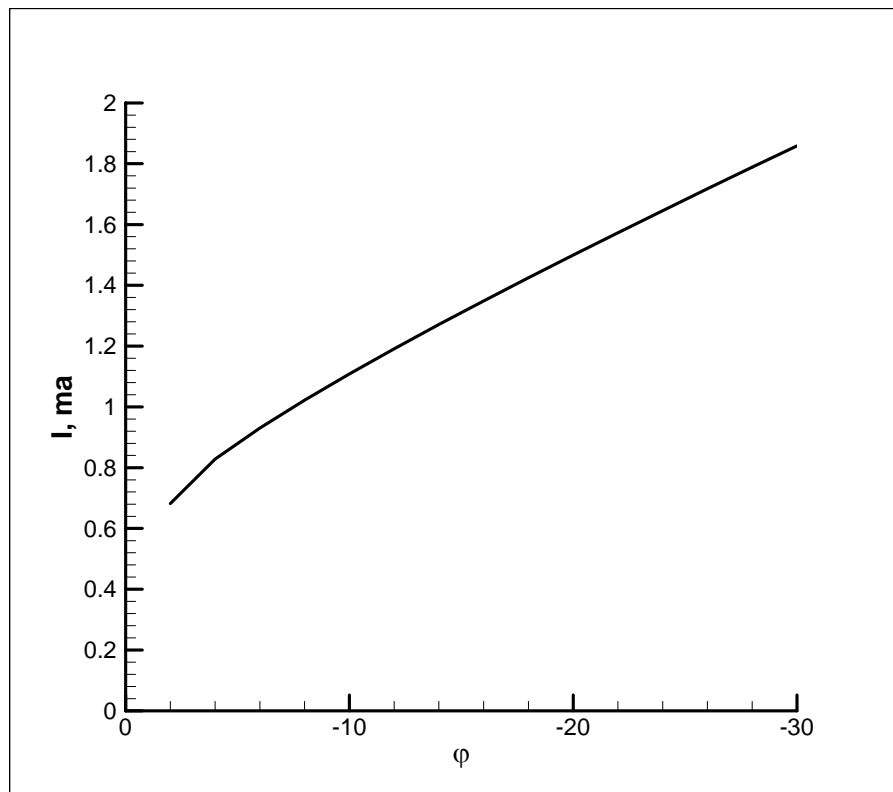


Fig.13. The computed voltage-current characteristic of the transversal cylindrical probe $R = 0.15$ mm, $T = 5000$ K, $N = 4 \cdot 10^{17}$ cm^{-3} , $v=660$ m/s, $D_i = 70$ cm^2/s , $N_i = 4 \cdot 10^{12}$ cm^{-3}

Comparison of the computed and measured parameters (including the voltage-current characteristics of the transversal cylindrical probe, and the computed and measured ion currents on the longitudinal and transversal cylindrical probes over the probe length, Fig.14, shows a reasonable correlation.

The last graph shows however that experimental ion currents for longitudinal and transversal cylindrical probes deviate much less than the computed ones. It may result from the fact that in experiments the truly longitudinal mode of the probe operation was not achieved: for so doing it would be necessary to provide very low turbulence and a highly parallel flow. The mode became closer to the transversal one at very low values of the angle between the probe axis and the flow. Due to these peculiarities, the longitudinal probes seem to be less applicable for the diagnostic purposes.

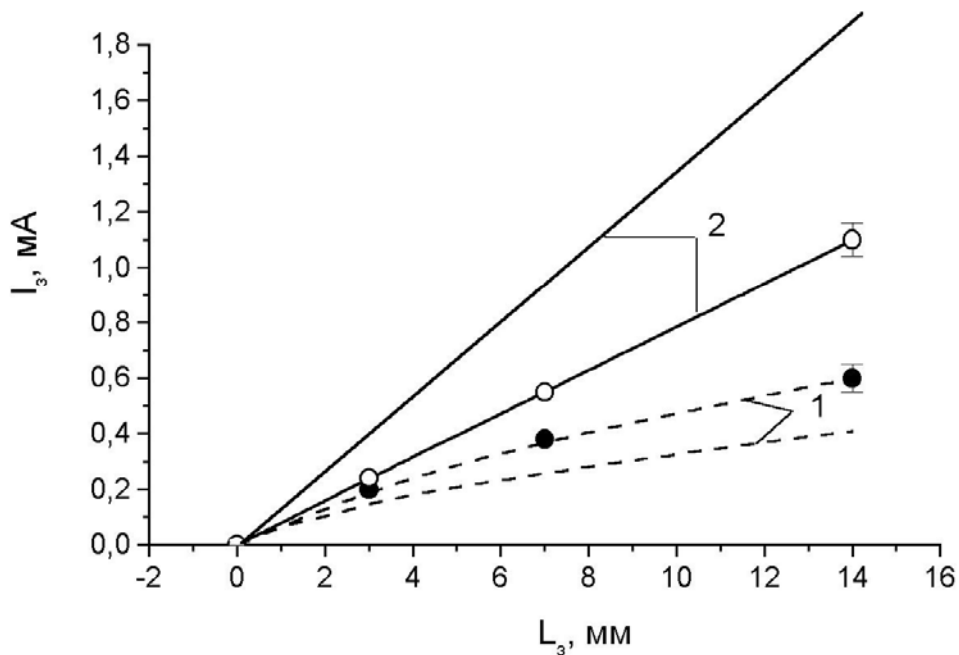


Fig.14. Comparison of the computed (lines) and measured (points with lines) ion currents on the longitudinal (1) and transversal (2) cylindrical probes over the probe length.
 $R_{pr} = 0.15$ mm, $T=5000$ K, $N = 4 \cdot 10^{17}$ cm⁻³, $v=660$ m/s, $D_i = 70$ cm²/s, $N_i = 4 \cdot 10^{12}$ cm⁻³, $U = 30V$.

§ 4. Electron part of probe characteristic

The ion branch of the computed voltage current characteristics can be wrong because of deviations from the self-similarity of the longitudinal dependences of the concentrations. In future studies it can prove to be better to consider a model, in which the longitudinal dependences of the concentrations are neglected, and the longitudinal dependence of the flow velocity is accounted for.

The electron branches of the voltage current characteristics have been studied with use of the model. Characteristic results are presented in Figs.15 - 20. The main positive ion was supposed to be H_3O^+ with the mobility at the atmospheric pressure being $\mu_1 = 8 \cdot 10^{-4} \text{ m}^2/(\text{V s})$, the electron mobility was taken to be $0,4 \text{ m}^2/(\text{V s})$, $T_g = 3000 \text{ K}$, $T_e = 3000 \text{ K}$.

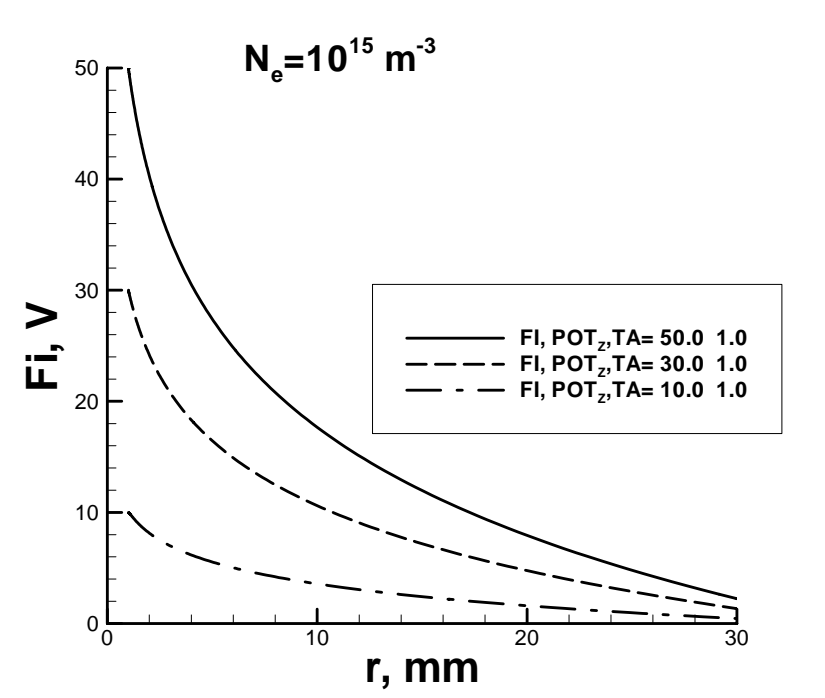


Fig.15. The spatial profiles of electric potential around probe
 $T_e/T = 1, n_e = 10^{15} \text{ m}^{-3}$

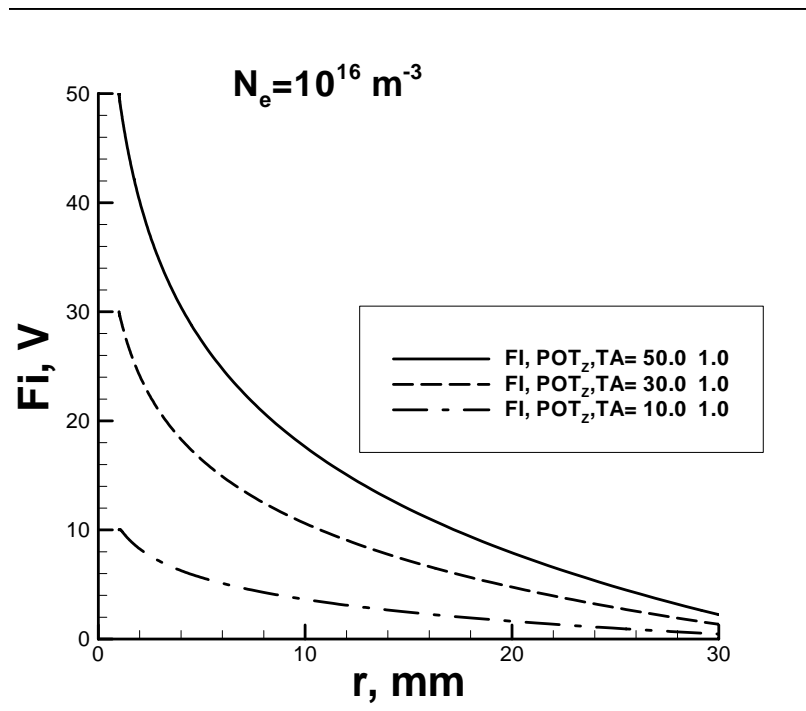


Fig.16. The spatial profiles of electric potential around probe.
 $T_e/T = 1, n_e = 10^{16} \text{ m}^{-3}$

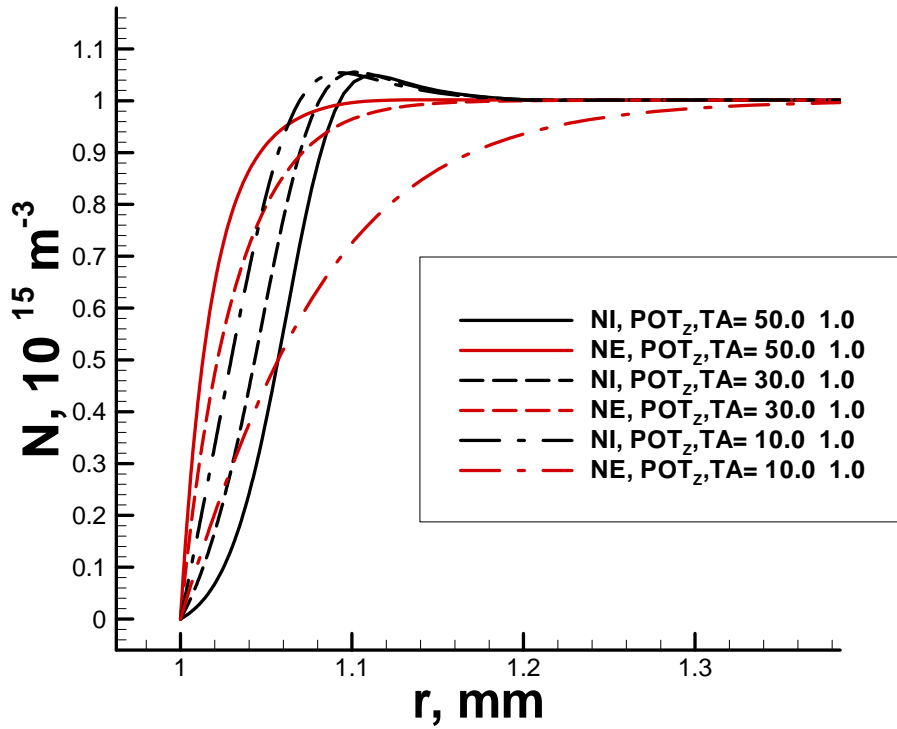


Fig.17. The spatial profiles of ion and electron densities around probe.

$$T_e/T = 1, n_e = 10^{15} \text{ m}^{-3}$$

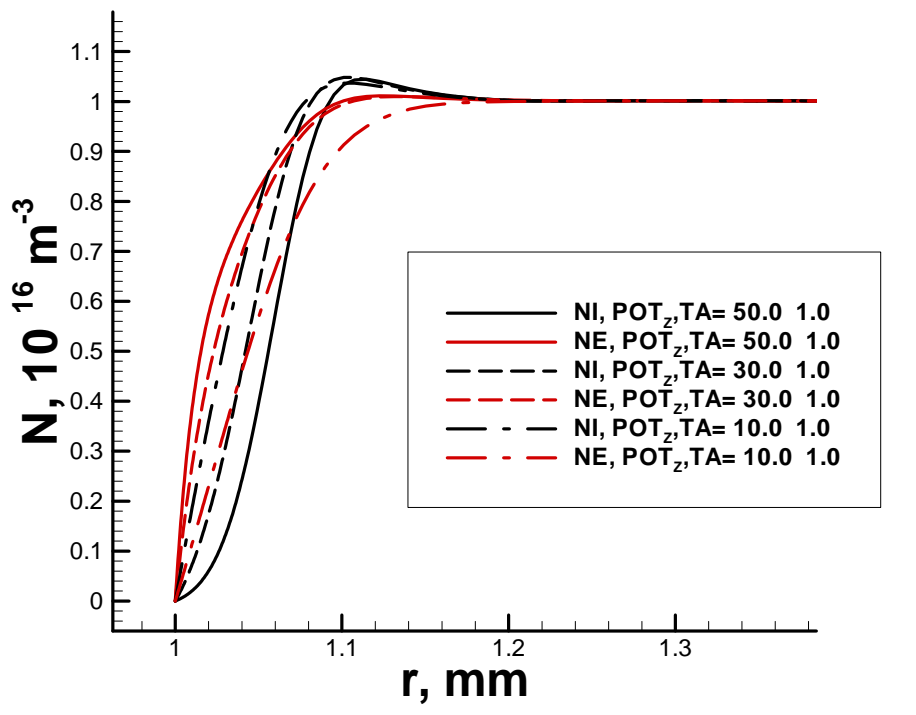


Fig.18. The spatial profiles of ion and electron densities around probe.

$$T_e/T = 1, n_e = 10^{16} \text{ m}^{-3}$$

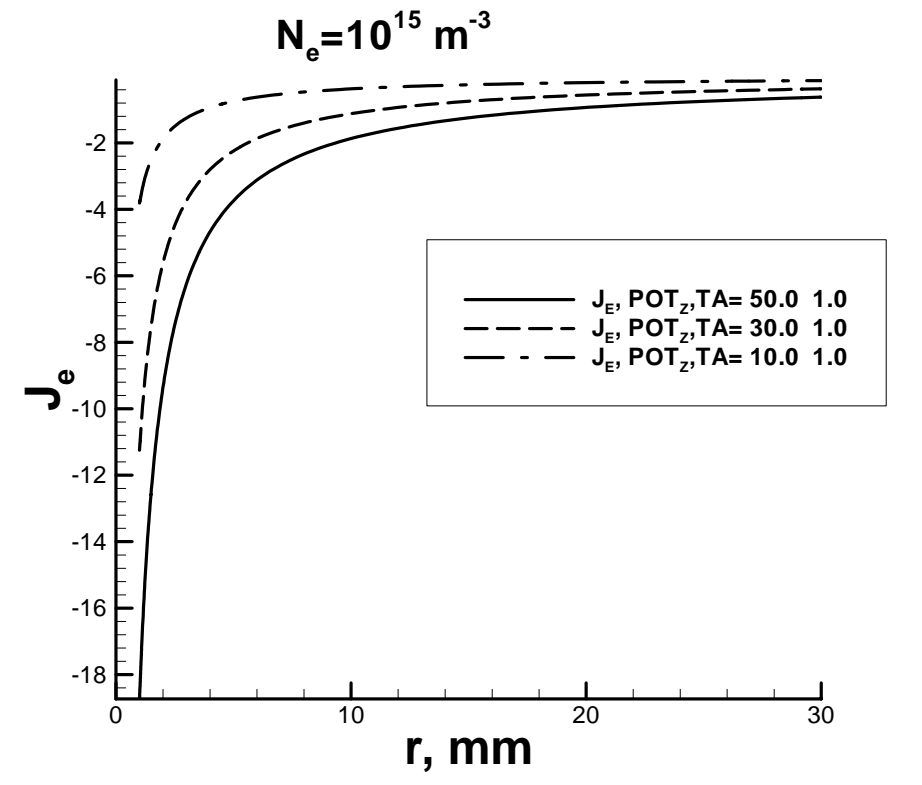


Fig.19. The spatial profiles of electron probe current at different probe potentials.
 $T_e/T = 1, n_e = 10^{15} \text{ m}^{-3}$.

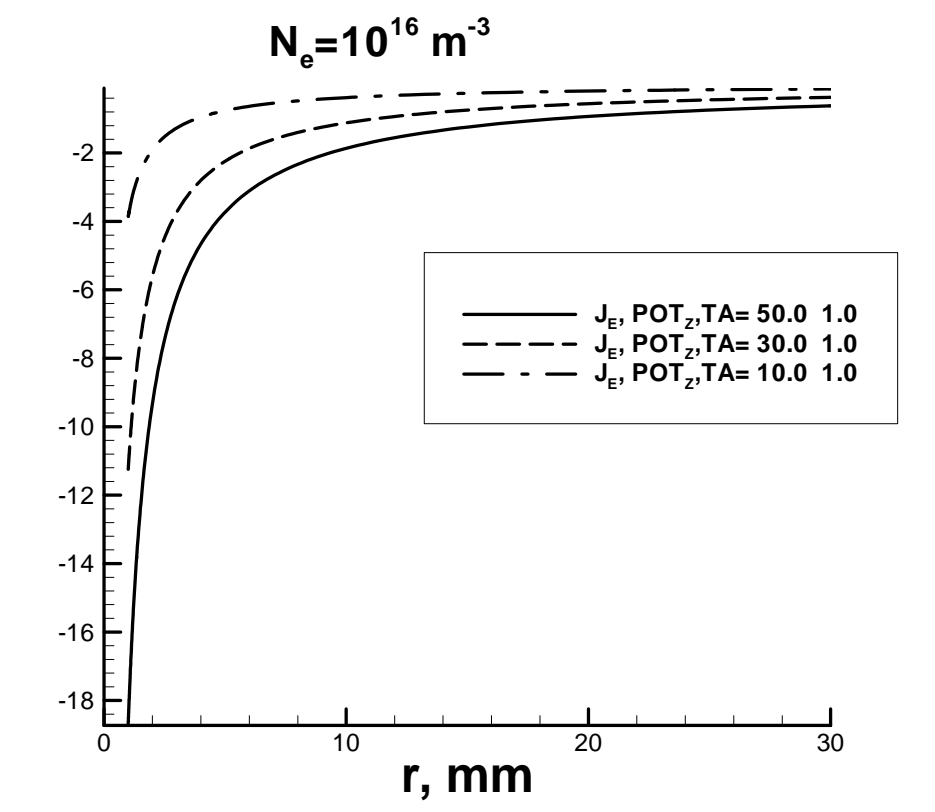


Fig.20. The spatial profiles of electron probe current at different probe potentials.
 $T_e/T = 1, n_e = 10^{16} \text{ m}^{-3}$.

One can conclude that under the conditions characteristic for the flame plasmas the voltage current characteristics are primarily defined by the electron drift in the plasma region. Note that the same conclusion has been worked out for these regimes as a result of the analytical studies for the transversal probes (see above).

REFERENCES

1. Benilov M.S. Theory of Electrical Probes in Flows of High Pressure Weakly Ionized Plasma (review). High Temperature. Vol. 26, No. 5, 1988, pp. 780-793 /Бенилов М.С. Теория электрических зондов в потоках слабоионизированной плазмы высокого давления. ТВТ.- Т. 26, №5.- 1988. С. 993-1003/
2. Neil Stahl, C.H.Su. Theory of Continuum Flush Probes. THE PHYSICS OF FLUIDS, V.14, N 7, p.1366-1376, 1971.
3. Г.Шлихтинг. Теория пограничного слоя. М. Наука. 1974
4. Chung P., Talbot L., Touryan K. Electric probes in stationary and flowing plasmas: Theory and application. New York. Springer-Verlag. 1975

CHAPTER Y.
METHODS OF THE DETECTION OF THE IGNITION PROCESS
AND MEASUREMENTS OF PLASMA PARAMETERS
OF A DISCHARGES IN A SUPERSONIC FLOW

§ 1. Spectroscopic method of the detection of the ignition process

1.1 Spectroscopic temporary measurement of relative intensities of active radicals in plasma of pulsed transversal discharge in a supersonic propane-air flow

Analysis of the radiation spectra of the transversal discharge in the supersonic air-propane mixture flows has shown that the atomic components (O, H, N), active radicals (CN, CH, OH) and molecules (C₂, N₂) were observed in condition at which the ignition take place.

The temporary measurements of relative intensities of various components were investigated for definition of the fact of ignition. Experiment was put as follows.

The measurements were performed in pulse mode of discharge. Quartz tube was used as combustor section of channel (see Chapter I, Fig.1.2). The temporal intensity of spectral lines or molecular bands were measurement by photoelectron amplifier at the large distances $z = 30$ cm (from the electrodes downstream. Such value of z exceeds the discharge length. Radiation signal propagates after electric breakdown of interelectrode gap practically instantly over the quartz tube, which carry out a role of optical lighthguide. The flow if there was an ignition, carries away a zone of burning. Intensity of weakened discharge radiation signal is closed to intensity of plasma of a flame. It allows in one measurement registering evolution of radiation of the plasma of the discharge chosen components and if there was an ignition, plasmas of a flame. Time evolution of a component which intensity of radiation is small in the discharge and is great in a flame, will allow defining the fact of ignition.

The temporary measurements of the luminescence of above mentioned components have shown that the evolution of radiation of components at the distances $z = 30$ cm from the electrodes downstream has been different. Luminescence of atomic components and CN ($\lambda = 380$ nm) has been observed for the discharge in supersonic airflow without propane. With addition of the propane the intensities of atomic components and CN varied.

So, a violet system of CN bands is present in the discharge radiation both of the air and air - propane mixture. The band (0,0) of this system at $\lambda = 3883 \text{ \AA}$ is the brightest. Waveforms of

intensity of this band (Fig 5.1) show that the intensity of the band rises with the rise of pulse duration in the case of the discharge in air-propane mixture.

Breakdown

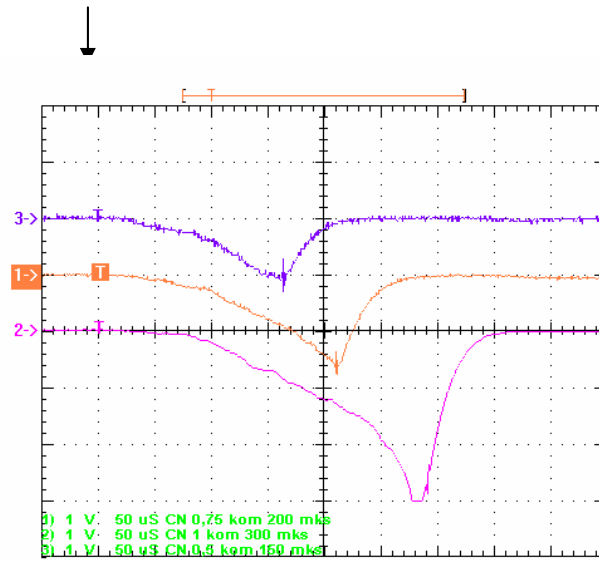


Fig.5.1 Waveforms of luminescence of CN ($\lambda = 3883 \text{ \AA}$) in plasma of the pulsed transversal discharge in air + propane supersonic flow. $P_0 = 4 \text{ atm}$, $p = 200 \text{ Torr}$.

3 - $\tau = 160 \mu\text{s}$, $I \approx 40 \text{ A}$, 1 - $\tau = 210 \mu\text{s}$, $I \approx 25 \text{ A}$, 2 - $\tau = 290 \mu\text{s}$, $I \approx 20 \text{ A}$.

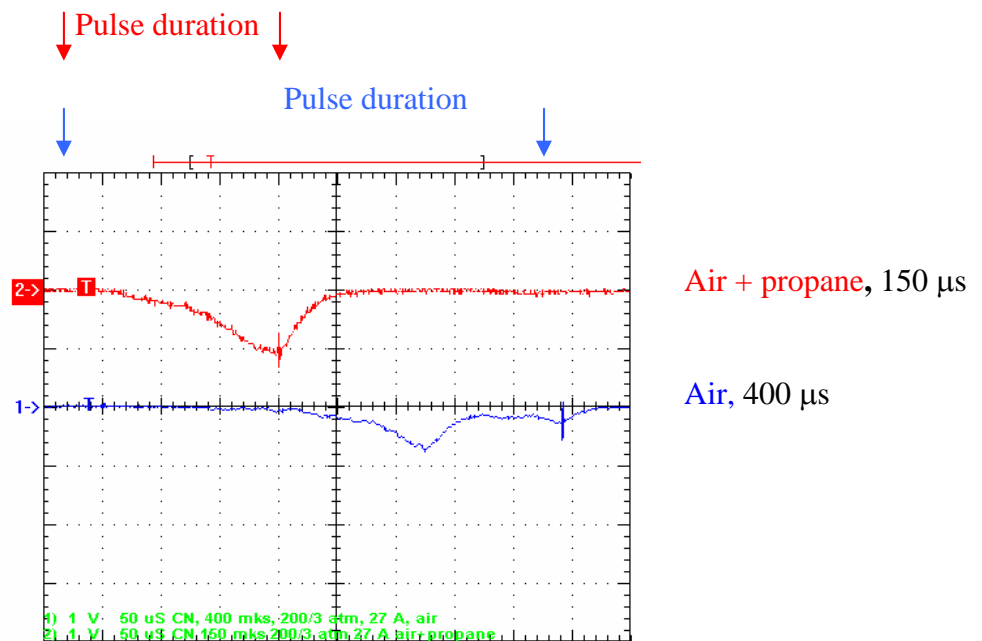


Fig.5.2. Waveforms of luminescence of CN ($\lambda = 3883 \text{ \AA}$) in plasma of the pulsed transversal discharge in air and air+propane supersonic flow.

1 – air, $\tau = 400 \mu\text{s}$, 2 – air+propane, $\tau = 150 \mu\text{s}$, $P_0 = 4 \text{ atm}$, $p = 200 \text{ Torr}$, $I \approx 27 \text{ A}$

This rise is observed even at decreasing of the discharge current. At the same time the band intensity in air is noticeably smaller than the band intensity for air-propane mixture even at long current duration and high values of current $I \approx 40 - 30$ A (Fig. 5.2).

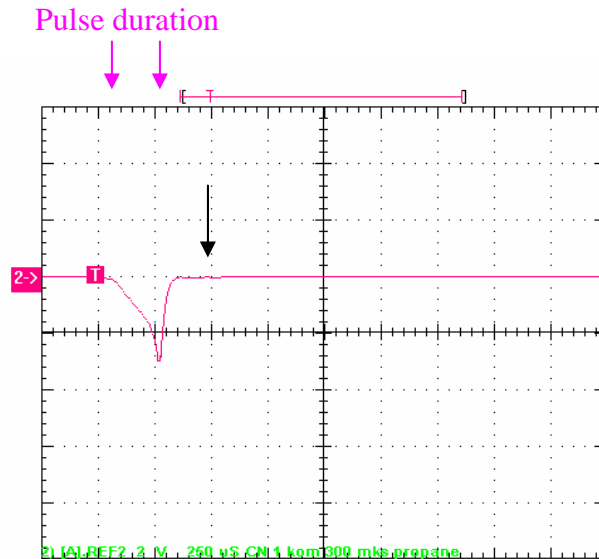


Fig.5.3. Waveforms of luminescence of plasma (4315 Å, CN) in plasma of the pulsed transversal discharge in the supersonic flow in the air-propane mixture.

$P_0 = 4$ atm, $p = 200$ Torr, $I = 20$ A, $\tau = 270$ μ s, $Z = 25$ cm. Scale factor: 250 μ s/div.

However, the radiation in all the cases drops to zero rather quickly (at typical time of about 50 μ s) after shut downing of the discharge pulse. As result CN radiation cannot be detected at distances of $z = 20 - 30$ cm from the electrodes downstream (Fig.5.3). The corresponding moment was shown by arrowed line on Fig.5.3. It means that CN radicals does not make any considerable input namely to the flame radiation.

The band of active radicals CH ($\lambda = 431,5$ nm) have proved to be the most convenient for detection of air-propane mixture ignition.

Typical waveforms of plasma luminescence $\lambda = 431,5$ nm in the pulsed transversal discharge in supersonic flow are presented in Fig.5.4. Experiments were carried out in cases of air, propane and air-propane mixture for different pulse duration at the following fixed parameters: the receiver pressure $p_0 = 4$ atm, the chamber pressure $p = 200$ Torr, the discharge current $I = 8$ A, the inter-electrode separation $L = 15$ mm , the axial coordinate $z = 25$ cm downstream the electrodes.

In case of airflow (curve 3, pulse duration $\tau = 200$ μ s), propane-flow (curve 6, pulse duration $\tau = 300$ μ s), or propane-air flow with short pulse duration (curve 4, $\tau = 100$ μ s) the

intensities of plasma radiation were very small. The increase of pulse duration is higher than some critical size (curves 5, $\tau = 150 \mu\text{s}$ and 2, $\tau = 200 \mu\text{s}$) results in a dramatic growth of the plasma radiation. These jump of plasma radiation appearance we connect with the fact of the ignition realization.

Breakdown

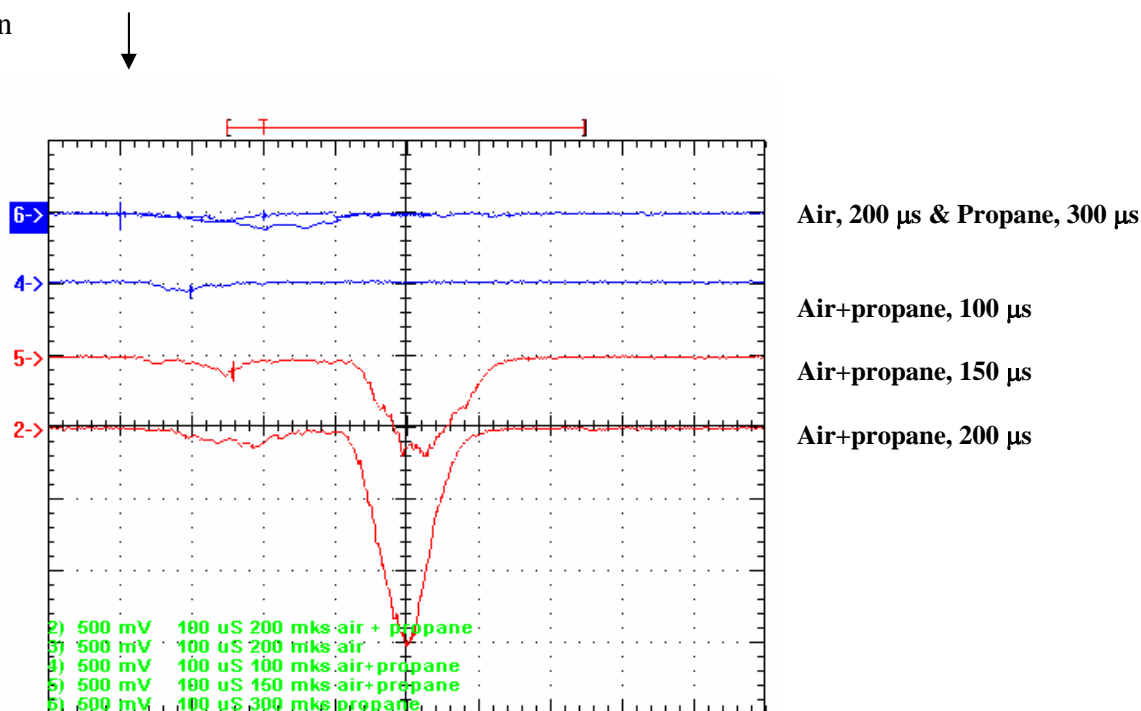


Fig. 5.4. Waveforms of plasma luminescence (4315 \AA , CH) in the pulsed transversal discharge in the supersonic flow in the air, propane and the air-propane mixture.

$P_0 = 4 \text{ atm}$, $p = 200 \text{ Torr}$, $I = 8 \text{ A}$. Axial coordinate $Z = 25 \text{ cm}$. Scale factor: $100 \mu\text{s}/\text{div}$.

Thus, the evolution of luminescence of CH can be used to testify the fact of ignition of a propane-air supersonic flow by pulse electric discharge.

1.2 Temporary measurement of relative intensities of active radicals in plasma jet, injected in a supersonic propane-air flow

Analysis of the radiation spectra in plasmadynamic discharge in supersonic air and air-propane mixture flow has been made. This analysis has shown that rich spectra were observed, in which the atomic components (O, H, N), active radicals (CN, CH, OH), molecules (C_2 , N_2) and other components were presented.

The temporary measurements of the luminescence radiation of components, observed in plasma of hydrocarbon flame (CH and C_2) have been produced to indicate the burning of

propane-air mixture. Experiments were carried out in cases of air and air-propane mixture at the following fixed parameters: the receiver pressure $P_0 = 4$ atm, the chamber pressure $p = 200$ Torr, the discharge capacity $C = 50 \mu\text{F}$. The discharge voltages were varied from 2.75 kV up 4.5 kV.

Breakdown

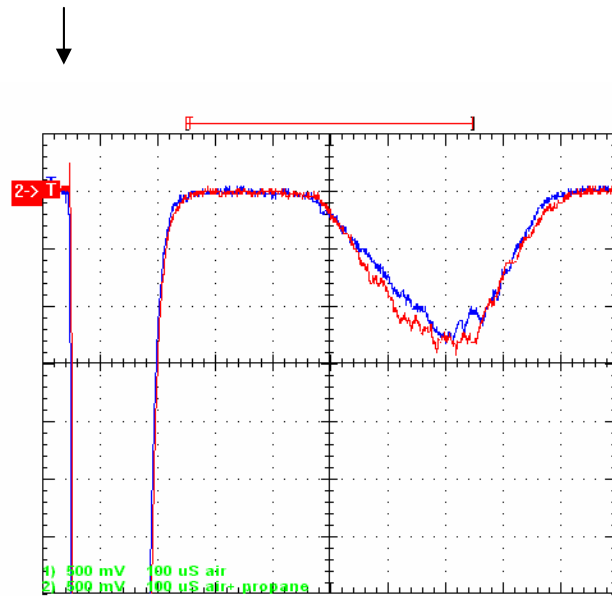


Fig. 5.5. Waveforms of luminescence of plasma ($\lambda=5165,2 \text{ \AA}$, C_2) at injection of plasmadynamic jet into supersonic propane-air flow. $U=2,75$ kV. $P_0 = 4$ atm, $p = 200$ Torr, stoichiometric propane-air ratio. $x= 32$ cm, scale factor: $100 \mu\text{s}/\text{div}$. Blue curve – airflow, red curve – air+propane mixture flow.

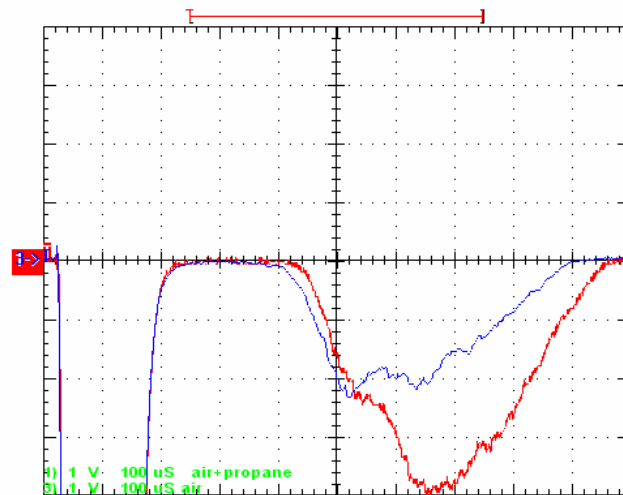


Fig. 5.6 Waveforms of a luminescence of plasma ($\lambda=5165,2 \text{ \AA}$, C_2) at injection of plasmadynamic jet into supersonic air and propane-air flow. $U=3,5$ kV. $P_0 = 4$ atm, $p = 200$ Torr, stoichiometric propane-air ratio. $x= 32$ cm, scale factor: $100 \mu\text{s}/\text{div}$. Blue curve – airflow, red curve – air + propane flow.

These measurements have been made at the distances $x \approx 30$ cm from the plasma generator downstream, at the moment $t \gg \tau$, where τ - the energy input pulse duration. Typical

value of τ was about 60 –70 μ s. During this time (on pulse stage) very high intensity of plasma luminescence was registered in all cases (see Fig.5.5 – 5.7).

The luminescence of C_2 ($\lambda=516$ nm) has been observed for the discharge in supersonic airflow without propane and for the discharge in supersonic propane-air mixture flow (Fig.5.5). The similar picture was observed for CH radical ($\lambda = 431$ nm). Thus, the luminescence of CH radicals was observed not only in a propane-air flow, but also in supersonic airflow as opposed to a case of pulse transversal discharge. An addition of the propane to result in changes the values of the intensities of C_2 and CH.

The difference between the intensity of luminescence of C_2 ($\lambda = 516$ nm) in supersonic airflow and air + propane mixture flow was observed at high values of input energy only (compare Fig.5.5 and Fig.5.6).

However, the luminescence of CH ($\lambda = 431$ nm) was change at all values of input energy (Fig.5.7).

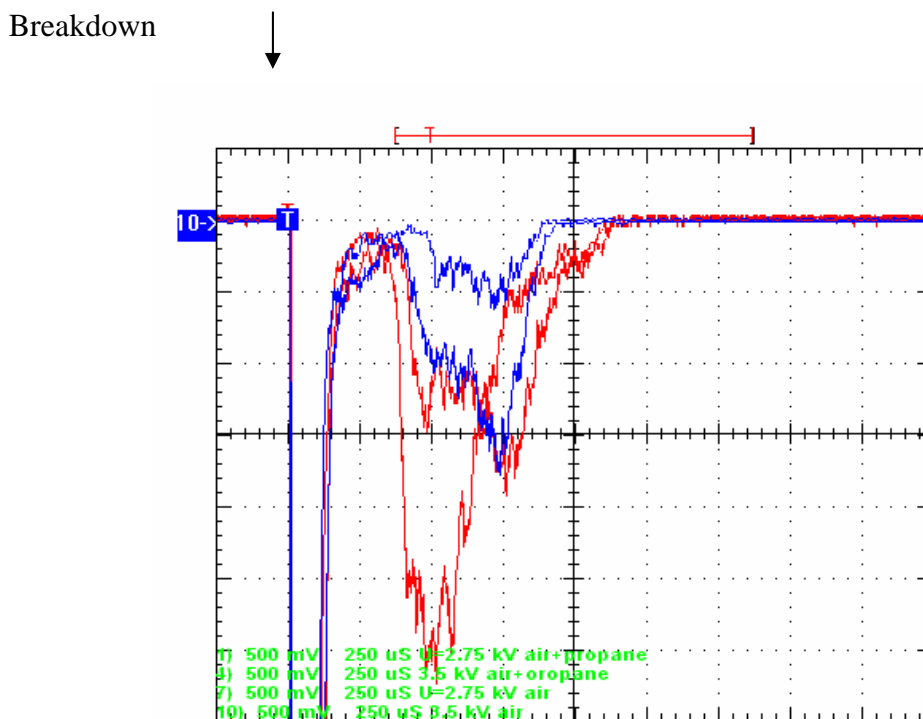


Fig. 5.7. The comparison of the waveforms of a luminescence of plasma ($\lambda=4315$ Å, CH) at injection of plasmadynamic jet into supersonic air and propane-air flow at two different discharge voltages ($U=2,75$ kV и $3,5$ kV).

$P_0 = 4$ atm, $p = 200$ Torr, $x = 32$ cm, scale factor: 250 μ s/div.

Blue curves: air, red curves: air + propane

Thus, the intensities of a band of active radical CH ($\lambda=431,5$ nm) was more convenient for detection of air-propane mixture ignition.

§ 2. Probe temporary measurements

If the length of transversal discharge along a flow is limited to some value, the zone of burning continuously drifts a flow. Therefore for definition of the fact of ignition it is necessary to divide in space the discharge plasma from the flame plasma, i.e. to execute measurements on distance, exceeding the length of the discharge.

Experiment was put as follows. Measurements were carried out into flame produced by transversal pulse electric discharge in supersonic propane-air flow at Mach number $M = 2$. The propane mass fraction was about the stoichiometric one. Regime of single pulse with pulse duration $\tau = 200 - 300 \mu\text{s}$ was used. The length of discharge L along the flow at this duration is equal to $L = v\tau \leq 18 \text{ cm}$ (see Chapter YI). The probe was located at axial coordinate $z = 32 \text{ cm}$ downstream the electrodes. The single cylindrical probe with a diameter of 1 mm and length of 10 mm was positioned in the aerodynamic channel end. Basic electrode was a metal grid $1\text{mm} \times 1 \text{ mm}$, executed from wire $\varnothing 0.3 \text{ mm}$.

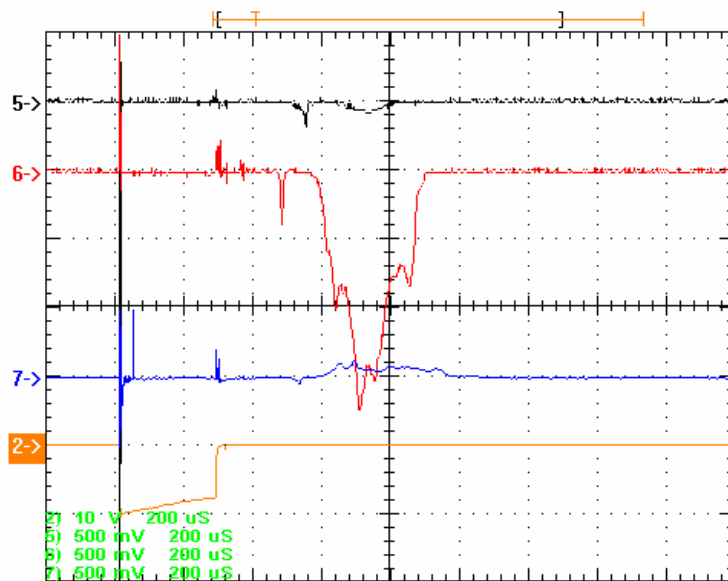


Fig.5.8. Waveforms of the probe currents demonstrating the fact of supersonic propane – air mixture flow ignition by the pulsed transversal discharge. $\tau = 300 \mu\text{s}$. $P_0 = 3 \text{ atm}$, $p = 200 \text{ torr}$. Probe bias $U = \pm 100 \text{ V}$ is for electron and ion current, respectively, $R_{pr} = 1 \text{ k}\Omega$, probe position $z \approx 32 \text{ cm}$.

Curves: 2 – the discharge current pulse, 5 – electron probe current in air flow, 6,7 – electron and ion probe currents in air-propane mixture flow at igniting value of discharge current ($I \sim 20 \text{ A}$), respectively.

Three layers of metal grid were used to increase the surface of basic electrode. This electrode was placed on distance of 3 cm from a probe downwards on a stream. A bias voltage $U(t) = \text{const}$ was applied between a probe and a basic electrode. Change of polarity of bias

allowed registering either electron, or ion probe current. The voltage proportional to probe current $I(t)$ was measured on resistance $R_{pr} = 1 \text{ k}\Omega$.

Typical waveforms of the probe currents were shown on Fig. 5.8. Signals of probe current were not detected in the cases of airflow, propane and air – propane mixture flow at discharge current below the ignition threshold.

These signals appearance we connect with the fact of the ignition realization. However, the value of ion probe current is very small: $I \sim 10 \text{ }\mu\text{A}$. Results presented in Fig.5.8 showed that a single probe method is more useful for detection of the ignition process since the electron part of the probe characteristic is more sensitive.

Thus, experimentally was shown that the fact of ignition and combustion of propane-air mixture supersonic flow may be tested by joint application of two methods: a) investigation of CH radicals band, $\lambda = 431.5 \text{ nm}$, luminescence evolution and b) investigation of the single electric probe currents evolution.

§ 3. The measurements of gas and vibrational temperatures

Radiation spectra of plasma of discharges in supersonic airflow at minimal full pressures $P_0 \approx 10^5 \text{ Pa}$ and ambient pressures $p < 10^4 \text{ Pa}$ are close to spectra of discharge in steady air under same pressures $p < 10^4 \text{ Pa}$. Under this condition the atomic components (O, H, N), active radicals (CN, CH, OH) and molecules (C_2 , N_2) are observed.

However the lines of the rotational structure of the second positive system of N_2 are dominated in wavelengths range 370 – 390 nm. (Fig.5.9), and radiation of this system is used for measurements of gas temperature of air plasma of discharges in supersonic flow.

The gas temperature was identified with rotation temperature of the basic state $X^1\Sigma_g^+$. Rotation temperature has been measured over relative intensities of lines of the rotational structure of the band (0;2) of the second positive system of N_2 (the transition $\text{C}^3\pi_u - \text{B}^3\pi_g$, $\lambda = 380,5 \text{ nm}$) (Fig.5.10.):

$$0,89 \cdot \ln(I_{ik}/i) = C - j^* \cdot (j^* + 1)/T_R.$$

where I_{ik} - intensity of a rotation structure spectral line I_{ik} , that corresponds to a transition between l-th and k-th states, j^* is a total molecular moment of momentum, i – is a quantum mechanical coefficient of intensity, C is a constant. Here one can take v_{ik}^4 to be a constant (the corresponding error $\approx 0.5\%$ is negligible), The rotation constant for upper state at radiation

transition $B' = 1.826$ is close to the rotation constant $B'' = 2.01$ for the basic state $X^1\Sigma_g^+$. As result rotation temperature $T_R = T_g B'/B''$ is close to gas temperature.

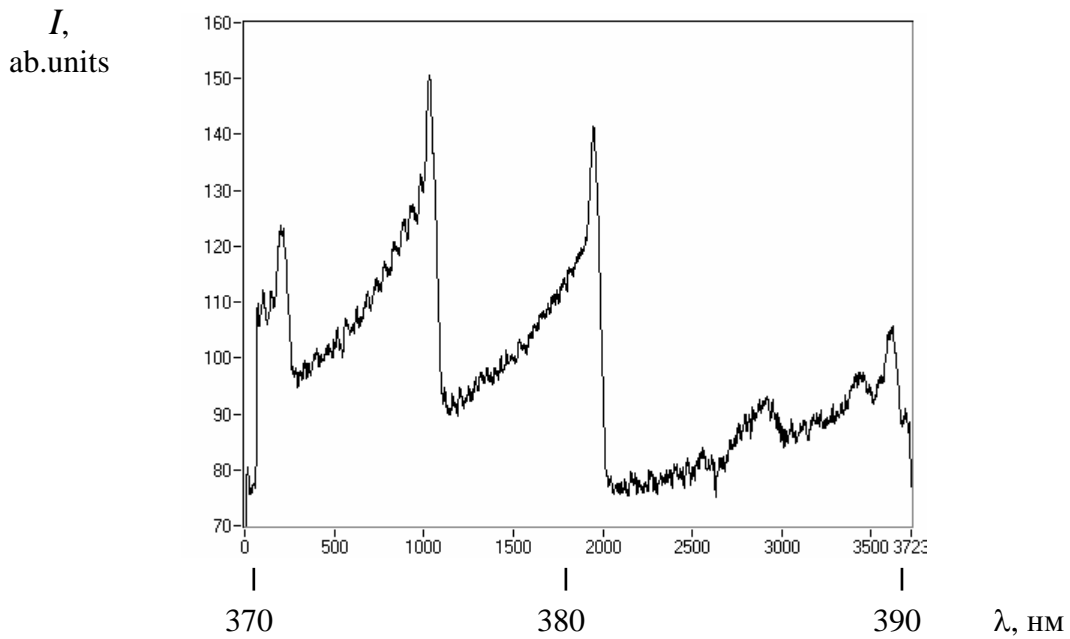


Fig.5.9 The radiation spectrum of the plasma of the discharge in supersonic airflow at $\lambda = 370$ - 390 nm. $p = 5,3 \cdot 10^3$ Pa, $P_0 = 10^5$ Pa, $M \approx 2$, $D_0 = 10$ mm, $I = 2.5$ A, $z = 1$ cm.

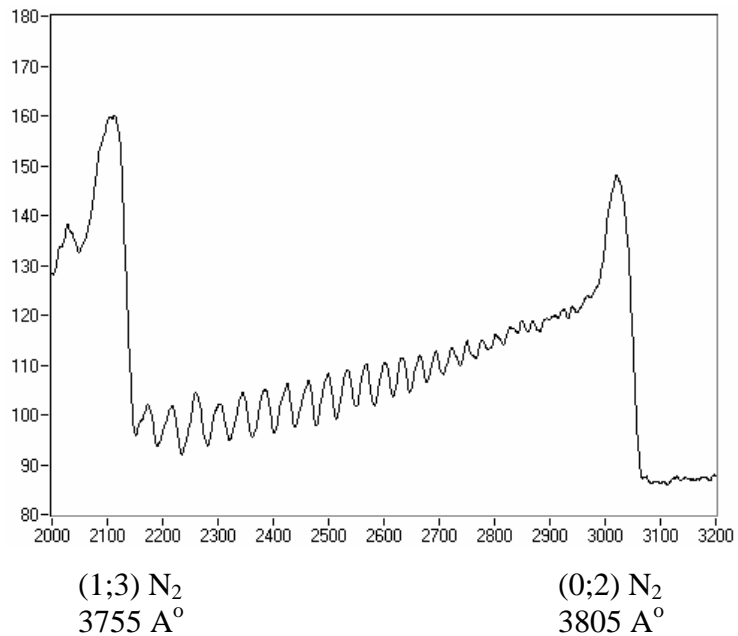


Fig.5.10. The radiation spectrum of the second positive system of N_2 of the plasma of the discharge in supersonic airflow.

$p = 5,3 \cdot 10^3$ Pa, $P_0 = 10^5$ Pa, $M \approx 2$, $D_0 = 10$ mm, $I = 2.5$ A, $z = 1$ cm.

However the intensities of lines of the rotational structure of the second positive system of N_2 , which is used for measurements of gas (rotational) temperature of air plasma, falls at growth of full pressure very sharp. Radiation spectra of plasma of pulse-periodic discharge at pressure $P_0 = 2 \cdot 10^5$ Pa was shown in Fig.5.11. It's seems that radiation intensities of the molecular bands of CN dominate in wave lengths range 365 – 395 nm. The relative value of the molecular bands the second positive system of N_2 ((0,2) $\lambda = 380.5$ нм, (1,3) $\lambda = 375.5$ нм, (2,4) $\lambda = 371.0$ нм), and first negative system N_2^+ (0,0) $\lambda = 391.4$ нм) were very small. As result, plasma temperature at $P_0 > 10^5$ Pa has to evaluate by the relative intensities of the molecular bands of CN (0,0) и (1,1) with quantum wavelengths $\lambda=388.3$ и 387.2 nm. This temperature is vibrational temperature. CN temperature data were considered at high values of full pressure as the upper limit of gas temperature.

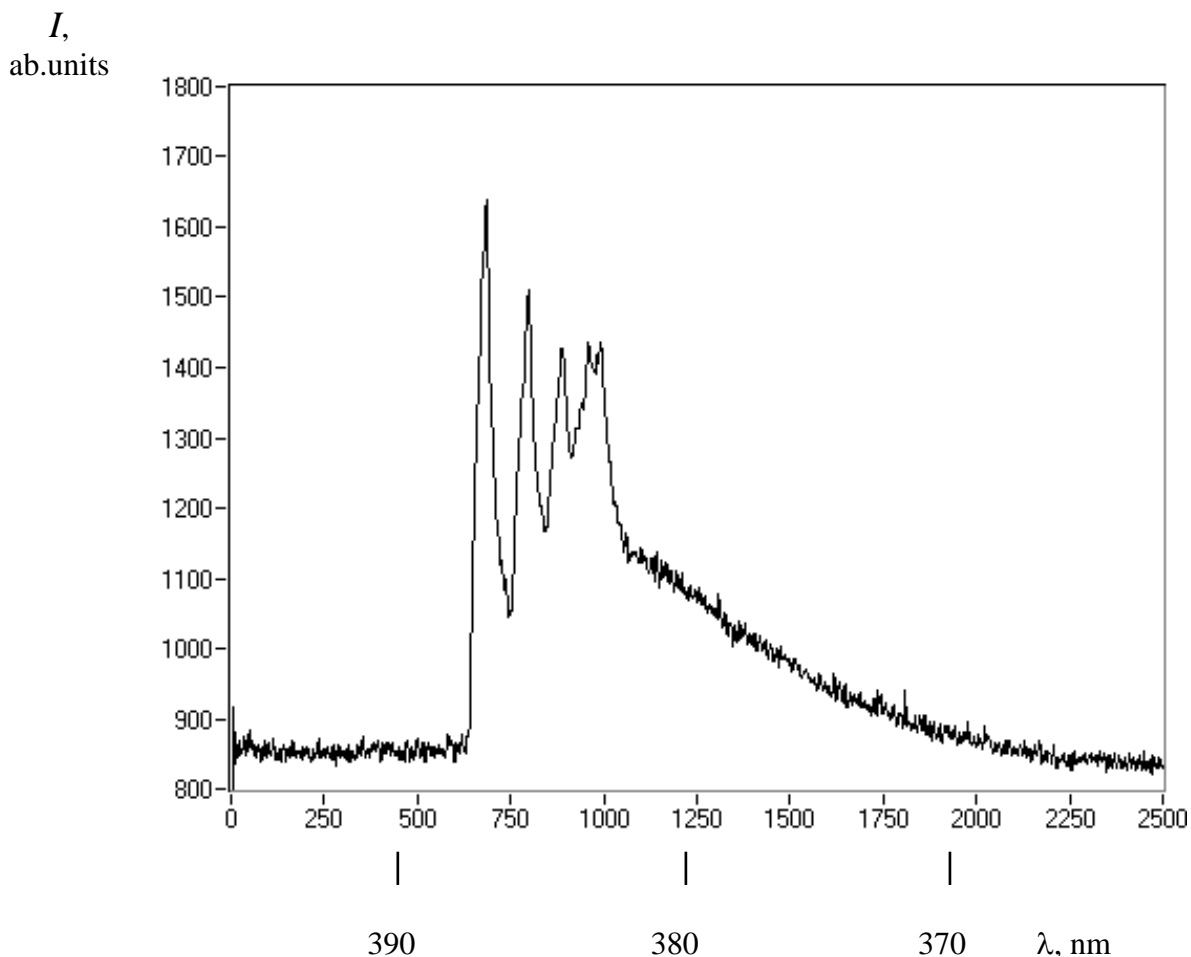


Fig.5.11 The radiation spectrum of the plasma of the discharge in supersonic airflow at $\lambda = 365$ - 395 nm.

$p = 1,3 \cdot 10^4$ Pa, $P_0 = 2 \cdot 10^5$ Pa, $M \approx 2$, $D = 12$ mm, $I \approx 20$ A, $\tau = 600$ μ s, $f = 10$ Гц, $z = 1$ cm.

Gas temperature as a function of full pressure for fixed discharge current is presented in the Fig.5.12. Measurements were performed in the pulsed discharge at pulse duration $480 \mu\text{s}$ in the current generator mode. The jet off-design power was $n = 2$. The radiation was detected from a region at a distance $z \approx 2 \text{ cm}$ from electrodes down a flow. Generally speaking, data obtained in the result of CN molecular bands relative intensities analysis at $P_0 > 1 \text{ atm}$ reflect an excitation temperature – the discharge vibrational temperature of molecules. It is easy to see that there is the excess of the temperature value determined by CN over the temperature value obtained by rotational temperature of the second positive N_2 system. It is naturally to expect that this difference has to decrease with increasing of pressure, so one can consider the temperature values found by CN to be the upper limit for the gas temperature. Then from the data presented in Fig.5.12 follows that the averaged value of the upper limit of the gaseous temperature at $P_0 = 4 \text{ atm}$ is smaller than that at $P_0 = 1 \text{ atm}$.

Thus the temperature has a tendency to decrease when a density of gas flowing out of a nozzle increases (i.e. in the case of full pressure increasing) in difference to its dependence in motionless air.

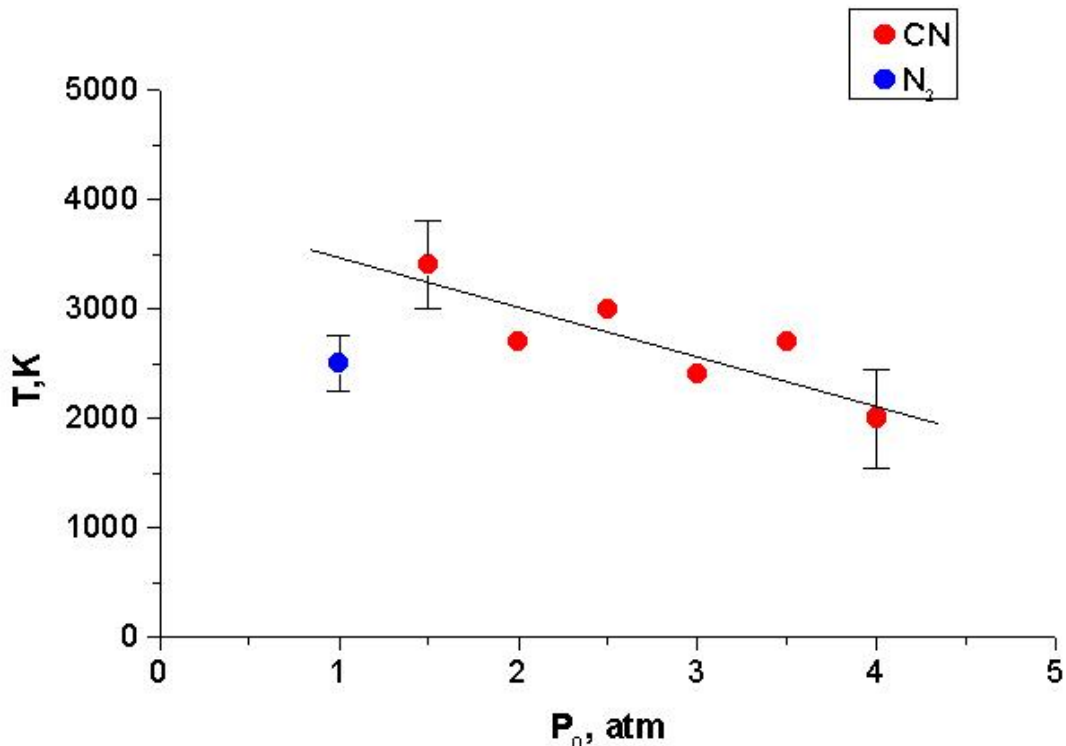


Fig.5.12. Gas temperature as a function of full pressure.
 $M = 2$, $n \equiv p^* / p = 2$, $I = 8 \text{ A}$, $\tau = 480 \mu\text{s}$, $L = 12 \text{ cm}$, $z = 2 \text{ cm}$.

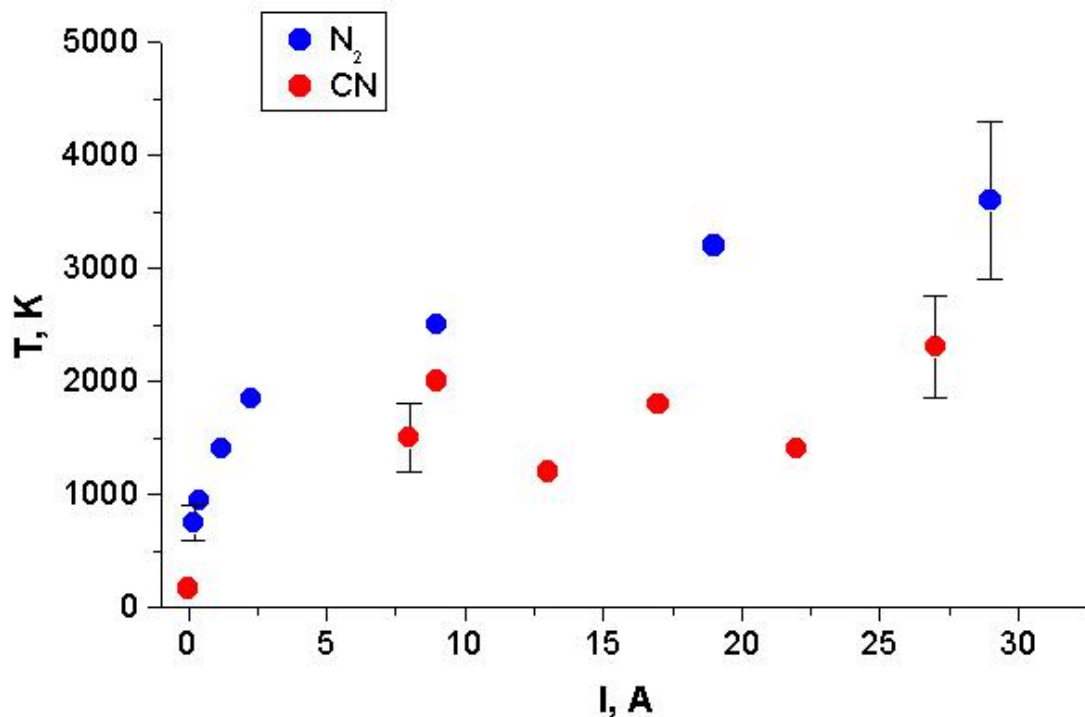


Fig.5.13. Gas temperature as a function of discharge current in plasma of the transversal discharge in supersonic airflow. $M = 2$, $p = 200$ Torr, $z = 1$ cm.

• - $P_0 = 1$ atm, $p = 40$ torr; • - $P_0 = 4$ atm.

Temperature drop is observed at full pressure increasing from $P_0 = 1$ atm to $P_0 = 4$ atm at all currents (Fig.5.13).

In general we have to conclude that experimentally obtained gas temperature absolute values at high currents reach several thousands degrees though they stay smaller than the value of the electron temperature $T_e \approx 10^4$ K, calculated for these conditions.

So plasmas in conditions under the investigation is nonequilibrium one, it is insufficient to know the gas temperature value for determining of its conductivity, and direct measurements of the electron concentration are necessary.

§ 4. Probe measurements of plasma density

4.1. Double probe characteristics in plasma of igniting discharges

4.1.1 Plasma jet injected into a supersonic flow

The voltage bias $U(t)$ was applied between two probes to measure the I-V probe characteristic. This bias changed linearly from a minimal voltage of -30 V to a maximal voltage of $+30$ V during $10 \mu\text{s}$. Typical waveforms of a double probe current $i(t)$ with the corresponding probe bias in plasma jets injected into a supersonic propane-air flow are demonstrated in Fig.5.14.

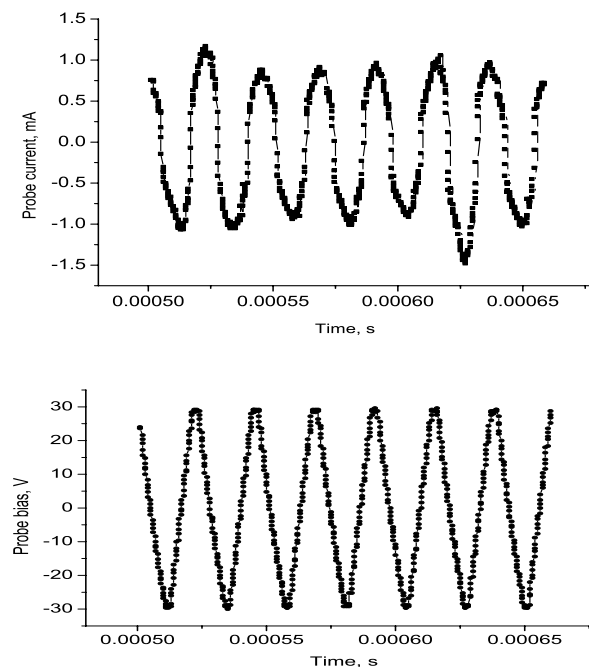


Fig.5.14 Waveforms of the double probe current (upper curve) and bias voltage (lower curve) at an injection of the plasmadynamic jet into supersonic propane – air mixture flow.

I-V probe characteristic was determined with the help of developed program. The set of probe characteristics constructed on a base of these data is represented in Fig.5.15.

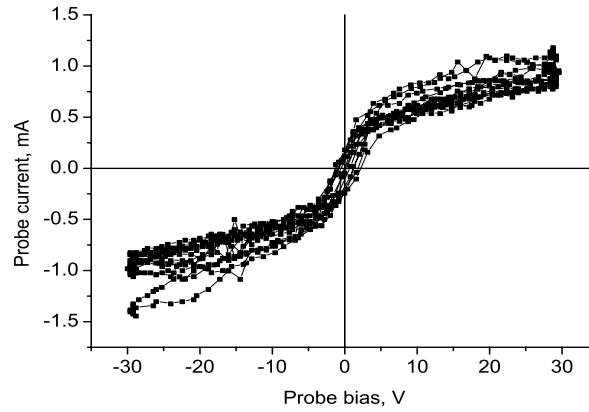


Fig.5.15 Double probe I – V characteristics at the plasmadynamic jet injection to the supersonic propane- air flow. $P_0 = 4$ atm, $p = 300$ Torr. $U = 4,25$ kV, $C = 50$ μ F. Symmetric double probe: $\varnothing 0.3$ mm, $L = 10$ mm. $z = 32$ cm.

It is visible, that ion parts of the double probe characteristics trend to a saturation. The probe characteristic fluctuates during the measurement period. This fact may be connected with the plasma density variations in the supersonic flow. The value of these variations can reach 50%.

The comparison of the measured characteristic of a double probe and of an ionic part of the characteristic simulated according Chapter IY for conditions of experiment is submitted on Fig.5.16. It is visible, that both qualitative and the quantitative consent between calculation and experiment is observed.

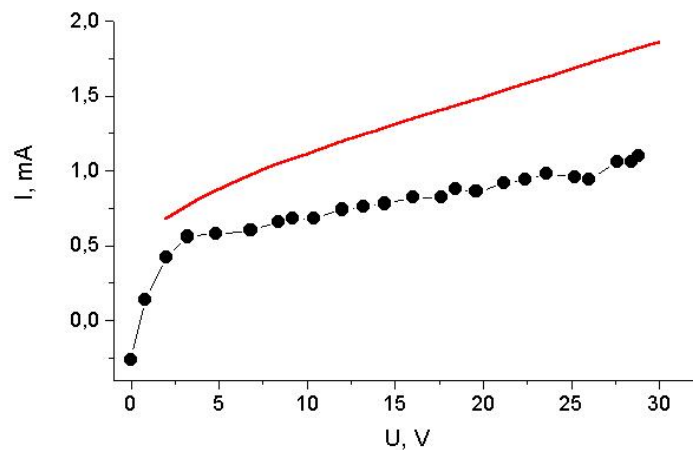


Fig.5.16. Comparison of measured (\bullet) and calculated (—) I-V probes characteristics of transversal double probes in pulse plasma jet, injected in a supersonic airflow.

Experiment conditions: $M = 2$, $p = 100$ Torr, $P_0 = 2$ atm, $C = 50$ μ F, $U = 2.5$ kV, $z = 22$ cm.

Double probe $\varnothing 0.3 \times 14$ mm, distance between probes $D = 4$ mm.

Simulation conditions: $R = 0.15$ mm, $T_e = T_i = T_g = 5000$ K, $N_i = 4 \cdot 10^{12}$ cm^{-3} , $v = 660$ m/s, $D_i = 70$ cm^2/c .

Difference of absolute values of currents does not exceed 70 %. This result is good as this mistake includes also mistakes of definition of density of gas, electron and ion temperatures, mobility of ions.

Comparison of characteristics of double transversal and longitudinal probes was carried out. These results are submitted on Fig.5.17. It is visible, that values of ion saturation current on longitudinal probe are lower than values of a current of a transversal probe under the same conditions. This result will completely be coordinated to the results of numerical simulation submitted in Chapter IY.

However application of longitudinal probes in supersonic flows does not result in simplification of the description of ion collection by a probe.

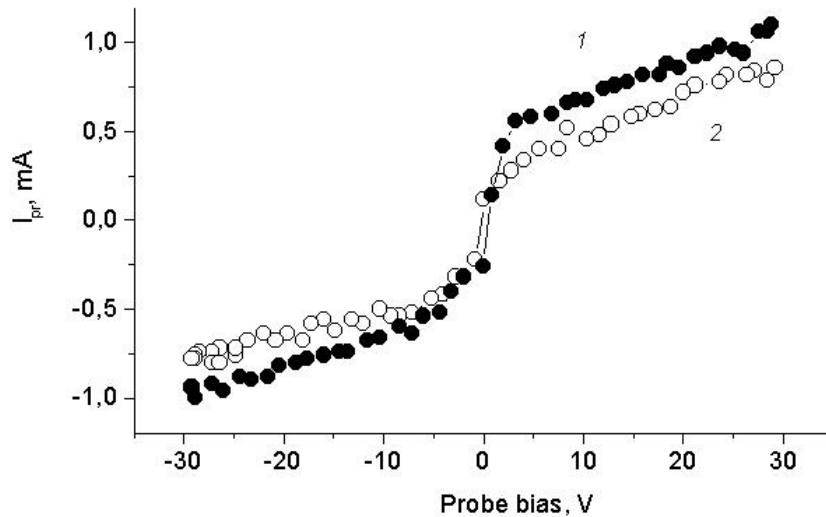


Fig.5.17. I-V probe characteristics of transversal (1) and longitudinal (2) double probes in pulse plasma jet, injected in a supersonic airflow.

$M = 2$, $p = 100$ Torr, $P_0 = 2$ atm, $C = 50 \mu\text{F}$, $U = 2.5$ kV, $z = 22$ cm.

Double probe $\varnothing 0.3 \times 14$ mm, distance between the probes $D = 4$ mm.

4.1.2 Pulse and DC discharge in supersonic flow.

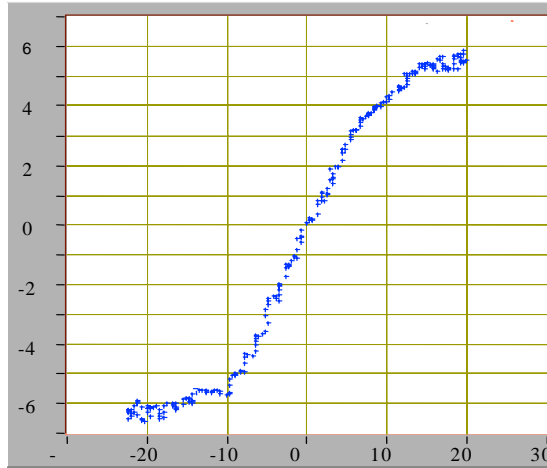
The application of only the double probes is possible in the case of the transversal electric discharges in the supersonic flow. Two typical double probe voltage - current characteristics in the airflow plasma are represented in Fig.5.18.

Little differences in double probe characteristics take place at an addition of propane to the supersonic airflow.

One can see that ion parts of the probe characteristics are close to those of the pulsed jet. Modes of the probe operation in the plasma parameter range of igniting discharges are the intermediate

ones from the analytical approach point of view. Results of our computer simulations (Chapter IY) are applicable in this case.

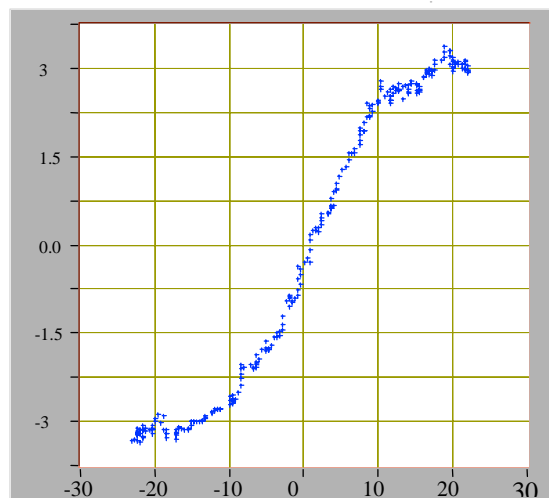
Probe current, mA



I = 11A

Probe bias, V

Probe current, mA



I = 5 A

Probe bias, V

Fig.5.18. The double probe voltage - current characteristic in the plasma of the pulse transversal discharge in the supersonic airflow.

Cylindrical probe: $\varnothing = 0.3$ mm, axial position $z = 4$ cm. $P_0 = 1$ atm, $p = 40$ Torr, $\tau = 300$ μ s.

Gas temperature achieves values more than 1000 K in conditions of igniting discharges (see Fig. 5.12-5.13 and Chapter VI), therefore at flow Mach number $M = 2$ a mode of probe operation is subsonic as a rule. Numerical simulation shows, that in conditions of experiments

the mode of saturation with a nonzero inclination of the characteristic is realized. Therefore for a determination of ion density the model of an ion saturation current for subsonic flow can be applied.

The review of the works devoted to a mode of ion saturation current, is executed within the framework of the project 1867p []. Results of numerical simulation (Chapter IY) show that take into account the difference between ion and electron temperature of plasmas.

In the frameworks of a simple model [I.16] analogous to [I.7] one can show that the dimensionless densities of electron j_- and ion saturation currents j_+ on a cylindrical and spherical probe are equal:

$$j_{\pm} = (1 + \tau^{\mp}) \frac{\partial n}{\partial r} \Big|_{r=1} .$$

Here r - dimensionless radial coordinate in terms of probe radius R , $\tau = T_+/T_-$. The model assumes the constancy of temperatures through the field of flow.

The numerical calculations are conducted in []. The relation for dimensionless current i is convenient to present as the dependence on an electrical Reynolds number:

$$i = 0.58 (1 + \tau^{-1})^{0.6} Re^{0.4}, \quad (1)$$

The dimensional current on a full surface of a cylinder is equal

$$I = 2 \pi e N_{\infty} D_+ L i \quad (2)$$

With the account mistakes of definition of density of gas, electron and ion the mistake of concentration can be estimated in size about 100 %.

4.2 Single probe characteristics in plasma

4.2.1 Plasma jet injected into a supersonic flow

In the case of plasma jets with a shot time of energy input sufficient for ignition supersonic propane-air mixture flow both double and single probes can be used for investigations of plasmas in a flow in contrast to the case of pulsed and DC transversal discharges where only double probes are appropriate.

The single cylindrical probe was positioned in the aerodynamic channel end. Basic electrode was a metal grid $1\text{mm} \times 1\text{mm}$, executed from wire $\varnothing 0.3\text{mm}$. Three layers of metal grid were used to increase the surface of basic electrode. This electrode was placed on distance

of 3 cm from a probe downwards on a stream. Typical waveforms of a single probe current with the corresponding probe bias in plasma jets injected into a supersonic propane-air flow on interval of time $640 \mu\text{s} - 710 \mu\text{s}$ after breakdown are demonstrated in Fig.5.19. The probe characteristics constructed on a base of these data is represented in Fig.5.20.

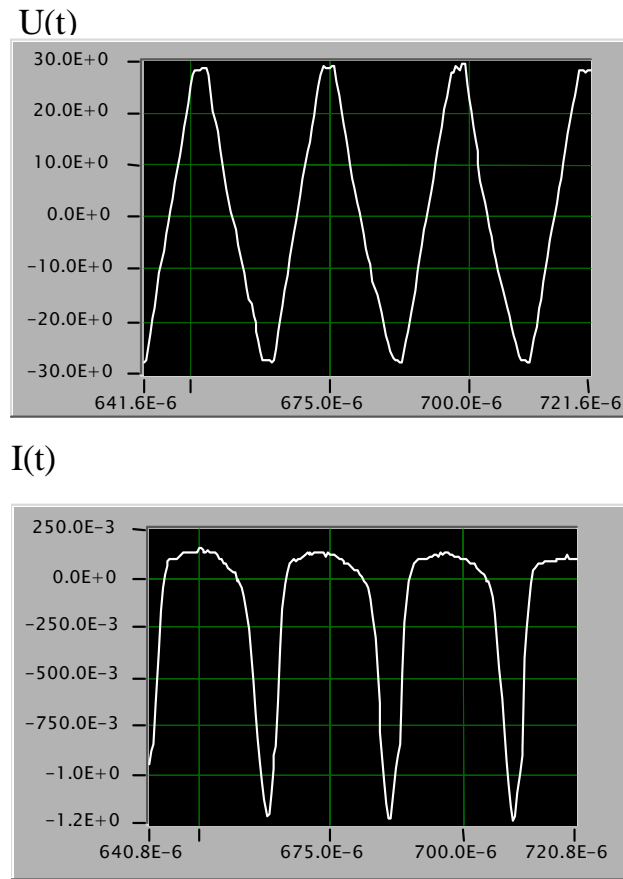


Fig.5.19 Waveforms of the bias voltage (upper curve) and single probe current (lower curve) at an injection of the plasmadynamic jet into supersonic propane – air mixture flow.

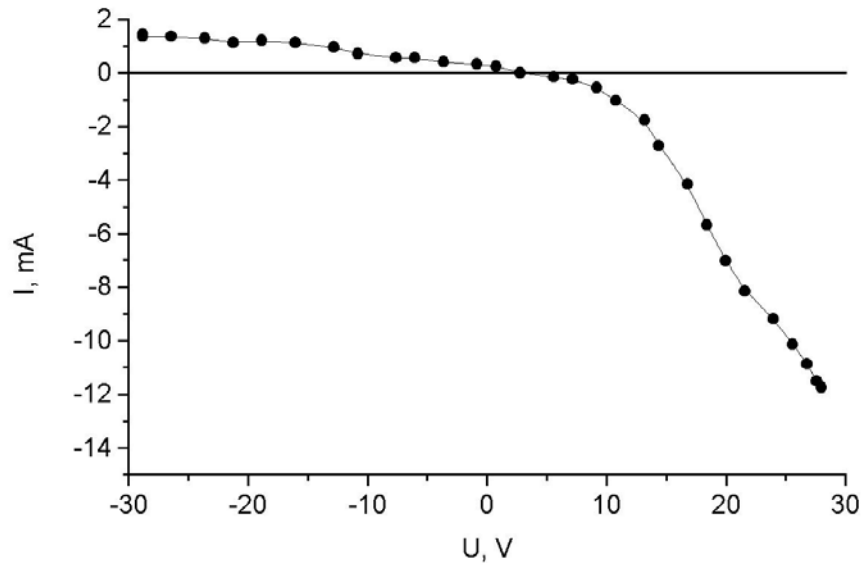


Fig.5.20. I-V probe characteristics of single transversal probe in pulse plasma jet, injected in a supersonic airflow. $P_0 = 1 \text{ atm}$, $p = 50 \text{ torr}$, $U = 4.25 \text{ kV}$.
Cylindrical probe: $\varnothing = 0.3 \text{ mm}$ x 15 mm , axial position $z = 32 \text{ cm}$.

I-V characteristic of single probe is more sensitive to fluctuations of parameters of plasma, than I –V characteristic of a double probe. It is visible on Fig 5.19, that peak values probe current vary in an examined interval a little. Therefore during measurement characteristic, equal $10 \mu\text{s}$, properties of propane-air plasma do not vary. It guarantees correct measurement I – V characteristic of a probe.

One can see that the electron part of probe characteristic is close to the linear function. So, the type of measured probe characteristics is close to those of the characteristics, which take place under the pulse plasma jet injection to steady air [1,2]. Since the plasma temperature is high, then the flow around the probe mode is the subsonic one, analogous to the jet outflow to the steady air [1,2]. Such probe operation modes in collision high-density plasma flows have been studied primarily analytically under the conditions of significant influence of the Debye layer on a basis of the asymptotic analysis in a totality of extreme cases [3].

4.2.2 Plasma of flame ignited by the pulse transversal discharge in the supersonic propane-air flow.

Experiment was performed analogy to experiments described in § 2 of this Chapter, only instead of constant probe bias the variable bias was used. The typical single probe voltage -

current characteristics in the propane-air flame plasma in the supersonic propane-air flow is presented in Fig.5.21.

The values of the ion probe current is about the ones in the propane- burning Meker burner, the absolute value of the ion probe current is small ($\sim\mu\text{A}$).

Plasma density in propane – air mixture flame produced in a Meker burner at atmospheric pressure (according to [4]) was equal to $n_e \sim 10^9 - 10^{10} \text{ cm}^{-3}$. The main ion was H_3O^+ [4].

In the case of the supersonic flow the signal/noisy ratio can be low. As the result, the it is more convenient to use the electron part of probe characteristic, i.e. the positively biased probe, which collects much higher electron currents due to the higher mobility of electrons.

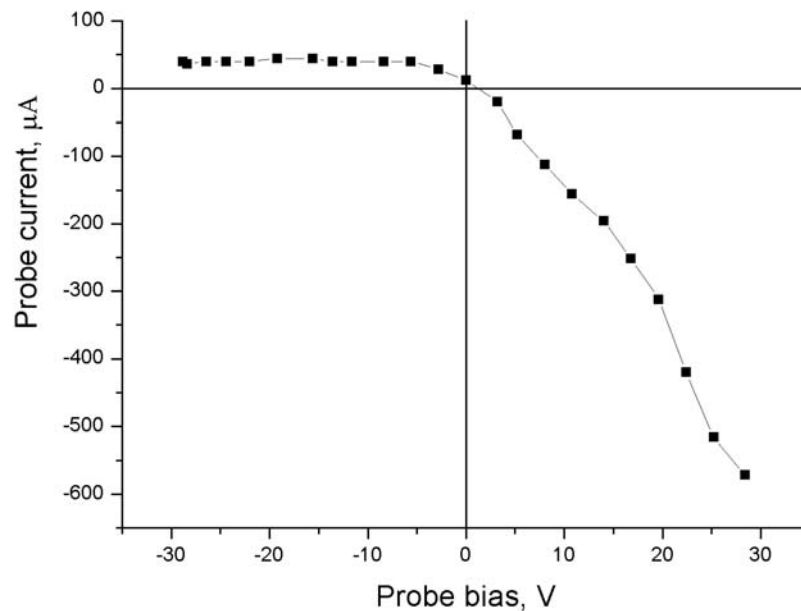


Fig.5.21. The single probe voltage - current characteristic in the propane-air flame plasma in the supersonic propane-air flow.

Cylindrical transversal probe: $\varnothing = 1 \text{ mm} \times 10 \text{ mm}$, axial position $z = 32 \text{ cm}$. $P_0 = 3 \text{ atm}$, $p = 200 \text{ torr}$.

The supersonic propane-air flow has been ignited by transversal pulse discharge.

The dimensionless parameters of probe characteristic under these assumptions in our conditions are:

- Electric Reynolds number $Re_e = uR/D_i \approx 200$,
- $\varepsilon = (r_D/r_p)^2 \approx 10^{-2}$

The type of probe characteristic is determined according to theoretical analysis (see [5]) the value of product of ε by Re^2 . In this case $\varepsilon Re^2 \gg 1$, then the main part of probe voltage drops in the zone of unperturbed flow and I-V characteristic has to tend to linear.

The type of experimental characteristics is close to the type of theoretical characteristics. The evaluation of plasma density shows that the magnitude of n_i is about 10^{10} cm^{-3} .

REFERENCES

1. Anders A., Ershov A.P., Isaev K. Sh., and Timofeev I.B. High Temperature. 1987. V. 25, No. 4, p. 743.
2. Ershov A. P., Imad I. Kh., Timofeev I. B. *et al.* High Temperature. V.31 No. 4 1993. P. 531.
3. Benilov M.S. High Temperature. Vol. 26, No. 5, 1988, P. 780.
4. J.Dawe, Syed A.H.Rizvi, and Peter R.Smy. IEEE TRANSACTIONS ON PLASMA SCIENCE, Vol.21, No.1, 1993, PP. 202-208.
5. Benilov M.S.,Bochkarev G.G., Buznikov A.V. ,German V.O., Kovbasyuk V.I. Academy of Science News. Liquid and Gas Mechanics. No.1. Pp.150-160, 1983.

CHAPTER VI.

PLASMA PARAMETERS OF IGNITING DISCHARGES IN SUPERSONIC FLOW

§ 1. Parameters of electrode discharges in supersonic airflow

1.1 The longitudinal discharge in the supersonic gas flow

The circuit with an additional electrode was used for creation of the longitudinal discharge [1]. High-voltage electrode of the discharge and grounded additional electrode were placed in a plane, perpendicular supersonic flow, on a distance about 10 mm. Second grounded electrode of the discharge was placed along a flow on a distance L about 3 – 15 cm.

Typical waveforms of the discharge voltage U , the current of initial perpendicular discharge (between perpendicular electrodes) I_{trans} and one of longitudinal discharge I_{long} are shown in Fig.6.1. After the breakdown between a high-voltage electrode of the discharge and grounded additional electrode the plasma discharge channel of a pulsed discharge is sweeping down by a flow with a speed equal to that of the flow; as a consequence its length grows continuously up to closure of longitudinal discharge gap. Up to this moment the discharge voltage of initial transversal discharge U growth proportional to its length, $I_{trans} = \text{const}$, $I_{long} = 0$. After the switchover to longitudinal discharge $U \approx \text{const}$, $I_{trans} = 0$, $I_{long} = \text{const}$. According to results of [1], the small oscillations of longitudinal discharge voltage are observed.

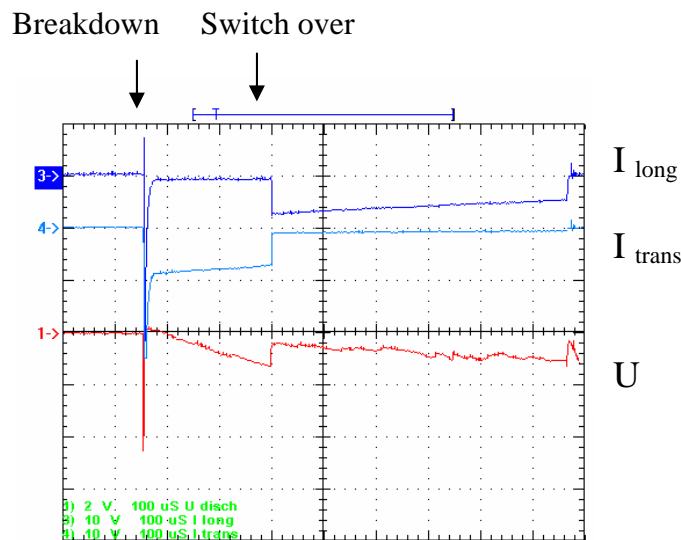


Fig.6.1. Waveforms of the voltage on the discharge U , the current between perpendicular electrodes I_{trans} and the current between longitudinal electrodes I_{long} .
 $P_0 = 4 \text{ atm}$, $p = 200 \text{ Torr}$, $\tau = 800 \text{ } \mu\text{s}$, $L = 10 \text{ cm}$.

Appearance of longitudinal discharge in supersonic airflow is shown in Fig.6.2.

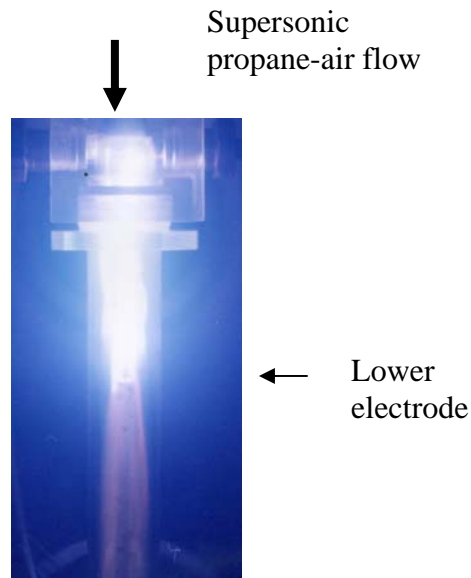


Fig.6.2. Photo of longitudinal discharge in supersonic air-propane flow
 $P_0 = 4 \text{ atm}$, $p = 200 \text{ Torr}$, $\tau = 800 \mu\text{s}$, $L = 10 \text{ cm}$.

Thus, two distinctions between this longitudinal discharge from longitudinal discharge, investigated in [1] take place:

- The pulse mode with long time duration has been used
- The discharge in aerodynamic canal but free jet has been investigated.

1.2 The transversal discharge in the supersonic gas flow

Integral topology of transverse to flow DC discharge' luminescence (during an exposure time of a second's hundredth part) is well known: thin channels are extending along a flow behind discharge's electrodes. Their brightness considerably exceeds those of their bridging region, so the discharge channel seems to be unconnected.

This picture is typical both for small and hypersonic Mach numbers of wind tunnels and jets (Fig.6.3). Change to a pulse discharge with varying pulse duration τ does not lead to changing of an integral luminescence topology (now during a pulse), but it changes only a discharge's extension along a flow. The latter at first linearly increases with a flow velocity, then it slows down and comes to a value close to those of the constant current case at the given gasdynamic flow's properties. Hence, it is evident that transverse discharge's plasma is drifted by a flow, however, a way of the current connection and factors limiting discharge extension along a flow stay unclear.

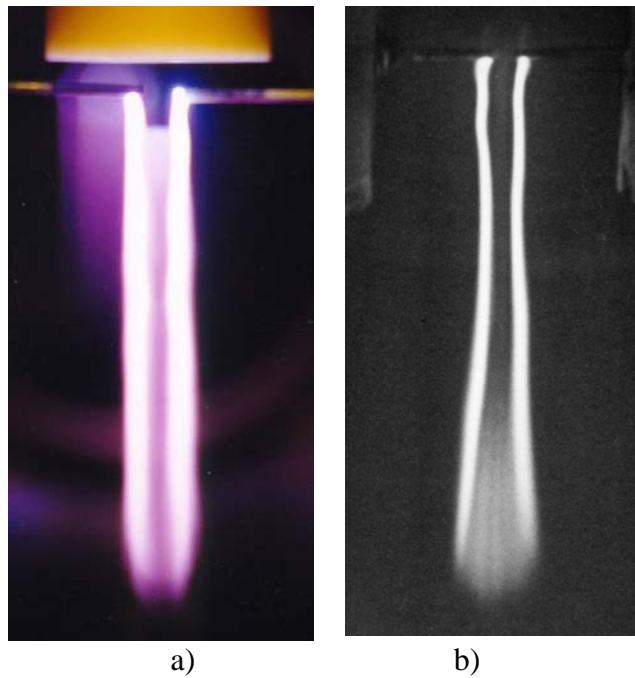


Fig.6.3. DC transversal discharges in supersonic airflows.
 a) air jet, $M = 2$; b) wind tunnel, $M = 6$.

Mechanism of a current connection

At the same time the pulse mode, with relatively not complicated way of high discharge current generating, allows to apply a super speed photo detection method and to trace a discharge development in details. Such a panoramic picture of a transversal pulse discharge developing in a supersonic jet from a breakdown moment till the moment of quasi-stationary structure's creation is presented in Fig.6.4. A flow is directed top-down. We used a photo detector with a two rows insert in a mode of per-frame photography, duration of a frame was 16 or 32 μs . During a development the discharge goes away behind an illuminator. In Fig. 6.4 this moment corresponds to $\approx 256 \mu\text{s}$, maximal observed size is limited by $\approx 13 \text{ cm}$.

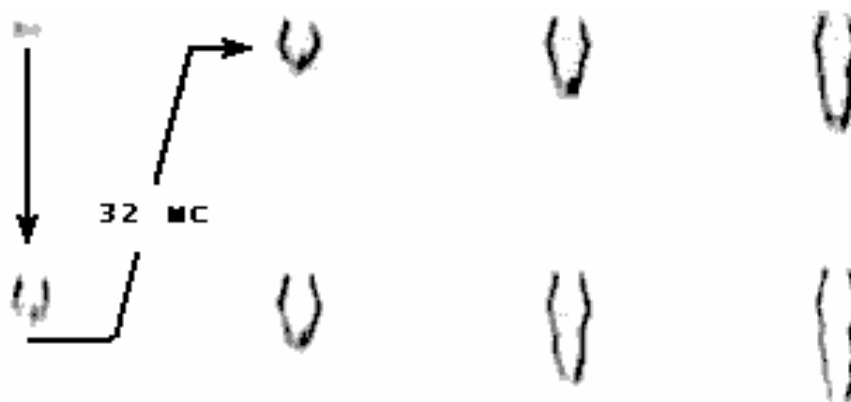


Fig.6.4. Dynamic of transversal discharge in a supersonic airflow.
 $P_0 = 2 \text{ atm}$, $p = 100 \text{ Torr}$, $M = 2$. Discharge current $I \approx 20 \text{ A}$.

From the point of view of the discharge propagation in space results of the super speed photo detection show that inputting of transport processes (ambipolar diffusion, thermal conductivity and drift) outside of near electrode regions is negligibly small. That is why a velocity of the discharge propagation and its configuration are set by corresponding flow's characteristics.

So the discharge with applied transversal field can not be stationary in principle since a part of the positive column is always perpendicular to a flow and is constantly drifted by it.

Instability's mechanism

Propagating discharge process along a flow can not be infinite and it breaks at some moment. Fig.6.4 illustrates this phenomenon. Discharge's extension sharply decreases and then the current's channel begins to be drifted out by a flow. The moment of the sharp decrease of the discharge's length is undoubtedly conditioned by the breakdown between the anode and the cathode streams. We managed to fix this directly at high speeds of the photography.

In Fig.6.5 one can see the going out (extincting) part of the discharge's channel. The breakdown in this case of strongly under expanded jet takes place near the Mach disk. One can see that a new, a shorter way of a current leads to a quick going out of a plasma glow in the remained discharge part. Later the discharge channel starts to drift by the flow again and the whole process repeats.

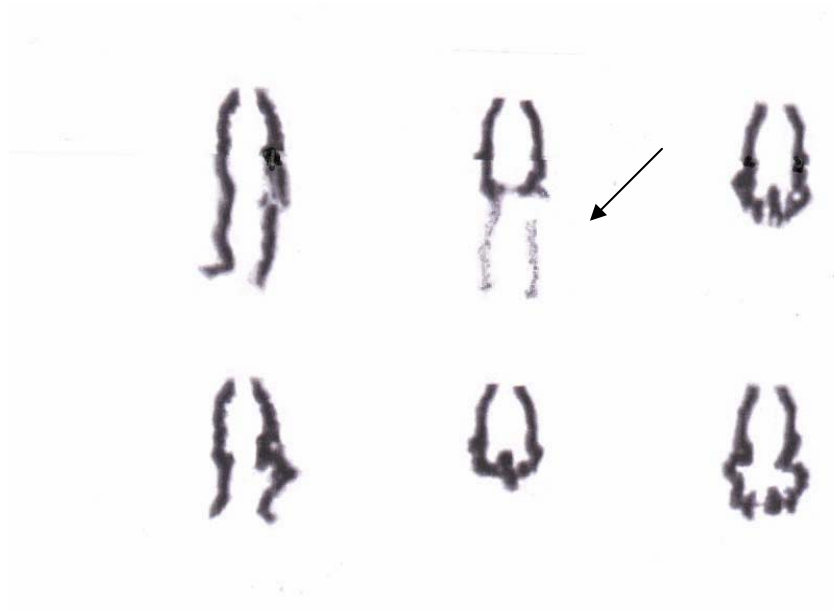


Fig.6.5 Secondary breakdown between the anode and cathode parts of discharge.
 $P_0 = 4 \text{ atm}$, $p = 100 \text{ Torr}$, $M = 2$, $I = 30 \text{ A}$. Interval between photos $16 \mu\text{s}$.

Quantitatively the process of the discharge developing in time is most simply illustrated by the typical voltage waveforms at the discharge's electrodes. Such waveforms with the current waveforms are represented in Fig.6.6.

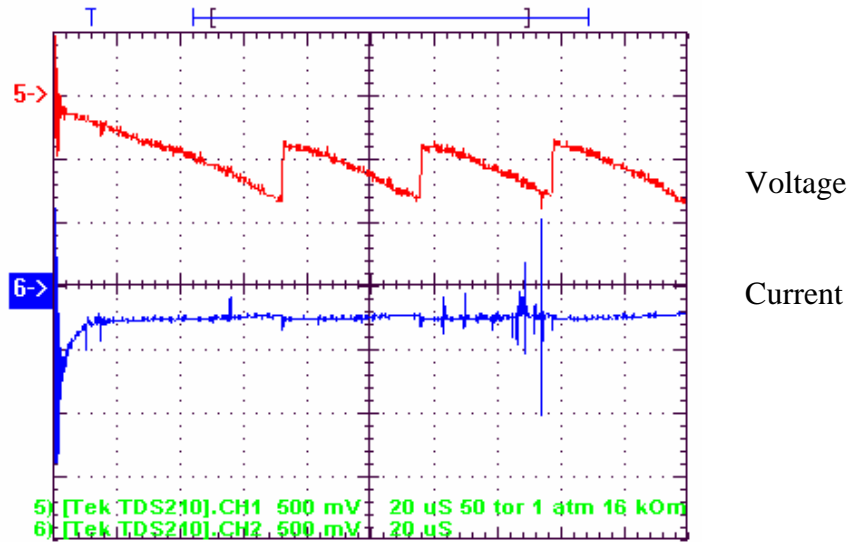


Fig.6.6. Waveforms of pulse discharge voltage and current.

$P_0 = 1 \text{ atm}$, $p = 45 \text{ Torr}$, $L = 6 \text{ mm}$, $\tau = 200 \text{ } \mu\text{s}$. Scale factors: $I - 1 \text{ A/div}$, $U - 1 \text{ kV/div}$.

Increasing of the discharge extension along a flow is accompanied by a monotonous and close to the linear voltage increasing at electrodes. After a definite time from the discharge's start this increasing breaks by the voltage sharp drop corresponding to the breakdown between the anode and the cathode streams. Position of the breakdown plain along a flow with respect to the electrodes determines the residual voltage drop at the discharge. Later the process repeats and the discharge turns to a vibrating mode.

Electric field in pulse transversal discharge

Continuous increasing of the discharge channel's length reveals that the discharge is unstable even in an idealized case of discharge feeding from the generator of current $I = I_0$. So in the classical discharge AVC, $U(I)$ - dependence, to each current value there will correspond a number values of potential difference between electrodes corresponding to definite time moments. That is why from the physical point of view there is a sense in an electric field dependence of current $E(I)$, but not $U(I)$ dependence. Results of floating potential measurements and of direct measuring of E by two floating probes, which signals came to the entrance of a differential amplifier have shown that the electric field strength changes in time rather slowly not

only in the anode but in the cathode discharge's part as well. An average field value $\langle E \rangle$ (over a whole discharge's length) can be determined also from the waveforms of the voltage at the discharge (Fig.4.5), since $\partial U / \partial t = \langle E \rangle v$. Essentially that in so doing a sum of near electrode potential drops is automatically excluded. In contrast to measurements of [1], current's generator acts as a source for discharge feeding.

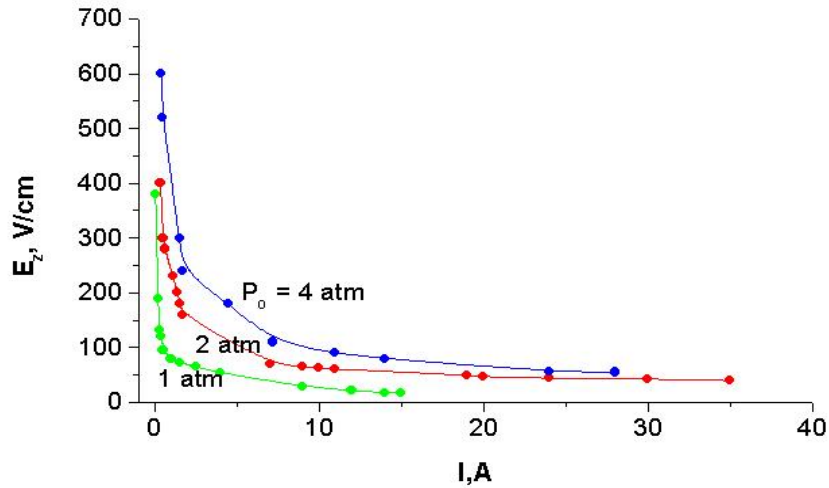


Fig.6.6a. An electric field versus current in the pulsed transversal discharge in a supersonic airflow. $M = 2$, $\tau = 200 \mu s$, $n \equiv p^* / p = 2$.

Data obtained by this way for the transversal discharge with respect to a discharge current in the three orders of magnitude range are presented in Fig.6.6. They are presented for fixed values of full pressure P_0 , since the pressure in the nearest (supersonic) jet's region, where the discharge burns, is determined by a pressure at a nozzle's cut but not by a pressure in a chamber.

It is easy to see that found dependencies $E(I)$ are the falling ones, and the electric field in a region of respectively small currents reaches values close to 1 kV/cm, then is quickly and strongly drops with the current's rise, almost for about an order of magnitude, and then changes weakly. A transition region from one mode to another corresponds to currents of $I \sim 1$ A and with pressure in a jet it moves to the side of high currents.

In an absence of a flow a current motion trough a gas is accompanied by a constriction. As usual a connection between a current and a field is close to the power dependence $I \sim E^{-m}$, in case of small currents, i.e. weakly constricted glow discharge, $m = 1$, and $I \sim E^{-1}$. Value of m rises with current's rise. It reaches $m = 3$, and $I \sim E^{-3}$ in case of big currents typical for arcs. Data presentation in a double logarithmic scale show that the power dependence with $m = 2 \pm 0,2$ corresponds to small currents in the region of quick field's drop. Value $m \approx 3$ corresponds to big

currents. So this discharge in typical for plasma aerodynamic experiments can be classified as intermediate between the strongly constricted and the burning arc discharge.

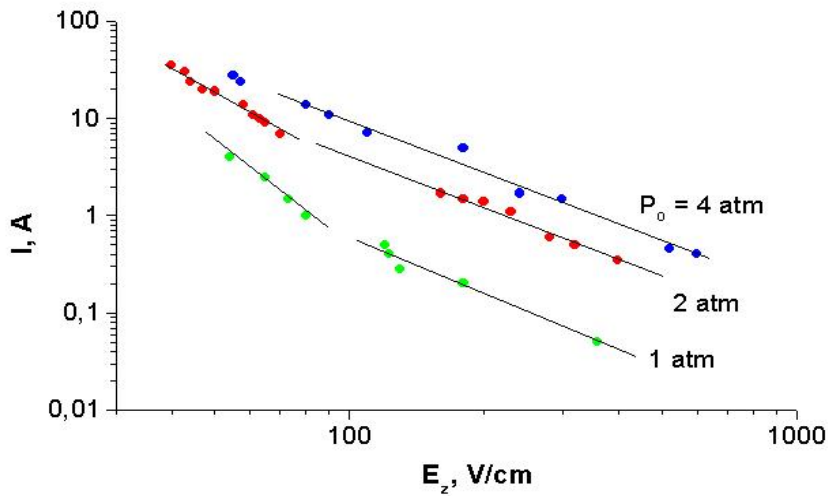


Fig. 6.6b. The discharge current versus an electric field in the pulsed transversal discharge in a supersonic airflow (the same experimental data, as Fig. 6.6a).
 $M = 2$, $\tau = 200 \mu\text{s}$, $n \equiv p^* / p = 2$.

Character of $E(I)$ dependence is connected not only with temperature changing and respectively with a conductivity changing, but with a size of a current conducting region. Results of luminescent discharge channel measurements and of its hot region are represented in Fig.6.7.

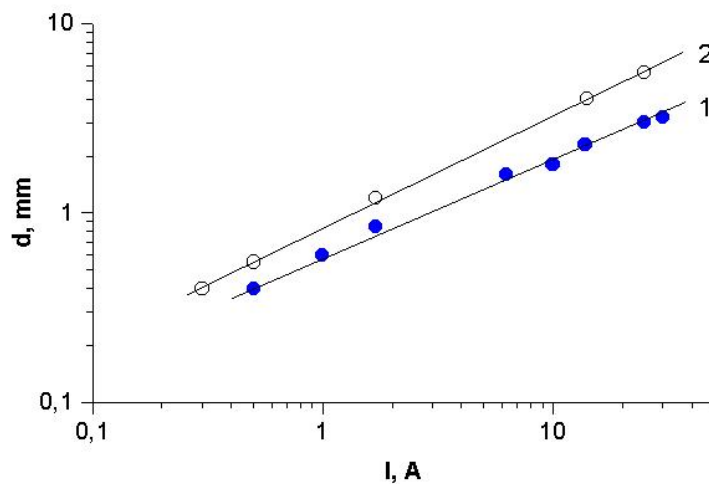


Fig.6.7. Pulse transversal discharge channels diameter versus current in supersonic airflow.
 $M = 2$, $\tau = 200 \mu\text{s}$, $P_0 = 2 \text{ atm}$, $p = 100 \text{ Torr}$.
 Curve 1 – photography with a blue filter (CC-8), curve 2 – photography without a filter.

One can see that the channel's diameter rises with the current according to a law $d \sim E^{-0.5}$. A diameter of the hot region in this case is by $\approx 1,5$ -2 times less than those of the luminescent region.

It was shown earlier [1] and confirmed now that the neutral particle temperature is slowly decreasing along a airflow. Thus, we can operate the mean gas temperature of main part of discharge. The correlation between this mean gas temperature and discharge current is shown in Fig.6.8.

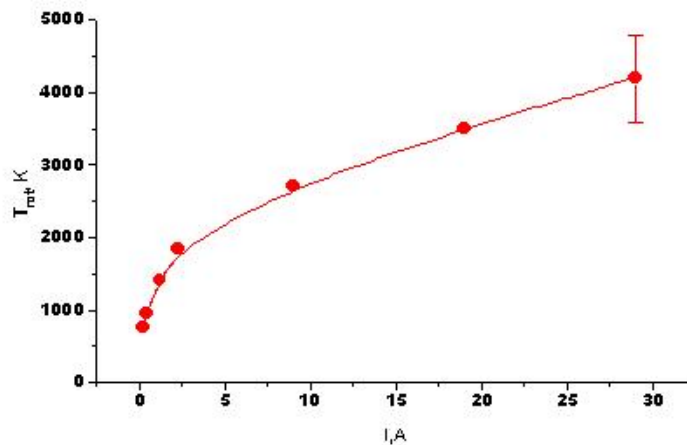


Fig.6.8 a. Mean gas temperature as a function of discharge current
 $P_0 = 1 \text{ atm}$, $p = 40 \text{ torr}$, $M = 2$, $L = 12 \text{ mm}$, $z = 1 \text{ cm}$.

One can easily see that the temperature in linear scale rises quickly at small currents (in the glow discharge mode) up to $T=2000 \text{ K}$ value and then its rise slows down. Such a behavior is practically opposite to the behavior of an electric field with a current.

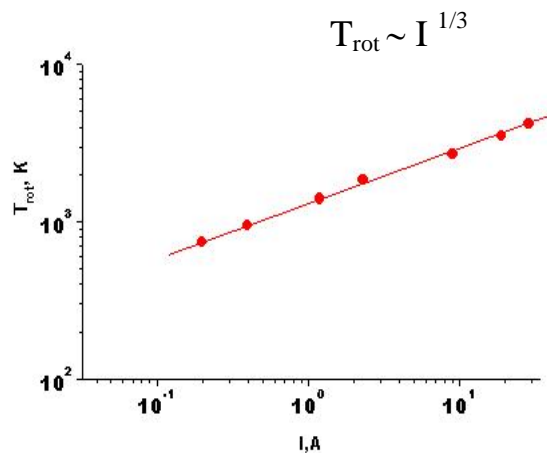


Fig.6.8 b. Mean gas temperature as a function of discharge current (the same data)
 $P_0 = 1 \text{ atm}$, $p = 40 \text{ torr}$, $M = 2$, $L = 12 \text{ mm}$, $z = 1 \text{ cm}$.

It is typical that temperature - current dependence has a direct power law (see Fig.6.8 b). $T \sim I^{1/3}$ in studied range of parameters.

Temperature drop is observed at full pressure increasing from $P_0=1$ atm to $P_0=4$ atm at all currents (compare Fig.6.8a and Fig.6.9) though this difference is insignificant at small currents.

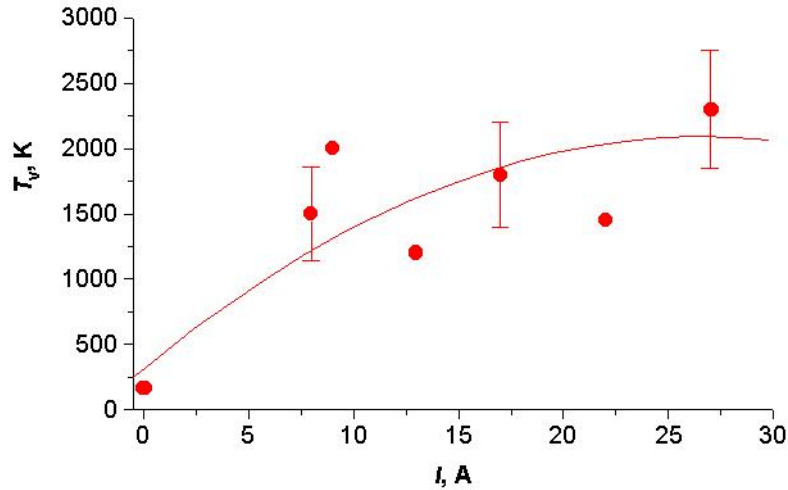


Fig.6.9. Mean gas temperature as a function of discharge current
 $P_0 = 4$ atm, $p = 200$ torr, $M = 2$, $\tau = 480 \mu\text{s}$, $L = 12$ mm, $z = 2$ cm.
 Temperature measurements have been performed on relative intensities of CN bands.

In general we have to conclude that experimentally obtained gas temperature absolute values at high currents reach several thousands degrees though they stay smaller than the value of the electron temperature $T_e \approx 10^4$ K, calculated for these conditions. So plasmas in conditions under the investigation is nonequilibrium one, it is insufficient to know the gas temperature value for determining of its conductivity, and direct measurements of the electron concentration are necessary.

Results of measurements show, that electron densities in the anode and the cathode discharge regions differ not more than by 2 times and they decrease not more than by 2 – 3 along the channel length. This drop is caused evidently by an expansion of the discharge channel along an axial coordinate. So for the determined range z one can use an average concentration value. Determined charged particle concentration – discharge current dependence is shown at Fig. 6.10. Measurements were made at $z = 3$ cm with a help of automatized scheme with optical separation [1].

In Fig. 6.10 a one can see data obtained both by the probe method and based on Stark effect. At that the concentration values were determined from the data about the ion current. In analysis were considered two mechanisms of ion reaching the probe: one of them was connected with diffusion and another with the drift. It is easy to see that calculation results in the case of small currents (corresponding to high electric fields in the plasma) at drift mechanism supposition correspond more to Stark effect measurements than calculations at diffusion mechanism supposition.

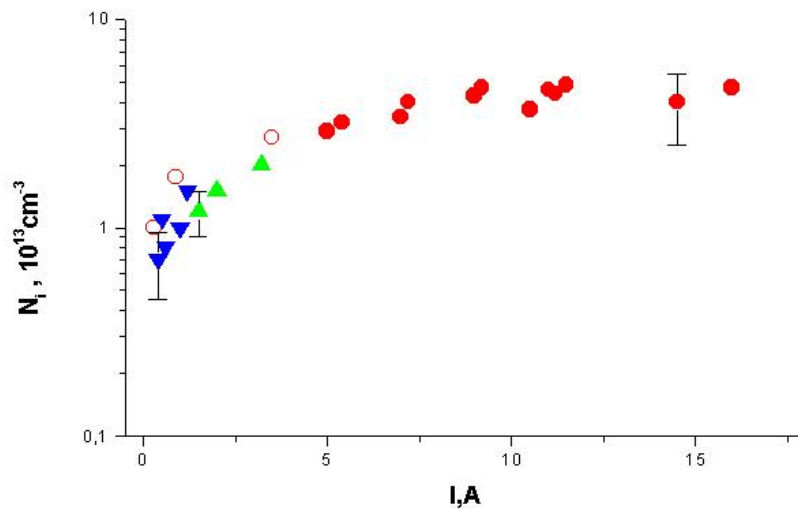


Fig.6.10 a. Plasma density versus discharge current.

$P_0 = 1 \text{ atm}$, $p = 40 \text{ Torr}$, $z = 3 \text{ cm}$.

○ – diffusion $\varnothing 0,2 \text{ mm}$, ● – diffusion $\varnothing 0,3 \text{ mm}$ ▼ – drift $\varnothing 0,5 \text{ mm}$, ▲ Stark

One can see that the concentration quickly increases at small currents and then its rise slows down. The same data expressed in double logarithmic scale, see Fig. 4.10 b, show that the concentration behavior can be described by the power dependence:

$$N_i \sim \begin{cases} I^{2/3}, & I < 1 \text{ A} \\ I^{1/3}, & I > 1 \text{ A} \end{cases}$$

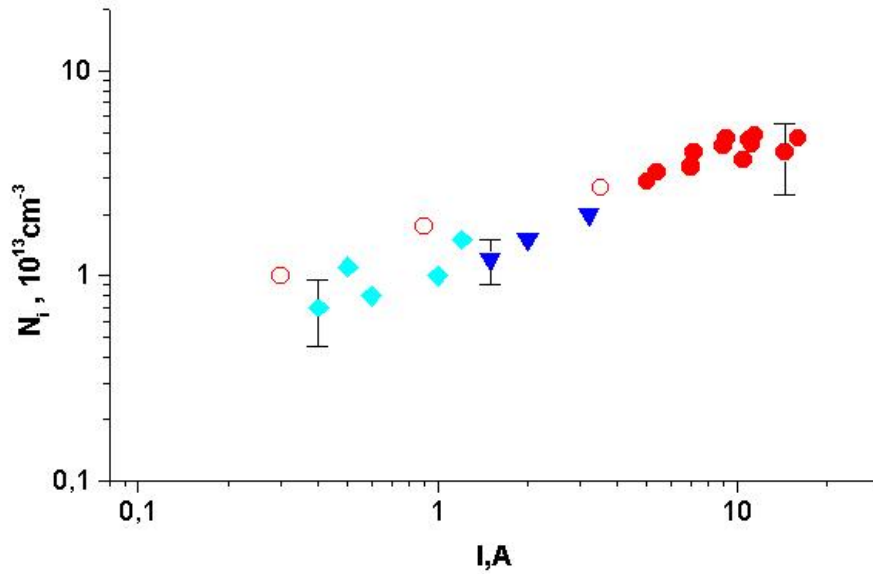


Fig.6.10 b. Plasma density versus discharge current.

$P_0 = 1 \text{ atm}$, $p = 40 \text{ Torr}$, $z = 3 \text{ cm}$

○ – diffusion \varnothing 0,2 mm, ● – diffusion \varnothing 0,3 mm, ◆ - drift \varnothing 0,5 mm, ▼ – Stark .

§ 2. Parameters of electrode ignition discharge in supersonic propane-air flows

The investigation of the transversal discharge in supersonic propane-air flow was performed in case of scheme of test channel, showed in Fig.1.2 – 1.3 of Chapter I. Typical view of the ignition process of the air-propane mixture with the help of pulsed-periodic discharge in the supersonic channel was shown in Fig.6.11.

The main measurements of plasma parameters were performed under the chamber pressure $p = 200 - 300 \text{ torr}$, total pressure $P_0 = 2 \text{ atm}$, stagnation temperature $T_0 = 300 \text{ K}$. Under these conditions the propane mass fraction was about the stoichiometric one.

A single pulse mode was used. The discharge current varied from 2 up to 40 A, the duration of the input energy pulse varied from 50 up to 1000 μs .



Fig.6.11. The supersonic propane-air flow ignition by transversal pulse-periodic discharge. The pulse duration $\tau=200 \mu\text{s}$, the pulse repetition rate $f=10 \text{ Hz}$, discharge current $I=20 \text{ A}$.

The comparison of electric fields in plasmas of pulsed transversal discharges in supersonic flows of the air and the air-propane mixture are presented in Fig.6.12.

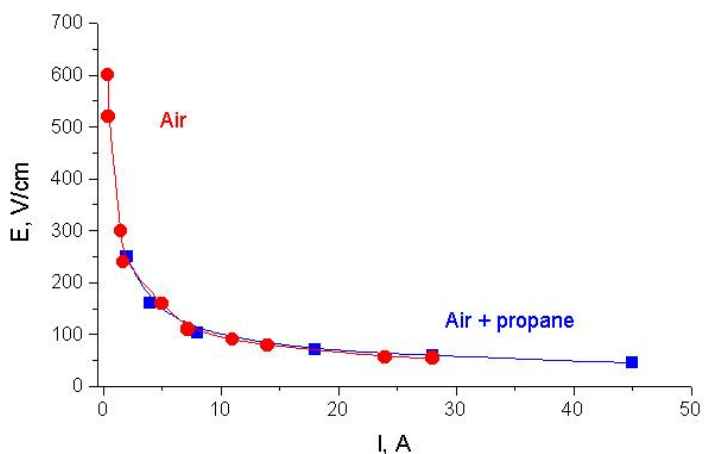


Fig.6.12. Comparison of the values of electric field in plasmas of the pulsed transversal discharge in the supersonic flow in the air and in the air-propane mixture.

$P_0 = 4 \text{ atm}$, $p = 200 \text{ torr}$, $M = 2$. $\tau = 1 \text{ ms}$, $D_0 = 15 \text{ mm}$.

● – air , ■ – air+propane (stoichiometric ratio).

One can see that the addition of propane up to stoichiometric ratio has no influence on the value of the discharge electric field. As a result, data measured in a discharge in a supersonic airflow may be used for the corresponding discharge in an air-propane supersonic flow.

Discharge plasma temperature value in air – propane mixture supersonic flow is significantly higher (see Fig.6.13) than those in the supersonic airflow at the same full pressure, where it does not exceed 2000 K (see Fig.6.9). Undoubtedly that such considerable temperature jump (with respect to air plasmas) can be explained only by the fact of propane – air mixture ignition. One can see that the plasma temperature is achieved the value about 3500 K at $z \geq 3$ cm and slowly decreasing along a flow.

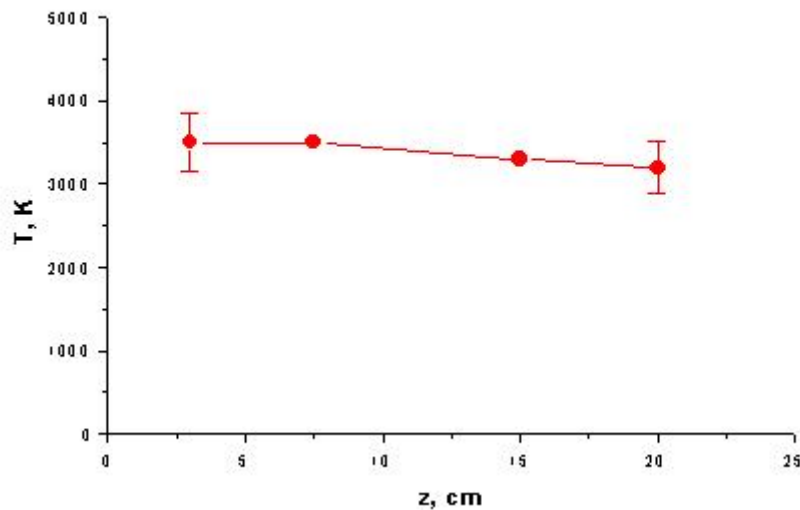


Fig.6.13. Temperature distribution in plasma of pulse-periodic longitudinal discharge in supersonic propane-air flow along the axis of flow.

$p = 200$ Torr, $P_0 = 4$ atm, $M \approx 2$, $L = 10$ cm, $\tau = 480$ μ s, $I = 8$ A.

The range of parameters of the pulsed transversal electric discharge, in which the ignition of the propane-air mixture flow is observed, is shown in Fig.6.14. It seems that there is an electric power density threshold of combustion. Under the condition of our experiment ($P_0 = 4$ atm, $p = 200$ Torr, $M = 2$) this threshold is equal to about 0.5 kW/cm, at smaller electric power density the combustion is not observed.

The growth of electric power density results in reduction of the pulse duration. The dependence between the electric power density and the pulse duration is close to $I E \sim \tau^{-m}$, where $m \approx -1$.

Under the higher level of electric power density, shock wave generation is observed.

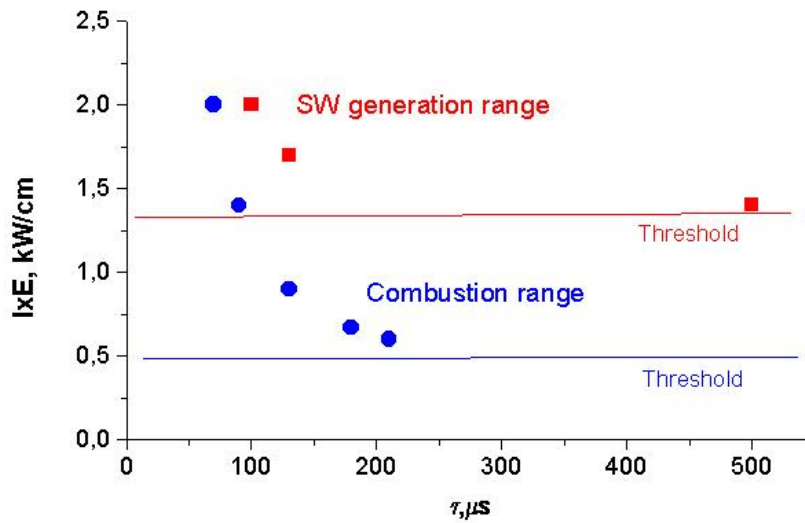


Fig.6.14. Threshold electric power in the plasma of the pulsed transversal discharge in the supersonic air-propane flow over the pulse duration
 $P_0 = 4 \text{ atm}$, $p = 200 \text{ Torr}$, $M = 2$.

The value of τ is proportional to a discharge size along a flow (see §2) in studied range of parameters, it means that approximately constant value of energy inputted to a discharge $W_{thresh} \approx (IU\tau)_{thresh}$ corresponds to an ignition boundary. Experimental results in these coordinates are presented in Fig. 6.15.

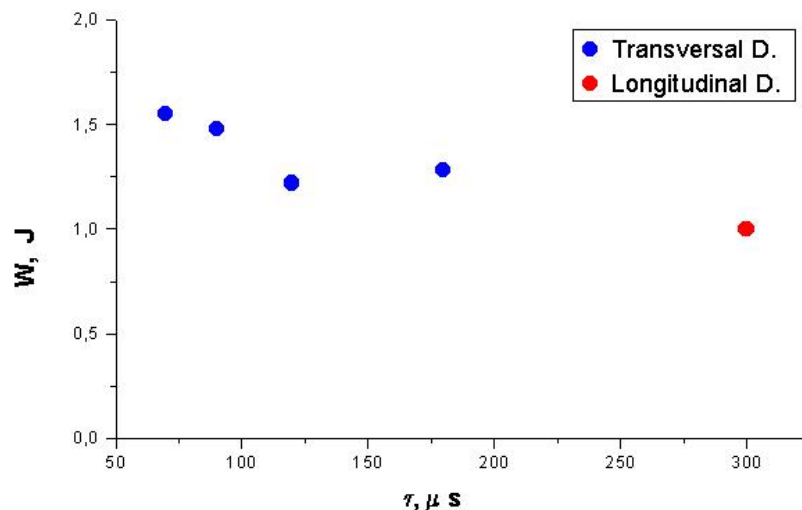


Fig.6.15. Threshold ignition energy value of supersonic propane-air mixture flow by a longitudinal and transversal discharges with respect to pulse duration. A point at $\tau = 300 \mu\text{s}$ corresponds to the longitudinal discharge. $P_0 = 4 \text{ atm}$, $p = 200 \text{ Torr}$, $M = 2$.

One can see that a value of energy inputted to a discharge, which determines an ignition threshold, is weakly dependent on pulse duration, and in essence it determines the ignition. If it is so, then at constant value of a discharge current I and pulse duration τ there has to be a discharge length (determining U and W_{thresh} as well), below which the ignition will not occur.

The longitudinal discharge allows varying a discharge gap length at constant pulse duration. Typical waveforms of CH radiation at different discharge lengths are presented in Fig. 6.16. One can see that the ignition does not occur at decreasing of the discharge length below some definite value. Boundary value of energy inputted to a longitudinal discharge is shown in Fig. 6.15. It is close to the energy value necessary for ignition caused by the transversal discharge.

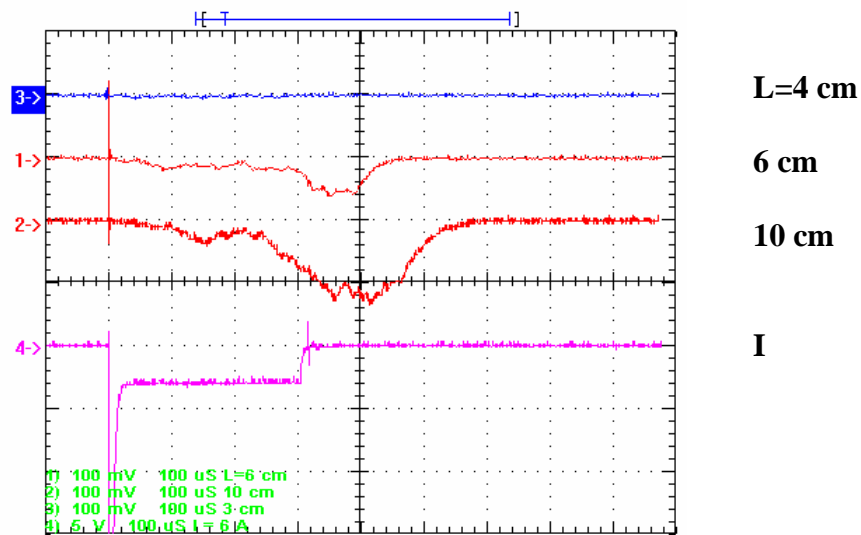


Fig.6.16. The influence of length of longitudinal discharge on ignition of supersonic propane-air flow. $p = 200$ Torr, $P_0 = 4$ atm, $M \approx 2$, $I = 6$ A, $\tau = 300$ μ s. Waveforms of CH radiation at different discharge length L : $L = 4$ cm (curve 3), $L = 6$ cm (curve 1), $L = 10$ cm (curve 2). Curve 4 is the waveform of discharge current pulse.

§ 3. Macroscopic parameters of a plasmadynamic discharge in a supersonic air and propane - airflows

Series of experiments have been carried out for plasma jet generated by a pulsed plasmatron to investigate mode generation. Plasma jet was injected into steady air. An external electrical discharge parameters were measured by a low-inductance voltage divisor (the discharge gap voltage over time) and the Rogowsky belt (the discharge electric current over time). The signals were registered by a memory oscilloscope.

Waveforms of the discharge voltage and electric current for a 50- μF capacity are typical for plasmadynamic discharges (Fig.6.17). The first current half-period is 28 μs long, and the second lasts for 40 μs . The maximal electric current I_{max} is 12 kA, the discharge voltage U_{max} is up to 3.2 kV. Under conditions of our experiments, these values varied in the ranges of $I_{\text{max}} = 10 \div 20$ kA, $U_{\text{max}} = 2 \div 4$ kV.

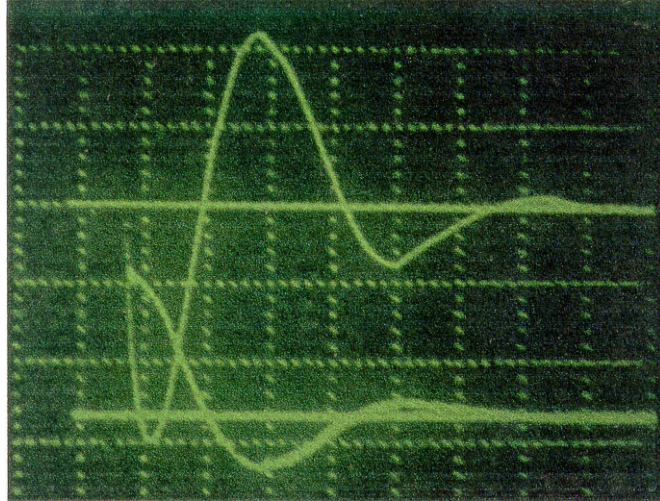


Fig.6.17. Typical view of discharge voltage and electric current waveforms.

The oscilloscope traces can also yield the discharge electric power over time, as well as the energy input into the plasma (Fig.6.18 a,b).

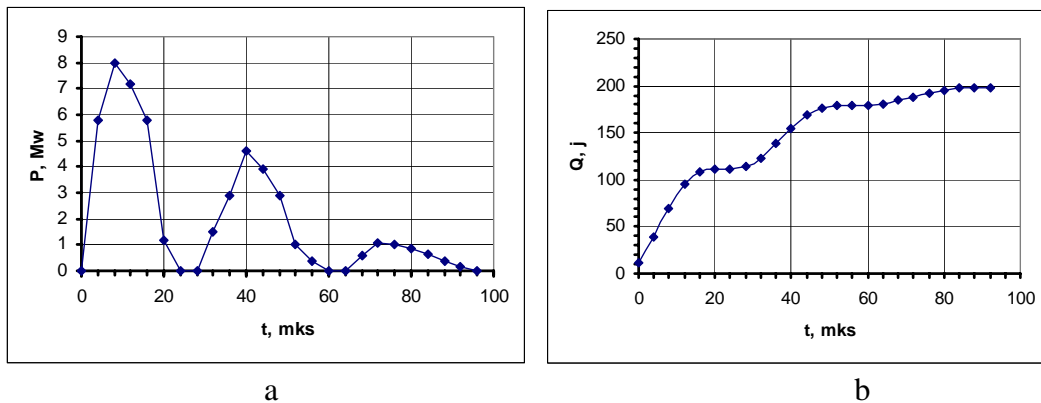


Fig.6.18. An electric power (a) and energy input into the plasma (b) versus time.

Such computations have shown that the main part of energy is supplied during the first two half-periods, i.e. during 65-70 μs . Note that, according to optical and probe measurements, the total lifetime of the discharge plasma before its decay is 400-600 μs .

A high-speed photo camera was applied for studying spatial and temporal characteristics of the plasma jets generated by the plasmatron. The exposition time of a frame was 16 μs (the mirror rotation frequency was 15000 revolutions per minute).



Preliminary experiments have been carried out for plasma flows into the steady atmosphere. For so doing, the plasma generators had been fixed in a gas/vacuum chamber with a possibility of a broad range air pressure variation. Structures similar to those studied in [1] have been observed. A peculiarity of these discharges is a low (1.4...2.3) ratio of the internal diameter of the carrier (1) and the external diameter of the rod electrode (4) in a comparison with values (3...5) characteristic for “classical” MPC (magnetoplasma compressor) discharges.

Frames of Fig.6.19 show typical dynamics of the plasma jet under conditions, which provide formation of plasma jets close to the classical magnetoplasma compressor (MPC) jets. One can see the cumulative phase of the discharge with further formation of the plasma jet. Analogous high speed photographs have yielded the plasma jet length and the speed of jet propagation over time for various discharge conditions.

Fig.6.19 A typical dynamics of the plasma jet in steady air. The exposition time of a frame was 16 μs .

Fig. 6.20 shows plasma size evolution. One can see that during the first phase the speed of plasma jet propagation is high, but then the plasma length stabilizes. Maximal length of plasma jets after the main energy input period achieves 50...90 mm.

An analysis of such graphs shows that during the first half-period of the electric current the speed of plasma jet propagation is as high as 1...3 km/s. During the second half-period is much lower (500...800 m/s). After that the speed drops to values less than 100 m/s.

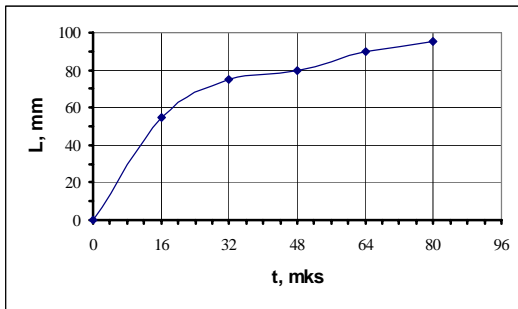


Рис. 6.20a. Plasma jet length over time.
 $C = 100 \mu\text{F}$, $U = 3.5 \text{ kV}$, $p = 200 \text{ Torr}$.

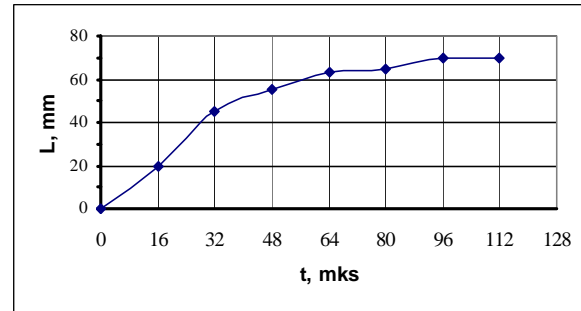


Рис. 6.20b. Plasma jet length over time.
 $C = 50 \mu\text{F}$, $U = 3.5 \text{ kV}$, $p = 300 \text{ Torr}$.

The next series of experiments was bound with studies of ignition by the pulsed plasmatron. In these experiments the plasmatron was fixed in the newly developed discharge chamber (see Ch.1) so that its muzzle was 2 mm apart from the gas flow channel, and the angle between the axes of the plasmatron and the channel was 135° . The capacity C was as a rule $50 \mu\text{F}$, the initial voltage of the capacitor was (2.5 - 4) kV. Under these conditions the plasma jet dynamics is analogous to the classical MPC discharge jet dynamics.



Fig.6.21. Photo frames of plasma jet injected into propane-air flow.
 $C = 50 \mu\text{F}$, $U = 3 \text{ kV}$, $p = 300 \text{ Torr}$, $P_0 = 3 \text{ atm}$.

Typical photo frames are shown in Fig.6.21. Series of such frames yield plasma jet length over time. Unfortunately, excess exposition in the plasma jet radiation makes it difficult to determine the jet size during the cumulative stage; before and after this stage, the plasma jet boundary is well seen.

Fig. 6.22 shows typical dependencies of the plasma jet length over time as deduced from the photo frames. One can see that during the cumulative stage the speed of plasma jet propagation in a supersonic gas flow (0.9...1.5 km/s) practically coincides with that in a steady gas. Later, when the plasma leaves the discharge chamber, its speed approaches the speed of the supersonic gas flow (500...650 m/s).

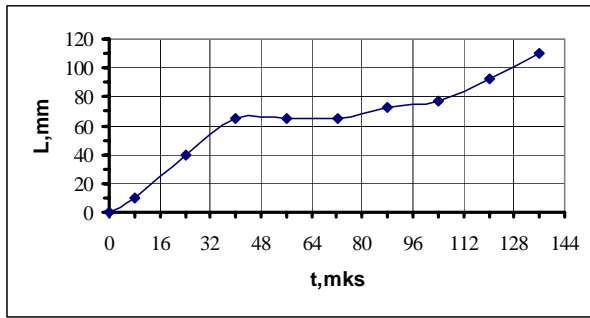


Рис. 6.22a.

Plasma jet length over time for a discharge in the channel with airflow.

$C = 50 \mu\text{F}$, $U = 4.5 \text{ kV}$, $p = 300 \text{ Torr}$, $P_0 = 3 \text{ atm}$.

$v_i = 1.6 \text{ km/s}$, $v_f = 0.7 \text{ km/s}$,

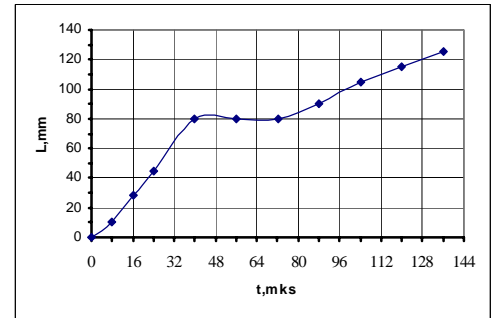


Рис. 6.22b.

Plasma jet length over time for a discharge in the channel with a flow of a combustible propane-air mixture.

$C = 50 \mu\text{F}$, $U = 4.5 \text{ kV}$, $p = 300 \text{ Torr}$, $P_0 = 3 \text{ atm}$.

$v_i = 2 \text{ km/s}$, $v_f = 0.7 \text{ km/s}$,

Note that during the first, cumulative phase, when the plasma jet propagation speed is high, a gas dynamical blockage of the supersonic gas flow is possible, which can result in its partial or full stopping. During next stages the gas flow recovers. Such a gas dynamical blockage, according to the probe measurements, can result in formation of two sequent plasma volumes, which travel down the quartz channel with the gas flow.

§ 4. Plasma density of a plasmadynamic discharge in a supersonic air and propane – air mixture flows

Three pairs of $\varnothing 0.3 \text{ mm}$ molybdenum probes were sealed into the tube, the first of them was 12 cm from the electrodes, the rest were positioned with a 10-cm separation from each other. The fourth $\varnothing 1 \text{ mm}$ probe was positioned in the channel end.

Temporary dependencies of the plasma jet length and distributions of charged particles density along the channel can be determined with use of probes with a fixed bias voltage.

The comparison of the plasma jet length over time deduced from the probe signals and deduced from the photo frames are shown in Fig. 6.23. One can see that the speed of plasma jet propagation in a supersonic gas flow deduced from the probe signals is closed to that deduced from the photo frames despite of a variation of full and ambient pressures. Absolute value of initial speed of jet is defined mainly the value of discharge energy content, whereas the value of final speed is close to speed of a flow.

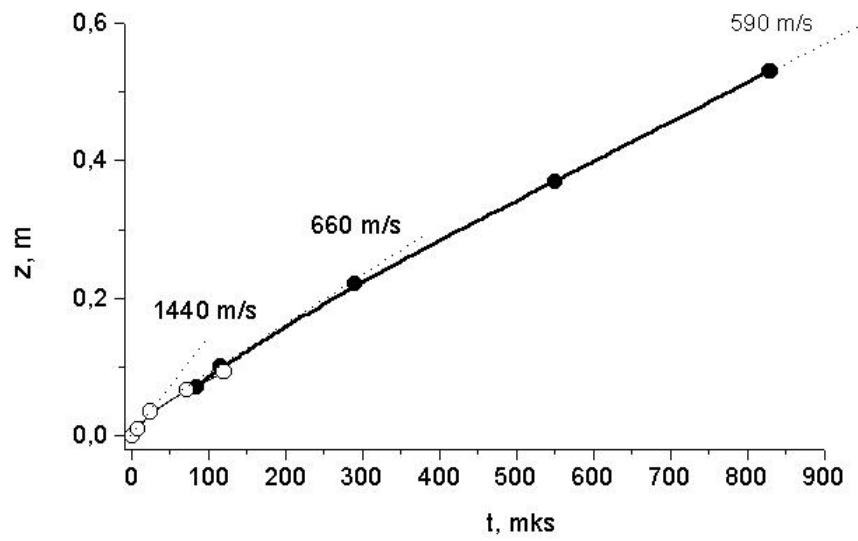


Fig.6.23. Plasma jet length over time for a discharge in the channel with airflow.
 ○ - high speed photo measurements, $C = 50 \mu\text{F}$, $U = 3.0 \text{ kV}$, $p = 300 \text{ Torr}$, $P_0 = 3 \text{ atm}$.
 ● - probe measurements, $C = 50 \mu\text{F}$, $U = 3.0 \text{ kV}$, $p = 100 \text{ Torr}$, $P_0 = 2 \text{ atm}$.

Axial distribution of the maximal value of probe current is shown on Fig.6.24. One can see that this distribution is described by power dependence with an exponent $n \approx -2.2$.

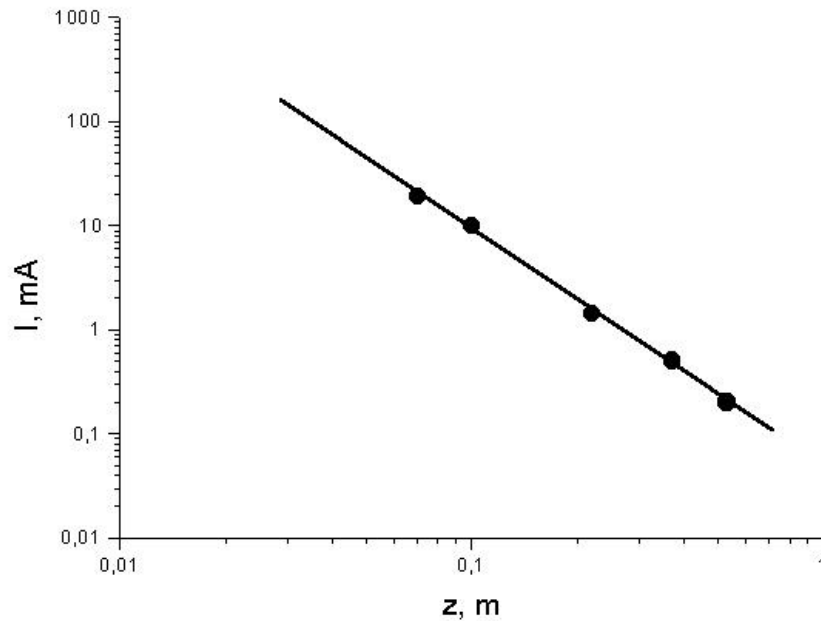


Fig.6.24. Axial distribution of the maximal value of probe current.
 $C = 50 \mu\text{F}$, $U = 2.5 \text{ kV}$, $p = 100 \text{ Torr}$, $P_0 = 2 \text{ atm}$. Transversal probe $\varnothing 0.3\text{mm} \times 14\text{mm}$.

The model of an ion saturation current for subsonic flow can be applied for a determination of ion density n_i . It is possible to believe, that electron temperature is closed to ion temperature. In this case the formula, approximating the results of calculations is [2]:

$$i = 0,43 Re_e^{0,42} \quad (1),$$

where i is dimensionless ion saturation current, Re_e - electric Reynolds number $Re_e = uR/D_i$. The transition to a dimensional current I_i is carried out by the relation:

$$I_i = 4 \pi e n_i D_i L I \quad (2),$$

where D_i is ion diffusion coefficient, L is probe length.

The value of D_i is proportional to neutral particle density. For check of the formula (2) we have carried out measurements of probe ion saturation current at various values of full pressure. These results are shown in Fig.6.25a, b. One can see that ion probe current is inversely proportional to neutral particle density according to formula (2).

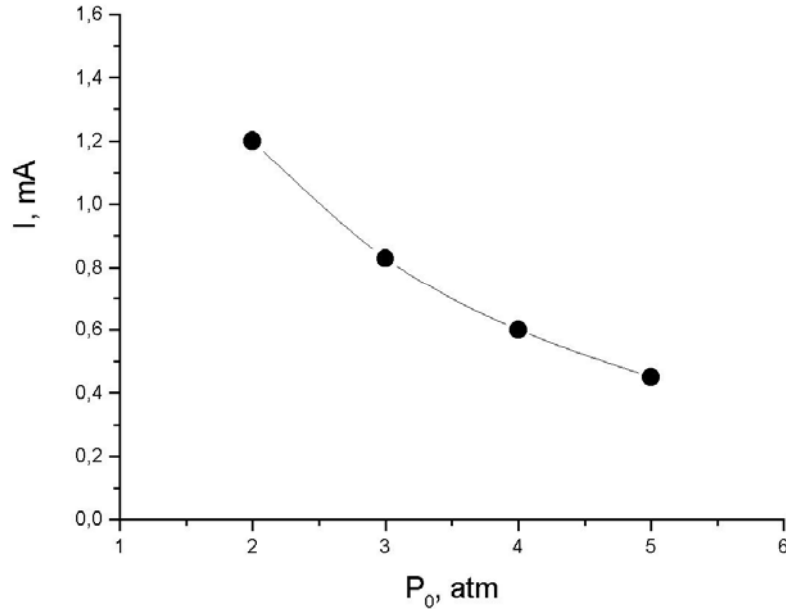


Fig.6.25a. Probe current in plasma jet, injected into supersonic flow, versus full pressure. $C = 50 \mu\text{F}$, $U = 3.5 \text{ kV}$, $p = 100 \text{ Torr}$, $z = 22 \text{ cm}$. Transversal probe $\varnothing 1\text{mm} \times 10\text{mm}$.

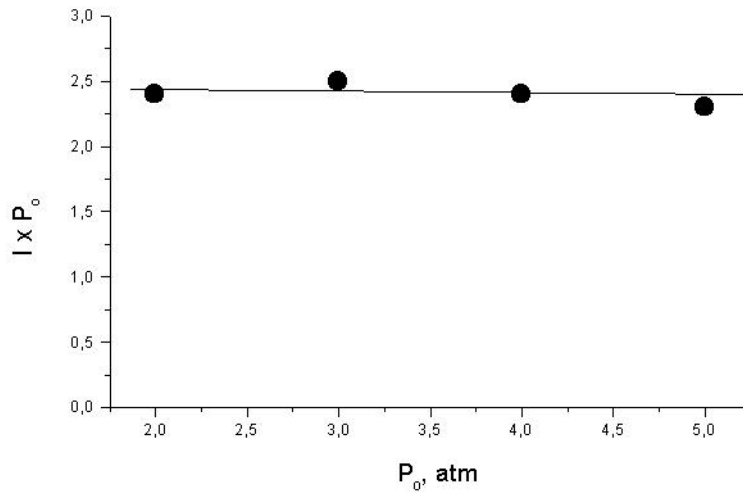


Fig.6.25b. The same data in new axes $I \times P_0, P_0$.

The results of evaluation of plasma density under the formulas (1) – (2) in case of Fig.6.24 are shown in Fig.6.26. One can see, that the magnitude of n_i at axial distances $z \sim 10 - 30$ cm are about $10^{13} - 10^{12} \text{ cm}^{-3}$ accordingly in typical cases of experiments (pressure p is about 100 – 300 Torr, $U = 2.5 - 4 \text{ kV}$, $C = 50 \mu\text{F}$)

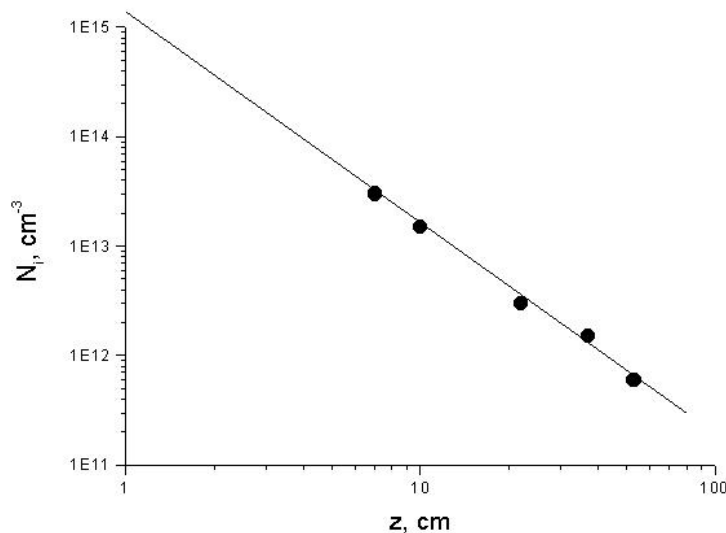


Fig.6.26. Axial distribution of the maximal values of plasma jet density, injected into supersonic airflow. $C = 50 \mu\text{F}$, $U = 2.5 \text{ kV}$, $p = 100 \text{ Torr}$, $P_0 = 2 \text{ atm}$.

The results of measurements of I – V characteristics of double probe at injection of plasmadynamic jet into propane-air supersonic flow were shown that the addition of propane

changes the double probe characteristics slightly. Plasma jet with a small values of input energy time is allowed us to apply not only double but single probes in contrast to case of pulse transversal discharge. A single probe method application is more useful in this case, as electron part of probe characteristic is more sensitive.

Thus the influence of propane addition to air has been performed in single probe mode.

Probe measurements have been performed at the voltage bias $U(t)$ which change linearly from a minimal voltage of -30 V to a maximal voltage of $+30$ V during $10 \mu\text{s}$. The waveforms of a single probe current $i(t)$ allow to not only to measure characteristics of a probe, but also to describe temporary evolution of plasma density. This evolution is described by evolution of amplitude of probe current.

The measurements were carried out in a regime of single pulse with a voltage of the generator being equal to 4.25 kV. The values of the pressure in the chamber, the pressure in the receiver of the compressor were varied. The influence of variation of these parameters on the temporary dependence of probe current in the $x = 32$ cm cross section of the channel is shown in Fig.6.27—6.30.

Change of chamber pressure in 2 times result in relatively small change of probe current (Fig.6.27). However increase of the pressure in the receiver of the compressor result in proportional decrease of electron current as well as it was observed in case of an air jet (Fig.6.28).

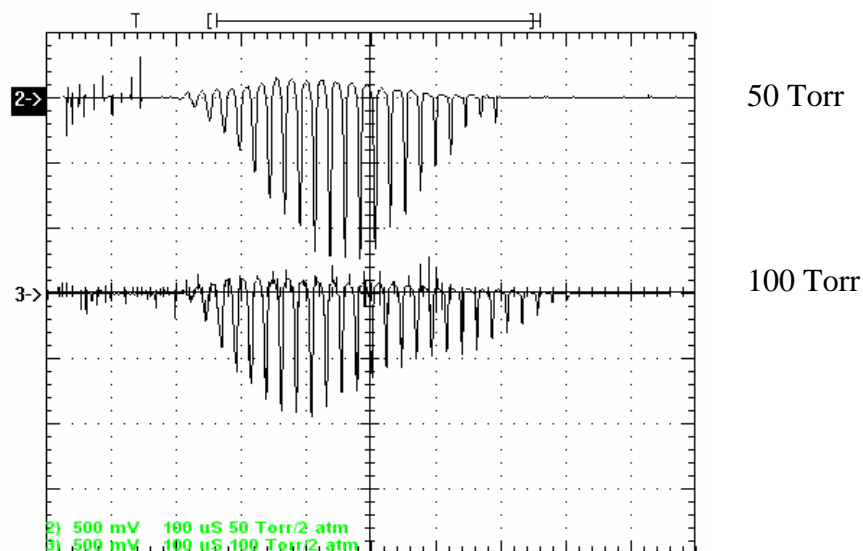


Рис.6.27. The influence of variation of the pressure in the chamber on the temporary dependence of ion and electron probe current at injection of plasmadynamic jet into supersonic airflow.

$$P_0 = 2 \text{ атм}, U = 4,25 \text{ кВ}, C = 50 \mu\text{F}.$$

$$\text{Single probe } \varnothing 0.3 \text{ мм}, L = 10 \text{ мм}, x = 32 \text{ см}.$$

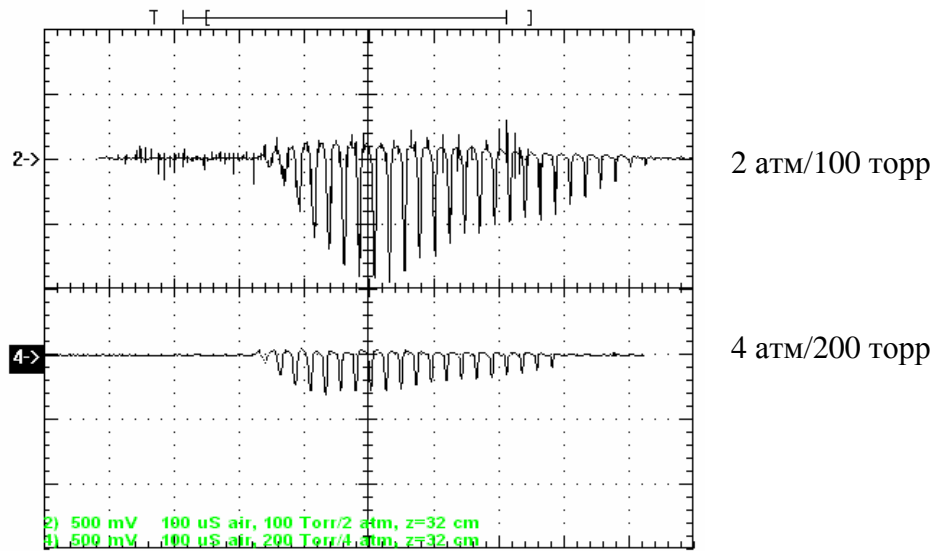


Fig.6.28. The influence of variation of the pressure in the receiver of the compressor on the temporary dependence of ion and electron probe current at injection of plasmadynamic jet into supersonic airflow.

$$P_0/p = 2, U = 4,25 \text{ kV}, C = 50 \text{ }\mu\text{F}.$$

Propane addition to airflow has resulted in change of small value in the signal of electron probe current in case of small pressure $p = 100 \text{ Torr}$ (Fig.6.29). However at more high values of pressure the growth as values of probe current as duration of current were observed (Fig.6.30).

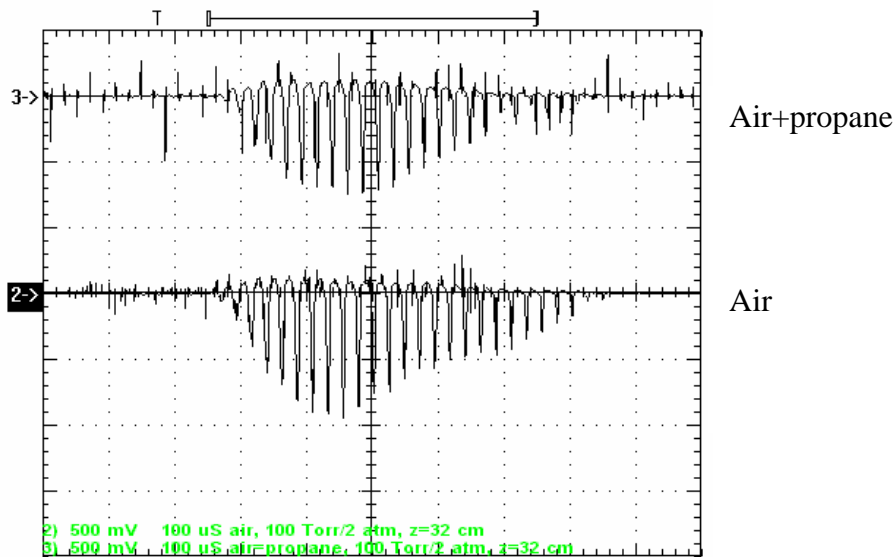


Fig.6.29. The comparison of temporary dependence of ion and electron probe current at injection of plasmadynamic jet into supersonic air and propane-air flows at low chamber pressure.

$P_0 = 2 \text{ атм}$, $p = 100 \text{ Torr}$. $U = 4,25 \text{ kV}$, $C = 50 \text{ }\mu\text{F}$.

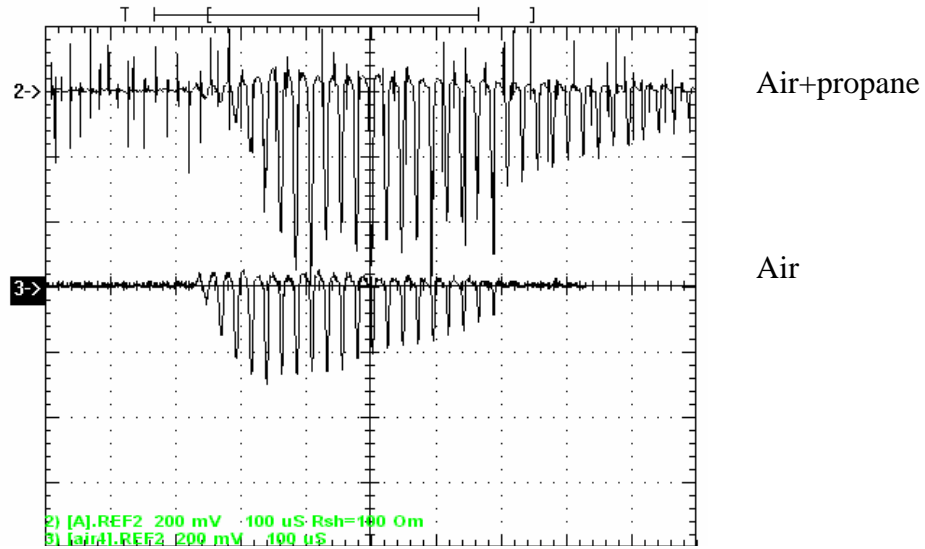


Fig.6.30. The comparison of temporary dependence of ion and electron probe current at injection of plasmadynamic jet into supersonic air and propane-air flows at high chamber pressure.

$p = 200 \text{ топп}$, $P_0 = 4 \text{ атм}$. $U = 4,25 \text{ kV}$, $C = 50 \text{ }\mu\text{F}$.

References to Chapter VI.

1. Final Project Technical Report of ISTC 1867p. Development of Methods for Diagnostics of Discharges in Supersonic Flows. Moscow. September 2001.
2. A.P. Ershov, N.V.Ardelyan, V.L.Bychkov, V.A.Chernikov, V.M.Shibkov, O.S.Surkont I.B.Timofeev. Mechanisms of transversal electric discharge sustantion in supersonic air and propane-air flows 41st Aerospace Sciences Meeting and Exhibit and 5th Weakly Ionized Gases Workshop, Reno, Nevada, 6-9 Jan.2003 AIAA 2003-0872
3. A.Ershov, N.Ardelyan, S.Chuvashev, V.Shibkov, I.Timofeev. Probe diagnostics of gas discharges in supersonic airflows. AIAA Journal, Vol. 39, No 11. P.2180, 2001.
4. Ardelyan N.V., Bychkov V.L., Gordeev O.A., Ershov A.P., Timofeev I.B. Peculiarities of transversal discharge in a flow as non self maintained in air. II. Theoretical model of electric discharge in a supersonic flow.

CHAPTER VII.
SIMULATION OF AN IGNITION DISCHARGE IN A SUPERSONIC
PROPANE-AIR MIXTURE FLOW

§ 1. Heat source model of the discharge
in supersonic air-propane mixture flow

The heat source model of gas discharge [1,2] was employed for description of propane-air supersonic flow ignition. The laminar flow was described by Navier-Stokes equations with additional source term in energy equation.

Heat supply power distribution in source is given by Gauss law

$$\omega_h = c_h(z) \exp(-(r/\beta_h(z))^2),$$

where z is distance from the source origin coinciding with cathode, r is distance from source axes, $\beta_h(z)$ and $c_h(z)$ is specified functions of z . Function $c_h(z)$ is defined in terms of total heat supply $P_h(z)$ in cross-section $z = const$.

$$P_h(z) = 2\pi \int_0^{\infty} \omega_h r dr$$

For short initial region $z_{cb} \leq z \leq z_{ce}$ modeling cathode region it is given $P_h(z) = P_c$ and $\beta_h(z) = \beta_c$. In other discharge region $z_{ce} < z < z_{de}$ values of these functions are specified as $P_h(z) = P_s$ and $\beta(z) = a_h \sqrt{z + b_h}$. Parameters a_h and b_h are defined from conditions $\beta(z_{ce}) = \beta_c$, $\beta(z_e) = \beta_e$, where z_e and β_e are specified parameters.

The gas-phase models

For description of propane-air mixture ignition and burning were used three thermally equilibrium gas-phase models

- global model, including 5 species (C_3H_8 , O_2 , N_2 , H_2O , and CO_2) and single global reaction ;
- quasi-global model, including 11 species (C_3H_8 , O_2 , N_2 , H_2O , CO_2 , H_2O_2 , CO , H_2 , OH , O , H), one global reaction, and detailed reactions (Table 1 a,b);

- model with detailed reactions mechanism, including 30 species ($C_3H_8, O, H, O_2, N_2, H_2, CO, OH, H_2O, HO_2, H_2O_2, HCO, CO_2, CH, CH_2, CH_3, CH_4, C_2H, C_2H_2, C_2H_3, C_2H_4, C_2H_5, C_2H_6, C_3H_5, C_3H_6, C_3H_7i, C_3H_7n, CH_2O, CH_2OH, CH_3OH$) and 70 chemical reactions (Table 2 a, b).

Global reaction mechanism [3]

Single global reaction: $C_3H_8 + 5O_2 \Rightarrow 3 CO_2 + 4 H_2O$

reaction rate: $\omega = A \exp(-E/T)[C_3H_8]^\alpha [O_2]^\beta$ mol/cm³s, [] – mole fraction, mol/cm³

$A=1.0 \times 10^{12}$, $E = 15100$ K, $\alpha = 0.1$, $\beta = 1.65$

Quasi-global reaction mechanism [3]

Global reaction: $C_3H_8 + 1.5O_2 \Rightarrow 3 CO + 4 H_2$,

reaction rate: $\omega = A \exp(-E/T)[C_3H_8]^\alpha [O_2]^\beta$ mol/cm³s, [] – mole fraction, mol/cm³

$A=1.5 \times 10^{12}$, $E = 15100$ K, $\alpha = 0.1$, $\beta = 1.65$

Elementary dissociation-recombination reactions

Reverse rate constants $k_r = AT^n \exp(-E/T)$, cm⁶/mol²s

Table 1 a

Reaction	E,K	A	n
O ₂ + M ⇌ O + O + M	0.	4.70e15	-0.28
H ₂ O + M ⇌ OH + H + M	0.	9.26e13	1.
H ₂ + M ⇌ H + H + M	0.	7.50e12	1.
OH + M ⇌ O + H + M	0.	2.00e12	1.
CO ₂ + M ⇌ CO + O + M	2063.	5.90e15	0.
HO ₂ + M ⇌ H + O ₂ + M	-500.	1.65e15	0.
HO ₂ + M ⇌ O + OH + M	0.	1.00e17	0.
H ₂ O ₂ + M ⇌ OH + OH + M	-2510.	9.10e14	0.

Elementary exchange reactions

Reverse rate constants $k_r = AT^n \exp(-E/T)$, cm³/mol s

Table 1 b

Reaction	A	n	E, K
H + O ₂ = OH + O	1.30e13	0.	0.
O + H ₂ = OH + H	7.33e12	0.	3670.
H + H ₂ O = OH + H ₂	2.19e13	0.	2590.
O + H ₂ O = OH + OH	5.75e12	0.	394.
O ₂ + OH = O + HO ₂	5.00e13	0.	500.
OH + OH = H + HO ₂	2.50e14	0.	1000.
H ₂ + O ₂ = H + HO ₂	2.50e13	0.	350.
H ₂ O + O ₂ = OH + HO ₂	5.00e13	0.	500.
H ₂ O ₂ + O ₂ = HO ₂ + HO ₂	1.00e13	0.	500.

HO2	+	H2	=	H2O2	+	H	1.70e12	0.	1887.
H2O	+	HO2	=	H2O2	+	OH	1.00e13	0.	900.
CO2	+	H	=	CO	+	OH	1.50e07	1.3	-400.
CO2	+	O	=	CO	+	O2	3.14e11	0.	18900.
CO2	+	OH	=	CO	+	HO2	1.50e14	0.	11902.

Detailed reaction mechanism [4]

Elementary dissociation-recombination reactions

Reverse rate constants $k_r = AT^n \exp(-E/T)$, $\text{cm}^6/\text{mol}^2 \text{s}$

Table 2 a

Reaction			E, K	A	n
O2	\Leftrightarrow	O + O	0.	2.9e17	-1.
H2O	\Leftrightarrow	OH + H	0.	2.2e22	-2.
H2	\Leftrightarrow	H + H	0.	1.8e13	-1.
OH	\Leftrightarrow	O + H	0.	1.0e16	0.
CO2	\Leftrightarrow	CO + O	2060.	5.9e15	0.
HO2	\Leftrightarrow	H + O2	0.	2.3e18	-0.8
HO2	\Leftrightarrow	OH + O	0.	1.0e17	0.
H2O2	\Leftrightarrow	OH + OH	0.	3.25e22	-2.0
HCO	\Leftrightarrow	CO + H	0.	1.1e15	0.
CH4	\Leftrightarrow	CH3 + H	0.	2.5e11	1.0
CH2O	\Leftrightarrow	HCO + H	0.	4.7e15	0.
C2H4	\Leftrightarrow	C2H2 + H2	0.	1.9e16	0.
C2H5	\Leftrightarrow	C2H4 + H	0.	6.3e13	0.
C2H6	\Leftrightarrow	CH3 + CH3	0.	3.6e13	0.
C3H6	\Leftrightarrow	C2H3 + CH3	0.	3.5e10	0.
C3H7I	\Leftrightarrow	C2H4 + CH3	0.	1.0e11	0.
C3H7N	\Leftrightarrow	C2H4 + CH3	0.	1.6e11	0.
C3H7N	\Leftrightarrow	C3H6 + H	0.	2.9e14	0.
C3H8	\Leftrightarrow	CH3 + C2H5	0.	2.0e17	-1.8
C3H8	\Leftrightarrow	C3H7n + H	0.	3.6e13	0.
C3H8	\Leftrightarrow	C3H7i + H	0.	2.4e13	0.
CH2OH	\Leftrightarrow	CH2O + H	0.	1.4e14	0.

Elementary exchange reactions

Reverse rate constants $k_r = AT^n \exp(-E/T)$, $\text{cm}^3/\text{mol s}$

Table 2 b

Reaction			A	n	E,K
OH	+	O = H + O2	2.00e14	0.	8455.
OH	+	H = O + H2	5.06e04	2.67	3160.
H2O	+	H = H2 + OH	1.00e08	1.60	1661.
O	+	H2O = OH + OH	1.50e09	1.14	50.
OH	+	OH = HO2 + H	1.50e14	0.0	503.
H2	+	O2 = HO2 + H	2.50e13	0.0	348.
H2O	+	O2 = HO2 + OH	6.00e13	0.0	0.
H2O	+	O = HO2 + H	3.00e13	0.0	866.
OH	+	O2 = HO2 + O	1.80e13	0.0	-204.

H2O2	+	O2	=	HO2	+	HO2	2.50e11	0.0	-624.
H2O	+	OH	=	H2O2	+	H	1.00e13	0.0	1802.
H2O	+	HO2	=	H2O2	+	OH	5.40e12	0.0	503.
CO2	+	H	=	CO	+	OH	4.40e06	1.5	-372.
HCO	+	O	=	CH	+	O2	3.00e13	0.0	0.
HCO	+	CO	=	CO2	+	CH	3.40e12	0.0	348.
CO	+	H2	=	HCO	+	H	2.00e14	0.0	0.
CO	+	H2O	=	HCO	+	OH	1.00e14	0.0	0.
CO	+	HO2	=	HCO	+	O2	3.00e12	0.0	0.
CH	+	H2	=	CH2	+	H	8.40e09	1.5	169.
HCO	+	H2	=	CH2O	+	H	2.50e13	0.0	2008.
HCO	+	OH	=	CH2O	+	O	3.50e13	0.0	2008.
HCO	+	H2O	=	CH2O	+	OH	3.00e13	0.0	604.
CH2	+	H2	=	CH3	+	H	1.80e14	0.0	7574.
CH2O	+	H	=	CH3	+	O	7.00e13	0.0	0.
CH2O	+	OH	=	CH3	+	O2	3.40e11	0.0	4499
CH3	+	H2	=	CH4	+	H	2.20e04	3.0	4399.
CH3	+	OH	=	CH4	+	O	1.20e07	2.1	3835.
CH3	+	H2O	=	CH4	+	OH	1.60e06	2.1	1238.
C2H2	+	H	=	C2H	+	H2	1.10e13	0.0	1443.
CH2	+	CO	=	C2H2	+	O	4.10e08	1.5	854.
C2H	+	H2O	=	C2H2	+	OH	1.10e13	0.0	3522.
C2H2	+	H2	=	C2H3	+	H	3.00e13	0.0	0.
C2H2	+	HO2	=	C2H3	+	O2	5.40e11	0.0	0.
C2H3	+	H2	=	C2H4	+	H	1.50e14	0.0	5133.
C2H3	+	H2O	=	C2H4	+	OH	3.00e13	0.0	1515.
CH3	+	CH3	=	C2H5	+	H	3.00e13	0.0	0.
C2H4	+	HO2	=	C2H5	+	O2	2.00e12	0.0	2513.
C2H5	+	H2	=	C2H6	+	H	5.40e02	3.5	2621.
C2H5	+	OH	=	C2H6	+	O	3.00e07	2.0	2573.
C2H5	+	H2O	=	C2H6	+	OH	6.30e06	2.0	325.
C3H5	+	H2	=	C3H6	+	H	5.00e12	0.0	765.
C3H6	+	HO2	=	C3H7I	+	O2	1.00e12	0.0	2513.
C3H7n	+	H2	=	C3H8	+	H	1.30e14	0.0	4881.
C3H7i	+	H2	=	C3H8	+	H	1.00e14	0.0	4196.
C3H7n	+	OH	=	C3H8	+	O	3.00e13	0.0	2942.
C3H7i	+	OH	=	C3H8	+	O	2.60e13	0.0	2248.
C3H7n	+	H2O	=	C3H8	+	OH	3.70e12	0.0	829.
C3H7i	+	H2O	=	C3H8	+	OH	2.80e12	0.0	433.
CH2O	+	H2	=	CH2OH	+	H	3.00e13	0.0	0.
CH2O	+	HO2	=	CH2OH	+	O2	1.00e13	0.0	3619.
CH2OH	+	H2	=	CH3OH	+	H	4.00e13	0.0	3066.
CH2OH	+	H2O	=	CH3OH	+	OH	1.00e13	0.0	853.
C3H8	+	O2	=	C3H7n	+	HO2	5.50e05	1.5	0.
C3H8	+	O2	=	C3H7i	+	HO2	3.00e09	0.5	0.

Numerical method

Numerical integration of the governing equations was performed by TVD type difference scheme of second order accuracy. The spatial discretization of equations was made by using a finite volume technique with a central formulation over structured meshes. The inviscid fluxes through cells interfaces are calculated using exact Riemann problem solution defined by interfacial values of parameters in the adjoining cells. These values were calculated by limited one-dimensional extrapolation of primitive variables from cells centers to cells sides. Viscous fluxes through sides of cells were determined by the space centered difference formulas. Difference equations are solved with implicit two-layer iterative procedure. The flow field parameters were computed due Gauss-Seidel line relaxation numerical technique on every iteration.

Computation space domain was limited by boundaries: $0 \leq z \leq 14$ cm, $0 \leq r \leq 2$ cm accordingly experiment conditions. The non-uniform structured grid with number cells of 300×75 was used. The cells are condensed in heat source origin region in axial direction and near axis in radial direction.

§2. Results of simulation of ignition of supersonic propane-air mixture flow by electric discharge

The presented results are computed for experimental condition which took place at research of process of ignition by longitudinal and transversal discharges:

total pressure $P_0 = 4$ atm, total temperature $T_0 = 300$ K, Mach number $M = 2$ and stoichiometric composition of fuel mixture.

Comparison of the results received for all models considered above, was carried out. Comparison of model with quasi-global reaction mechanism and model with detailed reactions mechanism has shown, that difference of results is insignificant. The results received with the help of model with detailed reactions mechanism further are submitted.

In all cases it is supposed that $z_{cb} = 0.1$ cm, $z_{ce} = 0.2$ cm, $z_e = 12$ cm. The effects of the heat source power, geometry and time expansion type on the ignition process were studied.

The values of varied parameters are listed in Table 2

Table 2.

Case	z_{de} , cm	β_c , cm	β_e , cm	P_c , w/cm	P_s , w/cm				
1.1	14	0.01	0.15	125	50				
1.2	14	0.01	0.15	237.5	55				

1.3	14	0.01	0.15	150	60				
2.1	14	0.02	0.15	500	50				
2.2	14	0.02	0.15	550	55				
2.3	14	0.02	0.15	600	60				
	3	0.01	0.15						

Predicted distributions of temperature along axis are shown on Fig. 1. The distance Z on figures is measured from heat source origin. The temperature distributions in non-reacting gas flow with same heat supply are shown by dotted lines.

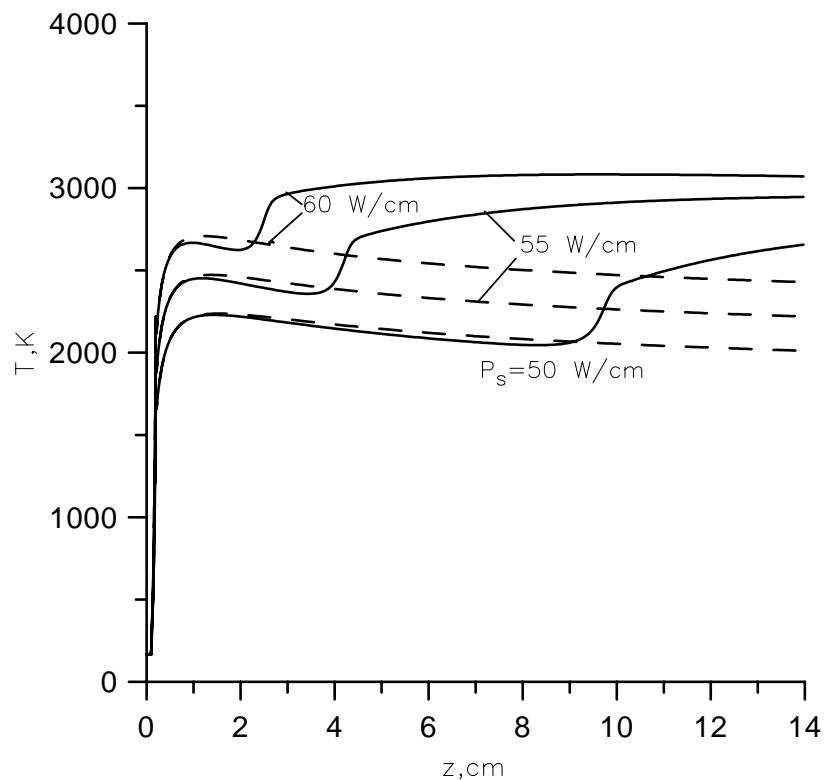


Fig.7.1. Gas temperature axial distributions in supersonic propane-air flow at some values of heat supply powers per unit length. $L_s = 14$ cm. Cathode region radius $\beta_c = 0.2$ mm. Dotted lines describe distributions in a non-reacting flow and continuous lines - reacting gas flow.

One can see that the temperature of non-reacting flow does not differ from a case when reactions of burning are possible. Sharp jump of temperature takes place only at a great distance (≈ 10 cm) and undoubtedly testifies to ignition of a flow. Results of calculations of propane mole fraction axial distributions (Fig.7.2) and especially CH mole fraction axial distributions (Fig.7.3) show also the fact of ignition. The increase of heat supply power results in faster ignition of a

flow, and characteristic length (time) of ignition corresponds to a given value of power. Also calculations show, that at reduction of power up to some critical value (~ 40 W/cm) ignition has no place even at the maximal length of a source.

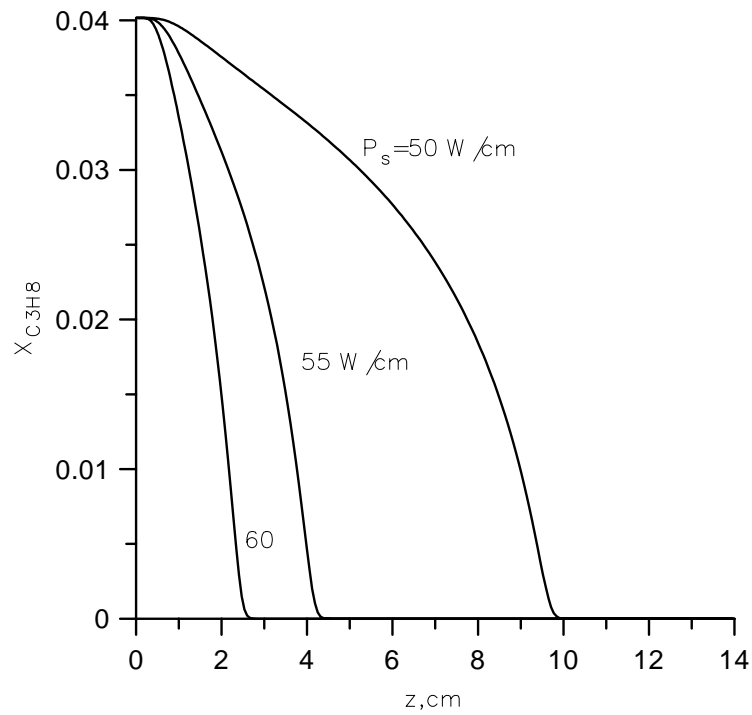


Fig.7.2. Propane mole fraction axial distributions in supersonic propane-air flow. $L_s = 14$ cm. $\beta_c = 0.2$ mm.

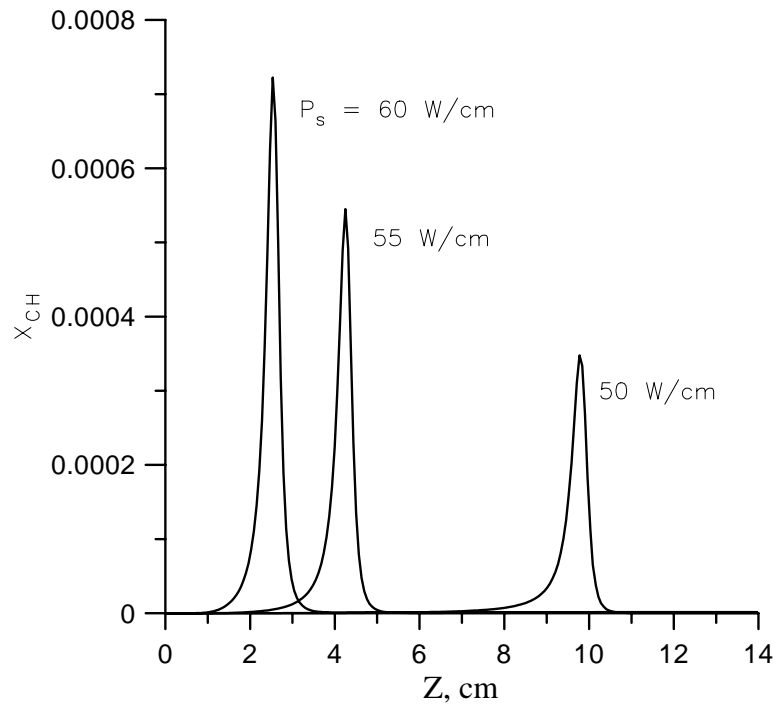


Fig.7.3. CH mole fraction axial distributions in supersonic propane-air flow at some values of heat supply powers per unit length. $L_s = 14$ cm, $\beta_c = 0.2$ mm.

Thus, in the consequence with experimental data there is the threshold value of heat supply power determining ignition. The value of a threshold in experiment is equal to about 500 W/cm of electric power. Computed value of the threshold of supply power enclosed in heating of gas, is equal to about 10 % from this value. 10 % heat to electric power ratio does not contradict the available data. It means that it is impossible to ignore the thermal mechanism of ignition of propane – air mixture flow completely.

Burning of a flow takes place also in a radial direction. Ignition occurs on an axis of a thermal source (since the temperature on an axis is maximal) and is accompanied by expansion of burned down propane zone with growth z (Fig. 7.4).

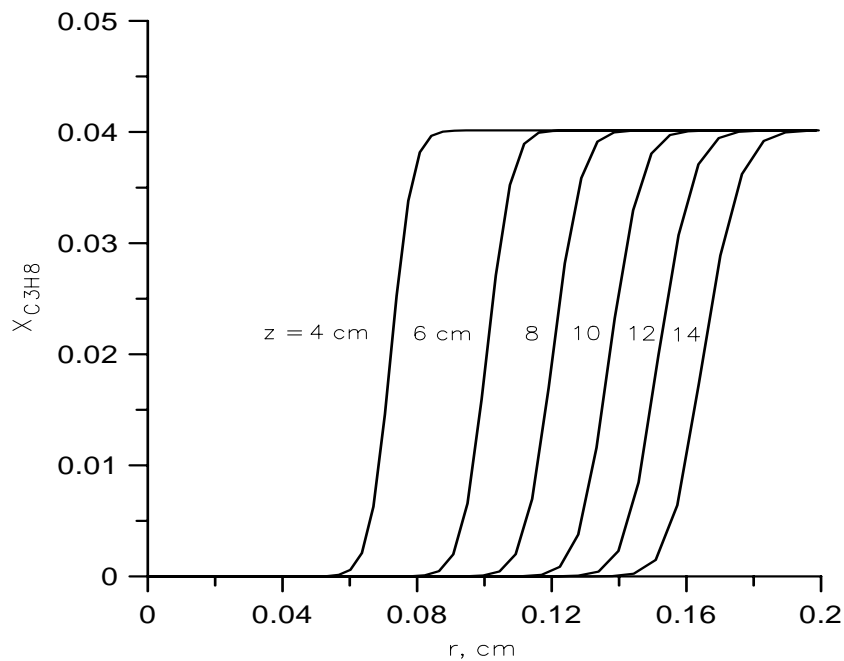


Fig.7.4 Propane mole fraction radial distributions in supersonic propane-air flow at some distances along flow.

$L_s = 14$ cm, $P_s = 60$ W/cm. $\beta_c = 0.2$ mm.

Influence of extent of a heat source along a flow on axial distribution of parameters is shown on Fig. 7.5 – 7.8. It is visible, that the axial temperature, if ignition has taken place, in case of even short ($L_s = 3$ cm) thermal source exceeds value of temperature for a non-reacting flow.

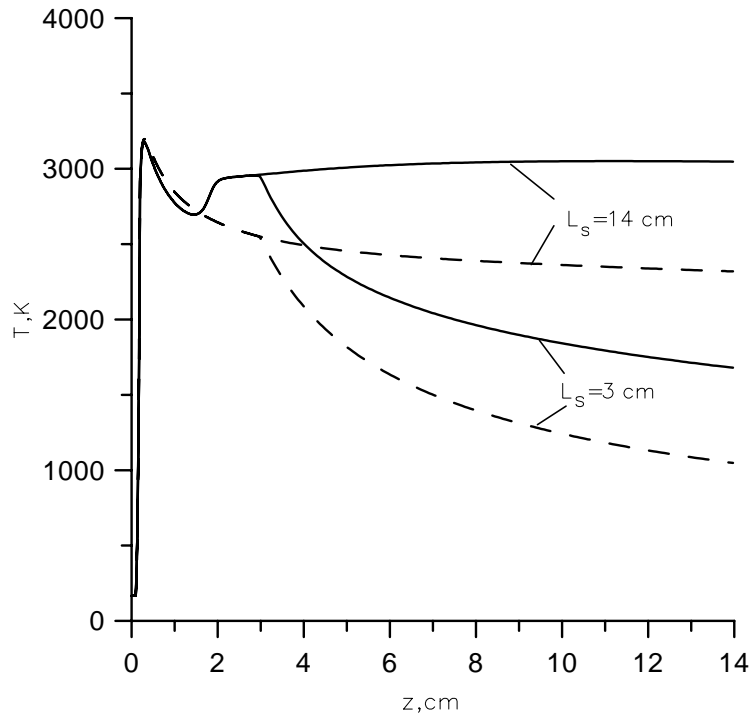


Fig.7.5. Gas temperature axial distributions in supersonic propane-air flow at some values of heat source expansion. Dotted lines describe distributions in a non-reacting flow and continuous lines - reacting gas flow. The heat supply power per unit length $P_s = 60 \text{ W/cm}$, $\beta_c = 0.1 \text{ mm}$

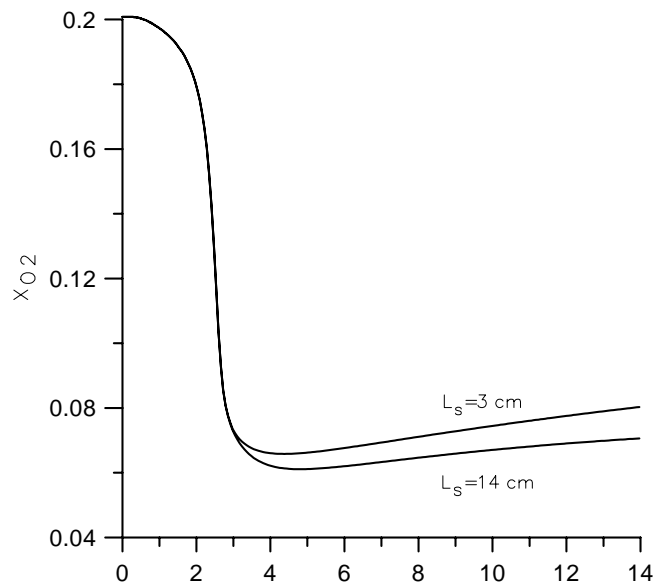


Fig.7.6. O_2 mole fraction axial distributions in supersonic propane-air flow at some values of heat supply length. $P_s = 60 \text{ W/cm}$, $\beta_c = 0.2 \text{ mm}$.

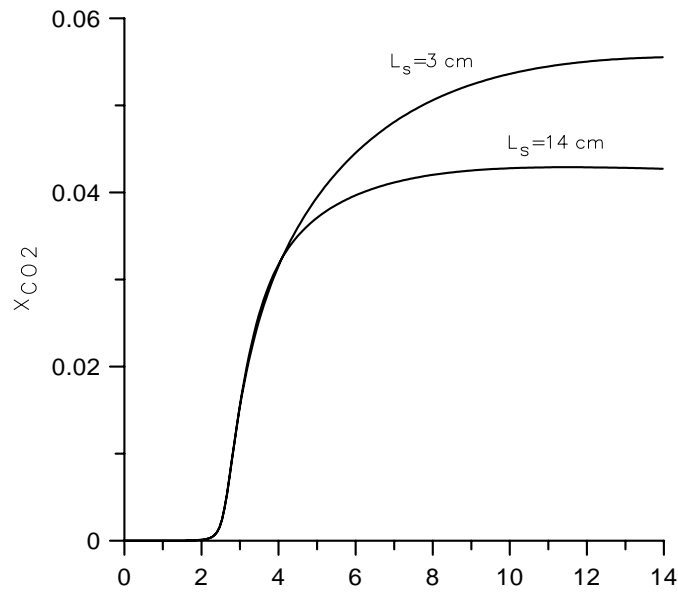


Fig.7.7. CO₂ mole fraction axial distributions in supersonic propane-air flow at some values of heat supply length. $P_s = 60$ W/cm, $\beta_c = 0.2$ mm.

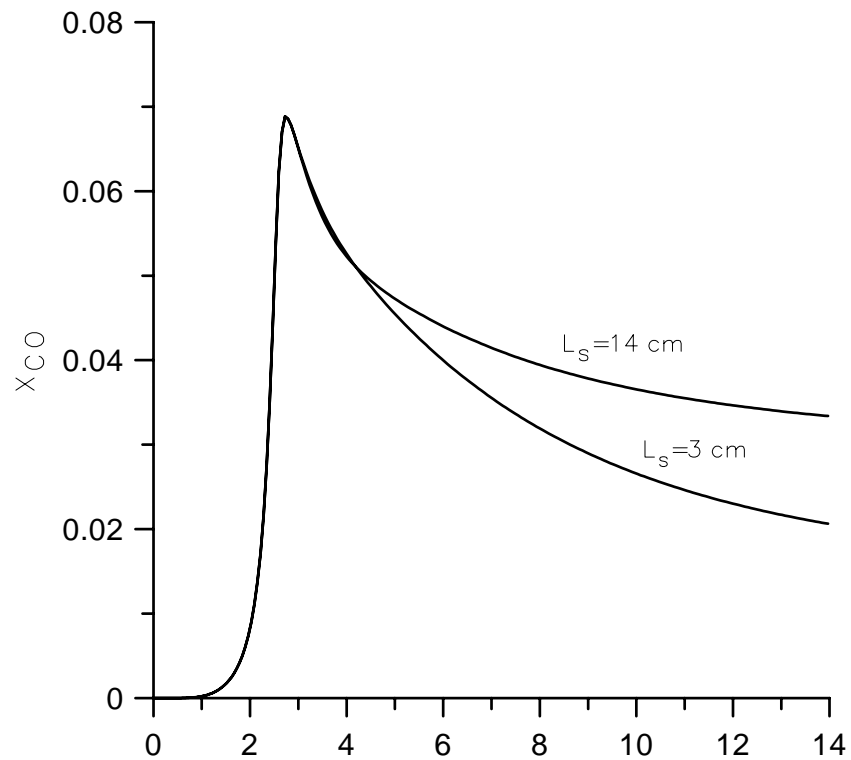


Fig.7.7. CO₂ mole fraction axial distributions in supersonic propane-air flow at some values of heat supply length. $P_s = 60$ W/cm, $\beta_c = 0.2$ mm.

REFERENCES TO CHAPTER VII.

1. Georgievsky P.Yu., Gromov V.G., Ershov A.P., et al. Gas discharge in supersonic flow // The 2nd Workshop on magneto-plasma-aerodynamics in aerospace applications. Moscow, 5 April -7 April 2000, P.143.
2. Chernikov V., Ershov A., Georgievsky P. et al. Features of Transversal Gas Discharge in Supersonic Gas Flow // 32nd AIAA Plasmadynamics and Lasers Conf. and 4th Weakly Ionized Gases Workshop. Anaheim, CA. 11–14 June 2001. AIAA-2001-3084.
3. Westbrook, C.K., Dryer, F.L. Simplified Reaction Mechanisms for the Oxidation of Fuels in Flames. Combustion Science and Technology, 1981, Vol.27, pp.31-43.
4. Katta, V.R., Roquemore, W.M. Simulation of Unsteady Flows in an Axisymmetric Research Combustor Using Detailed-Chemical Kinetics. AIAA/ASME/SAE/ASEE Joint Propulsion Conference & Exhibit, 34th, Cleveland, OH, July 13-15, 1998.

CONCLUSION

The complex of probe and spectroscopic methods which allow to determine parameters of discharge plasma of a fuel-air mixture, fact of ignition of propane - air mixture in a supersonic flows and parameters of flame plasma has been developed in the current project.

For these purposes an experimental installation has been created, which provided a supersonic ($M = 2$) air and propane-air mixture flow at the static pressure range 50 - 300 Torr with pulse-periodic transversal and longitudinal discharges and pulsed plasma jets.

The main efforts were required for application of the probe method for diagnostics of discharges in supersonic flows. Modes of probe-plasma interaction are numerous, and for a great part of them there exists no sufficient theory, which would make it possible to bind probe signals with plasma properties. For the purposes of diagnostics, it is necessary to develop fast algorithms of computation of voltage-current characteristics.

A certain further progress in covering the region of parameters of interest for plasma aerodynamic applications has been achieved.

A new analytical model for drift, diffusion and intermediate modes of probe operation in high-speed flows of dense weakly ionized plasma is suggested. It takes into account the effect of the second wire of the double probe and the leakage of the electron current. The model is valid for an arbitrary angle between the discharge field and the flow velocity. A comparison of analytical and experimental voltage-current characteristics is presented.

Another new analytical model for the modes, in which the probe current is limited by processes in the Debye double layer and in the ion drift region, has been developed for the characteristic high-speed flows of flame plasmas. The resulting voltage-current characteristics do not contradict with experimental data.

In further efforts, these two models, in the principle, could be combined into one, which would be capable of covering a wide range of plasma flow parameters, including the drift, diffusion and Debye double layer modes. For applicability of this model for diagnostics, a special fast image recognition algorithm could be developed.

Peculiarities of diagnostics of air-fuel mixtures have been considered. The results of computations on base of this model correspond with data of a detailed 2D numerical simulation and experimental voltage-current characteristics.

This 2D numerical model needs to be further improved to be able to account for the Debye layers; however, a large and lasting effort in fundamentals of applied mathematics is required for so doing.

The results of computations for air-fuel mixtures point on a necessity to investigate what kind of positive ions prevails in a plasma under investigation, for small quantities of components with low ionization potentials can affect the diagnostics.

A new numerical model based on a detailed 1D simulation of electron and ion fluids is developed. Results concerning the Debye and diffusion layers and the intermediate modes for dense weakly ionized gas flows (including the flows of pulsed discharge plasmas and flames) are presented. These results are in a reasonable agreement with the new experimental data, but they differ considerably from the earlier analytical works available from the literature. This model needs improvements for broadening the region of parameters where it is reliable.

The longitudinal positioning of probes has proved to be less advantageous than the transversal one.

Thus, to provide plasma diagnostics for the wide range of parameters characteristic for plasma aerodynamic applications, a considerably simple, but comprehensive analytical model is wanted. A prototype of such a model can be derived from the analytical models of the presented work. A considerable work of checking the model reliability for different combinations of parameters is required, for which purpose new numerical studies are necessary, as well as new experiments. The newly created numerical models could be used for such verification after certain modifications.

The new type of the probe measurement device fundamentally improving the temporary resolution was developed. The opportunity of circuit operation in immediate vicinity to investigated object was shown experimentally. Thus the time resolution of circuit will be defined by components.

I-V probe characteristics in discharge plasma and combustion plasma in the supersonic air and air-propane mixture were measured. The measurement time of characteristics was equal to no more than 10 μ s. The theoretical researches have allowed to substantiate techniques of definition of ion density in discharge plasma and electron density in flame plasma in supersonic flows.

The method of gas temperature measurement was adapted to experimental conditions. The intensities of lines of the rotational structure of the second positive system of N_2 , which has been used for measurements of gas (rotational) temperature of air plasma, falls at growth of full pressure $P_0 > 1$ atm very sharp. Especially it is true in case of air-propane plasmas. As result, plasma temperature has to be evaluated over the relative intensities of the molecular bands of CN.

Mechanism of sustention and the values of microscopic parameters of transversal electric discharge in supersonic air and propane-air flows were investigated.

Checking technique of ignition and combustion of propane- air mixture in supersonic flows was suggested. Experimentally was shown that the fact of ignition and combustion of propane-air mixture supersonic flow may be tested by joint application of two methods: a) investigation of CH radicals band, $\lambda = 431.5$ nm, luminescence evolution and b) investigation of the single electric probe currents evolution. The scope of this technique apparently is not limited to a case of a propane-air mixture, but can be distributed on other hydrocarbons-air mixtures.

The range of parameters of the pulsed transversal electric discharge, in which the ignition of the propane-air mixture flow is observed, is determined. It is experimentally shown, that there are the thresholds of ignition determined by electric power, extent of the discharge along a flow. Comparison of experimental results with results of numerical simulation of ignition of propane-air mixture flow by electric discharge shows, that it is impossible to ignore the thermal mechanism of ignition of propane – air mixture flow completely.

All types of discharges can be used for an ignition of propane-air mixture supersonic flow (in the case of the electrode discharges the threshold current has to be $I > 1$ A, the plasma density has to be $N > 10^{11}$ cm^{-3} in the case of plasma jets). The density of recombining plasma of the jet and the density of discharge plasmas are the values of the same order of the magnitude at times of hundreds of μ s. However, plasma jets injected into flows conserve high values of plasma density

at long distances from the plasma source in contrast to the longitudinal and transversal discharges. So the ignition range of plasma jets is much higher than of electric gas discharges but it is achieved due to higher energy inputs.

LIST OF PUBLISHED PAPERS AND REPORTS

1. Александров А.Ф., Ершов А.П., Сурконт О.С., Тимофеев И.Б., Тимофеев Б.И., Черников В.А., Черников А.В., Шибков В.М. Поперечные газовые разряды в сверхзвуковых потоках воздуха. Тезисы докладов XXIX Звенигородской конференции по физике плазмы и УТС. 25 февраля – 1 марта 2002 г., Звенигород, 2002г. с.208.
2. Ershov A.P., Bychkov V.L., Chernikov V.A., Shibkov V.M., Surcont O.S., Timofeev B.I., Timofeev I.B. Transversal electric discharges in supersonic airflow. The fourth workshop on magnetoplasma aerodynamics for aerospace applications. Moscow, 9 – 11 April 2002, p.67
3. А.П.Ершов, В.Л.Бычков, И.Б.Тимофеев, Б.И.Тимофеев, О.С.Сурконт, В.А.Черников, В.М.Шибков. Поперечные электрические разряды в сверхзвуковых потоках воздуха. Четвертое совещание по магнитоплазменной аэродинамике в аэрокосмических приложениях (Аннотации к докладам) Москва, 9-11 апреля 2002, Институт высоких температур РАН с.66
4. Ershov A.P., Bychkov V.L., Chernikov V.A., Shibkov V.M., Surcont O.S., Timofeev B.I., Timofeev I.B. Peculiarities of transversal discharge in a flow as non self maintained in air. 1. Transversal electric discharges in supersonic flows. International Workshop Thermochemical and plasma processes in aerodynamics. Saint Petersburg, 15-19 July 2002.P.134 – 137.
5. Ardelyan N.V., Bychkov V.L., Ershov A.P., Gordeev O.A., Timofeev I.B. Peculiarities of transversal discharge in a flow as nonself maintained in air. II. Theoretical model of electric discharge in a supersonic flow. . International Workshop Thermochemical and plasma processes in aerodynamics. Saint Petersburg, 15-19 July 2002. P.139 – 146.
6. Бычков В.Л., Ершов А.П., Сурконт О.С., Тимофеев Б.И., Тимофеев И.Б., Черников В.А., Шибков В.М. Особенности поперечного разряда в потоке, как несамостоятельного разряда в воздухе. I. Поперечные электрические разряды в сверхзвуковых потоках. Труды Международного Симпозиума Термохимические и плазменные процессы в аэродинамике. С-Петербург, 15-19 июля, 2002. С.130 – 134.
7. Арделян Н.В., Бычков В.Л., Ершов А.П., Гордеев О.А., Тимофеев И.Б. Особенности поперечного разряда в потоке, как несамостоятельного разряда в воздухе. II. Теоретическая модель электрического разряда в сверхзвуковом потоке. Труды Международного Симпозиума Термохимические и плазменные процессы в аэродинамике. С-Петербург, 15-19 июля, 2002. С.135 –142.

8. Ershov A.P., Bychkov V.L., Chernikov V.A., Shibkov V.M., Surkont O.S., Timofeev B.I., Timofeev I.B. Transversal electric discharges in supersonic airflow. Proceedings of the 4th Workshop on Magnetoplasma Aerodynamics for Aerospace Applications. Moscow, 9 – 11 April 2002, p.240-245.
9. A.P.Ershov, N.V.Ardelyan, V.L.Bychkov, V.A.Chernikov, V.M.Shibkov, O.S.Surkont, I.B.Timofeev. Mechanisms of transversal electric discharge sustantion in supersonic air and propane-air flows. 41st Aerospace Sciences Meeting and Exhibit and 5th Weakly Ionized Gases Workshop, Reno, Nevada, 6-9 January 2003. AIAA 2003-0872.
10. V.A.Chernikov, S.A.Dvinin, A.P.Ershov, I.B.Timofeev, V.M.Shibkov. The theory of direct current discharge in transversal gas flow. 41st Aerospace Sciences Meeting and Exhibit and 5th Weakly Ionized Gases Workshop, Reno, Nevada, 6-9 January 2003. AIAA 2003-1193.
11. A.P.Ershov. Annual technical report of ISTC Project # 2247p (From 1 February 2002 to 1 February 2003). Moscow. February 2003.
12. Александров А.Ф., Ершов А.П., Сурконт О.С., Тимофеев И.Б., Черников В.А., Шибков В.М. Применение импульсного разряда для воспламенения сверхзвукового потока пропан - воздушной смеси. Тезисы докладов XXX Звенигородской конференции по физике плазмы и УТС., 24 февраля–28 февраля 2003г Звенигород, с.221.
13. А.П.Ершов, Н.В.Арделян, А.В.Калинин, О.С.Сурконт, Б.И.Тимофеев, С.Н.Чувашев, В.М.Шибков. Зондовая диагностика в условиях воспламеняющих разрядов в сверхзвуковых потоках. Пятое совещание по магнитоплазменной аэродинамике в аэрокосмических приложениях (Аннотации к докладам) Москва, 7-10 апреля 2003, Институт высоких температур РАН с.59.
14. A.P.Ershov, N.V.Ardelyan, O.S.Surkont,, I.B.Timofeev, S.N.Chuvashev, V.M.Shibkov. Probe diagnostics for the conditions of igniting discharges in supersonic flow. The fourth workshop on magnetoplasma aerodynamics for aerospace applications. Moscow, 7-10 April 2003, p.60.
15. V.L.Bychkov, V.G.Gromov, A.P.Ershov, V.A.Levin,V.A.Chernikov, V.M.Shibkov, O.S.Surkont and I.B.Timofeev. An electrode ignition discharges in supersonic propane-air flows. Combustion and Atmospheric Pollution /edit by G.D.Roy, S.M.Frolov/, Moscow, Torus press, PP.278-282. 2003.
16. A.P.Ershov, V.A.Chernikov, V.M.Shibkov, O.S.Surkont, I.B.Timofeev, N.V.Ardelyan, S.N.Chuvashev, V.L.Bychkov, V.G.Gromov and V.A.Levin. Parameters of electrode ignition discharges in supersonic propane-air flows. International Workshop

- “Thermochemical and plasma processes in aerodynamics”. Saint Petersburg, 28-31 July, 2003.P.67-75.
17. А.Ф.Александров, Н.В.Арделян, А.П.Ершов, А.В.Калинин, О.С.Сурконт, Б. И.Тимофеев, В.М.Шибков. // Зондовая диагностика газоразрядной плазмы и плазмы пламени в сверхзвуковых потоках воздуха и пропан - воздушной смеси. Тезисы докладов 3 Всероссийской конференции «Физическая электроника» Махачкала, 23-26 сентября 2003 г., с.91-94.
 18. Н.В.Арделян, В.Л.Бычков, А.П.Ершов, А.В.Калинин, О.С.Сурконт, И.Б.Тимофеев, С.Н.Чувашев. Исследования высокоскоростных плазменных потоков для плазменной аэродинамики. 6-й международный симпозиум по радиационной плазмодинамике. Сб. научных трудов. Москва. 2003. С. 47-52.
 19. А.П.Ершов, И.Б.Тимофеев, В.А. Черников, С.Н.Чувашев. Плазмодинамические МПК – разряды для плазменной аэродинамики. 6-й международный симпозиум по радиационной плазмодинамике. Сб. научных трудов. Москва. 2003. С. 53-58.
 20. С.А.Двинин, А.П.Ершов, И.Б.Тимофеев, В.А. Черников, В.М.Шибков. Моделирование разряда постоянного тока в поперечном сверхзвуковом потоке газа.// Теплофизика высоких температур, 2004, 42, N 2.
 21. A.P.Ershov, N.V.Ardelyan, O.S.Surkont., I.B.Timofeev, S.N.Chuvashhev, V.M.Shibkov. Discharge and flame plasmas probe diagnostics in supersonic air-propane flows. 42nd AIAA Aerospace Sciences Meeting and Exhibit 5-8 January 11, 2004 Reno, Nevada, AIAA 2004-1016.
 22. А.Ф.Александров, А.П.Ершов, А.В.Калинин, О.С.Сурконт, Б. И.Тимофеев, В.М.Шибков. Автоматизированные схемы зондовых измерений в плазме разрядов в сверхзвуковых потоках газа. Тез. докл. XXXI Звенигородской конф. по физике плазмы и УТС. г.Звенигород 24 февраля–28 февраля 2004г. с.
 23. А.П. Ершов, О.С.Сурконт, И.Б. Тимофеев В.А. Черников, В.М.Шибков. Поперечные электрические разряды в сверхзвуковых потоках воздуха. Механизмы распространения и неустойчивости разряда // ТВТ. 2004. Т.42. №3. С.